

Letter from the Editors

Dear readers of *Acta Naturae*,
We would like to bring to your attention the 19th issue of our journal. Having analyzed the publication activity and citation impact, we are delighted to say that our journal has found its audience, and the level of publications is steadily increasing. The well-known consulting company *Macmillan Science Communication* collaborating with *Nature Publishing Group* has recently become interested in the journal. *Acta Naturae* has been selected among three Russian journals as a model for being promoted in Russia. Jointly with SkolTech, *Macmillan Science Communication* has elaborated a business plan aimed at arousing the interest of the audience in the journal and increasing the number of citations.

We still have a lot to achieve. It would be enough to mention that the impact factor of the oldest Russian journal “*Biokhimiya*” (Biochemistry, Moscow) in 2012 was 1.149, which actually is quite achievable for *Acta Naturae* in the near future (the impact factor of *Acta Naturae* in 2012 was 0.477). There is an appreciably large number of articles in our Editorial portfolio waiting to be published, which, however, does not increase the time required to publish a paper. In some cases, provided that two peer reviews are favorable, it takes less than two months to be published. Certainly, if repeated peer review is required, this time may be as long as 6 months. We are interested in increasing the number of fundamental medicine articles and good reviews that would be useful for young scientists and even students.

In this issue you will find our usual sections and several interesting reviews, research articles, and the Forum section devoted to the results of the 38th Congress of the Federation of European Biochemical Societies (FEBS 38) that was held this summer in St. Petersburg. We call your attention to the review by E.A. Vas’kova et al. devoted to the phenom-

enon of “epigenetic memory” of pluripotent stem cells. Our journal has been paying due attention to the problems of stem cell reprogramming and this publication will contribute to the already available findings in this area. The next review (A.L. Rippa et al.) covers the modern trends in regenerative medicine. It focuses on the role of integrins in the formation of the epidermis. The third review is devoted to aptamers (A.V. Lakhin et al.). These mimetics are likely to grab a special spot in biopharmaceutics in the near future.

The research section starts with an article by R. Shakh-Makhmud and O.N. Il’inskaya that looks into the role of ribonuclease in resistance to the pandemic influenza A (H1N1) virus. The article by P.G. Georgiev et al. focuses on the classical problems of molecular biology. Its title is rather provoking: “Competition within Introns: Splicing Wins Over Polyadenylation via a General Mechanism”. The article by V.I. Tishkov et al. is devoted to classical enzymology and describes the structural aspects of α -amino acid ester hydrolase. The problems of innate immunity are discussed in the paper by E.R. Sadchikova. We welcome good articles in the area of neurophysiology: in particular, the paper by A.L. Zefirov et al. (researchers from the very strong Kazan school) is published in this issue. The mechanisms of autoimmune pathologies and models of these diseases are discussed in articles by Ya.A. Lomakin et al. and A.G. Sobolev et al. The molecular mechanisms of stress are considered in the study by D.N. Baryakin et al. The articles by the research team of S.B. Seredenin and A.N. Ver-evkin are devoted to the investigation of the mechanisms of pathological conditions and the designing potential drugs for patients with depression and type 2 diabetes mellitus.

We sincerely wish you the New Year 2014 filled with health and success! ●

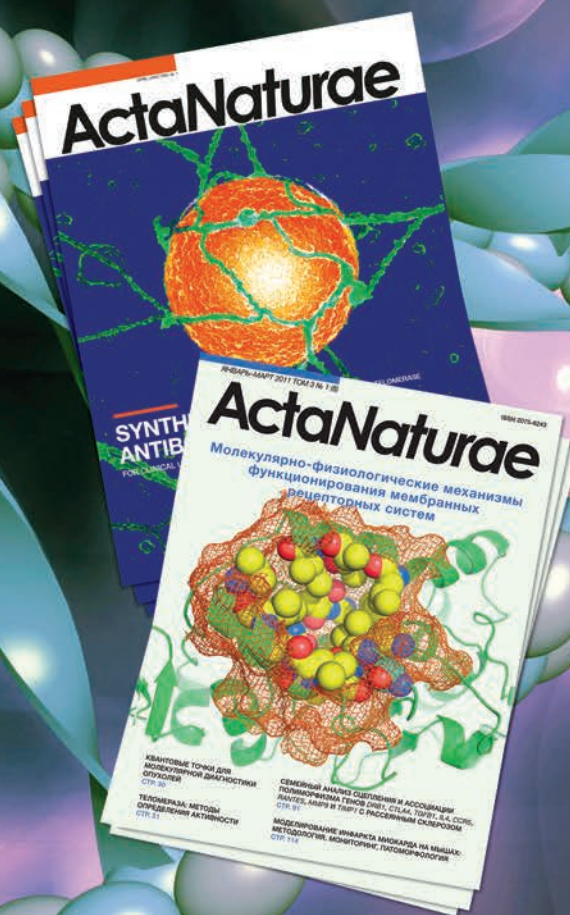
Editorial Board

ActaNaturae

SUBSCRIPTION TO

Acta Naturae journal focuses upon interdisciplinary research and developments at the intersection of various spheres of biology, such as molecular biology, biochemistry, molecular genetics, and biological medicine.

Acta Naturae journal is published in Russian and English by Park Media company. It has been included in the list of scientific journals recommended by the State Commission for Academic Degrees and Titles of the Ministry of Education and Science of the Russian Federation and the Pubmed abstracts database.



SUBSCRIBE AT THE EDITORIAL OFFICE

Leninskie Gory, 1-75G, Moscow, 119234 Russia
Telephone: +7 (495) 930-87-07, 930-88-51
Bio-mail: podpiska@biorf.ru
Web site: www.actanaturae.ru

SUBSCRIBE USING THE CATALOGUES OR VIA THE INTERNET:

ROSPECHAT (The Russian Press)
Indices: 37283, 59881
www.pressa.rosp.ru

INFORMNAUKA
Index: 59881
www.informnauka.com

INTER-POCHTA
17510
www.interpochta.ru

INFORMATION FOR AUTHORS:

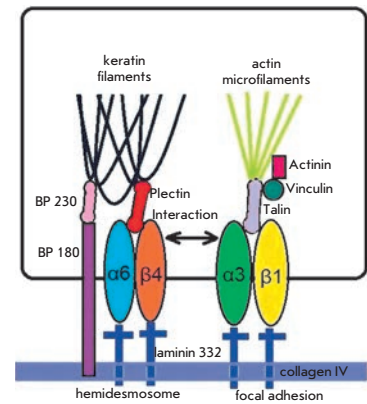
If you would like to get your research paper published in *Acta Naturae* journal, please contact us at journal@biorf.ru or call +7 (495) 930-87-07.



The Role of Integrins in the Development and Homeostasis of the Epidermis and Skin Appendages

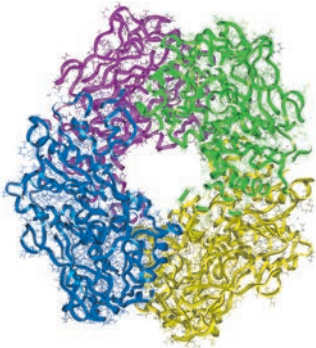
A.L. Rippa, E.A. Vorotelyak, A.V. Vasiliev, V.V. Tersikh

Integrins play a critical role in the regulation of adhesion, migration, proliferation, and differentiation of cells. Development of mice with tissue-specific integrin genes knockout and determination of the genetic basis for a number of skin diseases in humans showed the significance of integrins in the biology, physiology, and morphogenesis of the epidermis and hair follicles. This review discusses the data on the role of different classes of integrin receptors in the biology of epidermal cells, as well as the development of the epidermis and hair follicles.



Integrin receptors in cell-matrix interactions

3D Structure Modeling of Alpha-Amino Acid Ester Hydrolase from *Xanthomonas rubrilineans*



S.A. Zarubina, I.V. Uporov, E.A. Fedorchuk, V.V. Fedorchuk, A.V. Sklyarenko, S.V. Yarotsky, V.I. Tishkov

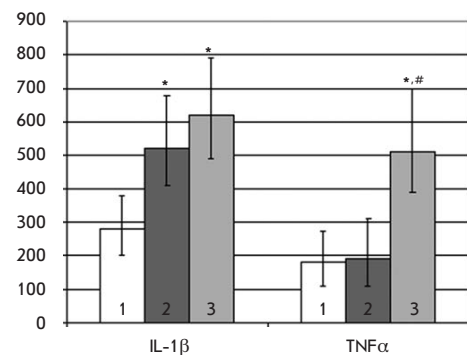
Alpha-amino acid ester hydrolase (AEH) is a promising biocatalyst for β -lactam antibiotics synthesis of penicillins and cephalosporins. The structure of AEH from *Xanthomonas rubrilineans* (XrAEH) was simulated using the homology modeling method, and its active site was analyzed. The structures of XrAEH complexes with ampicillin, amoxicillin, cephalexin, *D*-phenylglycine and 4-hydroxy-*D*-phenylglycine methyl esters were obtained by docking. Antibiotic agents for whose synthesis this enzyme would show the highest efficiency were determined.

General view of the XrAEH tetramer

Neolactoferrin As a Stimulator of Innate and Adaptive Immunity

A.D. Chernousov, M.F. Nikonova, N.I. Sharova, A.N. Mitin, M.M. Litvina, P.E. Sadchikov, I.L. Goldman, A.A. Yarinin, E.R. Sadchikova

The innovative product Neolactoferrin is a natural combination of recombinant human lactoferrin (90%) and goat lactoferrin (10%) isolated from the milk of transgenic goats carrying the full-length human lactoferrin gene. The effect of Neolactoferrin on human immune system cells was studied. Neolactoferrin was shown to exhibit an immunotropic activity and to hinder the development of immune inflammatory processes. Iron saturation of Neolactoferrin increases its pro-inflammatory activity.



Effects of Neolact (2) and Neolact enriched in iron (3) on monocyte secretion of cytokines IL-1 β and TNF α

Founders

Ministry of Education and
Science of the Russian Federation,
Lomonosov Moscow State University,
Park Media Ltd

Editorial Council

Chairman: A.I. Grigoriev
Editors-in-Chief: A.G. Gabibov, S.N. Kochetkov

V.V. Vlassov, P.G. Georgiev, M.P. Kirpichnikov,
A.A. Makarov, A.I. Miroshnikov, V.A. Tkachuk,
M.V. Ugryumov

Editorial Board

Managing Editor: V.D. Knorre
Publisher: K.V. Kiselev

K.V. Anokhin (Moscow, Russia)
I. Bezprozvanny (Dallas, Texas, USA)
I.P. Bilenkina (Moscow, Russia)
M. Blackburn (Sheffield, England)
S.M. Deyev (Moscow, Russia)
V.M. Govorun (Moscow, Russia)
O.A. Dontsova (Moscow, Russia)
K. Drauz (Hanau-Wolfgang, Germany)
A. Friboulet (Paris, France)
M. Issagouliants (Stockholm, Sweden)
A.L. Konov (Moscow, Russia)
M. Lukic (Abu Dhabi, United Arab Emirates)
P. Masson (La Tronche, France)
K. Nierhaus (Berlin, Germany)
V.O. Popov (Moscow, Russia)
I.A. Tikhonovich (Moscow, Russia)
A. Tramontano (Davis, California, USA)
V.K. Švedas (Moscow, Russia)
J.-R. Wu (Shanghai, China)
N.K. Yankovsky (Moscow, Russia)
M. Zouali (Paris, France)

Project Head: S.B. Nevskaya

Editor: N.Yu. Deeva

Strategic Development Director: E.L. Pustovalova

Designer: K.K. Oparin

Photo Editor: I.A. Solovey

Art and Layout: K. Shnaider

Copy Chief: Daniel M. Medjo

Address: 119234 Moscow, Russia, Leninskiye Gory, Nauchny
Park MGU, vlad.1, stroeniye 75G.

Phone/Fax: +7 (495) 930 88 50

E-mail: vera.knorre@gmail.com, mmorozova@strf.ru,
actanaturae@gmail.com

Reprinting is by permission only.

© ACTA NATURAE, 2013

Номер подписан в печать 17 декабря 2013 г.

Тираж 200 экз. Цена свободная.

Отпечатано в типографии «МЕДИА-ГРАНД»

CONTENTS

Letter from the Editors 1

FORUM

FEBS 38 in St. Petersburg 6

REVIEWS

E.A. Vaskova, A.E. Stekleneva,
S.P. Medvedev, S.M. Zakian
“Epigenetic Memory” Phenomenon
in Induced Pluripotent Stem Cells 15

A.L. Rippa, E.A. Vorotelyak, A.V. Vasiliev,
V.V. Terskikh
The Role of Integrins in the Development
and Homeostasis of the Epidermis
and Skin Appendages 22

A.V. Lakhin, V.Z. Tarantul, L.V. Gening
Aptamers: Problems, Solutions
and Prospects 34

RESEARCH ARTICLES

R. Shah Mahmud, O.N. Ilinskaya
Antiviral Activity of Binase against
the Pandemic Influenza A (H1N1) Virus 44

M. Tikhonov, P. Georgiev, O. Maksimenko
Competition within Introns: Splicing
Wins over Polyadenylation
via a General Mechanism 52

S.A. Zarubina, I.V. Uporov, E.A. Fedorchuk,
V.V. Fedorchuk, A.V. Sklyarenko,
S.V. Yarotsky, V.I. Tishkov
**3D Structure Modeling
of Alpha-Amino Acid Ester Hydrolase
from *Xanthomonas rubrilineans*.....62**

A.D. Chernousov, M.F. Nikonova, N.I. Sharova,
A.N. Mitin, M.M. Litvina, P.E. Sadchikov,
I.L. Goldman, A.A. Yarilin, E.R. Sadchikova
**Neolactoferrin As a Stimulator
of Innate and Adaptive Immunity71**

M.M. Abdrakhmanov, A.M. Petrov,
P.N. Grigoryev, A.L. Zefirov
**Depolarization-Induced
Calcium-Independent Synaptic
Vesicle Exo- and Endocytosis
at Frog Motor Nerve Terminals77**

D.N. Baryakin, D.V. Semenov, A.V. Savelyeva,
O.A. Koval, I.V. Rabinov, E.V. Kuligina,
V.A. Richter
**Alu- and 7SL RNA Analogues Suppress
MCF-7 Cell Viability through Modulating
the Transcription of Endoplasmic Reticulum
Stress Response Genes83**

Y. A. Lomakin, M. Yu. Zakharova,
A. A. Belogurov, N. A. Bykova, M. A. Dronina,
A. E. Tupikin, V. D. Knorre, A. N. Boyko,
A. V. Favorov, M. R. Kabilov,
N. A. Ponomarenko, A. G. Gabibov
**Polyreactive Monoclonal Autoantibodies in
Multiple Sclerosis: Functional Selection from
Phage Display Library and Characterization by
Deep Sequencing Analysis94**

S.B. Seredenin, T.A. Voronina,
T.A. Gudasheva, T.L. Garibova,
G.M. Molodavkin, S.A. Litvinova,
E.A. Elizarova, V.I. Poseva
**Antidepressant Effect of Dimeric
Dipeptide GSB-106, an Original
Low-Molecular-Weight Mimetic
of BDNF 105**

A.G. Soboleva, V.V. Sobolev, S.A. Bruskin,
A.V. Mezentsev
**Three-Dimensional Model of Mouse
Epidermis for Experimental Studies
of Psoriasis110**

T.N. Popova, A.A. Agarkov, A.N. Verevkin
**Intensity of Free Radical Processes
in Rat Liver under Type 2 Diabetes
and Introduction of Epifamin.....118**

Guidelines for Authors..... 123

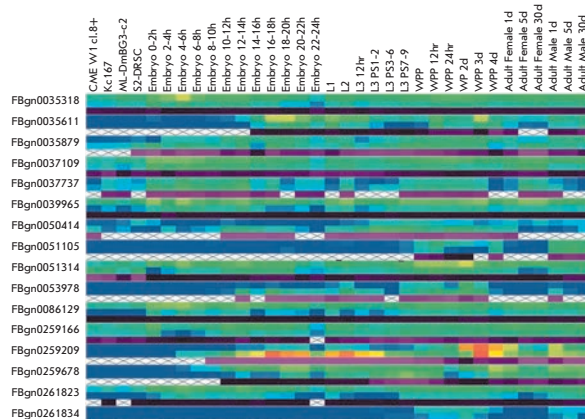


IMAGE ON THE COVER PAGE
Heat map illustrating the expression patterns of the genes

FEBS 38 in St. Petersburg

For the Russian scientific community working in the field of life sciences, the year 2013 was marked by a high-profile event, namely the 38th Congress of the Federation of European Biochemical Societies (FEBS), held in St. Petersburg on July 6–11. The event was covered by the media (it should be mentioned that the RIA Novosti news agency was the official partner of the Congress); however, many things remained behind the scenes. *Acta Naturae* and its staff took an active part in the organization of the forum. In this year's final issue, we would like to share our impressions "from inside the event" and to analyze it.

SOME STATISTICS AND COMPARISON WITH WESTERN COUNTRIES

FEBS brings together over 36,000 researchers from 35 National European biochemical societies. Its activities extend far beyond the congress' platform. The FEBS structure includes journal committees (FEBS Journal; FEBS Letters, etc.), "Science and Society," "Women in Science," an Educational Section, a Scholarship Committee, etc. FEBS is a very democratic organization and holds regular elections of the executive group and chairmen of the committees.

FEBS Congresses have been held annually in European countries for nearly 40 years and bring together the European scientific community working in the field of life sciences. Over the recent years, the subject matter of the Congress has significantly expanded and currently overlaps with the subject of congresses on biophysics, neuroscience, and immunology to some extent. This trend is not incidental, since the drive toward increasing specialization of research areas, which is characteristic of the end of the XX century, tends to be replaced by making research more universal and by combining disciplines and experimental approaches. The introduction of "omics," deep sequencing, application of NMR platforms, X-ray analysis using QM/MD methods do allow one to use the comprehensive ap-

Table 1. The number of participants by country (data for the leading 20 countries are shown)

	Russia	864		Korea	53
	Turkey	151		Ukraine	52
	Poland	115		Portugal	46
	Italy	112		Japan	31
	USA	111		Israel	29
	Germany	107		Greece	27
	United Kingdom	95		Netherlands	27
	Czech Republic	84		Romania	26
	France	83		Croatia	23
	Spain	73		Hungary	23

proach in attempting to solve the problems of biology and molecular medicine. This situation could not but affect the programs of large international forums. Requirements to their organization have tightened dramatically. Today, the participation of thousands of people at the same time (a sort of scientific

"flash mob") requires an enormous organizing effort to create a special scientific atmosphere that would be interesting for several generations of researchers, from undergraduate and graduate students to the greatest scientists on the apex of their career. Despite the economic problems in Europe, the FEBS brand

Table 2. Major and satellite symposia of the 38th FEBS Congress**Major symposia****I. Mechanisms of Genetic Control****ORGANIZATION OF EUKARYOTIC GENOMES (S1)** Chairpersons: Wendy Bickmore, S. Razin**RNA WORLD (S2)** Chairpersons: O. Dontsova, Eric Westhof**DNA DAMAGE AND REPAIR (S3)** Chairpersons: E. Gromov, O. Lavrik, Leon Mullenders**EVOLUTIONARY GENOMICS (W4)** Chairpersons: K.G. Scriabin, Huanming Yang**NUCLEIC ACID TARGETS AND THERAPEUTICS (W5)** Chairperson: V. Vlasov**II. Biocatalytic Mechanisms and Protein Dynamics****BIOCATALYSIS: GENERAL PROBLEMS (S6)** Chairpersons: M. Blackburn, A. Gabibov**PROTEIN STRUCTURE AND FOLDING (S7)** Chairpersons: Cyrus Chothia, A. Finkelstein**PROTEIN DYNAMICS (W8)** Chairpersons: A. Arsenyev, O. Fedorova, Jaak Jarv**ENZYMES REACTING WITH ORGANOPHOSPHORUS AGENTS (W9)** Chairpersons: Patrick Masson, S. Varfolomeev**ALEXANDER BRAUNSTEIN MEMORIAL SYMPOSIUM: ENZYMES, COFACTORS, MECHANISMS (W10)**

Chairpersons: T. Demidkina, Andrea Mozzarelli, V. Tishkov

III. Mechanisms of Communication and Signaling**ION CHANNEL SIGNALING: FROM SPATIAL STRUCTURES TO PHYSIOLOGICAL MECHANISMS (S11)**

Chairpersons: A. Kaznacheeva, O. Kryshchal, Alan North, V. Tsetlin

MEMBRANE TRANSPORT AND SECRETION: FROM NEPHRONS TO NEURONS (S12) Chairpersons: Qais Al-Awqati,

Dominique Eladari, A. Petrenko

BIOCHEMISTRY OF STRESS RESPONSE (S13) Chairpersons: B. Margulis, Gabriele Multhoff**“MITOCHONDRIOLOGY”: NEW APPROACHES IN BIOENERGETICS (S14)** Chairpersons: Sergio Papa, V. Skulachev**CELLULAR MECHANISMS OF PROTEOLYSIS (S15)** Chairpersons: Aaron Ciechanover, Helle Ulrich**IV. Molecular Mechanisms of Disease****BIOCHEMISTRY FOR MEDICINE: DRUG DESIGN AND DIAGNOSTICS (S16)** Chairpersons: A. Egorov, A. Kiselev,

S. Komissarenko, Tomas Zima

BIOCHEMISTRY OF NEOPLASTIC TRANSFORMATIONS (S17) Chairpersons: G. Georgiev, Joseph Shlessinger**MECHANISMS OF G PROTEIN SIGNALING (S18)** Chairpersons: Andrew Goryachev, Alfred Wittinghofer**BIOCHEMISTRY OF NEURODEGENERATION (S19)** Chairpersons: Yves Agid, M. Ugriumov**PHOTORECEPTION AND BIOCHEMISTRY OF VISION (S20)** Chairpersons: Karl-Wilhelm Koch, M. Ostrovsky**STEM CELLS: FUNDAMENTALS AND APPLICATIONS (S21)** Chairpersons: Clare Blackburn, A. Tomilin**V. Biochemical Mechanisms of Immune Defense****MOLECULAR BASIS OF AUTOIMMUNITY (S22)** Chairpersons: Jean Francois Bach, Ludwig M. Sollid**IMMUNOCHEMISTRY AND BIOENGINEERING (S23)** Chairpersons: S. Deev, Andreas Plückerthun**B CELLS IN INFLAMMATION AND DISEASE (W24)** Chairpersons: Elias Toubi, Moncef Zouali**VI. General Aspects of Biochemistry****PROTEOMICS AND PEPTIDOMICS (S25)** Chairpersons: V. Govorun, V. Ivanov**METABOLISM OF MARINE ORGANISMS: STRUCTURE AND ACTIVITIES (S26)** Chairpersons: V. Stonik**BIOCHEMISTRY OF PLANTS (S27)** Chairpersons: A. Grechkin**GLYCOBIOLOGY: CARBOHYDRATE-PROTEIN RECOGNITION (S28)** Chairpersons: N. Bovin, Monica Palcic**BIOINFORMATICS (W29)** Chairpersons: M. Gelfand, E. Koonin**SYSTEMS BIOLOGY (W30)** Chairpersons: I. Goryanin, Daniel Thomas, M. Samsonov**BIOGENIC POLYAMINES IN CELL METABOLISM (W31)** Chairpersons: Robert Casero, A. Chomutov, Heather Wallace**BIOCHEMISTRY OF INVERTEBRATES (W32)** Chairpersons: A. Granovich, Jorgen Markl, N. Mikhailova**BIOENGINEERING: FUNDAMENTALS AND APPLICATION (W33)** Chairpersons: V. Popov, V. Shvydas**FEBO Symposia and Satellite Symposia****WOMEN IN SCIENCE** Chairperson: Cecilia Arraino**SCIENCE AND SOCIETY. CANCER: MECHANISMS, TREATMENT, PREVENTION AND PERSONALIZED MEDICINE****PERSPECTIVES** Chairpersons: Jacques-Henry Weil, Alexander Eggermont, M. Lichinitser**EDUCATION IN BIOCHEMISTRY “BOLOGNA PROCESS - DEBATE “PRO” AND “CONTRA”** Chairpersons:

Ferdinand Hucho, T. Ovchinnikov

FEBS EDUCATION COMMITTEE WORKSHOP: LIFE SCIENCE. EDUCATIONAL CRITERIA Chairpersons: Gül Güner

Akdogan, Keith Elliott

EMBL-RUSSIA: COOPERATION BETWEEN RUSSIA AND EUROPE IN THE FIELD OF LIFE SCIENCES

Chairpersons: Iain Mattaj, V. Panchenko

SATELLITE SYMPOSIUM “NMR IN BIOLOGY” Chairman: Isabella C. Felli**SCIENTIFIC MEETING ON GENOCENTRIC PROJECT “HUMAN PROTEOME”** Chairpersons: Juan Pablo Alba, A.

Archakov, William Hancock, Young Ki-Paik

brought together large audiences: Prague, 2009 (1,900 delegates), Gothenburg, 2010 (1,600 participants), Turin, 2011 (1,850 people), Seville 2012 (2,000 people).

We just could not lower the bar. There were more than 2,400 people present at the Congress in St. Petersburg; as we can see this is a record for the recent years (Table 1).

This fact has surprised the FEBS management, which originally was friendly but also displayed some mistrust. How could this be achieved? We managed to gather a unique team of speakers. Eleven Nobel laureates, living legends of science in the XX and XXI centuries, participated in the Congress. There is another interesting testimony of the scientific and political foresight of the convener of the symposium “Membrane Transport and Secretion: From Nephrons to Neurons,” Prof. Alexander Petrenko, who invited James Rothman as the key lecturer. James Rothman won the Nobel prize in the fall of 2013, well after the Congress. The program of the Petersburg Congress included 40 symposia with more than 320 speakers (Table 2).

This was a definite semantic and financial risk. The number of speakers was about twice as high as the average number of those at the congresses of the past years. Aptly described by Prof. Israel Pecht, Secretary General of FEBS, “There were two FEBS congresses gathered in St. Petersburg.” There were no empty lecture halls. The scientific community migrated between the meeting rooms in an intense rhythm. The only inconvenience was the lack of quality sound insulation between the lecture halls.

We managed to ensure a high level of “internationalism” amongst lecturers. As shown in Table 3, the number of Russian lecturers was

significant but not dominant, as unfortunately happened in some other FEBS congresses.

This fact was in no way associated with the level of Russian science. We could have gathered many more reports from Russia, but in this case one of the main objectives of the high-level Congress would not have been fulfilled, i.e. various national scientific schools would not have been represented. There were a lot of Americans at the Congress in St. Petersburg. FEBS combats this tendency, but we did not succumb to the pressure and opted for the “quality of science” rather than geopolitical issues. At the same time, we managed to attract very high-quality lecturers from the “Eastern bloc” (Table 3). We collected suggestions from the national committees of post-Soviet and East European countries and convinced the leaders of the symposia to include them in the program.

Table 3. Number of invited lecturers by country

USA	62	Japan	5
Russia	45	Finland	3
Germany	45	Hungary	3
The United Kingdom	44	Poland	3
France	27	Sweden	3
Italy	14	Denmark	3
Switzerland	14	Canada	2
Israel	12	Czech Republic	2
Spain	8	Norway	2
Portugal	6	South Africa	2
Ukraine	6	Belgium	1
China	4	Greece	1
Netherlands	4	Croatia	1

From this point of view, the Petersburg Congress compares favorably with the Congresses of the previous years. It will be very interesting to see how varied the national representation at the 2014 Congress in Paris and 2015 Congress in Berlin will be.

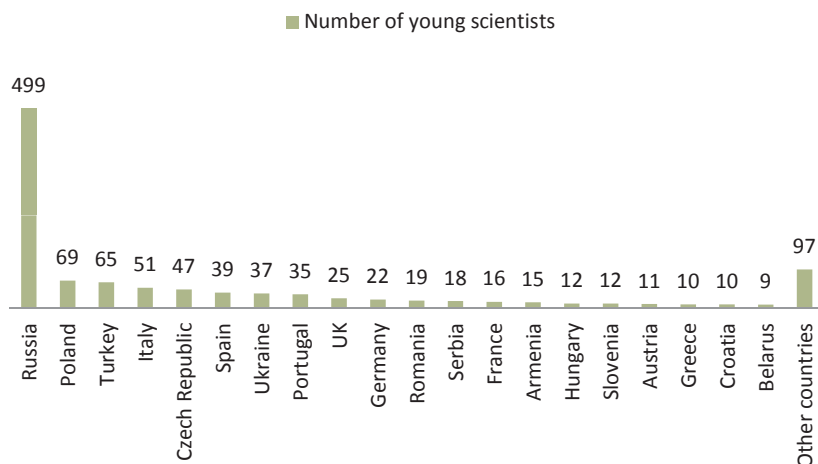
We managed to attract a lot of young people: 1,118 participants were young scientists under the age of 35 (see diagrams). Young delegates participated in the Young Scientists Forum (117 participants led by Cand. Chem. Sciences Alexei Belogurov), the FEBS Bursaries program (265 people), and they won the contest for young scientists supported by the Ministry of Education and Science of the Russian Federation (252 people). A unique atmosphere of communication and ability to see and talk to leaders of the world’s scientific elite was created.

The cultural heritage of Russia, St. Petersburg, and its surroundings were crucial in attracting delegates to the 38th FEBS Congress. The Congress opening ceremony was held in the Oktyabrsky Hall; after the ceremony and plenary lectures of Nobel Laureate Jules Hoffmann, who was introduced to the Congress by Academician Konstantin Skryabin and Sir Alan Fersht, the Swan Lake ballet was performed. An overnight visit to the Hermitage and its outstanding collection was organized with the help of Academician Oleg Kiselev (chairman of the St. Petersburg Biochemical Society) and Director of the State Hermitage Mikhail Piotrovsky.

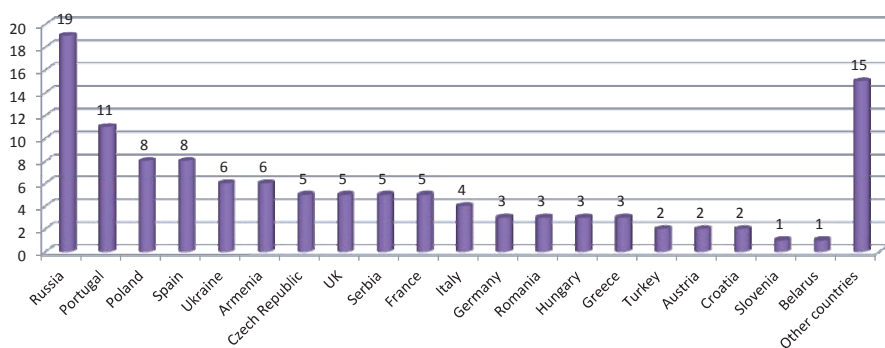
WHY RUSSIA NEEDED THIS FORUM

It is rather complicated and costly to organize such a high-level Congress, and mobilizing considerable resources is required. However, we should take an interest as to why other countries with a developed scientific infrastructure compete for

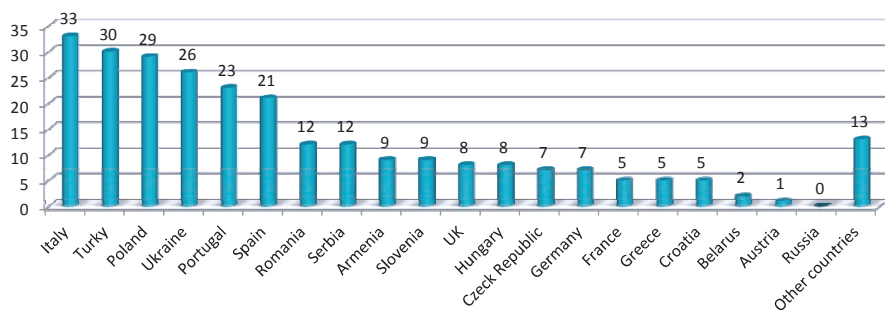
Distribution of young scientists in the Forum by country (a total of 1,118 people)



FEBS Young Scientists Forum - distribution of the participants over countries (a total of 117 people)



Distribution of FEBS bursary winners over countries (a total of 252 winners)



the right to host FEBS Congresses. Obviously, science in the modern world is becoming the privilege of rich countries. In this regard, the intension to be “in the global trend” spurs national biochemical societies to mobilize and host congresses with the support of their govern-

ments. The Soviet Union only once had the honor of hosting an FEBS Congress. In 1984, Academician Yuri Ovchinnikov organized the remarkable 16th FEBS Congress with the participation of Linus Pauling, Dorothy Hodgkin, and other great scientists of that time.

The 38th FEBS Congress confirmed that a significant number of Russian scientists are on par with their peers throughout the world, since the vast majority of Symposia (33 out of 40), along with the European and American chairpersons, were chaired by Russian scientists, notably not those who have immigrated abroad, but the researchers heading laboratories in Russia. Thus, the representatives of Russian science are known abroad, and they are able to gather decent and qualified foreign colleagues and to organize a thematic forum. This conclusion is important not only for us. Foreign colleagues could see that Russian science has not perished and that Russian scientists can be invited as co-authors in major European and international projects. Many foreign delegates shared a positive experience obtained from the summary reports and poster presentation of young Russian scientists. For young scientists, it was a great school of presentations and communication with their peers and with the world’s scientific leaders. The section on the problems of biochemical education chaired by professors Tatiana Ovchinnikova and Ferdinand Hucho worked perfectly at the Congress.

The Congress has shown that the Russian life science has a future and is interesting to the world; however, we need to properly manage existing and incoming human resources, as well as instrumental and reagent facilities. Articles that unreasonably criticize the Russian scientific school are harmful and often cause confusion even among foreign colleagues. However, stagnation in development and underestimation of the need for participation in the “international division of scientific labor” are unacceptable. The Congress has shown that the “point of no return” has been passed and that Russia has a future in the field of Bioscience.

FEBS 38 AND ADMINISTRATIVE BODIES

FEBS congresses usually attract the attention of the government bodies of the host countries. City mayors and ministers deliver addresses at opening ceremonies. The organizing committees are always concerned with this public image-related section. The 38th Congress was no exception. It was historically important to mention the role of the Skolkovo Foundation in the initiation of government solutions associated with the Congress. Viktor Vekselberg, on behalf of the Skolkovo Foundation, had addressed a request to support the initiative of the Russian Biochemical Society to hold the Congress in St. Petersburg to the Russian Federation government. St. Petersburg was chosen as the FEBS Congress venue for 2013 (a competitive bidding was held, and the city was selected on the second run). Dmitry Medvedev had signed an Order of the RF Government specifying which spheres certain ministries and agencies were to be in charge of during preparations for the Congress. Dmitry Livanov was appointed Congress chairman.

The most problematic issue was the one associated with getting visas for foreign participants. We were aware of the fact that the issue of borders for most Europeans and young people in particular has fell into oblivion. A typical illustration of this situation was the familiarization visit of the FEBS Young Scientists section in the winter of 2013, when despite our explanations and visa assistance, one of the members of the mission (Alice Verchere from France) came to Russia without a visa. Actually, the FEBS management insisted on a visa-free regime for the participants. The Ministry of Foreign Affairs of the Russian Federation and the Ministry of Education and Science came up with the most optimal alternative for issuing free-of-charge visas using telex

confirmation (this method worked almost without glitches). Now we can state with assurance that everyone who wanted to visit the Congress managed to do so (with few exceptions). We would like to make special mention of the excellent work of Senior Advisor of the Ministry of Foreign Affairs Alexander Pavlushko, consuls and advisors of the Ministry of Foreign Affairs Denis Klyukin (Washington), Andrey Ignatov (Strasbourg), Alexander Bessarabov (Paris), Konstantin Dorokhin (Madrid), Yury Klimenko (Barcelona), and Vladimir Beletsky (Bonn). The Ministry of Education and Science and its staff contributed greatly at different stages of the preparation process. Then-Deputy Minister Igor Fedyukin and current Deputy Minister Alexander Povalko, who quickly joined the preparation process, rendered invaluable assistance. A lot was done by Director of the Department of Foreign Affairs Evgeny Ugrinovich, Deputy Director Alexander Sumbatyan, and ministry staff Vladimir Arbuzov and Albert Garmash.

The chairman of the State Duma Committee on Science and Science-intensive Technologies, academician Valery Chereshnev, made a fundamental contribution to the solution of critical problems. Lyudmila Ogorodova (who was the deputy chairperson of the Committee at the time and is currently a deputy minister of the Ministry of Education and Science) also contributed to the solution of a number of problems associated with preparations for the Congress. At the Russian Academy of Sciences, the burden of responsibility for the Congress rested on Vice President of the RAS, Academician Anatoly Grigoryev, who signed dozens of letters to ministries and agencies and solved a number of fundamental problems for the Congress. The administration of the St. Petersburg Research Center of the RAS, the St. Petersburg

Academic University, and Academician Zhores Alferov helped with successful resolution of numerous organizational problems for the Congress. The Young Scientists Forum would not have been possible without the active contribution of the First Pro-rector for research of the St. Petersburg Academic University, corresponding member of the RAS Mikhail Dubina. Invaluable assistance was provided by the administration of the St. Petersburg State Polytechnic University (the chancellor, corresponding member of the RAS Andrey Rudskoy, pro-rectors Dmitry Raichuk and Alexander Rechinsky). Participants of the Young Scientists Forum were accommodated in the campus of the St. Petersburg State Polytechnic University under the assistance of Viktor Ignatenko.

The Head of the Committee of Science and Higher Education at the St. Petersburg Administration, Andrey Maksimov, and his deputy, Irina Ganus, played a significant role at all the stages of preparations for the Congress. So did the Russian Foundation for Basic Research (and its chairman, Academician Vladislav Panchenko). The Foundation rendered an unprecedented support to the Congress, while Vladislav Panchenko participated in the opening ceremony and headed the session devoted to collaboration between the European Molecular Biology Laboratory and the Russian Foundation for Basic Research (EMBL-RFBR). Member of the Skolkovo Foundation Council Mikhail Kovalchuk also rendered invaluable assistance at the initial stage.

The opening ceremony of the Congress kicked off at 4 p.m. on July 6, 2013, with an address read by RF Government Vice-President Arkady Dvorkovich from the Chairman of the Government of the Russian Federation Dmitry Medvedev to the Congress par-

ticipants. St. Petersburg Governor Georgy Poltavchenko delivered the welcome speech to the participants and guests of the Congress.

The time at which the Congress was held was a rather difficult one for Russian science. Several days before the opening of the Congress, a draft bill on the reform of the Russian Academy of Sciences was passed; so heated debates ensued. The RAS president, Academician Vladimir Fortov, called the conflicting parties to reconciliation; however, tensions ran high. Aaron Ciechanover (a member of the International Advisory Council and Nobel laureate) addressed the RF government asking for a solution to the situation. Many of the eleven Nobel Prize winners participating in the Congress backed the scientists' movement for amending certain provisions of the bill that would undoubtedly have a negative effect on the development of science in Russia. In his concluding address, Arkady Dvorkovich gave assurances to the scientific community that the RF government was concerned about the problems of scientists and that it would promote the development of science in our country.

FEBS 38, FUNDAMENTAL SCIENCE AND BIOTECHNOLOGY

The dispute over the relationship between fundamental and applied science has been going on for decades. This disagreement has taken on an international dimension; however, with the advent of advanced technologies in biotechnology and biopharmaceutics, the dispute seems to have been resolved (at least in Western countries). It is now unambiguously clear that no discipline can be referred to as "low-grade science" (e.g., biotechnology). Today, each breakthrough in biomedical research is a stepping stone toward actual application. This situation has much in common with the one that prevailed in

physics in the past (as well as in its current state), where most breakthroughs had resulted in high-tech weaponry. And mainstream physicists have direct participation in the implementation of "applied" developments.

During the 38th FEBS Congress, along with the fundamental symposia (Table 2), much attention was focused on biomedical research, oncology, autoimmune diseases, and biopharmaceutics. The entire "Science and Society" session (chaired by Jacques Henry Weil) was devoted to oncology issues. The Congress hosted a session by the "Skolkovo" Foundation that was organized by Deputy Director Alexander Chernov and Deputy Manager of the Biomed Cluster Gelena Lifshitz. The SkolTech University was represented by Prof. Konstantin Severinov.

The Ministry of Industry and Trade of the Russian Federation came up with an initiative to host a special session devoted to biopharmaceutics. The meeting operated under the auspices of then-Director of the Department of the Chemical-Engineering Complex and Bioengineering Technology of the Ministry of Industry and Trade of Russia and current Deputy Minister Sergei Tsyba and Director for International Economic Relations Alexei Gruzdev. It was an exciting session. The session was chaired by Academician Alexei Egorov on the Russian side and co-chaired by the director of pharmacology at Yale University, a foreign member of RAS, Prof. Joseph Schlessinger. The session speakers were Nobel Laureates Jean Marie Lehn, Jules Hoffmann, and Ada Yonath; the Russian side was represented by a mainstream researcher in the field of anticancer chemistry, Mikhail Lichinitser. The speakers discussed issues pertaining to the development of proteinase inhibitors, which are potential anti-cancer agents.

EXHIBITION

Historically, the FEBS congresses have hosted an interesting exhibition of devices and equipment. Antonina Shuvalova, commerce director at "Sigma Aldrich Rus," was heavily involved in the organization. The company, one of the general congress sponsors, provided printed materials for Congress participants. The Congress in Saint Petersburg was attended by 41 companies. AB SCIEX took a very interesting initiative to bring a demonstration bus to Saint Petersburg to run a course on mass spectrometry for students. This bus enjoyed much success with the participants, including Nobel Laureates Kurt Wüthrich, Ada Yonath, and Robert Huber.

WHAT WAS NEW TO SCIENTISTS AT THE CONGRESS IN SAINT PETERSBURG?

No doubt, plenary sessions were of much interest. Susumu Tonegawa, a Nobel laureate for his discovery of the genetic principle behind the generation of antibody diversity, covered his new projects on the "functional bioimaging" of brain parts. His article was published in *Science* after the Congress. The ex-president of the Scripps Research Institute, Prof. Richard Lerner, drew a complex picture of combinatorial biology in his plenary lecture. Joseph Schlessinger talked on new approaches to the development of antiproliferative agents. Nobel Laureate Jack Szostak presented new concepts of the evolution and origin of life.

WITHOUT WHOM THE CONGRESS WOULD HAVE BEEN IMPOSSIBLE

The chairman and secretary of the International Advisory Council of the Congress, Nobel Laureate Richard Roberts and Prof. Michael Blackburn, made an invaluable contribution to the preparation of the program. The role of Nobel Prize Winner Roger Kornberg was

also significant. The president of the Congress was academician Vladimir Skulachev.

In addition, Chairman of the Program Committee Sergey Kochetkov and Program Committee Secretary Marina Tretyak (who was in charge of all lecturers) contributed greatly. The role of the Congress secretary, Vera Knorre, was also invaluable. The abstracts of the participants were prepared by Congress Coordinator Alexandra Rogalskaya.

The primary sponsor of the Congress, the “Farmsintez” company, and its president Dmitry Genkin provided financial support and the technical staff to prepare and host the Congress. One of the leading financial specialists at the company, Igor Volodin, was the financial director of the Congress.

The companies “Legal Forum” headed by Olga Motenko and “Lumier Group” headed by Ekaterina Ivanova successfully performed delegate management and organi-

zational events, while the Lenexpo exhibition center headed by Sergey Voronkov mounted the pavilions.

The Park Media company (and personally Alexander Gordeev and Konstantin Kiselev, who assumed the burden of registering participants and supporting the Congress website) made an invaluable contribution from the earliest days until the final minutes of the Congress organization process.

SHOULD RUSSIA COMPETE FOR THE RIGHT TO HOST LARGE SCIENTIFIC CONGRESSES IN FUTURE!

Russia is destined to remain in the scientific community, and only the active participation of Russian scientists in large international forums can help our country retain ground. Some significant scientific events should of course be held in Russia.

HOW WILL THE SCIENTIFIC COMMUNITIES FORMERLY PART OF THE RUSSIAN ACADEMY OF SCIENCE FUNCTION IN THE ERA

OF THE FEDERAL AGENCY FOR SCIENTIFIC ORGANIZATIONS!

Most large congresses are held under the auspices of scientific communities. In Russia, such communities used to function as a single organization within the structure of the Russian Academy of Sciences. What will happen now? Who will be in charge of paying fees into international research organizations? Could it happen that the Russian scientific communities, which have such a rich history, are pushed to the margins of the reorganization processes? The new administration of the Academy and the Federal Agency for Scientific Organization will now have to solve these problems. ●

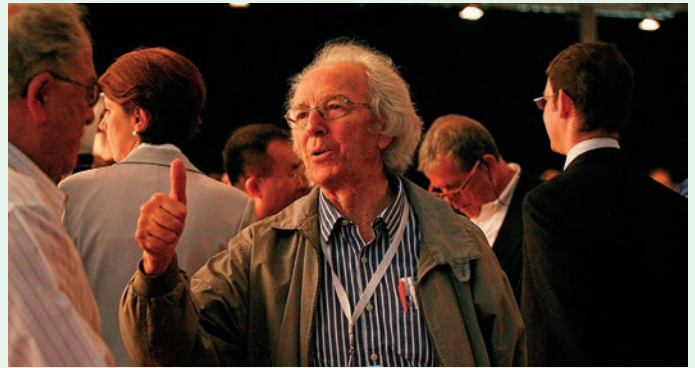
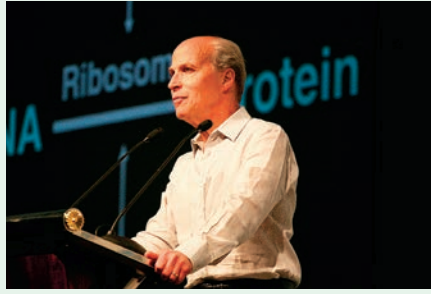
A.G. Gabibov,

Corresponding member of the Russian Academy of Sciences,
Professor,
Editor-in-Chief of Acta Naturae journal

FORUM



FORUM



"Epigenetic Memory" Phenomenon in Induced Pluripotent Stem Cells

E.A. Vaskova^{1,2,3}, A.E. Stekleneva^{1,2,3}, S.P. Medvedev^{1,2,3}, S.M. Zakian^{1,2,3,*}

¹Institute of Cytology and Genetics, Siberian Branch, Russian Academy of Sciences, prosp. Akad. Lavrentyeva, 10, Novosibirsk, Russia, 630090

²Meshalkin State Research Institute of Circulation Pathology, Rechkunovskaya Str., 15, Novosibirsk, Russia, 630055

³Institute of Chemical Biology and Fundamental Medicine, Siberian Branch, Russian Academy of Sciences, prosp. Akad. Lavrentyeva, 8, Novosibirsk, Russia, 630090

*E-mail: zakian@bionet.nsc.ru

Received 27.05.2013

Copyright © 2013 Park-media, Ltd. This is an open access article distributed under the Creative Commons Attribution License, which permits unrestricted use, distribution, and reproduction in any medium, provided the original work is properly cited.

ABSTRACT To date biomedicine and pharmacology have required generating new and more consummate models. One of the most perspective trends in this field is using induced pluripotent stem cells (iPSCs). iPSC application requires careful high-throughput analysis at the molecular, epigenetic, and functional levels. The methods used have revealed that the expression pattern of genes and microRNA, DNA methylation, as well as the set and pattern of covalent histone modifications in iPSCs, are very similar to those in embryonic stem cells. Nevertheless, iPSCs have been shown to possess some specific features that can be acquired during the reprogramming process or are remnants of epigenomes and transcriptomes of the donor tissue. These residual signatures of epigenomes and transcriptomes of the somatic tissue of origin were termed "epigenetic memory." In this review, we discuss the "epigenetic memory" phenomenon in the context of the reprogramming process, its influence on iPSC properties, and the possibilities of its application in cell technologies.

KEYWORDS pluripotency; reprogramming; epigenetics.

ABBREVIATION ESCs – embryonic stem cells; iPSCs – induced pluripotent stem cells; DMR – differentially methylated regions.

INTRODUCTION

Organism cells of any type have individual epigenomes: certain set and pattern of posttranslational covalent histone modifications and DNA methylation, and the presence of specific small non-coding RNAs. The combination of these factors forms a unique chromatin structure, which is inherent to cells of a special type.

Chromatin of pluripotent cells usually stays in the decompacted state and open configuration [1, 2]. Such a configuration promotes a dynamic posttranslational remodeling of histones and DNA methylation/demethylation processes during cell differentiation and specialization [3, 4]. The pluripotent cells also contain bivalent domains (i.e., the areas enriched in markers of both active and inactive chromatin together). Most bivalent domains are associated with the transcription start sites of the genes involved in the development. For example, bivalent domains were found in the genes of early mouse development (*Sox1*, *Pax3*, *Msx1*, and *Irx3*). A low transcriptional level is typical of these genes in pluripotent cells, while during differentiation the bivalent domains are converted into monovalent

ones with markers of either active or inactive chromatin; therefore, genes are either activated or suppressed, providing a certain type of cell specialization [1].

Two types of pluripotent cells are widely used in biomedicine today: embryonic stem cells (ESCs) and induced pluripotent stem cells (iPSCs). iPSCs are derived from somatic cells via ectopic overexpression of certain transcription factors, including *Oct4*, *Sox2*, *Klf4*, *c-Myc*, *Nanog*, and *Lin28*, or microRNAs [5–8]. iPSCs can be obtained at any period of human life and from various somatic cells (skin fibroblasts, keratinocytes, adipose stem cells, cells of peripheral blood, etc.); they are donor-specific (autologous). These are the reasons why the use of iPSCs is the preferred strategy in biomedicine and why a detailed, large-scale study of their properties and scope of clinical use is an urgent problem.

Based on today's knowledge, iPSCs and ESCs are known to have virtually the same properties: they express similar sets of genes and form teratomas containing the derivatives of all three germ layers. Mouse iPSCs at tetraploid complementation are capable of forming

chimeras and generating valid organisms [9]. Meanwhile, plenty of studies have produced evidence that the lines of iPSCs acquire a variety of genetic and epigenetic aberrations, including impaired functioning of imprinted genes, changed numbers of gene copies, point mutations, aberrant patterns of DNA methylation, etc. during the reprogramming process [10–14]. At that, both the aberrations acquired during reprogramming and some retained epigenetic markers of somatic cells cause differences in the epigenomes and transcriptomes of ESCs and iPSCs. This phenomenon of inheritance of the initial somatic epigenomes and transcriptomes by iPSCs is known as epigenetic memory [15–17].

An analysis of the identity of epigenomes and transcriptomes among iPSCs and their progenitor cells, the effects of epigenetic memory on iPSC properties, and the possibilities for its practical application in biomedicine are the main issues touched upon in this review.

THE EPIGENETIC MEMORY PHENOMENON IN THE PROCESS OF SOMATIC CELLS REPROGRAMMING TO THE PLURIPOTENT STATE

Advanced methods of high-performance analysis have proved the similarity of gene expression profiles, set, and distribution patterns of histone covalent modifications, DNA methylation, and microRNA expression in iPSCs and ESCs. However, minimal differences exist in their transcriptomes and epigenomes. Different patterns of DNA methylation in independent iPSC lines have been analyzed in a number of recent studies, cytosine methylation of DNA CpG-nucleotides being the most explored phenomenon [18]. CpG nucleotides can be scattered through a genome or concentrated in special regions known as CpG islands. The CpG islands typically reside near the gene promoters, and the high level of promoter methylation correlates with gene repression [19]. K. Kim *et al.* [16] analyzed, using Comprehensive High-throughput Array-based Relative Methylation (CHARM) analysis, DNA methylation patterns both in ESCs and iPSCs derived from two different somatic cell types: mouse hematopoietic progenitors and tail-tip fibroblasts. This approach allowed the authors to assess the methylation of approximately 4.6 million CpG nucleotides, including virtually all CpG islands and the adjacent areas but ignoring non-CpG methylation. Relative to ESCs, 3,349 differentially methylated regions (DMRs) were found in fibroblast-derived iPSCs, while only 516 were found in blood-derived ones. Notably, the CHARM analysis of the 24 mostly expressed DMRs has shown these regions to be associated with the genes involved in hemopoiesis (11 genes) and osteogenesis (3 genes). Thus, these results indicate that the genes initially responsible for cell specialization remain under-reprogrammed during the reprogramming of an iPSC.

The markers of skeletal musculature cells, *Cxcr4* and *Integrin B1*, are significantly expressed in iPSCs derived from mouse skeletal muscle precursors, while granulocyte markers, *Lysozyme* and *Gr-1*, are expressed in iPSCs from granulocytes. 1,388 differentially expressed genes were found by comparing the transcriptional profiles of two iPSC lines. At that, the results of the bioinformatics analysis of 100 genes with the maximum different expression levels allowed the authors to distribute them into groups of the genes involved in myofibrils and contactile fibers, muscle development, and β -cell and leucocyte activation [17]. Thus, these findings again attest to the epigenetic memory of iPSCs, in the form of retention of some specific traits of the initial somatic epigenomes and transcriptomes.

A similar phenomenon is also known in human iPSCs. K. Nishino *et al.* [20] performed a comparative analysis of DNA methylation in 5 lines of human ESCs, 22 iPSC lines, and 6 lines of initial somatic cells. Embryonic lung fibroblasts, amniotic and endometrial cells, cells of umbilical vein epithelium and menstrual blood, and skin fibroblasts were used as somatic progenitor cells. Methylation was analyzed using DNA Illumina's Infinium HumanMethylation27 BeadChip, with probes to 24,273 CpG sites within 13,728 genes. The methylation patterns of ~90% of CpG sites (17,572 sites) were similar in ES, iPS, and initial somatic cells, attesting to the fact that only 10% of CpG sites undergo modification and ensure the epigenetic variability of different types of cells. The comparison of pluripotent (ESC, iPSC) and initial somatic cells revealed 220 DMRs, 174 (79.5%) of which were hypermethylated in ESCs and iPSCs. These regions were associated mainly with the genes of transcription regulation. Interestingly, most of the hypomethylated DMRs localized within the CpG islands, while most of the hypermethylated DMRs resided beyond them. A comparison of DNA methylation in ESCs and iPSCs demonstrated that DMR numbers vary among the lines. In total, when a DMR was found in at least one of the iPSC lines under examination, 1,459 DMRs were found within 1,260 genes. Of special note, the DMR number is a totality of first the aberrant de novo methylated sites and, second, the sites inherited from the somatic cells of the initial types [20].

In addition, DNA methylation in human ESCs and iPSCs from neonatal umbilical blood (from two independent donors) was examined [21]. Consistent with the other studies, variation of the DNA methylation patterns among different lines was demonstrated, using a DNA-microchip including 5.2 million CpG sites that involved virtually all CpG islands and near sequences. At that, 267 of the 370 DMRs were acquired de novo as a result of reprogramming, while 75 were inherited by the epigenetic memory [21].

The studies described in [20] and [21] were performed using DNA microchips that allowed one to assess the genome-scale DNA methylation. However, advanced methods of molecular and genetic analysis allow a much more accurate and high-resolution examination of a cell's epigenome. For example, R. Lister *et al.* [22] used the highly sensitive MethylC-Seq method to compare the methylomes of several iPSC lines derived from somatic cells of various types using various approaches. The method allows to assess cytosine methylation at the entire genome level with nucleotide resolution. The examined iPSCs included iPSCs derived from adipocytes using transduction by retroviruses carrying cDNAs of the *OCT4*, *SOX2*, *KLF4* and *MYC* genes; iPSCs obtained using transduction by lentiviruses carrying cDNAs of the *OCT4*, *SOX2*, *NANOG* and *LIN28* genes; IMr90 lung fibroblasts, and three iPSC lines obtained from foreskin fibroblasts using unintegrated episome vectors. The methylation status of 75.7–94.5% of cytosine residues was assessed in all lines under examination [22] and, moreover, in both CpG and non-CpG dinucleotides (mCH, where H = A, C or T). Although the methylation patterns of CpG dinucleotides in ESCs and iPSCs were very similar, 1,175 DMRs were detected. The total length of individual DMRs was 1.68 Mb, varying from 1 to 11 kb per nucleotide. The distribution of DMRs over the genome was also heterogeneous: most DMR (80%) were associated with CG islands, 62% were near or inside the genes, and 29 and 19% were found within 2 kb from the transcription start or termination sites, respectively. Noteworthy, a group of shared DMRs was found in all the examined lines, in spite of the line-specific variations of the DMR number and localization. This fact attests to the existence of hot spots lacking epigenetic reprogramming, whose functions and roles in the genome remain poorly examined and need further analysis.

Moreover, the methylation patterns in the non-CpG regions were also different, although their general patterns in the genomes of ESCs and iPSCs were similar. A total of 29 non-CpG regions were detected [22]. The regions had a number of distinctive features: first, non-CpG-DMRs were rather extended: more than half of the DMRs were over 1 Mb long, and the total length of 29 DMRs was 32.4 Mb. Second, the genome localizations of non-CpG-DMRs and methylated CpG-DMRs were different: most non-CpG strongly biased towards centromeres and telomeres [22]. Notably, both K. Nishino *et al.* [20] and R. Lister *et al.* [21] detected 72 gene promoters undergoing differential methylation.

The DNA methylation profiles in five samples of mesenchymal stromal cells, eight different mesenchymal-derived iPSC lines, and three lines of human ESCs were compared using DNA microchips for

a thorough analysis of the localization and dynamics of the CpG methylation in their genomes [23]. The genome-average methylation rate was 17 CpG sites per gene, with an average methylation percentage of CpG sites – 49.4, 70.6, and 70.5% in mesenchymal stromal cells, iPSCs from mesenchymal stromal cells, and ESCs, respectively. These data indicate that the reprogramming process tends towards the remodeling of semi-methylated regions into methylated ones. A total of 185,246 CpG sites were differentially methylated; 33,941 of them underwent further demethylation, while 151,306 became hypermethylated in the iPSCs. The CpG sites were further classified into groups, according to their localization in the genome: the CpG sites localized 1,500 or 200 bp upstream the transcription start point; in the 5'-non-translated regions; in the first exon; in the 3'-non-translated regions of the genes, and in the inter-gene regions [24]. The average methylation level increased during reprogramming in all regions; however, the methylation level of the promoters and first exon areas decreased; at that, the hypo- and hypermethylated sites were located mainly in the inter-gene regions. In addition, the adjacent areas of CpG islands were analyzed as follows: 2 kb upstream or downstream a CpG island (shore regions), and 2 kb-long regions flanking the shore regions (shelf regions). All other CpG sites were united into an open sea. In the mesenchymal stromal cells, the average methylation level of CpG islands was much lower (22.2%) than in the shore (67.5%) and shelf (42.7%) regions, and in the open seas (61.8%) [24]. These data indicate that reprogramming-associated changes in the DNA methylation pattern occurred mainly beyond the CpG islands. 3,744 ESC-iPSC DMRs were detected, 3,134 of them being hypermethylated and 610 being hypomethylated in the iPSC cells as compared to ESCs [24]. It is interesting that the hypermethylated CpG sites in ESCs were localized mainly within 200 bp from the transcription start sites, in the first exons of the genes, and in the inter-gene regions, while in the iPSCs they localize 1,500 bp upstream the transcription start sites and in the inter-gene regions. A bioinformatics analysis demonstrated that 610 hypermethylated CpG sites in iPSCs were associated with the genes involved in keratinization and keratin-differentiation processes, as well as epidermis cell differentiation and epidermis development.

Thus, the methylation profiles of iPSCs and ESCs are also different: in ESCs, highly methylated regions mainly localize in the proximal regions of gene promoters, while in the iPSCs – in the distal regions of gene promoters, inter-gene and open sea regions, as well as in the genes involved in epidermis development.

Interestingly, regular DMR distribution can be seen at the chromosome level as well: there are more X-

chromosome-localized DMRs in the iPSCs carrying XX sex chromosomes than in the iPSCs with XY [20].

Therefore, the reprogramming of somatic cells into pluripotent ones is followed by the formation of DMRs, whose quantities vary depending on the initial cell type, reprogramming methods, culture conditions, etc. Most of these DMRs result from de novo aberrant methylation, while the smallest part is the consequence of epigenetic memory. Noteworthy, the formation of the DMRs resulting from the epigenetic memory is conditioned by both the initial type of somatic cells and the individual-specific patterns of DNA methylation in the cell donors. Special features of cell epigenomes were found even in monozygotic twins [23]. Part of these donor-specific epigenetic variations was unchanged during the reprogramming. For example, 1,129 differentially methylated CpG sites were detected using a comparative analysis of their methylation profiles in the iPSCs derived from the mesenchymal stromal cells of five different donors. These sites were associated mainly with the genes involved in the processing and presentation of antigens. The donor-specific DMRs localized mainly in gene bodies, the 3'-non-translated, and inter-gene regions [24].

Covalent histone modifications are involved in the maintenance of some epigenetic markers of initial-type somatic cells along with CpG methylation. Thus, in the iPSCs derived from β -cells of the human pancreas, the factor of PDX1 transcription was not repressed during re-programming. The method of chromatin immunoprecipitation demonstrated that an acetylated histone 3 associated with transcriptionally active chromatin is maintained in the promoters of the genes that encode insulin and PDX1 [15].

Thus, full-range genome-wide studies have demonstrated the presence of minimal differences in the patterns of DNA methylation, gene expression, and covalent histone modifications in these cells despite the close similarity among ESCs and iPSCs. One of the most topical issues is the impact of these differences on the properties of iPSCs.

EFFECT OF THE EPIGENETIC MEMORY ON THE PROPERTIES OF INDUCED PLURIPOTENT STEM CELLS

The inherited features of the epigenomes and transcriptomes of the initial cell types affect only a small portion of genes. To what extent the aberrant regulation of these genes affects the properties of the resulting iPSCs is currently an issue of special interest. It has been established that DMRs inherited through epigenetic memory cause a shift in the differentiation spectrum; that is, the iPSC lines differentiate into somatic cells of the initial type. Thus, it was demonstrated that mouse iPSCs derived from either blood or skin cells

possess different potentials of differentiation to either the hemopoietic or osteogenic direction, correspondingly. The iPSCs derived from blood cells more readily form hemopoietic colonies, while the iPSCs from skin cells form more colonies when differentiating in the osteogenic direction [16]. In addition, the differentiation potentials of human iPSCs from neonatal umbilical blood cells and foreskin keratinocytes have been assessed [21]. The expression levels of the early differentiation marker, the keratin-14 gene, were determined in embryoid bodies on the 6th day of culture. In iPSCs from keratinocytes, the expression of this gene was 9.4-fold higher, indicating a much higher differentiation potential for these cells towards keratinocytes as compared to that of iPSCs from the umbilical blood. This phenomenon is reciprocal: the differentiation potential of iPSCs from umbilical blood to hemopoiesis was much higher [21].

Another area where the epigenetical memory may cause serious problems is the use of iPSCs in *in vivo* studies. M. Stadtfeld *et al.* [25] examined murine iPSCs from various somatic progenitors: hemopoietic stem cells (11 lines), progenitor cells from the granulocyte-macrophage line (11 lines), granulocytes (9 lines), peritoneal fibroblasts (6 lines), tail fibroblasts (6 lines), and keratinocytes (6 lines). The cells of the most newly established lines when in tetraploid complementation contributed poorly to chimaeras and failed to support the development of entirely iPSC-derived animals. A comparison of mRNAs demonstrated that, in contrast to the ESC genes, the imprinted genes *Gtl2* (or *Meg3*) and *Rian* of *Dlk1-Dio3* locus proximal to the mouse *12qF1* were repressed both in most iPSC clones and in the initial somatic lines. It is common knowledge that the genes of this locus participate in the growth and differentiation of some tissues, as well as in postnatal neurological and metabolic processes [26]. A genome-wide analysis of the microRNA expression profile demonstrated that the expression patterns of 21 of the 336 (6.3%) microRNAs in ESCs differ from those in iPSCs, all of them being expressed from the *12qF1* chromosome and repressed in iPSCs. The chromatin immunoprecipitation method has demonstrated that the acetylation levels of the H3 and H4 histones and that of methylated *H3K4* associated with transcriptionally active chromatin are significantly lower in the iPSC *Dlk1-Dio3* locus [25].

It is worth mentioning that not all the imprinted genes inherit the epigenetical and transcriptional statuses of initial somatic cell lines. Quantitative PCR demonstrated that the expression of the other imprinted genes is clone-specific [16]. This fact is supported by the results of another study with iPSCs from neutral stem cells isolated from a partenogenetic mouse embryo. In

these cells, the expression levels of the cells with paternal imprinting, *Peg1* (or *Mest*), *Ndn* and *Snurf* determined using microchips, was much lower than those in somatic cells from the embryos obtained by normal biparental fertilization, since these genes were reactivated during reprogramming [27]. Thus, the epigenetic memory phenomenon has a real impact on iPSC characteristics, and the consequences of its presence may be serious. Therefore, this aspect needs careful consideration when using iPSCs in disease modeling or in regenerative cell medicine.

EFFECT OF CULTURE CONDITIONS AND CHEMICAL AGENTS ON THE EPIGENOME OF INDUCED PLURIPOTENT STEM CELLS

Minimal differences in the epigenomes and transcriptomes caused by the epigenetic memory or/and aberrant methylation de novo in PSCs and ESCs can result in rather significant changes in cells' characteristics. Some logical questions emerge in this case: what are the factors affecting the type and number of these differences? Are there any artificial conditions that would allow one to correct these effects? Conditions and duration of culturing are the first noteworthy factors affecting iPSC quality in general and the number of epigenetic markers in particular. Reprogramming is a gradual process, and remodeling of the cell transcriptome and epigenome also takes a certain number of replication runs and mitoses, and, hence, the number of passages. The higher the number of passages, the lower the number of epigenetic differences is (if any). For example, in 12 independent lines of mouse iPSCs from various cell types (β -cells, fibroblasts, T-cells, and granulocytes), the number of differentially expressed genes varied at early passages from 500 to 2,000 depending on a line, and it decreased substantially to ~50 (and even to zero in some lines) after 14 passages [17]. The disappearance of differences among the iPSC lines correlated with the emergence of bivalent domains, trimethylated *H3K4* (active chromatin marker) and *H3K27* (inactive chromatin marker), typical of pluripotent cells [17]. A study of the methylation patterns in 7 independent lines of human iPSCs has also demonstrated a significant decrease in DMR in various lines from 80–256 at early passages to 30–70 at the 30th-40th passages [20]. A decrease in DMR numbers increases the ability of a line to differentiate into any of the three germ layers with equal effectiveness. For example, the effectiveness of the ability of iPSCs from keratinocytes to form hemopoietic colonies during differentiation was very low because of the residual methylation of the genes involved in hemopoiesis (e.g., *HOXD8*). The *HOXD8* gene is significantly methylated in keratinocytes and, via the epigenetic memory, in iPSCs derived

from them. The level of its methylation decreases during culturing, while the ability of cells to differentiate into hemopoietic cells simultaneously increases. However, this effect was observed only in one of two clones. Hence, long culturing of iPSCs might affect certain genome loci, but this was true not for the entire genome and not for all iPSC lines [21].

Two hypotheses can explain the elimination of the molecular and functional differences in iPSC clones during culturing. One of the possible mechanisms is the passive loss of the somatic markers associated with DNA replication. The alternative version is clone selection during culturing aimed at retention of the clones with fewer initial characters. However, a number of observations evidence against the selection. Thus, the proliferation levels and growth rates of clones from one cell are the same at early and late passages of iPSCs. The number of passages (that is, the required number of replication runs) necessary to eliminate inter-clone molecular and epigenetic differences also depends on the initial type of somatic cells [17].

Meanwhile, some findings attest to the lack of a decrease in the DMR number during culturing. For example, no changes in the DMR number at early (~15) and late (~65) passages were detected with a methylome analysis [22]. Culture conditions (medium composition, concentration of O₂ and CO₂, etc.) and/or the use of supplementary chemical agents are the other factors that could potentially affect the DMR number in iPSCs. The quality of iPSCs can be significantly improved by optimal conditions. Thus, the use of a medium supplemented with serum surrogate or with a mixture of embryonic bovine serum and serum surrogate instead of embryonic bovine serum alone provided an increase in the yield of clones in which the imprinted *Meg3* gene from the *Dlk1-Dio3* locus was reactivated [28].

Various chemical agents affect the gene expression as well. For example, treatment of mouse iPSCs with trichostatin (histone deacetylase inhibitor) and 5-azacytidine (DNA methylase inhibitor) causes changes in the epigenome [16]. Treatment of mouse iPSC clones in which the imprinted *Dlk1-Dio3* locus was repressed with valproic acid (histone deacetylase inhibitor) caused reactivation of the locus genes. These iPSC cells in tetraploid complementation could affect the development of an organism [25].

Ascorbic acid (vitamin C) also affects the DNA methylation pattern [29]. For example, dose-dependent reactivation of the imprinted *Meg3* gene from the *Dlk1-Dio3* locus was observed in iPSCs cultivated in an ascorbic acid-supplemented medium. However, ascorbic acid did not cause full-range demethylation of the entire genome; it could prevent aberrant demethylation of the *Dlk1-Dio3* locus only, but it could not

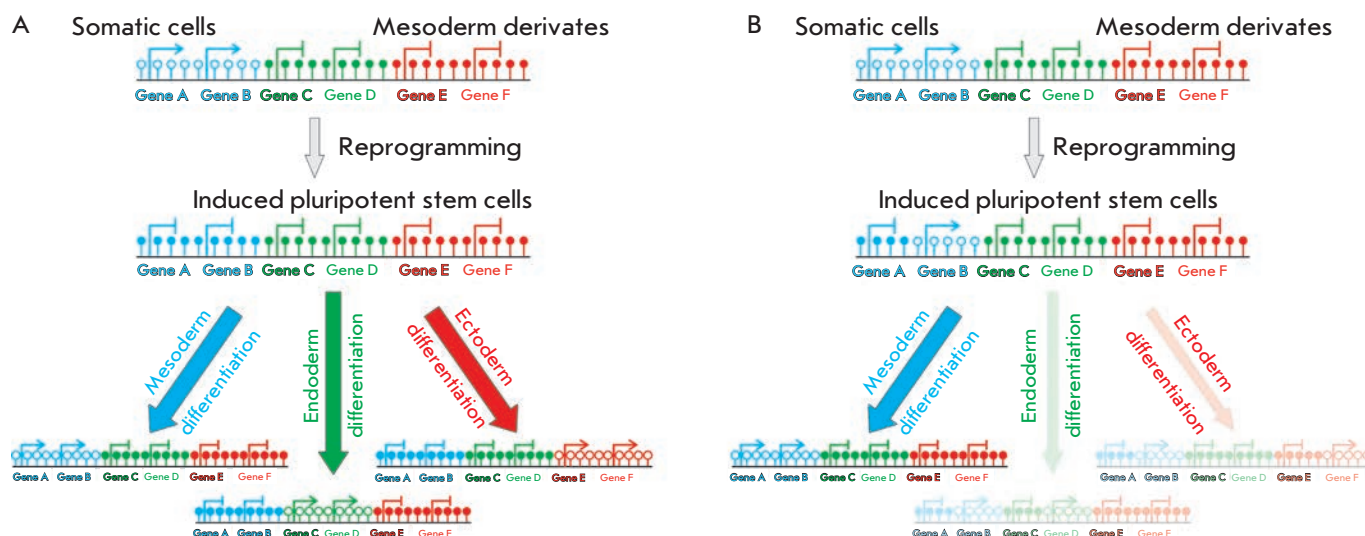


Figure. “Epigenetic memory” phenomenon in induced pluripotent stem cells. A – The “ideal” reprogramming process of somatic cells to pluripotency: differentiation of induced pluripotent stem cells into each of the germ layers is an equally likely event. B – As a result of the re-programming process induced pluripotent stem cells can retain some features of the epigenome of the donor tissue. This phenomenon shifts the differentiation: induced pluripotent stem cells preferentially generate derivatives of the donor somatic cell type

cause DNA demethylation in the stable clones of the iPSCs [28].

Meanwhile, the ability of cells to differentiate in a certain direction and their methylation profile can be restored by repeated reprogramming runs. For example, iPSCs from progenitors of a neural line had a very low ability to form colonies of hemopoietic cells. However, the reprogramming of these colonies significantly increased the formation of hemopoietic colonies by the secondary iPSCs [16]. Thus, iPSCs most closely similar to their standard, ESCs, can be obtained by varying the reprogramming system, culturing conditions, and duration, adding or removing chemical agents, etc. However, minimal differences in the transcriptomes and epigenomes of these cells still remain in any case. Is this factor a barrier for the practical use of iPSCs? This question is being currently discussed.

USE OF THE EPIGENETIC MEMORY PHENOMENON IN BIOMEDICINE

Biomedicine, as well as pharmacology, needs new, more perfect, model systems of diseases. These models should meet certain criteria: repeatability, availability, usability, unambiguous result interpretation, adequate transferability (i.e., translation of the results of fundamental studies into practical medicine) [30–33].

The available array of studies in this area has demonstrated that the use of iPSCs is one of the most prospective approaches. However, in order to establish an iPSC-based model of a human disease, one should consider all factors that could potentially affect the qual-

ity of the results. Epigenetic memory is one of the significant factors. Is this phenomenon an advantage or a disadvantage of iPSC-based models of human diseases? This is a pending issue. Let us consider the problems of modern medicine in the context of using iPSCs and try to solve one of these problems.

The availability of certain cell material suitable for study is the first urgent problem in cell replacement therapy. This problem can be subdivided further. First of all, it is associated with the availability of initial donor cells: this may be a problem, since obtaining biopsy material for many types of cells (e.g., neurons or epithelium of the internals) is a challenge. The second problem is the quantity of the available material, which is limited even when biopsy is available. Moreover, the cells are usually terminally differentiated, and, hence, their proliferative activity is limited. Therefore, all full-scale manipulation analyses cannot be performed using conventional methods. iPSCs obtained from a limited biopsy mass can solve the problem. Their proliferative potential is unlimited; therefore, they can be repeatedly differentiated into cells of the required type, providing thus an unlimited cell source for all relevant analyses and manipulations.

The next problem is correct and efficient differentiation of iPSCs into cells of a desired type. The protocols of targeted differentiation are available now for a limited number of cell cultures, although current information on signaling pathways and transcription factors related to development into a certain direction is plentiful. Therefore, even the availability of iPSC lines does not guarantee the obtaining of a certain narrowly

specialized cell type. This problem could be solved by the phenomenon of epigenetic memory. We suggest the following scheme for using this phenomenon for cell replacement therapy (see Figure). It is well known that epigenomes and transcriptomes of the initial cell type maintained in iPSCs make them differentiate into somatic cells of the initial type. Hence, it would be reasonable to use the biopsy material of cells of the same origin. A number of issues should be considered in this case: first, ten or more iPSC clones should be analyzed to choose the most optimal clones from the variances. Second, the overall transcriptome and methylome data must be compared with the available databases; this will allow a scientist to detect the so-called hot spots of underreprogramming that emerge via gene reactivation during the re-programming, and the spectra of the

genes with epigenetic markers inherited from the somatic cells of the progenitor type. Finally, the direction of cell differentiation could be predicted or changed, by special means, to a desirable one, after the genes affected by the epigenetic memory are examined at the functional level. Thus, this case allows us to demonstrate that the disadvantages of iPSC, such as the inheritance of a number of epigenome and transcriptome features caused by invalid reprogramming, can be converted into advantages. ●

This work was supported by the Ministry of Education and Science of the Russian Federation (Agreement № 8264) and the Russian Foundation for Basic Research (Grants № 11-04-00847-a, 12-04-00185-a and 12-04-00208-a).

REFERENCES

1. Bernstein B.E., Mikkelsen T.S., Xie X., Kamal M., Huebert D.J., Cuff J., Fry B., Meissner A., Wernig M., Plath K., et al. // *Cell*. 2006. V. 125. № 2. P. 315–326.
2. Spivakov M., Fisher A.G. // *Nat. Rev. Genet.* 2007. V. 8. № 4. P. 263–271.
3. Bibikova M., Chudin E., Wu B., Zhou L., Garcia E.W., Liu Y., Shin S., Plaia T.W., Auerbach J.M., Arking D.E., et al. // *Genome Res.* 2006. V. 16. № 9. P. 1075–1083.
4. Doi A., Park I.H., Wen B., Murakami P., Aryee M.J., Izzi-zarry r., Herb B., Ladd-Acosta c., Rho J., Loewer S., et al. // *Nat. Genet.* 2009. V. 41. № 12. P. 1350–1353.
5. Maherali N., Ahfeldt T., Rigamonti A., Utikal J., Cowan C., Hochedlinger K. // *Cell Stem Cell*. 2008. V. 3. № 3. P. 340–345.
6. Takahashi K., Tanabe K., Ohnuki M., Narita M., Ichisaka T., Tomoda K., Yamanaka S. // *Cell*. 2007. V. 131. № 5. P. 861–872.
7. Takahashi K., Yamanaka S. // *Cell*. 2006. V. 126. № 4. P. 663–676.
8. Yu J., Vodyanik M.A., Smuga-Otto K., Antosiewicz-Bourget J., Frane J.L., Tian S., Nie J., Jonsdottir G.A., Ruotti V., Stewart r., et al. // *Science*. 2007. V. 318. № 5858. P. 1917–1920.
9. Zhao X.Y., Li W., Lv Z., Liu L., Tong M., Hai T., Hao J., Guo C.L., Ma Q.W., Wang L., et al. // *Nature*. 2009. V. 461. № 7260. P. 86–90.
10. Pick M., Stelzer Y., Bar-Nur O., Mayshar Y., Eden A., Benvenisty N. // *Stem Cells*. 2009. V. 27. № 11. P. 2686–2690.
11. Hussein S.M., Batada N.N., Vuoristo S., Ching r.W., Autio R., Narva E., Ng S., Sourour M., Hamalainen R., Olsson C., et al. // *Nature*. 2011. V. 471. № 7336. P. 58–62.
12. Ben-David U., Benvenisty N., Mayshar Y. // *Cell Cycle*. V. 9. № 23. P. 4603–4604.
13. Martins-Taylor K., Xu r.H. // *Stem Cells*. 2011. V. 30. № 1. P. 22–27.
14. Sun B., Ito M., Mendjan S., Ito Y., Brons I.G., Murrell A., Vallier L., Ferguson-Smith A.C., Pedersen R.A. // *Stem Cells*. 2011. V. 30. № 2. P. 161–168.
15. Bar-Nur O., Russ H.A., Efrat S., Benvenisty N. // *Cell Stem Cell*. 2011. V. 9. № 1. P. 17–23.
16. Kim K., Doi A., Wen B., Ng K., Zhao R., Cahan P., Kim J., Aryee M.J., Ji H., Ehrlich L.L., et al. // *Nature*. 2010. V. 467. № 7313. P. 285–290.
17. Polo J.M., Liu S., Figueroa M.e., Kulalert W., Eminli S., Tan K.Y., Apostolou E., Stadtfeld M., Li Y., Shioda T., et al. // *Nat. Biotechnol.* 2010. V. 28. № 8. P. 848–855.
18. Adams R.L. // *Biochem J*. 1990. V. 265. № 2. P. 309–320.
19. Trowbridge J.J., Orkin S.H. // *Epigenetics*. 2010. V. 5. № 3. P. 189–193.
20. Nishino K., Toyoda M., Yamazaki-Inoue M., Fukawatase Y., Chikazawa E., Sakaguchi H., Akutsu H., Umezawa A. // *PLoS Genet*. 2011. V. 7. № 5. P. e1002085.
21. Kim K., Zhao r., Doi A., Ng K., Unternaehrer J., Cahan P., Hongguang H., Loh Y.H., Aryee M.J., Lensch M.W., et al. // *Nat. Biotechnol.* 2011. V. 29. № 12. P. 1117–1119.
22. Lister r., Pelizzola M., Kida Y.S., Hawkins R.D., Nery J.R., Hon G., Antosiewicz-Bourget J., O'Malley R., Castanon R., Klugman S., et al. // *Nature*. 2011. V. 471. № 7336. P. 68–73.
23. Kaminsky Z.A., Tang T., Wang S.C., Ptak C., Oh G.H., Wong A.H., Feldcamp L.A., Virtanen C., Halfvarson J., Tysk C., et al. // *Nat. Genet.* 2009. V. 41. № 2. P. 240–245.
24. Shao K., Koch C., Gupta M.K., Lin Q., Lenz M., Laufs S., Denecke B., Schmidt M., Linke M., Hennies H.C., et al. // *Mol. Ther.* 2012. V. 21. № 1. P. 240–250.
25. Stadtfeld M., Apostolou E., Akutsu H., Fukuda A., Follett P., Natesan S., Kono T., Shioda T., Hochedlinger K. // *Nature*. 2010. V. 465. № 7295. P. 175–181.
26. Da Rocha S.T., Edwards C.A., Ito M., Ogata T., Ferguson-Smith A.C. // *Trends Genet.* 2008. V. 24. № 6. P. 306–316.
27. Kim M.J., Choi H.W., Jang H.J., Chung H.M., Arauzo-Bravo M.J., Scholer H.R., Tae Do J. // *J. Cell Sci.* 2012. V. 126. № 11. P. 2516–2524.
28. Stadtfeld M., Apostolou E., Ferrari F., Choi J., Walsh R.M., Chen T., Ooi S.S., Kim S.Y., Bestor T.H., Shioda T., et al. // *Nat. Genet.* 2012. V. 44. № 4. P. 398–405
29. Wang T., Chen K., Zeng X., Yang J., Wu Y., Shi X., Qin B., Zeng L., Esteban M.A., Pan G., et al. // *Cell Stem Cell*. 2011. V. 9. № 6. P. 575–587.
30. Medvedev S.P., Shevchenko A.I., Zakian S.M. // *Acta Naturae*. 2010. V. 2. № 2. P. 18–28.
31. Cohen D.e., Melton D. // *Nat. Rev. Genet.* 2011. V. 12. № 4. P. 243–252.
32. Grskovic M., Javaherian A., Strulovici B., Daley G.Q. // *Nat. Rev. Drug Discov.* 2011. V. 10. № 12. P. 915–929.
33. Medvedev S.P., Grigor'eva E.V., Shevchenko A.I., Malakhova A.A., Dementyeva E.V., Shilov A.A., Pokushalov E.A., Zaidman A.M., Aleksandrova M.A., Plotnikov E.Y., et al. // *Stem cells Dev.* 2011. V. 20. № 6. P. 1099–1112.

The Role of Integrins in the Development and Homeostasis of the Epidermis and Skin Appendages

A.L. Rippa^{*1}, E.A. Vorotelyak^{1,2}, A.V. Vasiliev¹, V.V. Terskikh¹

¹ N.K. Koltzov Institute of Developmental Biology, Russian Academy of Sciences

² M.V. Lomonosov Moscow State University, Biological Department, Division of Cell Biology and Histology

*E-mail: rippa86@yandex.ru

Received 28.05.2013

Copyright © 2013 Park-media, Ltd. This is an open access article distributed under the Creative Commons Attribution License, which permits unrestricted use, distribution, and reproduction in any medium, provided the original work is properly cited.

ABSTRACT Integrins play a critical role in the regulation of adhesion, migration, proliferation, and differentiation of cells. Because of the variety of the functions they play in the cell, they are necessary for the formation and maintenance of tissue structure integrity. The trove of data accumulated by researchers suggests that integrins participate in the morphogenesis of the epidermis and its appendages. The development of mice with tissue-specific integrin genes knockout and determination of the genetic basis for a number of skin diseases in humans showed the significance of integrins in the biology, physiology, and morphogenesis of the epidermis and hair follicles. This review discusses the data on the role of different classes of integrin receptors in the biology of epidermal cells, as well as the development of the epidermis and hair follicles.

KEYWORDS basement membrane; hair follicle; differentiation; integrins; keratinocytes; migration; morphogenesis; proliferation; stem cells.

ABBREVIATIONS BM – basement membrane; ECM – extracellular matrix; HF – hair follicle; SCs – stem cells; ESCs – embryonic stem cells; integrin-linked kinase (ILK).

INTRODUCTION

Integrins are the major class of surface receptors that attach to the extracellular matrix (ECM) and are responsible for a cell's interaction with its environment; these receptors process external signals into intracellular ones and induce a number of regulatory cascades. Ultimately, this can lead to a variety of cellular responses. Signals that come from intracellular receptors can regulate adhesion, migration, growth, differentiation, and death of cells. Integrin dysfunction in animals causes the development of various pathologies.

Integrins are non-covalently attached heterodimer transmembrane receptors that consist of α - and β -subunits, forming a functional receptor. Today, a total of 18 α - and 8 β -subunits are known in vertebrates. These 26 subunits form at least 24 combinations of $\alpha\beta$ receptors (Fig. 1). Integrins are divided into three classes depending on the type of β -subunit. $\beta 1$ integrins form the most widespread group and usually bind to ECM proteins. $\beta 2$ integrins are expressed in leucocytes only; some of them can bind to the surface proteins of other cells. Some $\beta 3$ integrins are expressed in thrombocytes and megakaryocytes and play a major role in the adhesion processes and blood clotting. Other $\beta 3$ in-

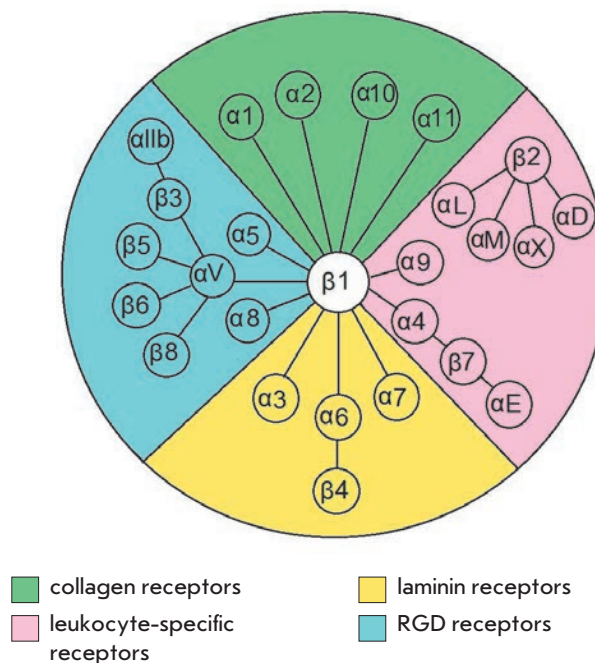


Fig. 1. Schematic representation of the heterodimeric integrin receptors family [1, 2]

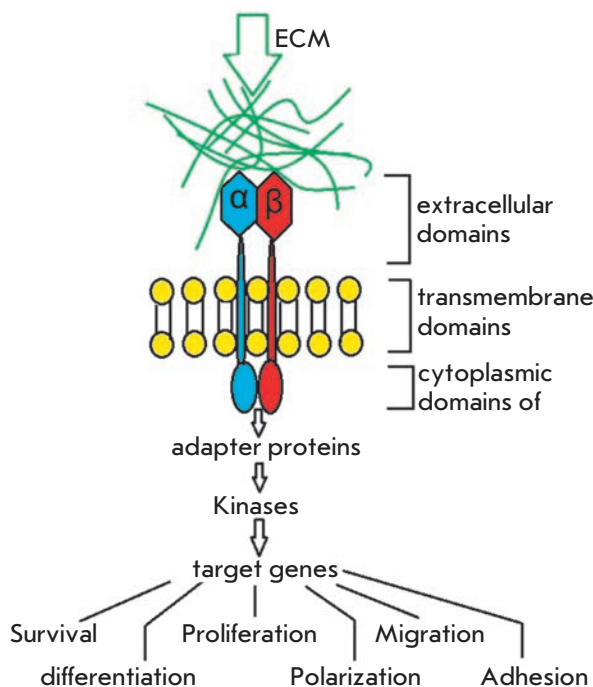


Fig. 2. The principle of action of extracellular signals on intracellular environment processes through integrin receptors

tegrins are expressed in endothelial cells, fibroblasts, and some types of tumor cells. Receptors comprising $\beta 4$ - $\beta 8$ subunits are rather few and have various structures; therefore, they cannot be included in any of the classes listed above [1, 2].

Integrin activation on the cytoplasmic membrane from inside the cell is responsible for cytoskeletal protein synthesis and can induce the expression of some genes. On the outer side of the cell, integrins can contact with the macromolecules of ECM or basement membrane (BM) and with the receptors of other cells, thereby forming the microsurrroundings of the cell. These interactions control intracellular processes and largely define the tissue structure (Fig. 2) [3, 4].

Integrins are responsible for the adhesion of epithelial cells to ECM by the formation of hemidesmosomes and focal adhesions.

Hemidesmosomes are stud- and rivet-like structures on the inner side of the cytoplasmic membrane of epithelial cells. They are formed by integrin $\alpha 6 \beta 4$ that uses the linker proteins plectins to attach to keratin filaments and strongly immobilize epidermis on the basement membrane mostly by binding to laminin 332 (Fig. 3).

Focal adhesions are more complicated structures that are formed from integrin association and are con-

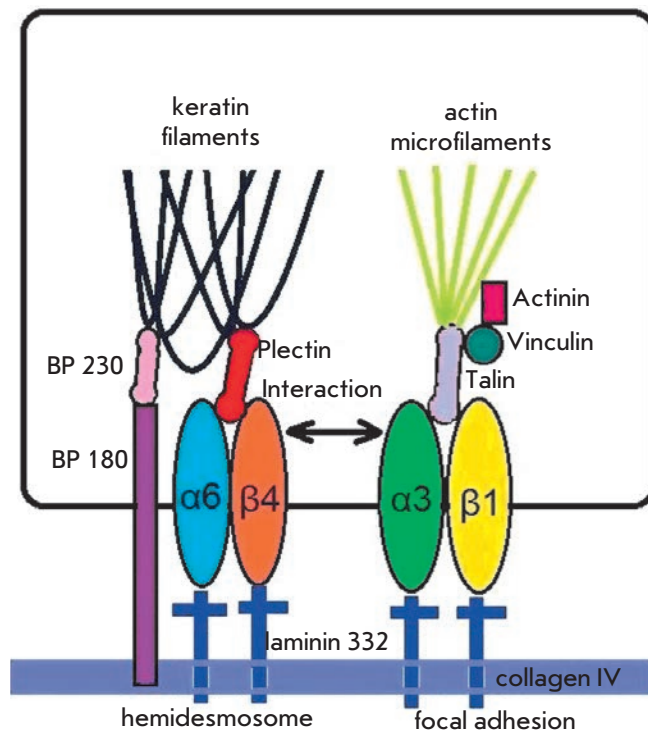


Fig. 3. Integrin receptors in cell-matrix interactions

nected to actin cytoskeleton by adapter proteins (talin, vinculin, a-actinin). The structure and morphology of these contacts are very dynamic. They can consist of hundreds of different proteins and perform adapter, signaling, and other functions. Focal adhesions are the so-called “data hubs” that regulate the protein signal flow and manage the biochemical signals of cellular responses to external stimuli (Fig. 3).

Integrin receptors play the key role in the formation and maintenance of the histotypical tissue structure. There is a vast amount of data supporting the role of integrins in the morphogenesis of skin epidermis and appendages, especially for the hair follicle (HF). The presence of hair is one of the defining characteristics of mammalian species. Hair has several functions, including thermoregulation, protection, sensory, and social ones. HF is developed and functions in close interaction between the epidermis and dermis. The epidermis component of HF consists of the hair matrix, the outer and inner root sheath, and the hair shaft. The dermis component of HF is represented by dermal papilla and the dermal sheath. The outer root sheath is connected to the basement layer of the epidermis from outside and to the inner root sheath from the inside; the latter surrounds the hair shaft. The outer root shaft has a thickening that is known as a bulge and contains stem cells

(SC). The base of HF (bulb) is made of specialized keratinocytes of the hair matrix and mesenchymal cells of dermal papilla. The hair shaft consists of terminal, differentiated keratinocytes (trichocytes) and originates from HF. The HF is also associated with the sebaceous glands, blood vessels, nerves, and an arrector pili muscle that is attached to the bulge (Fig. 4). In the postnatal period of life, the top part of HF (including the bulge and sebaceous gland) and dermal papilla stay intact, while the other HF part undergoes changes that can be subdivided into the growth phase (anagen), transition phase (catagen), and resting phase (telogen). In mice, the anagen stage starts from the formation of HF after 14.5 days of embryonic development and continues for up to 2 weeks after birth. After that, the catagen stage occurs, which lasts for approximately 1 week and is followed by the telogen stage of approximately the same duration [5].

In humans, the anagen stage of the scalp HF lasts for 2–7 years; the telogen stage lasts for up to 3 months, and after that the hair shaft is discarded. Every HF produces on average 20–30 hair shafts during a life. Normally ~95% of all HF is in the stage of anagen, and 5% is in the telogen phase [6].

The present work reviews the role of integrins which have an important function in skin biology and integrin-linked kinase (ILK), a transmitter of intercellular integrin signaling, the functions of which have not been fully elucidated.

EPIDERMIS INTEGRINS

There are several types of integrins that are found in the epidermis: $\alpha 3\beta 1$ (predominantly a receptor for laminin 332), $\alpha 6\beta 5$ (hemidesmosome component, receptor for laminin 332), and $\alpha 2\beta 1$ (receptor for collagen and laminin) [7]. Integrin $\alpha \nu \beta 5$ (receptor for vitronectin) is also one of the epidermal integrins, but it is expressed in lower amounts compared to other integrins [8]. In addition, basal keratinocytes of epidermis express integrins $\alpha 5\beta 1$ (receptor for fibronectin) and $\alpha 9\beta 1$ (receptor for tenascin C) [9, 10]. The group of $\beta 1$ integrins is generally located on the basal surface of keratinocytes [7, 8, 11] and is involved in the formation of focal adhesions. Integrin $\alpha 3\beta 1$ can be found on either the basal or lateral surfaces of basal keratinocytes to form intercellular contacts [12]. Under normal conditions, the expression of integrins is limited to the basal layer and outer root sheath of HF, except for integrin $\alpha \nu \beta 8$ that can be found in the suprabasal layers of the eyelid skin of mice [13]. During the wound healing process and other pathological conditions, including psoriasis and tumorogenesis, integrins are expressed by suprabasal keratinocytes [14]. Ectopic expression of $\alpha 2$, $\alpha 5$, and $\beta 1$ integrins in suprabasal skin layers lead to hyperpro-

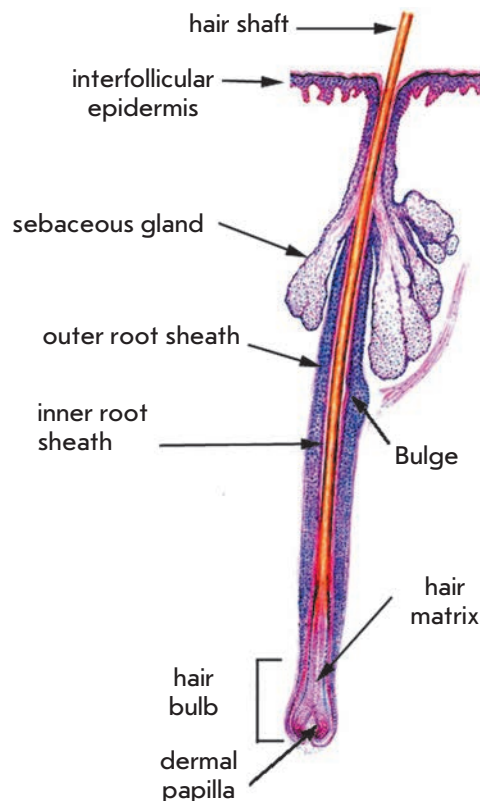


Fig. 4. The structure of the hair follicle [36]

liferation, differentiation disorders, and psoriasis-like phenotype formation [15].

The creation of tissue-specific integrin knockout mice and determination of the genetic basis of several skin diseases in humans has led to an understanding of the role of integrins in the physiology and morphogenesis of epidermis. It is assumed that integrins are involved not only in the binding of keratinocytes to the basal membrane, but also in the regulation of migration, proliferation, and differentiation of epidermal cells [6, 14, 16, 17].

INTEGRIN $\alpha 6\beta 4$

Initially, integrin specific antibodies were used to determine the role of integrins in the adhesion, migration, and initiation of terminal differentiation of keratinocytes; however, these antibodies disturbed the adhesion of cultured keratinocytes to different components of ECM [6, 16]. Creation of knockout mice without some integrins or their subunits allowed one to determine their role in the adhesion of keratinocytes to BM. For example, mice with deleted $\alpha 6$ and $\beta 4$ subunits die shortly after birth, are characterized by numerous blistering on the skin, and a stratified flat epithelium

caused by the absence of hemidesmosomes [18–20]. In humans, gene mutations in the $\alpha 6$ or $\beta 4$ subunit lead to the development of epidermolysis bullosa with stomach atresia, an autosomal disease in which skin blisters and gastrointestinal tract lesions emerge and require surgery immediately after birth [21].

Integrin $\alpha 6\beta 4$ attaches to laminin 332 in ECM and to keratin filaments inside the cell. This enables coordination of the cellular response depending on the condition of laminin molecules and, therefore, makes it possible to regulate keratinocyte adhesion, migration, and proliferation. This process possibly occurs through the NF- κ B or MAPK-pathway, which are initiated by $\beta 4$ integrin, or through small GTPase Rac1 activation. Moreover, $\alpha 6\beta 4$ integrin is required for the retention of hemidesmosome integrity. It was shown that phosphorylation of Ser1424 in the endodomain of $\beta 4$ integrin leads to disintegration of the hemidesmosomes that are located on the backside of the migrating cell [22]. Integrin $\alpha 6\beta 4$ can bind to collagen XVII type and plectin molecules. By using this binding and also by folding its cytoplasmic domain, integrin $\alpha 6\beta 4$ may be involved in the hemidesmosome assembly [12]. It has recently been shown that silencing of the $\alpha 6$ subunit expression causes a significant decrease in the expression of the $\alpha 3$ and $\alpha 2$ subunits on the surface of human keratinocytes. Interestingly, this type of cells lose the capability of rapid and directed migration on laminin and type I collagen surfaces. It is assumed that integrin $\alpha 6\beta 4$ can be the primary regulator of all other epidermal integrin types [23]. Meanwhile, in keratinocytes extracted from patients with $\beta 4$ gene mutation, the expression level of the $\alpha 3$ and $\alpha 6$ subunits remained within the normal range [24].

The data on the role of $\alpha 6\beta 4$ integrin in the cell migration process is still being debated. Possibly, this is connected to the partial interchangeability of the receptors $\alpha 3\beta 1$ and $\alpha 6\beta 4$ that can bind to laminin 332. According to entrenched notions, $\alpha 3\beta 1$ integrin upon binding to laminin 332 provides cellular adhesion, mobility, and assembly of laminin, whereas integrin $\alpha 6\beta 4$ upon binding with laminin 332 provides stable cell adhesion *via* the formation of hemidesmosomes (Fig. 3).

However, according to some data, the haptotactic migration along laminin 332 is facilitated by the combined action of both integrin receptors, and $\alpha 6\beta 4$ integrin has a transdominant inhibitory effect on $\alpha 3\beta 1$ (i.e., the function of $\alpha 3\beta 1$ can be suppressed upon $\alpha 6\beta 4$ binding). However, the use of anti- $\alpha 6\beta 4$ antibodies had no effect on chemotaxis [25]. Further, it was hypothesized that the inhibition of $\alpha 6\beta 4$ binding to a ligand leads to activation of an additional chemotactic pathway, which utilizes $\alpha 3\beta 1$ integrin, but cells migrate separately from each other [26]. Integrin- $\alpha 6\beta 4$ -deficient cells do not re-

spond to the addition of the epidermal growth factor (EGF) either due to a lack of interaction between the EGF receptor (EGFR) and $\beta 4$ or due to the suppression of integrin $\alpha 3\beta 1$ activity. In the case of $\alpha 6\beta 4$ expression and consequent binding upon the addition of EGF, activation of Rac1 was observed and led to the suppression and relocalization of $\alpha 3\beta 1$ integrin from basal focal adhesions to the area of intracellular connections. This contributed to the migration of keratinocytes as a single layer. It is assumed that integrin $\alpha 6\beta 4$ coordinates chemotaxis in the wound healing process. At wound sites, the kinetics of $\alpha 6\beta 4$ integrin binding to ECM proteins changes along with the synthesis rate of its components. During the migration, integrin $\alpha 6\beta 4$ binds to the secreted laminin 332. This enhances Rac1 activity and causes chemotaxis suppression (dependent on $\alpha 3\beta 1$), which could be necessary to maintain communication between the leading cells and the whole layer of epithelial cells [26].

INTEGRINS $\beta 1$

In addition to $\alpha 6\beta 4$ integrin, the connection to the basal membrane in the skin can be provided by integrins with a $\beta 1$ subunit in their structure.

As opposed to the knockout of subunits $\alpha 6$ and $\beta 4$, the complete knockout of $\beta 1$ integrins leads to early natal destruction, which makes it impossible to define its role in the skin [27, 28].

Trying to estimate the role of $\beta 1$ integrins in epidermis biology, keratinocytes were derived from a $\beta 1$ -null-ESC mouse. The $\beta 1$ -null-ESC line was obtained with a transfection vector that deactivates the $\beta 1$ integrin gene [29]. $\beta 1$ -null-ESC expressed simple keratins *in vitro*, but they were incapable of differentiating into keratinocytes and expressing the epidermal specific keratins 14, 10, and involucrin.

It is interesting that in teratomas, which are formed after subcutaneous transplantation of $\beta 1$ -null-ESCs into syngeneic mice, the expression of $\alpha 6\beta 4$ integrin, keratins 14, 10, and involucrin was found, attesting to the differentiation of these cells into keratinocytes.

$\beta 1$ -null-keratinocytes were also found in the epidermis of chimeric mice (wild type/ $\beta 1$ -null); these mice were characterized by a normal skin. ECM proteins assembly was significantly disturbed (smaller number, thinner, and shorter BM protein filaments) in the $\beta 1$ -null-ESC, but it was in the normal range in the teratomas and skin of chimeric mice [30].

Since keratinocytes and dermal fibroblasts contribute to the formation of BM [31], the authors suggested that the inability of $\beta 1$ -null-ESC to *in vitro* differentiate into keratinocytes could be a result of the inability to produce BM proteins rather than the absence of $\beta 1$ subunits alone. The observed *in vivo* differentiation

into keratinocytes could happen due to the formation of BM proteins by wild type cells from the surrounding tissue [30].

However, later experiments showed that there is at least one other possible explanation for the observed phenomena. Neither contact with the BM nor the presence of normal epidermal keratinocytes does restore the ability of $\beta 1$ -null-ESC to differentiate into keratinocytes [32]. In the study performed on the de-epithelized "dead" dermis with a retained BM, $\beta 1$ -null-ESC did not differentiate into keratinocytes. Co-culturing with normal epidermal keratinocytes was not effective, either. However, introduction of normal dermal fibroblasts into the dermis led to the formation of a high number of epidermal cysts from wild-type ESC and also some keratin-14-positive cells that were differentiated from $\beta 1$ -null-ESC. Fibroblasts in the tissue stimulated the differentiation of keratin-14-positive cells in embryoid bodies of wild-type and $\beta 1$ -null cells. It was shown that the keratinocyte growth factor (KGF), fibroblast growth factor 10 (FGF10), and transforming growth factor $\alpha 1$ (TGF α) that were all expressed by fibroblasts would stimulate ESC to differentiate into epidermal type cells. Meanwhile, the effect of the growth factors was more obvious in the $\beta 1$ knockout cells [32]. This could be explained by the fact that the concentration of growth factors in the growth medium was not the limiting factor for wild-type ESC. Therefore, for the stimulation of $\beta 1$ -null-ESC differentiation one needed to use a high concentration of inducers. These findings confirm the well-known synergism of integrins and growth factors and also indicate its presence at early stages of development, including the skin development process. It should also be noted that ESC of $\beta 1$ gene knockout mice were unable to grow in the presence of feeder cells, while for wild-type ESC the non-proliferating fibroblasts are necessary as a feeder culture. In this regard, the question about the role of feeder cells in ESC differentiation into keratinocytes arises.

Development of technologies for the generation of mice with tissue-specific gene knockout has allowed investigators to avoid difficulties in the investigation of the mutations that lead to natal embryo death. In order to investigate the consequences of epidermis specific deletion of $\beta 1$ integrins, mice with alleles flanked by the LoxP-sites of the $\beta 1$ subunit gene were crossbred with mice expressing Cre-recombinase under the control of keratin 14 and the promoter of 5 genes, which are activated in the basal layer of embryonic epidermis [33, 34]. The offspring of these mice exhibited epidermal blistering, but less developed than that in the mice with subunits $\alpha 6$ or $\beta 4$ knockout.

In the thin and fragile skin of mice with epidermis-specific $\beta 1$ subunit knockout (keratin-14-promoter-

controlled Cre-recombinase) there was an almost complete lack of BM, hemidesmosomes instability, a sharp decline of the proliferative potential of epidermis, and the inability of developing HF to invaginate into the dermis. These pups usually died within several hours after birth, possibly due to the lack of an epidermal barrier and dehydration. Nevertheless, the keratinocyte terminal differentiation program remained the same [33], which was contrary to the findings of some studies performed using transfection of mutant $\beta 1$ subunits *in vitro* and studies of keratinocyte cultures [35,37]. The findings indicate the crucial role of integrins containing the $\beta 1$ subunit in the maintenance of the proliferative capacity of the developing epidermis [33]. The inability of developing HF to invaginate into the dermis is rather interesting. The molecular mechanisms underlying the process of invagination of the growing HFs and their remodeling of ECM have not been thoroughly studied. Clearly, an important role in this process is played by integrins, particularly those containing the $\beta 1$ subunit.

Mice with $\beta 1$ subunit knockout in the embryo skin (Cre-recombinase controlled by the keratin 5 promoter gene) were developed. These mice were viable for 4 – 6 weeks [34], and by that time they had completely lost their HFs. Mutant mice were developing anomalies of HF and progressing hair loss due to a decrease in the proliferation of hair matrix cells. As a result, the deformed HF were replaced by macrophage infiltration; the epidermis of the back skin thickened; the basal layer of the epidermis was disorganized; cells had an abnormal morphology, irregularities in the formation of BM were observed; the number of hemidesmosomes decreased; and blistering developed. In contrast to the previous study, there was an increase in the number of layers of differentiated keratinocytes in the epidermis. The integrity of the BM surrounding the HF was not disrupted, possibly due to lower mechanical stress compared to the interfollicular epidermis or the lower structural dependence of the BM around the HF on $\beta 1$ integrins. Finally, the dermal fibrosis was developed in these mice [34]. There was also a reduction in the keratinocyte proliferative potential, and some researchers suggest that this may be caused not by the lack of a $\beta 1$ subunit, but by an associated decrease in integrin $\alpha 6\beta 4$ expression.

The results obtained in both studies investigating the impact of the deletion of $\beta 1$ integrins in embryonic epidermis attest to the important role of $\beta 1$ integrins in the formation of HF, organization of BM, and proliferation and differentiation of keratinocytes. HFs are known to be degenerated and to be incapable of cyclical changes when integrin $\beta 1$ is removed. Thus, it was assumed that $\beta 1$ integrins are involved in the retention of the SC compartment or SC activation during the initiation of

the anagen phase [34]. However, results of epidermis-specific $\beta 1$ integrin gene knockout were different depending on which particular tissue-specific gene (K5 or K14) was used for Cre-recombinase activation.

Some of the mice with tissue-specific $\beta 1$ integrin gene knockout were able to live for a relatively long time. This allowed one to conduct wound-healing experiments, which confirmed that $\beta 1$ was required for keratinocyte migration [38].

Epidermis-specific deletion of the $\beta 1$ integrin that was induced in embryogenesis [33, 34] did not allow one to fully assess its impact on proliferation, differentiation, development, and maintenance of the HF programs due to the developing fibrosis, inflammation or death of animals. To distinguish the primary effects of the $\beta 1$ subunit knockout from secondary ones, researchers compared the effects of $\beta 1$ integrin gene knockout in the 14.5-day mouse epidermis (using Cre-recombinase under the control of the keratin 5 gene promoter, K5Cre $\beta 1$ null) and induced deletions in adult epidermis (with 4-hydroxytamoxifen and CreER-recombinase under the control of the keratin 14 gene promoter, K14CreER) [39]. In the first case (K5Cre $\beta 1$ null), the authors observed an increased number of differentiated cell layers, degeneration of the HF and sebaceous glands, reduced proliferation, and separation of the epidermis from the underlying derma. These animals were found to have abnormal collagen type IV accumulation and laminin 332 in the derma. The removal of $\beta 1$ integrin subunits in the embryonic epidermis (K5Cre $\beta 1$ null) caused a disruption in terminal differentiation, which led to an increased number of cell layers expressing the markers typical of differentiated keratinocytes (keratin 10, kornifin, lorikrin and transglutaminase 1). These findings are in disagreement with data indicating the retention of the epidermal cell differentiation program in mice with tissue-specific $\beta 1$ integrin knockout [33]. The remaining HF still expressed SC markers at a high level. In the second case (K14CreER), knockout of $\beta 1$ genes in the adult animal epidermis led to minor changes in the epidermis. The main abnormality observed was an increase in the number of melanocytes. Disturbance of interfollicular epidermis differentiation and reduced size of the sebaceous glands were also observed. HF remained, but the outer root sheaths of HF were increased, some HF bulbs were thin and elongated, and a significant number of proliferating cells were found in some areas of interfollicular epidermis. The high expression of SC markers in the bulge area remained on day 30 after treatment with hydroxytamoxifen.

The phenotypic changes observed after the removal of $\beta 1$ integrins in mature epidermis were much less pronounced than those that occurred after the dele-

tion of genes during fetal development. In both cases, no obvious changes in the HFSC compartment were observed [39].

Since the described animal models with different $\beta 1$ subunit expression defects did not take into account the contribution of specific integrins α -subunits to regulation, the effect of $\alpha 3\beta 1$ integrin lacking on mature skin and the development of the HF was studied [40].

$\alpha 3\beta 1$ integrin is abundantly expressed in the skin; it localizes between hemidesmosomes and connects the BM to the actin cytoskeleton *in vivo*. Inactivation of the $\alpha 3$ -integrin subunit resulted in the death of pups shortly after birth; kidney and lung defects were observed in the animals [41]. Pups of $\alpha 3$ null-mice developed blisters on footpads, while the structure of hemidesmosomes remained normal. An analysis of the laminin 332 expression showed disorganization of the BM zone. The program of epidermis differentiation and stratification was unchanged [42]. Subsequent experiments showed that integrins $\alpha 3\beta 1$ and $\alpha 6\beta 4$ were not important for morphogenesis and homeostasis in the epidermis of the developing skin if the epidermis remained attached to the dermis. Mouse embryos lacking these integrins had a normal proliferation program and apoptosis rate in the intact BM areas until blister formation [43]. It was the contact between the epidermis and dermis, which was ensured by an unknown compensatory mechanism for a short period, which was important. With the development of blisters during embryogenesis, the intensity of apoptosis increased. Unfortunately, the morphogenesis of HF upon removal of integrins $\alpha 3\beta 1$ or $\alpha 6\beta 4$ has not been discussed [43].

To further investigate the consequences of integrin $\alpha 3\beta 1$ removal, the skin of newborn knockout animals was implanted in nude mice. In mature grafts, disruption of BM organization in interfollicular epidermis was observed and severe morphological abnormalities of HF occurred after the first development cycle: HF growth retardation, disorganization of F-actin in HF, fragmentation of HF, variation in pigment accumulation, and the formation of HF clusters. A closer look at the transplants led to the conclusion that $\alpha 3\beta 1$ integrin was not required for the differentiation of a mature interfollicular epidermis but was necessary for the regulation of various processes of morphogenesis and maintenance in HF. With $\alpha 3\beta 1$ integrin deletion, a mature skin can fully develop and form the HF and sebaceous glands, therefore suggesting that $\alpha 3\beta 1$ integrin is not required to maintain epidermal SC. However, significant disturbances emerged in HF after the first cycle; proliferation and apoptosis decreased, thus indicating a longer resting phase of the HF, while the formed clusters may result from unsuccessful attempts by HF to start the next growth phase. These data show that $\alpha 3\beta 1$ integrin

plays an important role in the specific regulation of the morphology of HF during the catagen phase of the HF cycle [40].

Taking into account the data on the role of $\beta 1$ integrins in the formation and maintenance of HF, proliferation and differentiation of keratinocytes, structuring of BM, and possible involvement in the maintenance or activation of the SC population, one can assume that at least the expression of the key genes involved in the development and formation of HF was altered in mice with activated $\beta 1$ integrin receptors. The phenotypic changes observed during the inactivation of these genes were similar to the phenotype that develops due to $\beta 1$ integrin gene knockout.

Some transcription factors, such as hairless, complex β -catenin-LEF-1-TCF-1, or Sonic hedgehog, were found to be involved in the proliferation of hair matrix keratinocytes and HF primordia [44, 45]. The mutant phenotype leading to the inactivation of these proteins partially overlaps with the $\beta 1$ -null-HF phenotype. On day 15 after birth, mice with a hairless mutation had premature apoptosis and increased proliferation rate of hair bulb matrix keratinocytes; improper location of the inner root sheath and outer root sheath atrophy was observed. The outer root sheath and hair bulb were broken down into separate cell clusters [44]. Mice with gene LEF-1 inactivation lacked whiskers and HF, as was observed in mice with epidermis-specific $\beta 1$ integrin gene knockout [46]. Mouse skin grafts of *Shh*^{-/-}, which were implanted into immunodeficient animals, could correctly differentiate to form hyperproliferative follicle-like structures that are incapable of producing mature hair shafts [47, 48]. It is interesting to see whether the keratinocyte-specific mutations leading to enhanced activity of these proteins are able to at least partially restore the $\beta 1$ -null-HF phenotype.

INTEGRIN-LINKED KINASE

Binding to a ligand induces integrin clustering, giving rise to complexes consisting of a large number of molecules. The affinity of integrin ligands is regulated by intracellular signals, thus activating integrins. The key activation regulators are talins and kindlins, which bind to the $\beta 1$ and $\beta 2$ integrin cytoplasmic domains [49]. The intracellular signaling pathway upon binding of integrins to ECM proteins has not been fully studied. Integrins lack either enzymatic activity or actin binding sites. It is assumed that signals are transmitted by various kinases and protein mediators.

It is most likely that integrin binding to the actin cytoskeleton is mediated by talin, α -actinin, and vinculin. Talin is required for stress transmission to the substrate via the formation of adhesive contacts, binding of integrin to the cytoskeleton, and subsequent cell

flattening [50]. Talin can bind integrins to actin via different ways: directly and through vinculin, which in turn binds to α -actinin and actin. Removal of α -actinin also inhibits the formation of adhesive contacts, but its role in the force transmission to the substrate has not been studied yet [51]. Vinculin gene knockout, contrary to the talin and α -actinin genes, has no dramatic consequences. Apparently, vinculin is important for adhesion strength but is not critical for their formation [52].

Integrin-mediated contacts are very complex structures which can include over 150 different molecules [53, 54]. These complexes comprise integral membrane proteins (integrins, syndecans), actin binding proteins (talin, vinculin, α -actinin), and signaling and adapter proteins (Src tyrosine kinase, focal adhesion kinase (FAK), paxillin and ILK) [55–60]. Focal adhesions also contain p21-activated kinase (PAK), Rho GTPases, which regulate the actin polymerization, myosin 2 contraction, microtubules dynamics and organization [61], calcium-dependent calpain 2 protease [62] and tyrosine phosphatase SHP-2 [63], which are likely to temporarily bind to adapter proteins and regulate their migration.

Protein kinase ILK, another component of focal adhesions [59], was originally identified as a protein interacting with $\beta 1$ integrins [64]. ILK is required for survival, migration, and cell adhesion. It mediates the interactions with various proteins, including $\beta 1$ and $\beta 3$ integrins, PINCH, paxillin and parvins, thus acting as a mediator between integrins and the actin cytoskeleton [59, 65].

ILK kinase activity and phosphorylation of some proteins, including protein kinase B (PKB/Akt) and glycogen synthase kinase 3 β (GSK 3 β), have been described in several papers [71, 73].

GSK 3 β was found in the bulge area of mature human HF tissue cultures, where it co-localizes with bulge markers, such as cytokeratin 15, 19, and CD200. Inhibition of glycogen synthase activity in this region increases the proliferation rate of outer root sheath cells, suggesting a possible involvement of GSK 3 β in maintaining the SC compartment of HF [66]. The development and cyclic changes in HF in a postnatal organism substantially depend on GSK 3 β inactivation [67, 68]. Active and unphosphorylated GSK 3 β can bind and phosphorylate β -catenin with the APC protein, resulting in the degradation of β -catenin. Phosphorylation of GSK 3 β inactivates the kinase and leads to the stabilization and translocation of β -catenin into the nucleus, where it interacts with the DNA-binding Lef1/Tcf proteins, which activate the transcription of target genes, such as the cyclin D genes, homeobox-containing transcription factors *c-myc*, Lef 1, and hair keratins [69, 70]. ILK, by phosphorylating GSK 3 β [71, 72] or inhibiting

the β -catenin degradation complex [73], can modulate β -catenin stability and thus play an important role in HF morphogenesis.

Nevertheless, the functions of ILK have not been completely elucidated, since both *in vitro* and *in vivo* findings indicate that ILK exhibits an adapter rather than kinase activity [74–80]. It is assumed that ILK contains a pseudo-kinase site that cannot be phosphorylated [81]. Thus, the degree of GSK 3 β and PKB/Akt phosphorylation in fibroblasts lacking ILK was the same as that in the control. Apparently, ILK is not involved in the phosphorylation of these kinases [74].

This hypothesis is confirmed by additional data showing that ILK regulates neither the phosphorylation of GSK 3 β , nor stability or activity of β -catenin in the HF, nor the cell differentiation matrix to the inner root sheath and the hair shaft. Keratinocyte-specific ILK (K5-Cre) gene knockout in mouse (keratin 5 gene promoter controlled Cre-recombinase) led to the disturbance of keratinocyte adhesion and BM integrity, blisters formation, keratinocyte ectopic proliferation in the suprabasal layers, abnormal keratinocyte differentiation, epidermal hyperplasia, defects in HF formation, and alopecia. The disruption of HF formation is associated with the accumulation of proliferating cells in the outer root sheath; while cell differentiation in the HF matrix and maintenance of SC remained the same. Mice with ILK gene knockout lived for a long time [80].

In contrast to the knockout of β 1-integrin genes, which reduces the proliferation of epidermal keratinocytes and HF matrix cells [33, 34], the knockout of ILK (K5-Cre) led to an insignificant decrease in the number of proliferating cells in the HF matrix. On the contrary, a substantial increase in the number of proliferating cells was observed in the outer root sheath. Since outer root sheath cells originate from the CD34⁺ stem cell population in the bulge [82], the authors checked whether the absence of ILK affects this population of cells. HF was found to contain CD34⁺-cells that will differentiate into transient cells. Since proliferating cells were accumulated in the outer root sheath but not in the hair matrix, a conclusion was made that ILK was required so that transient cells could migrate into the matrix and a hair bud could form during the anagen phase.

Interestingly, the absence of ILK in the keratinocyte culture influenced the formation of focal adhesions and prevented sustained directional migration. Cells also exhibited weak integrin mediated adhesions, and therefore did not capture lamellipodia, leading to changes in migration [80].

The consequences of ILK removal induced by cDNA expression in Cre-recombinase under the control of the keratin 14 gene promoter (K14-Cre) were also stud-

ied. In contrast to K5-Cre tissue-specific knockout [80], mice survived on average for up to 4 days after birth when this method was used for ILK gene inactivation. It should be noted that with β 1 integrin gene knockout, when the expression of Cre-recombinase was controlled by the keratin 14 gene promoter, the animals died soon after birth; while surviving for up to 6 weeks when the keratin 5 gene promoter was used [33, 34]. These differences can be explained if one takes into account the fact that keratin 14 expression starts after 11.5 days of embryonic development [83], and keratin 5 expression starts after 15 days [80], when the epidermis is already stratified and HF morphogenesis has begun. Such phenotypic differences may reflect the manifestation of the activity of keratin genes or differences in the intensity and/or expression time of the Cre-transgene and the ILK gene inactivation during embryogenesis.

Hence, deletion of ILK using the K14-CRE system weakened the morphogenesis of HF. Since the HF proliferation decreased, the number of HF decreased and morphogenesis could not be fully completed. The absence of ILK caused abnormalities in hemidesmosomes and triggered multiple formation of micro-blisters, dearrangement of keratinocytes in the suprabasal layers and the actin cytoskeleton, impaired adhesion, polarization, and migration.

ILK is considered to be a β 1-integrin target. The absence of ILK and β 1-integrins in the skin leads to a number of similar disturbances, including abnormal formation and performance of HF, a decrease in the proliferative activity of follicular keratinocytes, and blisters development.

Keratinocytes lacking ILK developed defects in adhesion and proliferation *in vitro*. The reduced proliferation rate resembled the disorders observed in HF but not those in interfollicular epidermis. The normal proliferation of primary keratinocytes in a cell culture is known to depend on the activation of α 3 β 1-integrins [84]. Taking in account the fact that the primary keratinocyte culture consists of transient and committed progenitor cells, the reduction in the proliferation rate of keratinocytes lacking ILK could be a result of intracellular β 1-integrin signaling disruption in this cell population. Possible disorders in SC proliferation could also be the cause, but this hypothesis is yet to be verified.

Upon ILK gene inactivation, adhesion and proliferation disturbances, as well as polarization and migration of murine keratinocytes in the cell culture, were observed [85]. The key event in polarization is the activation of Rac1 on the leading edge of the cell, causing the formation and stabilization of lamellipodia with integrin α 3 β 1 [86]. Infection of cells with an adenovirus carrying a constitutively active Rac1 reduces the polarization defects in ILK-deficient keratinocytes. Thus,

ILK is a crucial component of the signaling pathway, which connects integrin stimulation with Rac1 recruitment to the membrane, with spreading activation and directed migration of keratinocytes [85]. Lamellipodia stabilization defects could also be observed if the normal cells were transfected with the mutant Rac1 gene. Rac1 alone is not sufficient to stabilize lamellipodia, since the Rac1 constitutive expression in integrin- $\alpha3\beta1$ -deficient keratinocytes did not restore the type of migration [86].

The consequences of ILK inactivation in the HFSC were studied using tissue-specific knockout of the K15-Cre system that is specific of the HFSC [87].

During the induced inactivation of ILK in HFSC, hair follicles were able to enter the anagen phase. Stem cells from the bulge lacking ILK successfully migrated from the bulge and differentiated into cells of the outer root sheath and HF matrix and entered the growth phase. Consequently, the absence of ILK in the HFSC affects neither their migration nor their ability to produce a population of transient cells for the regeneration of HF. Meanwhile, the *in vitro* behavior of keratinocytes isolated from the bulge area of test mice (K15-Cre) differed from that of the controls. The adhesion efficiency to ECM-coated plastic was low. These findings coincide with the data obtained from keratinocytes isolated from the neonatal mouse epidermis, in which ILK was removed using K14-Cre [85]. The absence of ILK in HFSC mainly manifested itself as a reduction in the ability of bulge cells to differentiate into interfollicular epidermis cells during wound healing. Closure of the wounds on the back of experimental animals occurred later than that in the control group. The few bulge keratinocytes, which participated in the epidermis regeneration, were characterized by a low proliferative potential. Consequently, the ILK is required for the migration of bulge stem cell progeny into regenerating epidermis and for proliferation during wound re-epithelization. Taking into account the adhesion and migration defects of the keratinocytes derived from neonatal mice with epidermis-specific ILK deletion [80, 85], as well as the data on ILK inactivation in bulge SCs [87], one can assume that ILK mediates the interaction between cells and ECM, and that it contributes to the immobilization of keratinocytes on the basal membrane.

The molecular pathways modulated by ILK remain insufficiently studied. To fill in the gaps in our understanding of the role of ILK in the epidermis, some researchers have tried to determine gene expression by a microarray analysis [88]. For this purpose, gene expression in normal murine epidermis on day 3 after birth was compared to that in the epidermis with an inactivated ILK gene using tissue-specific knockout (K14-Cre). It was found that 27% of the transcripts were

expressed at a lower level. These transcripts encoded hair-specific keratins and proteins associated with them, such as keratin 31, the keratin-associated protein 3-3 and others, which is consistent with the disruption observed in the HF. The expression levels of desmoglein 4 (a protein important for the structural integrity of cuticle desmosomes and the HF cortex) and trichohyalin (a component of the inner root sheath) were 18- and 28-fold lower than the normal ones, respectively. A significant decrease in the expression level of these genes is consistent with the notion of the ILK expression importance after stages 4–5 of follicle formation.

ILK also plays an important modulating role in epidermal keratinocyte differentiation and formation of the epidermal barrier. This explains the lower expression of the genes encoding the key enzymes and factors which are required for protein crosslinking and lipid biosynthesis (e.g., transglutaminase 3, the substrate for transglutaminases Prr9, and others) observed in mice with epidermis ILK inactivation.

In the absence of ILK in the epidermis, expression of the genes involved in the Wnt and Shh signaling pathways was higher. Under normal skin morphogenesis, these signaling pathways are active at the early stages of HF development, while their activity decreases at later stages. Suspension of HF development at stages 2–4 in postnatal epidermis with the absence of ILK may be an indication of an increased expression of Wnt and Shh signaling pathway genes.

A transcriptome analysis of postnatal epidermis with ILK gene knockout revealed its role in HF development, keratinocyte maturation, and formation of the barrier function, as well as in pigmentation and regenerative processes [88].

INTEGRINS $\beta1$ AS MARKERS OF EPIDERMAL SCs

The behavior of SCs is controlled by the interaction between the internal transcriptional programs and external signals [89]. External signals are provided by the local microenvironment or niche where stem cells are located. ECM is an important component of the stem cell niche [90–93].

In the bulge region where HFSC are located, the ECM composition significantly differs from the composition of the remaining epidermis portions [94, 95]. Several-fold overexpression of collagen types VI, XVI, II, V, tenascin C, periostin, cysteine-rich glycoprotein nephronectin and other ECM components are observed in this region. The functional significance of these differences remains poorly investigated. Direct involvement of ECM and integrin receptors in the regulation of the fate of epidermal SC is doubtless. Interestingly, the composition of the ECM in the central portion of the cornea, which contains differentiating cells, and in

the limb that contains corneal SC also differs considerably. The limb area is enriched in collagen VII, XVI and IV, tenascin C, vitronectin, and laminin [96]. Hence, the integrin types that are expressed in these areas of cornea vary as well. Slowly proliferating and retaining the DNA label, limb cells are characterized by an over-expression of $\beta 1$, $\beta 4$, and $\alpha 6$ integrins. Small clonogenic cells of corneal rings were extracted on the basis of the $\alpha 6^{\text{bright}}/\text{CD}71^{\text{dim}}$ phenotype [97], which was also used to isolate the population of epidermal SC [98].

It has recently been shown that integrins can be used to enrich a SC population derived from various tissues [99–102].

In a human keratinocyte culture, the population of SC and transiently amplified cells were separated according to the $\beta 1$ -integrin expression level and the rate of adhesion to ECM proteins. The SC population with high levels of $\beta 1$ -integrin expression had a high colony forming efficiency and adhered to ECM proteins much faster than the cells of the transient compartment, which underwent terminal differentiation after one or five division cycles [103]. Cell motility depends on integrin expression levels, with motility being inhibited at high expression levels, and the medium level is the most favorable for cell motility [104]. Thus, transient cells that weakly express $\beta 1$ -integrin should have considerably higher motility than the strongly expressing SC, which was confirmed using time-lapse shooting. Moreover, transient cells were dispersed in a high-density cell culture, as opposed to SCs, which were arranged compactly [11].

High expression of $\beta 1$ -integrin (bright fluorescence after antibody staining) was used as a marker to determine the spatial organization of SCs and their progeny in human epidermis [11]. Keratinocytes with a low expression of these integrins originated from the SC compartment and started to rapidly proliferate and undergo differentiation.

In mouse epidermis, $\beta 1$ -integrins are expressed intensively in the bulge zone of HF and are widely used as markers for this region [68]. However, the use of the $\beta 1$ -integrin expression for human HF bulge cells is not possible, since they are expressed throughout the external layer of the outer root sheath, connective tissue sheath, and in the dermal papilla [105].

Similar results were obtained during the evaluation of the $\beta 1$ -integrin expression in tissue cultures of human scalp HF. The co-expression of fibronectin and tenascin C was also observed at the $\beta 1$ -integrin immunoreactivity sites. Researchers found no significant increase in $\beta 1$ -integrin immunoreactivity *in situ* in the bulge area. The use of $\beta 1$ -integrin activating antibodies and RGD tripeptides (Arg-Gly-Asp), which simulate natural ligands, contributed to the growth of the HF

tissue cultures extracted by *in vitro* microdissection, and it prevented their spontaneous regression. Thus, despite the lack of $\beta 1$ -integrin overexpression in human HFSCs, their signaling pathways play a role in the control of follicle growth. This approach may become a potential tool for preventing hair loss in humans via direct stimulation of the intracellular $\beta 1$ -integrin signaling pathway [106].

It was shown that $\beta 1$ integrins and MAP-kinase contribute to the *in vitro* maintenance of the SC compartment. Transfection of a human keratinocyte culture with a retrovirus containing a mutant integrin $\beta 1$ subunit (dominant negative mutation) decreased the surface expression level of these subunits, cell adhesion level, and MAP-kinase activation. This resulted in the differentiation of SCs [17].

A skin chemical carcinogenesis model was used to show that epidermis-specific $\alpha 3$ -integrin gene knockout slows the initiation step under the action of 7,12-dimethylbenz(α)anthracene and facilitates the exit of HFSC from the niche and their differentiation, thus preventing the accumulation of the transformed cells in the skin. Further treatment with phorbol ester caused no tumor progression in the experimental animals. Meanwhile, under prolonged exposure to DMBA alone in a single component protocol, tumor progression with transition to the malignant form was more effective and occurred at a higher rate in the epidermis of animals with α integrin gene knockout, although the number of malignancy lesions was lower [107].

$\beta 1$ integrins are required for apical localization of the protein complexes that regulate the asymmetric division of epidermal SCs, which ensures balance between the stem and progenitor cells localized on the BM and their differentiating progeny in the suprabasal layers of the epidermis [108].

Integrins can directly activate growth factor receptors in the absence of these factors [109].

Integrin receptors combine the functions of mechanical attachment of cells to the substrate and bidirectional signaling. On one hand, they provide an adequate cellular response to the signals from the environment; on the other hand, they allow the cell to modulate its microenvironment by itself. The adhesion of basal cells to the BM in the epidermis is critical for a firm connection between the epidermis and dermis, for maintaining its histotypical epidermal structure, and performance of its protective functions. However, integrins have other functions as well. In addition to participating in the assembly of BM proteins, integrins monitor the orientation of the mitotic spindle and the apical localization of the protein complex during the asymmetric division of basal keratinocytes, contributing to the continuous regeneration of the epidermis and maintaining

a pool of basal keratinocytes. Integrins adjust the migration, proliferation, and differentiation of epidermal cells, thus eventually determining the morphogenesis of the skin and its appendages. Abnormal integrin expression results in a delay in HF development during

embryogenesis or in degradation and loss of hair follicles in adulthood. Abnormalities in the integrin expression may be the underlying reason of a number of pathological conditions, including malignization. ●

REFERENCES

1. Hynes R.O. // *Cell*. 2002. V. 110. № 6. P. 673–687.
2. Barczyk M., Carracedo S., Gullberg D. // *Cell Tissue Res*. 2010. V. 339. № 1. P. 269–280.
3. Bouvard B., Brakebusch C., Gustafsson E., Aszódi A., Bengtsson T., Berna A., Fässler R. // *Circ. Res*. 2001. V. 89. № 3. P. 211–223.
4. Bokel C., Brown N.H. // *Dev. Cell*. 2002. V. 3. № 3. P. 311–321.
5. Stenn K.S., Paus R. // *Physiol. Rev*. 2001. V. 81. № 1. P. 449–494.
6. Gray J., Dawber R. *A Pocketbook of hair and scalp disorders: an illustrated guide*. Blackwell Science, 1999. 116 p.
7. Adams J.C., Watt F.M. // *J. Cell Biol*. 1991. V. 115. № 3. P. 829–841.
8. Hertle M., Adams J., Watt F.M. // *Development*. 1991. V. 112. № 1. P. 193–206.
9. Adams J.C., Watt F.M. // *Cell*. 1990. V. 63. № 2. P. 425–435.
10. Palmer E.L., Ruegg C., Ferrando R., Pytela R., Sheppard D. // *J. Cell Biol*. 1993. V. 123. P. 1289–1297.
11. Jensen U.B., Lowell S., Watt F.M. // *Development*. 1999. V. 126. № 11. P. 2409–2418.
12. Hashmi S., Marinkovich M.P. // *Clin. Dermatol*. 2011. V. 29. № 4. P. 398–411.
13. Stepp M.A. // *Dev. Dyn*. 1999. V. 214. № 3. P. 216–228.
14. Watt F.M. // *EMBO J*. 2002. V. 21. № 15. P. 3919–3926.
15. Carroll J.M., Romero M.R., Watt F.M. // *Cell*. 1995. V. 83. № 6. P. 957–968.
16. Watt F.M., Kubler M.D., Hotchin N.A., Nicholson L.J., Adams J.C. // *J. Cell Sci*. 1993. V. 106. P. 175–182.
17. Zhu A.J., Haase I., Watt F.M. // *Proc. Natl. Acad. Sci. USA*. 1999. V. 96. № 12. P. 6728–6733.
18. Dowling J., Yu Q.C., Fuchs E. // *J. Cell Biol*. 1996. V. 134. № 2. P. 559–572.
19. Georges-Labouesse E., Messaddeq N., Yehia G., Cadalbert L., Dierich A., LeMeur M. // *Nat. Genet*. 1996. V. 13. № 3. P. 370–373.
20. Van der Neut R., Krimpenfort P., Calafat J., Niessen C.M., Sonnenberg A. // *Nat. Genet*. 1996. V. 13. № 3. P. 366–369.
21. Ashton G.H., Sorelli P., Mellerio J.E., Keane F.M., Eady R.A., McGrath J.A. // *Br. J. Dermatol*. 2001. V. 144. № 2. P. 408–414.
22. Germain E.C., Santos T.M., Rabinovitz I. // *Mol. Biol. Cell*. 2009. V. 20. № 1. P. 56–67.
23. Kligys K.R., Wu Y., Hopkinson S.B., Kaur S., Platanias L.S., Jones J.C. // *J. Biol. Chem*. 2012. V. 287. № 22. P. 17975–17984.
24. Sehgal B.U., DeBiase P.J., Matzno S., Chew T.L., Claiborne J.N., Hopkinson S.B., Russell A., Marinkovich M.P., Jones J.C. // *J. Biol. Chem*. 2006. V. 281. № 46. P. 35487–35498.
25. Hintermann E., Bilban M., Sharabi A., Quaranta V. // *J. Cell Biol*. 2001. V. 153. № 3. P. 465–478.
26. Russell A.J., Fincher E.F., Millman L., Smith R., Vela V., Waterman E.A., Dey C.N., Guide S., Weaver V.M., Marinkovich M.P. // *J. Cell Sci*. 2003. V. 116. P. 3543–3556.
27. Fassler R., Meyer M. // *Genes Dev*. 1995. V. 9. P. 1896–1908.
28. Stephens L.E., Sutherland A.E., Klimanskaya I.V., Andrieux A., Meneses J., Pedersen R.A., Damsky C.H. // *Genes Dev*. 1995. V. 9. P. 1883–1895.
29. Fässler R., Pfaff M., Murphy J., Noegel A.A., Johansson S., Timpl R., Albrecht R. // *J. Cell Biol*. 1995. V. 128. № 5. P. 979–988.
30. Bagutti C., Wobus A.M., Fassler R., Watt F.M. // *Dev. Biol*. 1996. V. 179. № 1. P. 184–196.
31. Marinkovich M.P., Keene D.R., Rimberg C.S., Burgeson R.E. // *Dev. Dyn*. 1993. V. 197. № 4. P. 255–267.
32. Bagutti C., Hutter C., Chiquet-Ehrismann R., Fässler R., Watt F.M. // *Dev. Biol*. 2001. V. 231. № 2. P. 321–333.
33. Raghavan S., Bauer C., Mundschau G., Li Q., Fuchs E. // *J. Cell Biol*. 2000. V. 150. № 5. P. 1149–1160.
34. Brakebusch C., Grose R., Quondamatteo F., Ramirez A., Jorcano J.L., Pirro A., Svensson M., Herken R., Sasaki T., Timpl R. // *EMBO J*. 2000. V. 19. № 15. P. 3990–4003.
35. Levy L., Broad S., Diekmann D., Evans R.D., Watt F.M. // *Mol. Biol. Cell*. 2000. V. 11. № 2. P. 453–466.
36. <http://www.vetmed.vt.edu/education/curriculum/vm8054/Labs/Lab15/Lab15.htm>
37. Hotchin N.A., Gandarillas A., Watt F.M. // *J. Cell Biol*. 1995. V. 128. № 6. P. 1209–1219.
38. Grose R., Hutter C., Bloch W., Thorey I., Watt F.M., Fässler R., Brakebusch C., Werner S. // *Development*. 2002. V. 129. № 9. P. 2303–2315.
39. Lopez-Rovira T., Silva-Vargas V., Watt F.M. // *J. Invest. Dermatol*. 2005. V. 125. № 6. P. 1215–1227.
40. Conti F.J., Rudling R.J., Robson A., Hodivala-Dilke K.M. // *J. Cell Sci*. 2003. V. 116. P. 2737–2747.
41. Kreidberg J.A., Donovan M.J., Goldstein S.L., Rennke H., Shepherd K., Jones R.C., Jaenisch R. // *Development*. 1996. V. 122. № 11. P. 3537–3547.
42. DiPersio C.M., Hodivala-Dilke K.M., Jaenisch R., Kreidberg J.A., Hynes R.O. // *J. Cell Biol*. 1997. V. 137. № 3. P. 729–742.
43. DiPersio C.M., van der Neut R., Georges-Labouesse E., Kreidberg J.A., Sonnenberg A., Hynes R.O. // *J. Cell Sci*. 2000. V. 113. P. 3051–3062.
44. Panteleyev A.A., Botchkareva N.V., Sundberg J.P., Cristiano A.M., Paus R. // *Am. J. Pathol*. 1999. V. 155. № 1. P. 159–171.
45. Oro A.E., Scott M.P. // *Cell*. 1998. V. 95. № 5. P. 575–578.
46. Van Genderen C., Okamura R.M., Farinas I., Quo R.G., Parslow T.G., Bruhn L., Grosschedl R. // *Genes Dev*. 1994. V. 8. № 22. P. 2691–2703.
47. St-Jacques B., Dassule H.R., Karavanova I., Botchkarev V.A., Li J., Danielian P.S., McMahon J.A., Lewis P.M., Paus R., McMahon A.P. // *Curr. Biol*. 1998. V. 8. № 19. P. 1058–1068.
48. Chiang C., Swan R.Z., Grachtchouk M., Bolinger M., Litingtung Y., Robertson E.K., Cooper M.K., Gaffield W., Westphal H., Beachy P.A. // *Dev. Biol*. 1999. V. 205. № 1. P. 1–10.
49. Shattil S.J., Kim C., Ginsberg M.H. // *Nat. Rev. Mol. Cell Biol*. 2010. V. 11. № 4. P. 288–300.

REVIEWS

50. Zhang X., Jiang G., Cai Y., Monkley S.J., Critchley D.R., Sheetz M.P. // *Nat. Cell Biol.* 2008. V. 10. № 9. P. 1062–1068.
51. Choi C.K., Vicente-Manzanares M., Zareno J., Whitmore L.A., Mogilner A., Horwitz A.R. // *Nat. Cell Biol.* 2008. V. 10. № 9. P. 1039–1050.
52. Xu W., Baribault H., Adamson E.D. // *Development.* 1998. V. 125. № 2. P. 327–337.
53. Geiger B., Spatz J.P., Bershadsky A.D. // *Nat. Rev. Mol. Cell Biol.* 2009. V. 10. № 1. P. 21–33.
54. Geiger B., Yamada K.M. // *Cold Spring Harb. Perspect Biol.* 2011. V. 3. № 5. P. a005033
55. Turner C.E. // *Nat. Cell Biol.* 2000. V. 2. № 12. P. E231–E236.
56. Zamir E., Geiger B. // *J. Cell Sci.* 2001. V. 114. P. 3577–3579.
57. Frame M.C. // *J. Cell Sci.* 2004. V. 117. P. 989–998.
58. Mitra S.K., Hanson D.A., Schlaepfer D.D. // *Nat. Rev. Mol. Cell Biol.* 2005. V. 6. № 1. P. 56–68.
59. Legate K.R., Montanez E., Kudlacek O., Fassler R. // *Nat. Rev. Mol. Cell Biol.* 2006. V. 7. № 1. P. 20–31.
60. Huttenlocher A., Horwitz A.R. // *Cold Spring Harb. Perspect Biol.* 2011. V. 3. № 9. P. a005074.
61. Ridley A.J. // *Bioessays.* 1994. V. 16. № 5. P. 321–327.
62. Beckerle M.C., Burridge K., DeMartino G.N., Croall D.E. // *Cell.* 1987. V. 51. P. 569–577.
63. Yu D.H., Qu C.K., Henegariu O., Lu X., Feng G.S. // *J. Biol. Chem.* 1998. V. 273. № 33. P. 21125–21131.
64. Hannigan G.E., Leung-Hagesteijn C., Fitz-Gibbon L., Coppolino M.G., Radeva G., Filmus J., Bell J.C., Dedhar S. // *Nature.* 1996. V. 379. P. 91–96.
65. Grashoff C., Thievensen I., Lorenz K., Ussar S., Fässler R. // *Curr. Opin. Cell Biol.* 2004. V. 16. № 5. P. 565–571.
66. Yamauchi K., Kurosaka A. // *Arch. Dermatol. Res.* 2010. V. 302. № 4. P. 263–270.
67. Fuchs E., Merrill B.J., Jamora C., DasGupta R. // *Dev. Cell.* 2001. V. 1. № 1. P. 13–25.
68. Huelsken J., Vogel R., Erdmann B., Cotsarelis G., Birchmeier W. // *Cell.* 2001. V. 105. № 4. P. 533–545.
69. Zhou P., Byrne C., Jacobs J., Fuchs E. // *Genes Dev.* 1995. V. 9. № 6. P. 700–713.
70. Logan C.Y., Nusse R. // *Annu. Rev. Cell Dev. Biol.* 2004. V. 20. P. 781–810.
71. Delcommenne M., Tan C., Gray V., Rue L., Woodgett J., Dedhar S. // *Proc. Natl. Acad. Sci. USA.* 1998. V. 95. № 19. P. 11211–11216.
72. Novak A., Hsu S.C., Leung-Hagesteijn C., Radeva G., Papkoff J., Montesano R., Roskelley C., Grosschedl R., Dedhar S. // *Proc. Natl. Acad. Sci. USA.* 1998. V. 95. № 8. P. 4374–4379.
73. Oloumi A., Syam S., Dedhar S. // *Oncogene.* 2006. V. 25. № 59. P. 7747–7757.
74. Sakai T., Li S., Dicheva D., Grashoff C., Sakai K., Kostka G., Braun A., Pfeifer A., Yurchenco P.D., Fassler R. // *Genes Dev.* 2003. V. 17. № 7. P. 926–940.
75. Lynch D.K., Ellis C.A., Edwards P.A., Hiles I.D. // *Oncogene.* 1999. V. 18. № 56. P. 8024–8032.
76. Zervas C.G., Gregory S.L., Brown N.H. // *J. Cell Biol.* 2001. V. 152. № 5. P. 1007–1018.
77. Mackinnon A.C., Qadota H., Norman K.R., Moerman D.G., Williams B.D. // *Curr. Biol.* 2002. V. 12. № 10. P. 787–797.
78. Hill M.M., Feng J., Hemmings B.A. // *Curr. Biol.* 2002. V. 12. № 14. P. 1251–1255.
79. Grashoff C., Aszodi A., Sakai T., Hunziker E.B., Fässler R. // *EMBO Rep.* 2003. V. 4. № 4. P. 432–438.
80. Lorenz K., Grashoff C., Torka R., Sakai T., Langbein L., Bloch W., Aumailley M., Fassler R. // *J. Cell Biol.* 2007. V. 177. № 3. P. 501–513.
81. Qin J., Wu C. // *Curr. Opin. Cell Biol.* 2012. V. 24. № 5. P. 607–613.
82. Blanpain C., Fuchs E. // *Annu. Rev. Cell Dev. Biol.* 2006. V. 22. P. 339–373.
83. Dassule H.R., Lewis P., Bei M., Maas R., McMahon A.P. // *Development.* 2000. V. 127. № 22. P. 4775–4785.
84. Manohar A., Shome S.G., Lamar J., Stirling L., Iyer V., Pumiglia K., DiPersio C.M. // *J. Cell Sci.* 2004. V. 117. P. 4043–4054.
85. Nakrieko K.A., Welch I., Dupuis H., Bryce D., Pajak A., St-Arnaud R., Dedhar S., D'Souza S.J., Dagnino L. // *Mol. Biol. Cell.* 2008. V. 19. № 4. P. 1462–1473.
86. Choma D.P., Pumiglia K., DiPersio C.M. // *J. Cell Sci.* 2004. V. 117. P. 3947–3959.
87. Nakrieko K.A., Rudkouskaya A., Irvine T.S., D'Souza S.J., Dagnino L. // *Mol. Biol. Cell.* 2011. V. 22. № 14. P. 2532–2540.
88. Judah D., Rudkouskaya A., Wilson R., Carter D.E., Dagnino L. // *PLoS One.* 2012. V. 7. № 5. P. e36704.
89. Watt F.M., Driskell R.R. // *Philos. Trans. R. Soc. Lond. B. Biol. Sci.* 2010. V. 365. P. 155–163.
90. Hall P.A., Watt F.M. // *Development.* 1989. V. 106. № 4. P. 619–633.
91. Scadden D.T. // *Nature.* 2006. V. 441. P. 1075–1079.
92. Spradling A., Drummond-Barbosa D., Kai T. // *Nature.* 2001. V. 414. P. 98–104.
93. Watt F.M., Hogan B.L. // *Science.* 2000. V. 287. P. 1427–1430.
94. Morris R.J., Liu Y., Marles L., Yang Z., Trempus C., Li S., Lin J.S., Sawicki J.A., Cotsarelis G. // *Nat. Biotechnol.* 2004. V. 22. № 4. P. 411–417.
95. Tumber T., Guasch G., Greco V., Blanpain C., Lowry W.E., Rendl M., Fuchs E. // *Science.* 2004. V. 303. P. 359–363.
96. Ordóñez P., Di Girolamo N. // *Stem Cells.* 2012. V. 30. № 2. P. 100–107.
97. Hayashi R., Yamoto M., Saito T., Oshima T., Okano T., Tano Y., Nishida K. // *Biochem. Biophys. Res. Commun.* 2008. V. 367. № 2. P. 256–263.
98. Li A., Simmons P.J., Kaur P. // *Proc. Natl. Acad. Sci. USA.* 1998. V. 95. № 7. P. 3902–3907.
99. Wagers A.J., Weissman I.L. // *Stem Cells.* 2006. V. 24. № 4. P. 1087–1094.
100. Stingl J., Eirew P., Ricketson I., Shackleton M., Vaillant F., Choi D., Li H.I., Eaves C.J. // *Nature.* 2006. V. 439. P. 993–997.
101. Shackleton M., Vaillant F., Simpson K.J., Stingl J., Smyth G.K., Asselin-Labat M.L., Wu L., Lindeman G.J., Visvader J.E. // *Nature.* 2006. V. 439. P. 84–88.
102. Watt F.M., Fujiwara H. // *Cold Spring Harb. Perspect Biol.* 2011. V. 3. № 4. P. a005124.
103. Jones P.H., Watt F.M. // *Cell.* 1993. V. 73. № 4. P. 713–724.
104. Huttenlocher A., Sandborg R.R., Horwitz A.F. // *Curr. Opin. Cell Biol.* 1995. V. 7. № 5. P. 697–706.
105. Kloepper J.E., Tiede S., Brinckmann J., Reinhardt D.P., Meyer W., Faessler R., Paus R. // *Exp. Dermatol.* 2008. V. 7. № 7. P. 592–609.
106. Kloepper J.E., Hendrix S., Bodo E., Tiede S., Humpries M.J., Philpott M.P., Fässler R., Paus R. // *Exp. Cell Res.* 2008. V. 314. № 3. P. 498–508.
107. Sachs N., Secades P., van Hulst L., Kreft M., Song J.Y., Sonnenberg A. // *Proc. Natl. Acad. Sci. USA.* 2012. V. 109. № 52. P. 21468–21473.
108. Lechler T., Fuchs E. // *Nature.* 2005. V. 437. P. 275–280.
109. Moro L., Venturino M., Bozzo C., Silengo L., Altruda F., Beguinot L., Tarone G., Defilippi P. // *EMBO J.* 1998. V. 17. № 22. P. 6622–6632.

Aptamers: Problems, Solutions and Prospects

A.V. Lakhin*, V.Z. Tarantul, L.V. Gening

Institute of Molecular Genetics, Russian Academy of Sciences, 2 Kurchatov Sq., Moscow, Russia, 123182

*E-mail: lahin9@mail.ru

Received 05.03.2013

Copyright © 2013 Park-media, Ltd. This is an open access article distributed under the Creative Commons Attribution License, which permits unrestricted use, distribution, and reproduction in any medium, provided the original work is properly cited.

ABSTRACT Aptamers are short single-stranded oligonucleotides that are capable of binding various molecules with high affinity and specificity. When the technology of aptamer selection was developed almost a quarter of a century ago, a suggestion was immediately put forward that it might be a revolutionary start into solving many problems associated with diagnostics and the therapy of diseases. However, multiple attempts to use aptamers in practice, although sometimes successful, have been generally much less efficient than had been expected initially. This review is mostly devoted not to the successful use of aptamers but to the problems impeding the widespread application of aptamers in diagnostics and therapy, as well as to approaches that could considerably expand the range of aptamer application.

KEYWORDS SELEX; aptamer; diagnostics; therapeutics; problems.

ABBREVIATIONS NAs – nucleic acids; IOP – initial oligonucleotide pool; PEG – polyethylene glycol; SELEX – systematic evolution of ligands by exponential enrichment; siRNA – small interfering RNA.

INTRODUCTION

Nucleic acids (NAs) were for a long time regarded only as compounds whose major functions were related to the storage of inherited information (DNA) and its transfer from gene to protein (RNA). However, as time has passed, new functions, such as enzymatic catalysis (performed by ribozymes) and transcription regulation, have been reported. The increasing number of such examples has forced the scientific community to reconsider its original opinion about the functions of NAs and to propose the so-called “RNA world theory” [1, 2]. According to this theory, NAs can perform very diverse functions and have probably ensured all the catalytic reactions for the period since life took hold on our planet [3]. The discovery of oligonucleotides that can specifically bind various target molecules and are known as aptamers was a valuable contribution to confirming the multifunctional nature of NAs [4, 5].

Aptamers are small (usually from 20 to 60 nucleotides) single-stranded RNA or DNA oligonucleotides able to bind target molecules with high affinity and specificity. Currently, a large number of generated aptamers can bind various targets, ranging from simple inorganic molecules to large protein complexes, and entire cells. In fact, aptamers are nucleotide analogues of antibodies, but aptamer-generation is significantly easier and cheaper than the production of antibodies [6, 7]. Moreover, aptamers are neither immunogenic nor toxic [8]. All these features make aptamers ideal candidates for diagnostic and therapeutic applications, pu-

rification of target molecules from complex mixtures, biosensor design, etc. [9, 10]. Aptamers are so widely applicable that new aptamer-related reports are published almost every day. A special database has been created (<http://aptamer.icmb.utexas.edu>) to classify the aptamer-related data and provide access to information about numerous, existing aptamers.

The basic methods used to engineer aptamers were described over 20 years ago [11, 12]. Aptamers are usually selected from the oligonucleotide collection that is known as the initial oligonucleotide pool (IOP) and includes 10^{14} – 10^{15} different oligonucleotides. IOP is often called a “combinatorial library.” This comparison is not quite accurate, since such a library contains all possible oligonucleotides of selected size by definition and is too big for practical purposes (a relatively small library contains about 10^{18} different oligonucleotides). IOP is an aliquot of the synthetic chemical combinatorial library and contains single-chained DNA or RNA oligonucleotides conditioned for binding to the target molecule. Oligonucleotides composing IOP include 30- to 50-nucleotide-long variable parts (each position can be occupied by one of four nucleotides). Variable parts of aptamers are flanked by constant fragments to make the necessary manipulations (such as amplification and transcription) possible. It should be noted that RNA aptamers provide a significantly greater structural diversity compared to DNA aptamers, but their application is fraught with problems (RNA molecules are easily degradable by different factors, such

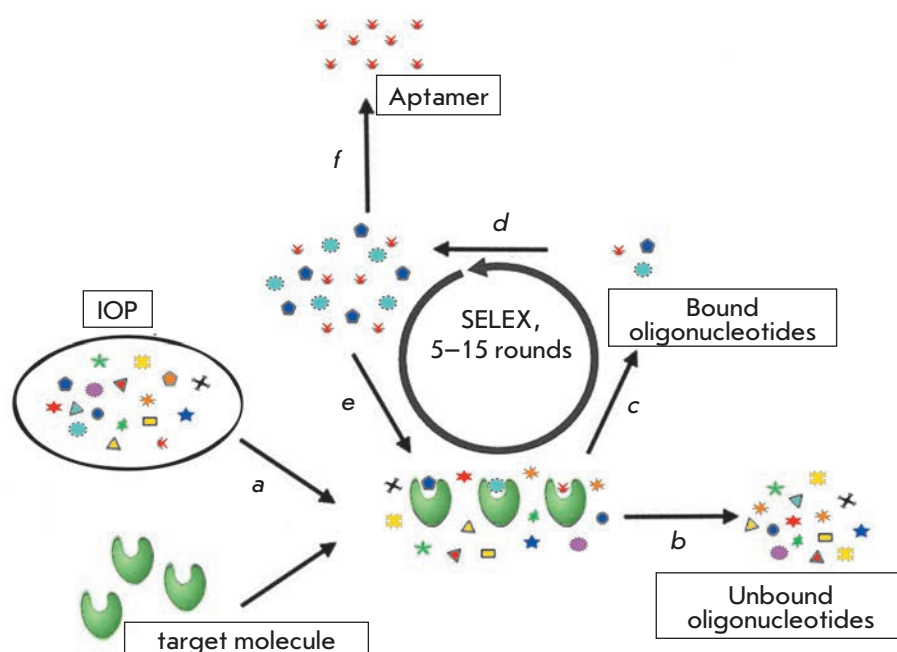


Fig. 1. Scheme of SELEX. (a) IOP is incubated with a target molecule. (b) Unbound oligonucleotides are separated from bound molecules by washing steps. (c) Bound oligonucleotides are eluted from the target molecule. (d) Eluted oligonucleotides are amplified using the PCR (DNA-SELEX) or RT-PCR (RNA-SELEX) technique. (e) The enriched pool is then subjected to further rounds of selection. (f) After 5–15 rounds, aptamers are cloned and analyzed in detail

as RNases, high temperature, alkaline medium etc.) [13, 14].

The conventional method for aptamer engineering known as SELEX (systematic evolution of ligands by exponential enrichment) can be conditionally separated into two alternating stages (Fig. 1). At the first stage, the original oligonucleotides are amplified by a polymerase chain reaction (PCR) to the desired concentration. In case of selection of RNA aptamers, the pool of single-chained oligoribonucleotides is generated by *in vitro* transcription of double-stranded DNA with T7 RNA-polymerase. For the selection of DNA aptamers, a pool of single-stranded oligodeoxyribonucleotides is generated by strand separation of double-stranded PCR products. At the second stage, the amplified pool is incubated with target molecules and interacting oligonucleotides are used for the first stage of the next SELEX round [7, 15].

Separation of oligonucleotides with higher affinity for target molecules and removal of unbound oligonucleotides are achieved through intense competition for binding sites. The selection pressure rises with every SELEX round. Maximum enrichment of the oligonucleotide pool with aptamers with the strongest affinity for the target molecule is usually achieved after 5–15 rounds [16, 17]. The SELEX method is applicable not only to the selection of aptamers capable of binding target molecules, but also to the selection of oligonucleotides with a particular enzymatic activity. In this case, the ability to catalyze the desired chemical reaction is used as a selection criterion [18, 19].

LIMITATIONS IN APTAMER APPLICATION AND POSSIBLE SOLUTIONS

The use of aptamers is fraught with problems that will be discussed in this review. The main bottlenecks limiting the wide application of aptamers are described below.

Problem 1. Aptamer degradation

The rapid degradation of aptamers (especially RNA aptamers) by nucleases in biological media, and in blood in particular, is a serious problem that puts limits on their practical application. The average time of oligonucleotide decay in blood ranges from several minutes to several tens of minutes depending on the oligonucleotide concentration and conformational structure. Since such a short time range is unacceptable for most therapeutic applications, several methods for protecting aptamers against degradation by nucleases have been developed.

One of the conventional methods used to generate nuclease-resistant aptamers is by performing SELEX with oligonucleotides containing modified nucleotides (Fig. 2). Special DNA and RNA polymerases that are able to utilise nucleoside triphosphate substrates with a modified, for example, 2' sugar position are used to generate such oligonucleotides. 2'-Amino pyrimidine nucleosides [20, 21], 2'-fluoropyrimidine nucleosides [22, 23], 2'-O-methyl purine, and 2'-O-methyl pyrimidine nucleosides [24, 25] are currently used for this purpose. The only aptamer approved for medical application known as Macugen (Fig. 3) is a vivid exam-

ple of an oligonucleotide modified using this approach [26]. Modification of nucleotides already included into aptamers could also be performed after the SELEX procedure; however, the inclusion of additional functional groups in this case can affect the specificity and affinity of an aptamer. Nevertheless, some modifications can increase aptamer resistance to nucleases without affecting their binding to target molecules. The most common and effective type of such aptamer improvements is the modification of 3'- and 5'-nucleotides [27]. Sometimes unmodified aptamers demonstrate very high resistance to degradation by blood nucleases [28]. This feature might be provided by the formation of specific three-dimensional structures that protect the 3'- and 5'-termini of aptamers against exonucleases.

The closed ring structures emerging after ligation of the 3'- and 5'-termini of the same aptamer are also highly resistant to degradation by nucleases. Several different aptamers can also be ligated to a closed structure with multiple specificities [29, 30]. The generation of such ring structures is an optimal approach for the regular injection of high amounts of aptamers, since the degradation products of some modified oligonucleotides have the potential of being toxic [31].

The novel approach to avoiding aptamer degradation by nucleases was provided by the development of "mirror aptamers" (Spiegelmers), which have an oligonucleotide backbone composed entirely of *L*-ribose (RNA Spiegelmers) or *L*-deoxyribose (DNA Spiegelmers). The development of Spiegelmers was favored by the fact that nucleases effectively cleave only *D*-, but not the unnatural *L*-oligonucleotides. However, if an aptamer with a known target is re-synthesized from *L*-nucleotides, this new aptamer will bind only an unnatural enantiomer protein containing *D*-amino acids. This problem can be solved if the primary selection of aptamers composed of *D*-nucleotides is performed using a synthetic *D*-protein. When selected aptamers are sequenced, they can be re-synthesized as Spiegelmers binding a natural *L*-protein. Such Spiegelmers are very stable and almost fully resistant to enzymatic degradation [32, 33].

Another approach to avoiding the problems related to aptamer degradation is by the recently developed method known as "aptamer displacement screening." This method is based on the screening of low-molecular-weight substances according to their ability to displace aptamers from the binding site of a target molecule (Fig. 4). It is presumed that the selected substance will have specificity and affinity similar to those of the displaced aptamer. The inhibitory effect of these low-molecular-weight compounds on protein targets is often identical to the effect of aptamers [34, 35].

Modification of 5'-terminus
(resistance
to 5'-exonucleases)

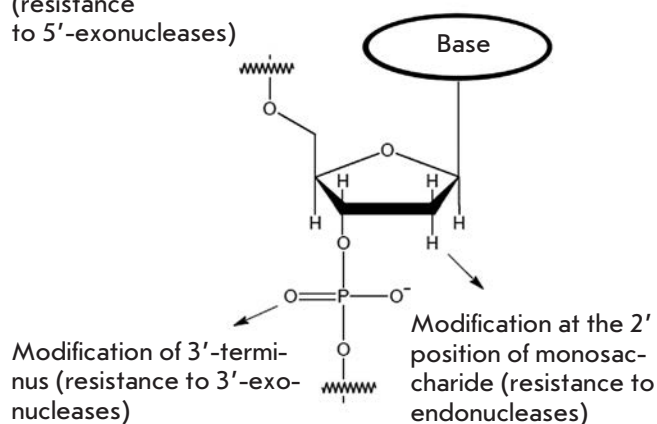


Fig. 2. Most frequently used modifications of nucleotides providing resistance of aptamers to nuclease degradation

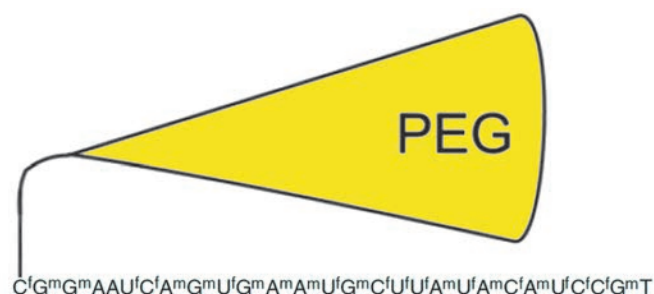
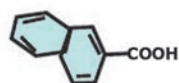


Fig. 3. The structure of the first FDA-approved aptamer, Macugen. The following modified nucleotides were used: f – 2'-fluoronucleotide, m – 2'-O-methylnucleotide. The aptamer was conjugated to 40 kDa PEG to avoid quick excretion during renal filtration

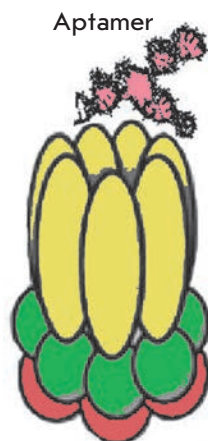
Problem 2. Aptamer excretion from the bloodstream by renal filtration

The removal of aptamers from the bloodstream via renal filtration complicates their therapeutic application. Most aptamers have a molecular weight ranging from 5 to 15 kDa (15–50 nucleotides), and they can be easily excreted by kidneys capable of removing substances with a molecular weight below 30–50 kDa. Conjugation of aptamers with polyethylene glycol (PEG) with a molecular weight of 20 or 40 kDa is the most common solution to this problem (Fig. 3). This method is currently being used to increase the bloodstream circulation time not only of oligonucleotides, but also of proteins, peptides and low-molecular-weight substances [36, 37]. The PEG-conjugated aptamers are excreted from the

Small molecule



Aptamer



Target molecule

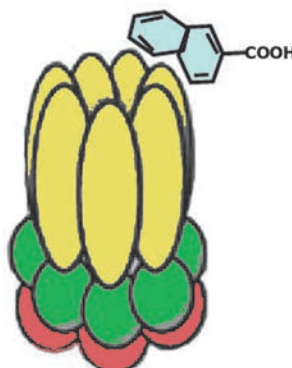


Fig. 4. Aptamer displacement screening. This approach allows one to select small molecules competing with an aptamer for the same binding site

bloodstream slowly (up to several days) and do not lose their specificity. And, besides, such PEG-conjugated aptamers are more effectively delivered to tissues and organs [38, 39]. As an alternative, aptamers could also be conjugated with cholesterol molecules. This modification also prolongs aptamer circulation in the bloodstream [40].

Problem 3. Control of the duration of action

The pharmacokinetic parameters of a drug (e.g., action duration) are very important in its therapeutic application. The duration of action depends on multiple factors, including degradation, involvement in metabolic processes, renal excretion, etc. All these factors should be taken into consideration before drug prescription, and sometimes they limit its application. The use of aptamers as drugs can often solve the problems associated with controlling the duration of action. One of the possibilities is to generate antidotes to aptamers by synthesizing a complementary oligonucleotide. Hybridization with antidote causes a change in aptamer conformation and complete loss of its ability to bind the target molecule (Fig. 5). The efficiency of this approach has been confirmed by experiments on animal models. An aptamer was delivered into the bloodstream and exhibited a therapeutic effect, while subsequent injection of an antidote inactivated the aptamer and stopped its action [41, 42]. The high efficiency of aptamer hybridization with an antidote in blood provides a unique opportunity to control the duration of the therapeutic action. It makes the application of aptamers preferable, since it is either impossible or very difficult to control the duration of action of antibodies or low-molecular-weight substances.

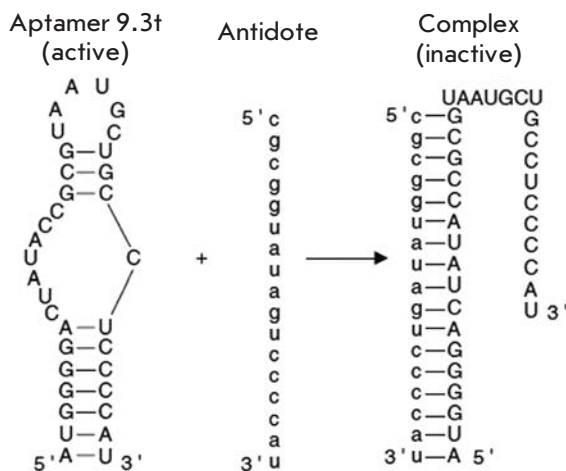


Fig. 5. Antidote-dependent regulation of aptamer functioning. The aptamer 9.3† is shown as an example [77]. This aptamer interacts with the coagulation factor IXa and has anticoagulation properties. Administration of a complementary antidote leads to quick inactivation of this aptamer and restoration of blood coagulation

Another effective and inexpensive way to control aptamer activity in the bloodstream without the necessity to generate a unique antidote is through the application of polycationic biopolymers that effectively bind polyanionic oligonucleotide molecules [43, 44]. Numerous polymers originally developed for gene therapy and delivery of DNA or siRNA possess the ability to bind NAs [45, 46]. Some low-molecular-weight molecules, such as porphyrin, can also bind particular conforma-

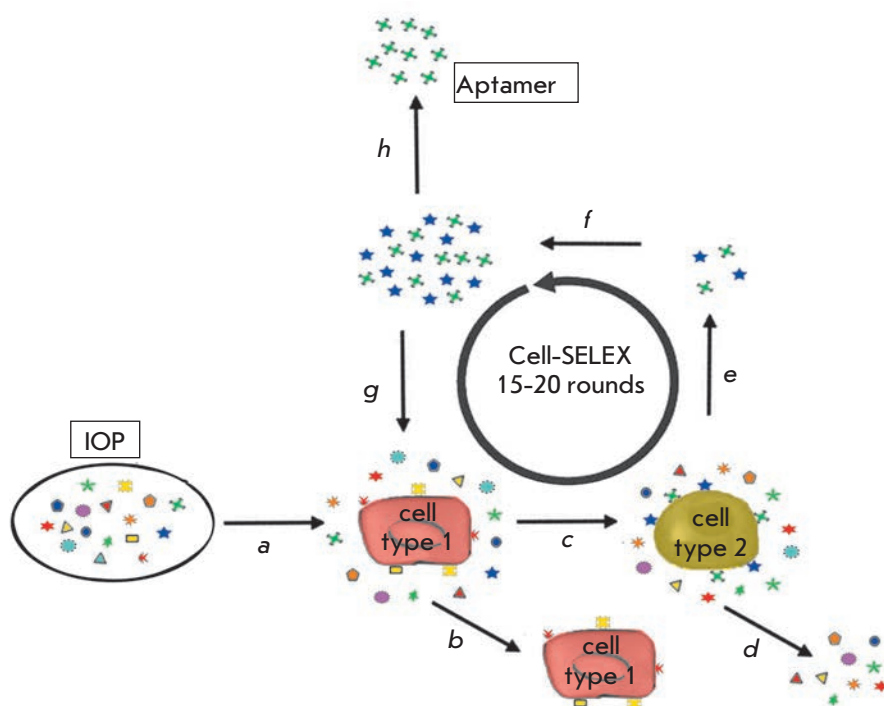


Fig. 6. Scheme of Cell-SELEX. (a) IOP is first incubated with a non-target cell in a negative selection step. (b) All oligonucleotides that show binding to the negative control cells are removed. (c) Unbound oligonucleotides from the negative step are added to the target cells in a positive selection step. (d) Unbound oligonucleotides from the positive step are separated from bound molecules by washing steps. (e) Oligonucleotides binding target cells are subsequently eluted. (f) Eluted oligonucleotides are amplified using the PCR (DNA-SELEX) or RT-PCR (RNA-SELEX) technique. (g) The enriched pool is then subjected to further rounds of selection. (h) After 15–20 rounds, aptamers are cloned and analyzed in detail

tional structures and inactivate an aptamer [47]. The blood does not contain significant amounts of NA due to the high activity of nucleases; therefore, it is presumed that biopolymers will bind preferentially foreign NAs (in particular, aptamers).

Another approach to controlling aptamer activity is inducible activation, i.e. conversion of an aptamer in an inactive form to an active one. For example, an inactive aptamer containing nucleotides with particular photosensitive modifications does not bind the target molecule. After being exposed to light with a particular wavelength, the aptamer loses its photosensitive groups and is converted into a functionally active state. This approach allows one to control both the time and site of aptamer activation [48, 49].

Problem 4. Interaction of aptamers with intracellular targets

Most aptamers were selected using molecules located on the cell surface or in the bloodstream. This potentially makes their application rather easy, since all that is needed to trigger the therapeutic effect is to deliver the aptamer into the bloodstream. However, some advances in the intracellular delivery of aptamers have recently been achieved. Special expression systems are able to generate aptamers inside cells and ensure their accumulation either in nucleus or in the cytoplasm. For example, transfection of cells with a recombinant vector expressing the aptamer sequence under a U6

promoter allows specific inactivation of nuclear target proteins [50, 51], while aptamer expression under a tRNA promoter ensures predominantly cytoplasmic localization of aptamers [52]. Cell-type-specific aptamer synthesis can be achieved by using directional viral expression systems that deliver vectors to particular cells [53, 54]. The concentration of expressed aptamers (also known as intramers) can be increased not only by using strong promoters that ensure a high level of expression, but also by limiting the rate of aptamer degradation by nucleases through protection of the 3'- and 5'- termini with additional structures (e.g., hairpins) [50].

Another way of delivering aptamers to intracellular target molecules is by the transfer of aptamers from the bloodstream to cells through receptor-dependent endocytosis [55, 56]. For example, endocytosis of aptamer binding prostate-specific membrane antigen (PSMA) provides effective and specific delivery of conjugated drugs to cancer cells expressing this antigen on their surface [57, 58].

Problem 5. Generation of aptamers using unpurified target proteins

Aptamer generation in most cases requires the availability of purified target molecules. Protein target molecules are expressed in cell cultures and purified by affine chromatography. These procedures are time- and labor-consuming, thus delaying the production of corresponding aptamers. Moreover, some proteins

are difficult to purify due to their chemical properties. Sometimes aptamers generated against target proteins expressed in prokaryotic cells do not interact with the same proteins expressed in eukaryotic cells due to post-translational modifications. These modifications can make epitopes of eukaryotic proteins inaccessible to aptamers generated against the proteins expressed in prokaryotic cells [59].

The modified SELEX protocol (Cell-SELEX) can be used to select aptamers that recognize cell-surface proteins [60, 61] (Fig. 6). Cell-SELEX allows to select aptamers located directly on the surface of live cells. It is also possible to generate aptamers that recognize specific microorganisms (e.g., such parasites as trypanosomes) [62, 63]. Cell-SELEX includes a negative selection step with a cognate cell type or cell line negative for target markers. One of the advantages of Cell-SELEX is that it does not require exhaustive information about cell-specific protein markers. The combination of negative selection with normal cells and positive selection with transformed cells will provide aptamers specific to tumor markers and promote the development of early cancer diagnostics.

The mutations that cause cancer first change the expression patterns, while the morphology of cells and tissues is changed later. The conventional methods of cancer diagnostics are focused mainly on morphological abnormalities and cannot recognize the early stages of cancer. This problem can be solved with Cell-SELEX-generated aptamers that recognize cancer cells. Aptamer microarrays can find trace amounts of cancer cells in the bloodstream [64, 65]. Marker-specific aptamers conjugated to gold particles are successfully used as contrasting agents for cancer-type specific diagnostics [66, 67].

New methods for the selection of aptamers that recognize intracellular target proteins in cell extracts have been developed [68, 69]. The negative selection step with extract from cognate cells lacking the target protein is included in SELEX when the target concentration is low. The resulting aptamer pool will be enriched in oligonucleotides that recognize the target protein. The negative selection step is unnecessary for target proteins with a high (1–10%) concentration [68, 69]. This SELEX modification allows fast generation of aptamers that recognize cell-type specific intracellular proteins. Target proteins can be further purified in native form by means of affinity chromatography on selected aptamers [70]. This approach can be useful for the analysis of purified enzymes, since fusion with affinity tags (GST, His, etc.) can unpredictably change enzyme properties [71].

Tissue-specific aptamers can be selected using a new approach known as *in vivo* SELEX [72]. A pool of nucle-

ase-resistant aptamers is injected into the bloodstream of an organism containing a specific tissue (e.g., tumor). This tissue is later excised; the aptamers are extracted, amplified, and re-injected into the target organism. Several rounds of such selection generate a pool of aptamers that target *in vivo* specific tissue. Many of these aptamers can migrate into cells and bind intracellular targets [72]. *In vivo* SELEX provides another significant advantage: the generated aptamers do not bind to blood or cell-surface proteins.

Problem 6. Aptamer cross-reactivity

Regardless of their high specificity, aptamers that recognize particular targets can also bind to molecules with a similar structure. Four aptamers against DNA-polymerase β generated in our laboratory can also bind and inhibit DNA polymerase α , which belongs to another DNA polymerase family [73]. Aptamer cross-reactivity can be an obstacle to their therapeutic application because of the possible side effects caused by aptamer interaction with other proteins; however, this problem can be avoided by introducing a SELEX negative selection step with structurally similar molecules. The results obtained in our laboratory confirm the efficiency of this approach. A more stringent SELEX protocol was used to produce a highly specific aptamer against DNA polymerase ι . This aptamer can bind neither to DNA polymerases α nor to β [74].

Problem 7. Automation of aptamer generation

Generation of aptamers seems to be a rather simple protocol, but in reality it is a time- and labor-consuming process. The selected aptamers sometimes turn out not to have the best affinity and specificity due to a suboptimal SELEX procedure. Automated SELEX [75, 76] allows one to avoid these problems and to generate aptamers with the required qualities within several days.

Another new method known as CE-SELEX (capillary electrophoresis SELEX) includes a modified stage of selection of target-bound oligonucleotides and allows to generate aptamers in one round. Nonequilibrium capillary electrophoresis of equilibrium mixtures (NECEEM) is used for aptamer fractioning. The entire selection procedure lasts 1–2 days and allows to select aptamers with strictly specified binding parameters K_d , K_{off} and K_{on} [77, 78].

CURRENT STATUS OF APTAMERS IN DIAGNOSTICS AND THERAPY

Mono- and polyclonal antibodies are routinely used for the diagnostics of various diseases. However, they can sometimes be successfully replaced by aptamers, especially when effective and specific binding to a target

molecule is required [79, 80]. Aptamers can recognize a membrane-immobilized protein in Western blotting protocols more effectively than antibodies can [81, 82]. ELISA protocols are also more sensitive when aptamers are used instead of antibodies [83, 84]. Similar to antibodies, aptamers can be used to purify target proteins [85, 86]. In contrast to antibodies, aptamers can be selected against non-immunogenic and toxic substances [87, 88].

Aptamers are also used as recognizing elements in biosensors [89, 90]. They are 10–100 times smaller than antibodies and can be arranged with a higher density on the biosensor surface. Aptamer-based biosensors require a smaller volume of the tested sample and can be re-used without loss of sensitivity [91, 92].

Aptamers are promising therapeutic agents, because they are cheap, non-immunogenic, and easy to modify. Inhibition of target enzymes is the main field of aptamer application as drugs. Aptamers inhibit target enzymes by binding to the catalytic center or inducing conformation changes in a protein's structure [93, 74]. However, when an aptamer is similar to an activating ligand, it can induce enzyme activation [94, 95].

Aptamer-based protocols of treatment of viral diseases are under development. Aptamers that recognize many viruses, including the human immunodeficiency virus (HIV), hepatitis C virus (HCV) and influenza virus, are already available [96, 97]. Aptamers can efficiently bind and inhibit many important viral enzymes, including reverse transcriptases, integrases, etc. However, the problem of effective delivery of aptamers or aptamer-expressing vectors into cells has yet to be solved. Nevertheless, aptamers can effectively bind viral capsid proteins. Such binding inhibits the interaction between viruses and cellular receptors and prevents viral entry into the cell [98, 99]. It makes the potential application of aptamers for antiviral prophylaxis or therapy much easier: aptamers can be injected intravenously or applied on the skin as a solution or ointment.

Aptamers against cell-type specific protein markers can be conjugated to drugs for targeted delivery. The following drug types can be used for conjugation to aptamers:

Toxic and radioactive substances that are inapplicable in therapy at high doses. They can be conjugated with aptamers and injected in low doses. These substances will subsequently concentrate locally (e.g. in tumor) to reach therapeutic doses [100, 101];

Easily degradable or excretable substances (e.g., siRNA). Cell- or tissue-specific delivery of siRNA conjugated to an aptamer removes the major obstacle to the therapeutic siRNA application [102, 103];

Drug-loaded nanoparticles. Animal models demonstrate the low efficiency of targeted delivery of nano-

particles conjugated to anti-tumor antibodies. These bulky conjugates are quickly removed from the bloodstream by phagocytes and demonstrate the low efficiency of delivery into solid tumors. Conjugates of nanoparticles with aptamers are significantly smaller and show better tissue penetration [104, 105]. The use of aptamer-conjugated liposomes for targeted drug delivery into cancer cells is the most promising area in this research; it has already proved efficient in some cases [106, 107]; and

Endogenous enzymes. Intracellular delivery of enzyme-aptamer conjugates can be used to restore the functional activity of cells if these enzymes are absent or dysfunctional [108].

CONCLUSIONS

Aptamers are a special class of substances that combine the advantages typical both of low-molecular-weight substances and proteins. Aptamers demonstrate an affinity and specificity similar to those of monoclonal antibodies. Meanwhile, aptamers are non-immunogenic and demonstrate high tissue penetration similar to that of small molecules. However, aptamers have not been commonly used thus far. The aptamer generation protocol SELEX was developed over 20 years ago, but only one aptamer, Macugen (or Pegaptanib), has been approved for therapeutic application (Fig. 3). Macugen binds to the vascular endothelial growth factor (VEGF) and blocks abnormal angiogenesis in the eye, thus preventing intraocular hemorrhage and loss of vision [26, 109].

Although aptamers have a number of advantages, it may seem rather strange that their share among modern therapeutic drugs is rather low. Aptamers are recently engineered substances, and this fact explains their rare application as therapeutic agents. For example, monoclonal antibodies were developed in 1975, but it was not until 1986 that the first antibody-based drug was approved by the U.S. Food and Drug Administration. The second drug of the type reached the pharmaceutical market in 1994, and now about twenty antibody-based drugs are used in clinic. The clinical trials may last for over 10 years and cost hundreds of millions of U.S. dollars. On the other hand, the first annual sales of Macugen (in 2005) have already exceeded 200 million U.S. dollars, a good incentive for the development of new aptamer-based drugs.

The use of aptamers in diagnostics has fewer limitations related to health risk, since there is no direct health risk in this case. In our opinion, the main obstacle to aptamer use in diagnostics is related to the lack of standardized protocols. The different aptamers generated in the same laboratory against the same target will differ in their primary structure, affin-

ity, specificity, and other chemical parameters. As a consequence, the protocol developed for one aptamer might appear inapplicable for another oligonucleotide. This circumstance creates a problem for aptamer application in the diagnostic of human diseases, which can be solved by generating standardized kits and protocols based on well-characterized aptamers with optimum characteristics. The constantly falling cost of chemical synthesis and generation of databases of characterized aptamers make this unification possible in the nearest future.

Almost all problems related to aptamer application have been solved to a certain extent, and we hope that these new substances will soon find extensive use both as scientific tools and as diagnostic and therapeutic agents. ●

This work was supported by the Program of the Presidium of the Russian Academy of Sciences "Molecular and Cell Biology," and the Russian Foundation for Basic Research (grants №№ 13-04-00598\13 and 13-04-00642\13).

REFERENCES

1. Gilbert W. // *Nature*. 1986. V. 319. P. 618.
2. Gold L., Janjic N., Jarvis T., Schneider D., Walker J.J., Wilcox S.K., Zichi D. // *Cold Spring. Harb. Perspect. Biol.* 2012. V. 4. P. a003582.
3. Cheng L.K., Unrau P.J. // *Cold Spring. Harb. Perspect. Biol.* 2010. V. 2. P. a002204.
4. Song K.M., Lee S., Ban C. // *Sensors (Basel)*. 2012. V. 12. P. 612–631.
5. Burnett J.C., Rossi J.J. // *Chem. Biol.* 2012. V. 19. P. 60–71.
6. Conrad R.C., Giver L., Tian Y., Ellington A.D. // *Meth. Enzymol.* 1996. V. 267. P. 336–367.
7. Kulbachinskiy A.V. // *Biochemistry (Moscow)*. 2007. V. 72. P. 1505–1518.
8. Bouchard P.R., Hutabarat R.M., Thompson K.M. // *Annu. Rev. Pharmacol. Toxicol.* 2010. V. 50. P. 237–257.
9. Cibiel A., Pestourie C., Ducongé F. // *Biochimie*. 2012. V. 94. P. 1595–1606.
10. Yang L., Zhang X., Ye M., Jiang J., Yang R., Fu T., Chen Y., Wang K., Liu C., Tan W. // *Adv. Drug. Deliv. Rev.* 2011. V. 63. P. 1361–1370.
11. Ellington A.D., Szostak J.W. // *Nature*. 1990. V. 346. P. 818–822.
12. Tuerk C., Gold L. // *Science*. 1990. V. 249. P. 505–510.
13. Hermann T., Patel D.J. // *Science*. 2000. V. 287. P. 820–825.
14. Nakamura Y., Ishiguro A., Miyakawa S. // *Genes Cells*. 2012. V. 17. P. 344–364.
15. Marimuthu C., Tang T.H., Tominaga J., Tan S.C., Gopinath S.C. // *Analyst*. 2012. V. 137. P. 1307–1315.
16. Mascini M., Palchetti I., Tombelli S. // *Angew. Chem. Int. Ed. Engl.* 2012. V. 51. P. 1316–1332.
17. Liu J., You M., Pu Y., Liu H., Ye M., Tan W. // *Curr. Med. Chem.* 2011. V. 18. P. 4117–4125.
18. Feldheim D.L., Eaton B.E. // *ACS Nano*. 2007. V. 1. P. 154–159.
19. Zaher H.S., Unrau P.J. // *RNA*. 2007. V. 13. P. 1017–1026.
20. Yan X., Gao X., Zhang Z. // *Genomics Proteomics Bioinformatics*. 2004. V. 2. P. 32–42.
21. Kuwahara M., Sugimoto N. // *Molecules*. 2010. V. 15. P. 5423–5444.
22. Li N., Nguyen H.H., Byrom M., Ellington A.D. // *PLoS One*. 2011. V. 6. P. e20299.
23. Derbyshire N., White S.J., Bunka D.H., Song L., Stead S., Tarbin J., Sharman M., Zhou D., Stockley P.G. // *Anal. Chem.* 2012. V. 84. P. 6595–6602.
24. Lebars I., Richard T., Di Primo C., Toulmé J.J. // *Blood Cells Mol. Dis.* 2007. V. 38. P. 204–209.
25. Hernandez F.J., Stockdale K.R., Huang L., Horswill A.R., Behlke M.A., McNamara J.O. 2nd. // *Nucl. Acid Ther.* 2012. V. 22. P. 58–68.
26. Siddiqui M.A., Keating G.M. // *Drugs*. 2005. V. 65. P. 1571–1579.
27. Mayer G. // *Angew. Chem. Int. Ed. Engl.* 2009. V. 48. P. 2672–2689.
28. Nitsche A., Kurth A., Dunkhorst A., Pänke O., Sielaff H., Junge W., Muth D., Scheller F., Stöcklein W., Dahmen C., et al. // *BMC Biotechnol.* 2007. V. 7. P. 48.
29. Mori Y., Nakamura Y., Ohuchi S. // *Biochem. Biophys. Res. Commun.* 2012. V. 420. P. 440–443.
30. Di Giusto D.A., Knox S.M., Lai Y., Tyrelle G.D., Aung M.T., King G.C. // *ChemBiochem*. 2006. V. 7. P. 535–544.
31. Levin A.A. // *Biochim. Biophys. Acta*. 1999. V. 1489. P. 69–84.
32. Eulberg D., Klussmann S. // *ChemBioChem*. 2003. V. 4. P. 979–983.
33. Turner J.J., Hoos J.S., Vonhoff S., Klussmann S. // *Nucl. Acids Res.* 2011. V. 39. P. e147.
34. Hafner M., Vianini E., Albertoni B., Marchetti L., Grune I., Gloeckner C., Famulok M. // *Nat. Protoc.* 2008. V. 3. P. 579–587.
35. Yamazaki S., Tan L., Mayer G., Hartig J.S., Song J.N., Reuter S., Restle T., Laufer S.D., Grohmann D., Krausslich H.G., et al. // *Chem. Biol.* 2007. V. 14. P. 804–812.
36. Pasut G., Veronese F.M. // *J. Control. Release*. 2012. V. 161. P. 461–472.
37. Milla P., Dosio F., Cattel L. // *Curr. Drug Metab.* 2012. V. 13. P. 105–119.
38. Tan L., Neoh K.G., Kang E.T., Choe W.S., Su X. // *Macromol. Biosci.* 2011. V. 11. P. 1331–1335.
39. Boomer R.M., Lewis S.D., Healy J.M., Kurz M., Wilson C., McCauley T.G. // *Oligonucleotides*. 2005. V. 15. P. 183–195.
40. Rusconi C.P., Roberts J.D., Pitoc G.A., Nimjee S.M., White R.R., Quick G. Jr., Scardino E., Fay W.P., Sullenger B.A. // *Nat. Biotechnol.* 2004. V. 22. P. 1423–1428.
41. Rusconi C.P., Scardino E., Layzer J., Pitoc G.A., Ortel T.L., Monroe D., Sullenger B.A. // *Nature*. 2002. V. 419. P. 90–94.
42. Bompiani K.M., Monroe D.M., Church F.C., Sullenger B.A. // *J. Thromb. Haemost.* 2012. V. 10. P. 870–880.
43. Oney S., Lam R.T., Bompiani K.M., Blake C.M., Quick G., Heidel J.D., Liu J.Y., Mack B.C., Davis M.E., Leong K.W., et al. // *Nat. Med.* 2009. V. 15. P. 1224–1228.
44. Bompiani K.M., Woodruff R.S., Becker R.C., Nimjee S.M., Sullenger B.A. // *Curr. Pharm. Biotechnol.* 2012. V. 13. P. 1924–1934.

45. Davis M.E., Pun S.H., Bellocq N.C., Reineke T.M., Popielarski S.R., Mishra S., Heidel J.D. // *Curr. Med. Chem.* 2004. V. 11. P. 179–197.
46. Mao H.Q., Leong K.W. // *Adv. Genet.* 2005. V. 53. P. 275–306.
47. Joachimi A., Mayer G., Hartig J.S. // *J. Am. Chem. Soc.* 2007. V. 129. P. 3036–3037.
48. Buff M.C., Schäfer F., Wulffen B., Müller J., Pötzsch B., Heckel A., Mayer G. // *Nucl. Acids Res.* 2010. V. 38. P. 2111–2118.
49. Brieke C., Rohrbach F., Gottschalk A., Mayer G., Heckel A. // *Angew. Chem. Int. Ed. Engl.* 2012. V. 51. P. 8446–8476.
50. Good P.D., Krikos A.J., Li S.X., Bertrand E., Lee N.S., Giver L., Ellington A., Zaia J.A., Rossi J.J., Engelke D.R. // *Gene Ther.* 1997. V. 4. P. 45–54.
51. Ausländer D., Wieland M., Ausländer S., Tigges M., Fussenegger M. // *Nucl. Acids Res.* 2011. V. 39. P. e155.
52. Chaloin L., Lehmann M.J., Sczakiel G., Restle T. // *Nucl. Acids Res.* 2002. V. 30. P. 4001–4008.
53. Mi J., Zhang X., Rabbani Z.N., Liu Y., Su Z., Vujaskovic Z., Kontos C.D., Sullenger B.A., Clary B.M. // *Nucl. Acids Res.* 2006. V. 34. P. 3577–3584.
54. Mayer G., Blind M., Nagel W., Böhm T., Knorr T., Jackson C.L., Kolanus W., Famulok M. // *Proc. Natl. Acad. Sci. USA.* 2001. V. 98. P. 4961–4965.
55. Davydova A.S., Vorobjeva M.A., Venyaminova A.G. // *Acta Naturae.* 2011. V. 3. № 4 (11). P. 12–29.
56. Meyer C., Eydeler K., Magbanua E., Zivkovic T., Pignaneau N., Lorenzen I., Grötzing J., Mayer G., Rose-John S., Hahn U. // *RNA Biol.* 2012. V. 9. P. 67–80.
57. Zhao Y., Duan S., Zeng X., Liu C., Davies N.M., Li B., Forrest M.L. // *Mol. Pharm.* 2012. V. 9. P. 1705–1716.
58. Min K., Jo H., Song K., Cho M., Chun Y.S., Jon S., Kim W.J., Ban C. // *Biomaterials.* 2011. V. 32. P. 2124–2132.
59. Liu Y., Kuan C.T., Mi J., Zhang X., Clary B.M., Bigner D.D., Sullenger B.A. // *Biol. Chem.* 2009. V. 390. P. 137–144.
60. Sun W., Du L., Li M. // *Curr. Pharm. Des.* 2011. V. 17. P. 80–91.
61. Ye M., Hu J., Peng M., Liu J., Liu J., Liu H., Zhao X., Tan W. // *Int. J. Mol. Sci.* 2012. V. 13. P. 3341–3353.
62. Göringer H.U. // *Trends Parasitol.* 2012. V. 28. P. 106–113.
63. Moreno M., González V.M. // *Curr. Med. Chem.* 2011. V. 18. P. 5003–5010.
64. Wan Y., Liu Y., Allen P.B., Asghar W., Mahmood M.A., Tan J., Duhon H., Kim Y.T., Ellington A.D., Iqbal S.M. // *Lab. Chip.* 2012. V. 12. P. 4693–4701.
65. Sheng W., Chen T., Kamath R., Xiong X., Tan W., Fan Z.H. // *Anal. Chem.* 2012. V. 84. P. 4199–4206.
66. Javier D.J., Nitin N., Levy M., Ellington A., Richards-Kortum R. // *Bioconjug. Chem.* 2008. V. 19. P. 1309–1312.
67. Khan S.A., Kanchanapally R., Fan Z., Beqa L., Singh A.K., Senapati D., Ray P.C. // *Chem. Commun. (Camb.)* 2012. V. 48. P. 6711–6713.
68. Kanoatov M., Javaherian S., Krylov S.N. // *Anal. Chim. Acta.* 2010. V. 681. P. 92–97.
69. Javaherian S., Musheev M.U., Kanoatov M., Berezovski M.V., Krylov S.N. // *Nucl. Acids Res.* 2009. V. 37. P. e62.
70. Han B., Zhao C., Yin J., Wang H. // *J. Chromatogr. B Anal. Technol. Biomed. Life Sci.* 2012. V. 903. P. 112–117.
71. Arnau J., Lauritzen C., Petersen G.E., Pedersen J. // *Protein Expr. Purif.* 2006. V. 48. P. 1–13.
72. Mi J., Liu Y., Rabbani Z.N., Yang Z., Urban J.H., Sullenger B.A., Clary B.M. // *Nat. Chem. Biol.* 2010. V. 6. P. 22–24.
73. Gening L.V., Klincheva S.A., Reshetnjak A., Grollman A.P., Miller H. // *Nucl. Acids Res.* 2006. V. 34. P. 2579–2586.
74. Lakhin A.V., Kazakov A.A., Makarova A.V., Pavlov Y.I., Efremova A.S., Shram S.I., Tarantul V.Z., Gening L.V. // *Nucl. Acid Ther.* 2012. V. 22. P. 49–57.
75. Cox J.C., Ellington A.D. // *Bioorg. Med. Chem.* 2001. V. 9. P. 2525–2531.
76. Eulberg D., Buchner K., Maasch C., Klussmann S. // *Nucl. Acids Res.* 2005. V. 33. P. e45.
77. Berezovski M., Drabovich A., Krylova S.M., Musheev M., Okhonin V., Petrov A., Krylov S.N. // *J. Am. Chem. Soc.* 2005. V. 127. P. 3165–3171.
78. Drabovich A.P., Berezovski M., Okhonin V., Krylov S.N. // *Anal. Chem.* 2006. V. 78. P. 3171–3178.
79. Soontornworajit B., Wang Y. // *Anal. Bioanal. Chem.* 2011. V. 399. P. 1591–1599.
80. Hong P., Li W., Li J. // *Sensors (Basel).* 2012. V. 12. P. 1181–1193.
81. Shin S., Kim I.H., Kang W., Yang J.K., Hah S.S. // *Bioorg. Med. Chem. Lett.* 2010. V. 20. P. 3322–3325.
82. Lee S., Song K.M., Jeon W., Jo H., Shim Y.B., Ban C. // *Biosens. Bioelectron.* 2012. V. 35. P. 291–296.
83. Wang Y., Xu D., Chen H.Y. // *Lab. Chip.* 2012. V. 12. P. 3184–3189.
84. Tan X., Chen W., Lu S., Zhu Z., Chen T., Zhu G., You M., Tan W. // *Anal. Chem.* 2012. V. 84. P. 8272–8276.
85. Orozco J., Campuzano S., Kagan D., Zhou M., Gao W., Wang J. // *Anal. Chem.* 2011. V. 83. P. 7962–7969.
86. Kökpinar O., Walter J.G., Shoham Y., Stahl F., Scheper T. // *Biotechnol. Bioeng.* 2011. V. 108. P. 2371–2379.
87. Bruno J.G., Richarte A.M., Carrillo M.P., Edge A. // *Biosens. Bioelectron.* 2012. V. 31. P. 240–243.
88. Lauridsen L.H., Shamaileh H.A., Edwards S.L., Taran E., Veedu R.N. // *PLoS One.* 2012. V. 7. P. e41702.
89. Huang Y., Zhao S., Chen Z.F., Shi M., Liang H. // *Chem. Commun. (Camb.)* 2012. V. 48. P. 7480–7482.
90. Han K., Liang Z., Zhou N. // *Sensors.* 2010. V. 10. P. 4541–4557.
91. Ocaña C., Pacios M., del Valle M. // *Sensors (Basel).* 2012. V. 12. P. 3037–3048.
92. Feng L., Chen Y., Ren J., Qu X. // *Biomaterials.* 2011. V. 32. P. 2930–2937.
93. Missailidis S., Hardy A. // *Expert. Opin. Ther. Pat.* 2009. V. 19. P. 1073–1082.
94. Huang Y.Z., Hernandez F.J., Gu B., Stockdale K.R., Nanapaneni K., Scheetz T.E., Behlke M.A., Peek A.S., Bair T., Giangrande P.H., et al. // *Mol. Pharmacol.* 2012. V. 82. P. 623–635.
95. Pastor F., Kolonias D., McNamara J.O. 2nd, Gilboa E. // *Mol. Ther.* 2011. V. 19. P. 1878–1886.
96. Zeller S.J., Kumar P. // *Yale J. Biol. Med.* 2011. V. 84. P. 301–309.
97. Binning J.M., Leung D.W., Amarasinghe G.K. // *Front. Microbiol.* 2012. V. 3. P. 29.
98. Gopinath S.C., Hayashi K., Kumar P.K. // *J. Virol.* 2012. V. 86. P. 6732–6744.
99. Mufhandu H.T., Gray E.S., Madiga M.C., Tumba N., Alexandre K.B., Khoza T., Wibmer C.K., Moore P.L., Morris L., Khati M. // *J. Virol.* 2012. V. 86. P. 4989–4999.
100. Zhang Y., Hong H., Cai W. // *Curr. Med. Chem.* 2011. V. 18. P. 4185–4194.
101. Orava E.W., Cicmil N., Gariépy J. // *Biochim. Biophys. Acta.* 2010. V. 1798. P. 2190–2200.
102. Zhu Q., Shibata T., Kabashima T., Kai M. // *Eur. J. Med. Chem.* 2012. V. 56. P. 396–399.
103. Neff C.P., Zhou J., Remling L., Kuruvilla J., Zhang J., Li H., Smith D.D., Swiderski P., Rossi J.J., Akkina R. // *Sci.*

REVIEWS

Transl. Med. 2011. V. 3. P. 66ra6.

104. Yu B., Tai H.C., Xue W., Lee L.J., Lee R.J. // Mol. Membr. Biol. 2010. V. 27. P. 286–298.

105. Talekar M., Kendall J., Denny W., Garg S. // Anticancer Drugs. 2011. V. 22. P. 949–962.

106. Aravind A., Jeyamohan P., Nair R., Veerananarayanan S., Nagaoka Y., Yoshida Y., Maekawa T., Kumar D.S. // Bio-technol. Bioeng. 2012. V. 109. P. 2920–2931.

107. Kang H., O'Donoghue M.B., Liu H., Tan W. // Chem. Commun. (Camb.) 2010. V. 46. P. 249–251.

108. Chen C.H., Dellamaggiore K.R., Ouellette C.P., Sedano C.D., Lizadjohry M., Chernis G.A., Gonzales M., Baltasar F.E., Fan A.L., Myerowitz R., et al. // Proc. Natl. Acad. Sci. USA. 2008. V. 105. P. 15908–15913.

109. Dombi T., Kwok K.K., Sultan M.B. // BMC Ophthalmol. 2012. V. 12. P. 37.

Antiviral Activity of Binase against the Pandemic Influenza A (H1N1) Virus

R. Shah Mahmud*, O.N. Ilinskaya

Institute of Fundamental Medicine and Biology, Kazan (Volga Region) Federal University,
Kremlyovskaya Str., 18, Kazan, Russia, 420008

*E-mail: raihan.shah@gmail.com

Received 15.05.2013

Copyright © 2013 Park-media, Ltd. This is an open access article distributed under the Creative Commons Attribution License, which permits unrestricted use, distribution, and reproduction in any medium, provided the original work is properly cited.

ABSTRACT The lack of effective antiviral drugs restricts the control of the dangerous RNA-containing influenza A (H1N1) virus. Extracellular ribonuclease of *Bacilli* (binase) was shown to manifest antiviral activity during single- and multi-cycle viral replication in the range of concentrations non-toxic to epithelial cells and 0.01–0.1 multiplicity of infection. During antiviral treatment for 15–30 min, the concentration of 1 µg/ml binase reduced the amount of focus-forming units of viruses by a factor of 3–10 and suppressed the virus-induced cytopathic effect in A549 human lung cells. The possible mechanisms of interaction between the virus and enzyme are discussed. Positive charges in both binase and viral hemagglutinin cause electrostatic interaction with negatively charged sialic acid on the host cell's surface followed by its penetration into the cell. Capsid elimination and release of viral RNA from endosome to the cytoplasm allows catalytic RNA cleavage by internalized binase. The data obtained confirm that binase is an effective antiviral agent against the pandemic influenza A (H1N1) virus. Certain progress in this field is associated with clarifying the detailed mechanism underlying the antiviral action of binase and development of the most effective way for its practical use.

KEYWORDS *Bacillus intermedius* ribonuclease; influenza A (H1N1) virus; A549 epithelial cell; cytotoxicity; antiviral activity.

ABBREVIATIONS FFU – focus-forming units, HA – hemagglutination, MOI – multiplicity of infection, AEC – 3-amino-9-ethylcarbazole, TPCK – L-1-Tosylamide-2-phenylethyl chloromethyl ketone.

INTRODUCTION

Over the past decades, researchers have focused on ribonucleases (RNases) as potential therapeutic agents. Some cytotoxic RNases are cancer-selective [1–3] and antivirally active [4, 5]. These properties are inherent to RNases of different origins; the most well-examined ones are onconases from oocytes of the northern leopard frog *Rana pipiens*, BS-RNase from bovine testicles, and microbial RNases from *Bacillus amyloliquefaciens* and *B. intermedius* (the new name of the species is *B. pumilus* [6]), barnase and binase, respectively. The pancreatic ribonuclease of cattle pancreas, commercially known as Ribonuclease amorphous, can be used to treat sinus infections and tick-borne encephalitis. However, an intracellular RNase inhibitor from human cells can decrease the activity of mammal RNases [7], thus restricting their medicinal use. In contrast to RNase A and RNase from human eosinophils, onconase and BS-RNase can suppress the replication of human immunodeficiency viruses type 1 in H9 leukemia cells without a toxic effect on the infected cells [4]. Binase, when injected intramuscularly into a site of street rabies virus inoculation in mice, guinea pigs, and rabbits,

has a considerable protective effect (40–67%) but does not suppress vaccine-induced antirabic immunity [5, 8]. An important point is that binase does not induce the synthesis of specific markers of the immune response, CD69 antigen and γ -interferon, in populations of CD8⁺ and CD4⁺ T lymphocytes; this fact indicates that the enzyme is devoid of the superantigenic properties inducing the polyclonal T-cell response [9]. Binase has been shown to decrease the infectious titer of the influenza type A (A/PR/8/34, A/Odessa/2882/82) and type B (B/Leningrad/369/76) viruses by two orders of magnitude, this activity being comparable with the activity of remantadin against the influenza A virus [10].

The search for effective antiviral products is an urgent task justified by the wide variability and global distribution of viruses. The aim of this study was to examine the action of binase on the pandemic influenza A/Hamburg/04/09 (H1N1) virus, the causative agent of the 2009 influenza epidemics. We found that a short-term (15–30 min) treatment of viruses with increasing concentrations of binase caused a proportional 3- to 10-fold decrease in the virus' ability to infect A549 lung adenocarcinoma cells. A binase concentration of

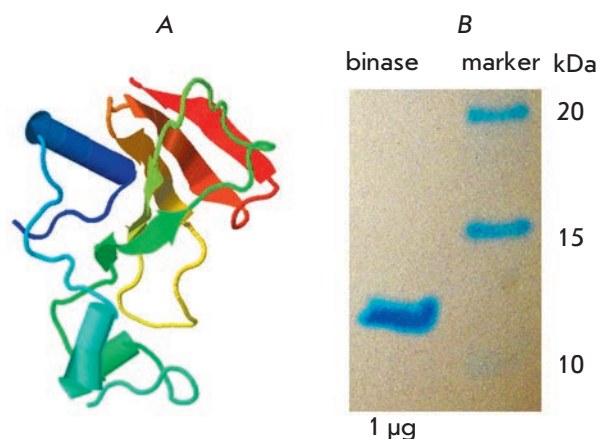


Fig. 1. Three-dimensional structure of RNase from *Bacillus pumilus* obtained using the Jmol program (www.jmol.org; binase PDB id: 1buj) (A); electrophoretogram confirming the purity of binase (B)

1 µg/mL was the most efficient and caused no inhibition of epithelial cells viability; this fact suggests that binase could be a promising antiviral agent.

EXPERIMENTAL

Bacterial RNase

The guanyl-specific RNase from *B. pumilus* 7P, binase, (12.2 kDa, 109 amino acid residues, pI 9.5) was homogeneously isolated from the culture fluid of *Escherichia coli* BL21 carrying the pGEMGX1/ent/Bi plasmid, according to A. Schulga *et al.* [11]. The molecular weight of binase, as well as its catalytic activity against synthetic substrates and high-polymeric yeast RNA, was already known (see Fig. 1A and [12, 13], respectively); specimen purity was confirmed by experiments (Fig. 1B).

Cell cultures

A549 (lung adenocarcinoma epithelial cell line) and MDCK II canine cocker spaniel kidney (from the collection of the Institute of Medicinal Virology Justus Liebig University, Giessen, Germany) were cultivated in DMEM supplemented with penicillin (100 U/mL), streptomycin (100 U/mL), and a 10% fetal bovine serum at 37°C and 5% CO₂.

Strain of the A/Hamburg/04/09 virus (H1N1) of influenza type A

The strain of the A/Hamburg/04/09 virus (H1N1) of influenza type A was obtained from the collection of the Giessen University in the form of a virus fluid. The

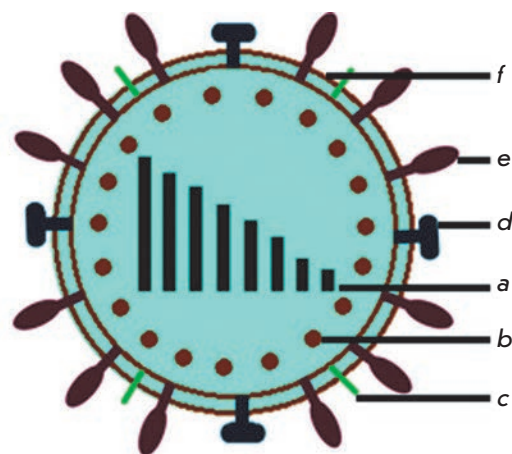


Fig. 2. Schematic representation of the influenza A (H1N1) virus. (a) 8 molecules of viral RNA coding the PB2, PB1, PA, HA, NP, NA, M (M1, M2) and NS (NS1, NS2) proteins; (b) structural protein M1; (c) integral membrane protein of the M2 ion channel; (d) neuraminidase; (e) hemagglutinin; (f) viral lipid bilayer

virus material was stored at -80°C. Schematic representation of the virus and its main components is provided in Fig. 2.

Cell viability

Cell viability in the presence of binase was determined from the activity of mitochondrial dehydrogenases converting the colorless derivative of the tetrazolium dye 3-(4,5-dimethylthiazol-2-yl)-2,5-diphenyltetrazolium bromide (MTT) (Sigma, Germany) into purple formazan crystals [14]. Staining intensity after a 24 or 48 h incubation of cells in the presence of 0.01–1000 µg/mL binase was determined from the absorbance of the formazan crystals dissolved in dimethylsulfoxide at 590 nm.

Ribonuclease activity

Ribonuclease activity in the culture medium of A549 cells was assessed from the amounts of acid-soluble products of the hydrolysis of yeast high-polymeric mRNA [15]. The amount of the enzyme that increased the optical density by one optical unit at 260 nm after incubation at 37°C for 1 h, calculated per mL of the enzyme solution, was taken as the activity unit.

Number of virus particles

The number of virus particles in the initial phage suspension was determined with a conventional hemagglutination assay of a 1.5% chicken erythrocyte suspension [16, 17]. The number of virus particles was expressed in hemagglutination units (HU) per mL, that

is, the maximum dilution of virus fluid able to cause hemagglutination of erythrocytes.

Infectious titer of the virus

An infectious titer of the virus was determined with the immunohistochemical techniques according to the number of focus-forming units (FFU) [18]. A virus suspension was added to the MDCK II monolayer and co-cultured at ambient temperature in the dark for 1 h; the virus suspension was then removed. The cells were further cultivated at 37°C and 5% CO₂ in a DMEM-Avicel supportive medium containing 1.25% of microcrystalline cellulose (FMC, Belgium), 0.36% of bovine serum albumin, and 1 µg/mL of trypsin treated with the TPCK chemotrypsin inhibitor (Sigma, USA). After 28 h of incubation, the culture medium was discarded, the cells were treated with ice Triton X-100 for 90 min, with mouse antibodies against the NP-protein of the influenza virus, and with the secondary anti-mouse antibodies conjugated to horseradish peroxidase (HRP)

(Santa Cruz Biotechnology, USA); and stained with AEC (Sigma, USA) in dimethylformamide. Thereafter, the plate was scanned to estimate the FFU number. An infectious titer was expressed in FFU/mL of the virus fluid.

Virus reproduction

Virus reproduction was assayed with a 1-day-old A549 monolayer culture (3×10^4 cells per well); the infection rate was 1 or 10 virus particles per 100 cells [multiplicity of infection (MOI) 0.01 or 0.1, respectively]. The binase effect on the virus infectivity was analyzed with the infection of A549 cells with RNase preincubated with the virus for 15–60 min. The cells were dark-incubated at room temperature for 1 h to adsorb the virus; the unadsorbed virus was removed, and the infected cells were incubated in DMEM supplemented with 0.36% of bovine serum albumin and 1 µg/mL of TPCK trypsin at 5% CO₂ and 37°C. After incubation for 12 to 24 h (single-cycle or multi-cycle virus reproduction, respectively), the supernatant was discarded and assayed for the FFU number. The cells were washed with a phosphate buffer and stained with 1.25% Coomassie Brilliant Blue (Merck, Germany) to visualize the cells that survived the infection. The experimental scheme is shown in Fig. 3.

Statistical analysis

The statistical analysis of the results from four runs of each experiment was performed by standard methods in Microsoft Excel 2010 and the SigmaPlot 10 software.

RESULTS AND DISCUSSION

Binase cytotoxicity against A549 adenocarcinoma cells

Binase at a concentration approaching 1 mg/mL of the medium (corresponding to 82 µM) exerts a concentration- and time-dependent inhibiting (up to the total cell lethality) effect on the viability of A549 human lung adenocarcinoma cells. The cytotoxic binase concentration that caused 50% cell lethality (CC₅₀) was 420–490 µg/mL after a one- or two-day exposure, respectively (Fig. 4 A, B). A concentration of 133 µg/mL caused 5% cell lethality during 24 h (CC₉₅) (Fig. 4A). This value was significantly lower (15 µg/mL) for a 48-h treatment (the data are not presented). Thus, the binase concentrations that have no toxic effect on the cells during 1-day exposure are below 133 µg/mL. These data are consistent with the values of binase cytotoxicity against A549 cells assessed earlier with the WST assay and cytometry [19]. Since binase cytotoxicity against malignant lung epithelial cells is more pronounced than their activity against normal cells [20], one can assume that even a tenfold increase in the

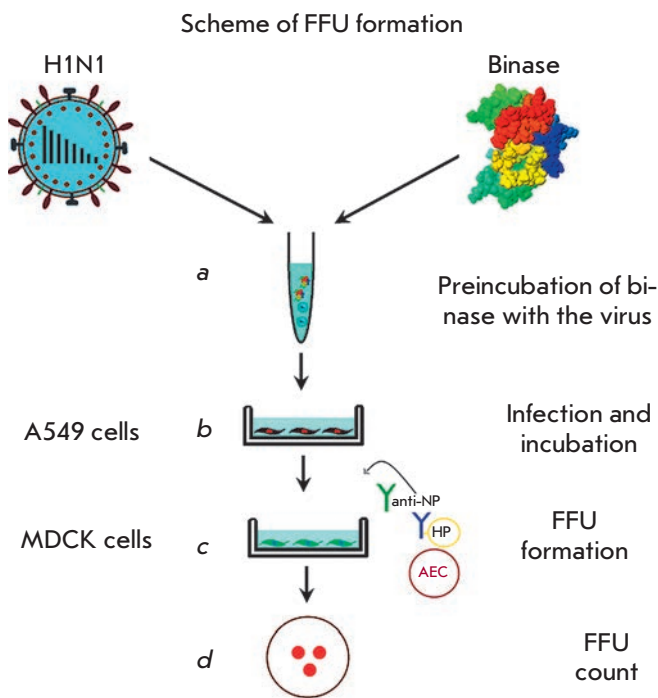


Fig. 3. Scheme of the experiment on FFU formation. (a) preincubation of viruses with binase (15–60 min); (b) A549 cells infected with binase-treated viruses, followed by incubation for 12–24 h; (c) A549 cell culture fluid tested for the presence of viruses detected by FFU in the MDCK cell culture by adding a primary viral anti-NP antibody and horseradish peroxidase conjugated anti-mouse secondary antibody after 28 h of cultivation; (d) direct count of FFU

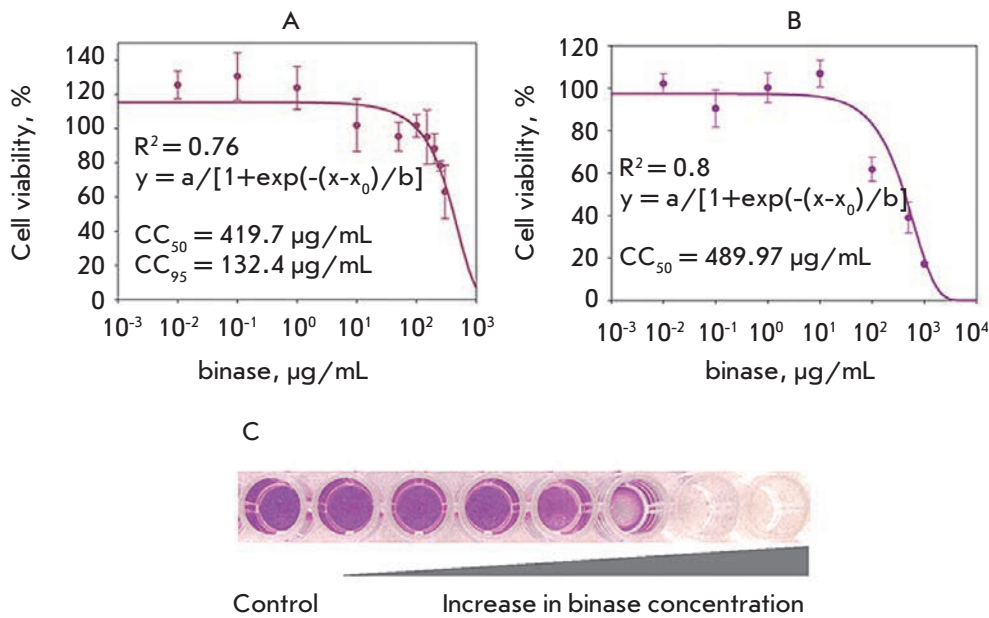


Fig. 4. Cell viability of A549 at different binase concentrations during 24 h (A) and 48 h (B) of incubation. The R-squared value calculated by SigmaPlot 10. CC_{50} and CC_{95} – the binase concentration which induces 50% and 5% cell death, respectively. (C) Visualization of A549 cell death at increasing binase concentration (MTT assay)

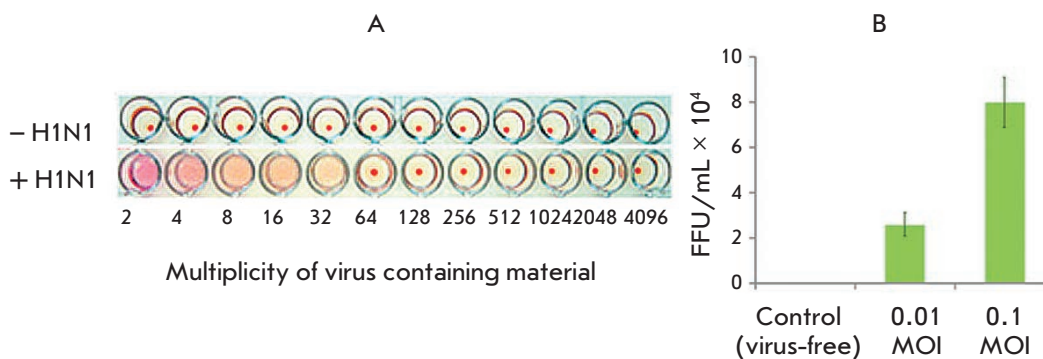


Fig. 5. Analysis of virus-containing material for the existence of viral particles by HA unit formation calculated as a multiplicity of dilutions (A) and FFU after cultivation of A549 cells for 24 h with different MOIs (B)

RNase concentration may have no negative effect on the viability of normal epithelial cells.

Most RNases involved in antiviral cell protection are synthesized by the host cells, and these enzymes direct the cells towards apoptotic death. In animals, the antiviral effect is exerted by ribonucleases from the RNase A family [21, 22], including RNase L, whose activation causes apoptosis in the infected cells [23]. Eosinophil ribonucleases reduce the *in vitro* infectivity of virus particles by penetrating into a virus' capsid and destroying its viral genomic RNA [24]. Examination of external RNases showed that a pancreatic RNase has anti-influenza activity on chicken embryos lacking a mammal ribonuclease inhibitor but had no inhibitory activity on mice [10]. Onconase can destroy the RNA of the human immunodeficiency virus while not affecting the RNA of the host cells [25]; however, a similar frog RNase from *Rana catesbeiana* not only inhibits the replication of the Japanese encephalitis virus, but also stimulates apoptosis in virus-infected cells [26]. We

found that when used at the aforementioned concentrations, binase causes no death of epithelial cells and, in addition, has no immunogenic properties and does not induce a superantigenic T-cell response [9]. This fact significantly increases the potential for the practical use of RNase.

Binase reduces the infectious titer of the influenza A (H1N1) virus

The hemagglutination assay showed that the initial virus fluid contained the A/Hamburg/04/09 virus with a hemagglutination titer of 32 HA units/mL (Fig. 5A). This value indicates that the content of virus particles in the suspension is sufficient, making it possible to analyze virus resistance to antiviral agents. Exposure of A549 cells to the virus at 0.1 and 0.01 MOI showed its high infectivity, while an increase in infection multiplicity was followed by an increase in the FFU number in the plate wells (Fig. 5B). The predicted rate of the virus material infectious titer was 5.8×10^6 FFU/mL.

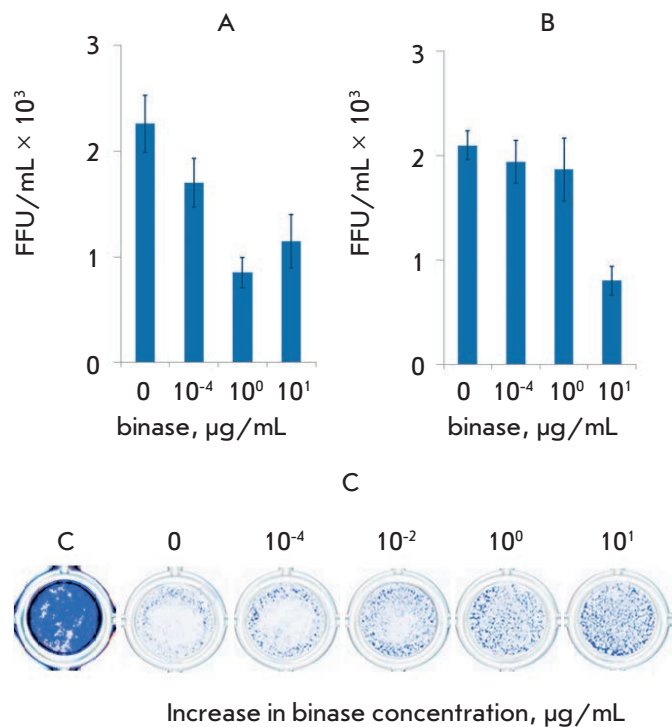


Fig. 6. Reduction of viral infectious units under binase treatment during 30 min (A) and 60 min (B) after preincubation with the enzyme; enhancement of survival of virus-infected cells after treatment with different concentrations of binase and incubation during 12 h. Visualization of A549 cells using a methylene brilliant blue dye (C)

To determine the antiviral effect of binase, the virus was co-preincubated with the enzyme at concentrations of less than cytotoxic (10⁻⁴–10¹ µg/mL) for 30 or 60 min; the A549 cells were infected with the resulting suspension, and the degree of their infection at 0.1 MOI was estimated.

At a single-cycle replication of virus, when the infected cells were cultivated for 12 h, the virus titer was proportional to the increase in the binase concentration (Fig. 6). Treatment with 1 µg/mL binase reduced virus reproduction threefold (Fig. 6A).

At a multi-cycle replication for 24 h, the antiviral effect of binase was higher: after 60 min of treatment with 10 µg/mL binase, virus reproduction decreased 6-fold (Fig. 7B). Death of A549 cells was caused by the cytopathic effect of the virus, both at single-cycle and multi-cycle replications (Figs. 6C, 7C, binase-free wells). However, the number of survived cells in a monolayer increased with the increasing binase concentration used for virus treatment. Maximum (up to 10-fold) inhibition of virus reproduction was observed one day after cell exposure to the virus preincubated with 1 µg/mL binase for 30 min (Fig. 7A).

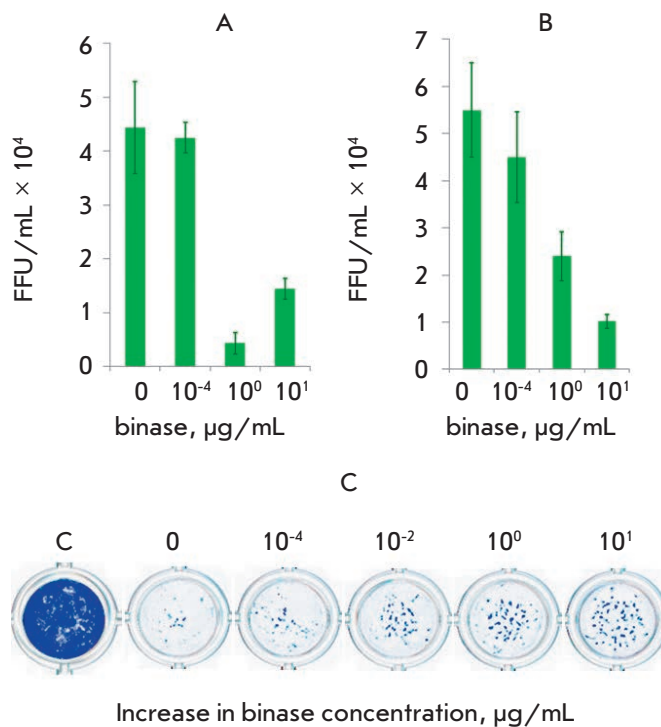


Fig. 7. Reduction of viral infectious units under binase treatment during 30 min (A) and 60 min (B) after preincubation with the enzyme; enhancement of survival of virus-infected cells after treatment with different concentrations of binase and incubation during 24 h. Visualization of A549 cells using a methylene brilliant blue dye (C)

The maximum effect of binase was achieved after multi-cycle virus replication; this was the reason for further assessment of the antiviral effect of binase one day after infection: the duration of the virus-enzyme preincubation period varied from 15 to 60 min, and the levels of A549 infection differed by two orders of magnitude (0.1 and 0.01 MOI) (Fig. 8A, table 1). The antiviral effect of binase depended both on the period of co-preincubation with the virus and on the degree of virus infection. The high infection level (0.1 MOI) could provide a higher possibility of virus contacts with binase molecules and, therefore, stronger binase effect compared to a low level of cell infectivity (0.01 MOI) (Table 1).

Independently of the cell infectivity level, the maximum antiviral effect was observed after 30 min of binase-virus co-preincubation; a longer period (60 min) of co-preincubation caused a threefold decrease in the antiviral effect (Table 1). With a low (0.01 MOI) level of cell infection, the antiviral activity of binase after 15 and 30 min enzyme treatments were virtually the same; therefore short-term (15 min) virus incubation with RNase can be regarded as sufficient for achieving

Table 1. Decrease in virus infectious titer compared to that in the initial viral fluid at multi-cycle infection under the binase effect depending on the cell infectivity level and duration of virus preincubation with the enzyme

Binase, $\mu\text{g/mL}$	Preincubation of virus with binase, min					
	15	30	60	15	30	60
	0.1 MOI			0.01 MOI		
0	100 \pm 25.3	100 \pm 19.2	100 \pm 18.1	100 \pm 21.0	100 \pm 7.4	100 \pm 35.4
1	17.5 \pm 9.0*	9.7 \pm 4.5*	43.6 \pm 9.4*	36.4 \pm 9.8*	27.5 \pm 3.5*	93.8 \pm 36.9

*Significant differences with binase treatment-free control. Virus titer in the initial material without binase treatment is taken as 100%.

Table 2. Increase in catalytic activity of binase in culture medium of A549 cells (U/mL) after 48 h cultivation

Binase, $\mu\text{g/mL}$	0 h	48 h
0	5.3 \pm 1.4	63.0 \pm 9.3
1	7107.1 \pm 770.7	4078.3 \pm 462.7
10	64600.0 \pm 6648.7	45000.0 \pm 5870.0

the optimal antiviral activity. During the preincubation period (15 min), 1 $\mu\text{g/mL}$ of binase decreased the number of virus particles in cells approximately sixfold at 0.1 MOI and threefold at 0.01 MOI (Table 1). An increase in the RNase concentration to 10 $\mu\text{g/mL}$ caused no decrease in the virus titer after a 30min treatment (Figs. 6A, 7A) but enhanced the antiviral effectiveness of binase after 60-min preincubation (Figs. 6B, 7B).

Thus, binase concentrations not toxic for A549 cells (1–10 $\mu\text{g/mL}$) inhibit the reproduction of the influenza A (H1N1) virus when pretreated with binase for 15–30 min.

Immunofluorescent methods demonstrated that binase had penetrated into the A549 cells even within the first hours of incubation [27]. The catalytic activity of the enzyme is known to be maintained in myeloid progenitor cells for 48 h [28]. We registered a decrease in binase catalytic activity in a culture medium of A549 cells treated with 1 and 10 $\mu\text{g/mL}$ binase (Table 2); this fact also attests to enzyme penetration into a cell. The mechanism of ribonuclease internalization is conditioned by the interaction between the cationic protein and the negative charge of the tumor cell surface; further cell penetration is provided by endocytosis [1]. Since the virus penetrates into a cell in a similar way,

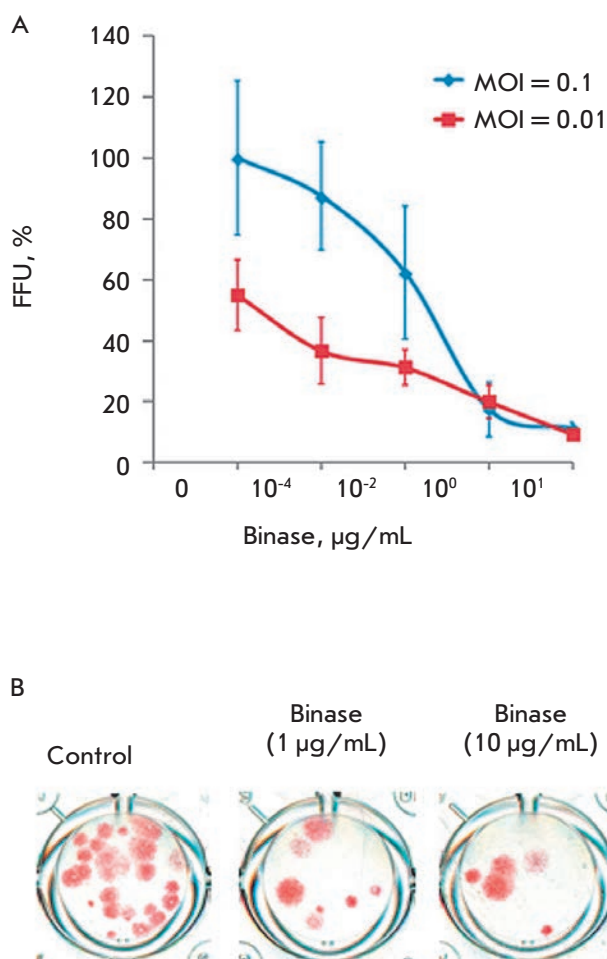


Fig 8. Reduction of viral infectious units under binase treatment after preincubation with the enzyme during 15 min (A) and visualization the FFU decrease in the MDCK cell culture. The value of FFU/mL of 0.1 MOI without treatment with binase was taken as 100%

binase–virus interaction can take place inside the cell as well (in particular, inside endosomes). The receptors of the influenza virus hemagglutinin on the host cell surface carry a negative charge provided by the sialic acid [29, 30]; hence, binase can interact with the surface of such cells via the electrostatic mechanism and penetrate into them independently of the virus. In the virus-infected cells, binase will cleave the viral RNA for at least 48 h until it is hydrolyzed by cell proteases [28]. It is noteworthy that the high temperature resistance of binase and maintenance of its activity in a wide pH range [31] is one of the significant factors conditioning its use.

Binase demonstrates antiviral activity against the viruses of rabies, the hoof-and-mouth disease, some plant viruses, and the seasonal influenza virus [8, 10, 32]. Up to 500 thousand human deaths are caused annually by the influenza virus. According to the WHO, the pandemic influenza caused by the A virus (H1N1) alone affected 414,000 humans, 5,000 cases ending in a fatal outcome (www.who.int). The continuous evolution of the virus due to the antigen drift and mixing of viral genetic material limits the efficiency of currently recognized protective strategies, including vaccination and administration of neuraminidase inhibitors. This fact explains the importance of a new therapeutic strategy, whose effectiveness would be independent of a virus' subtype. Our data show the high promise of developing the bacterial RNase-based strategy. A binase possessing a number of advantages as compared to its eukaryotic analogs (resistance to an inhibitor of mammalian RNases and easy production) can become the next-generation antiviral agent.

CONCLUSION

The high death rates that accompany influenza impose a serious social and economic burden on society; therefore, containing pandemics of influenza A type/H1N1 viruses is one of the urgent tasks facing the scientific community. Rapid spreading of a viral infection can be

checked by using broad-specificity drugs whose effectiveness is independent of particular mutations in the virus' genome. We have shown that concentrations of secretable ribonuclease from *B. intermedius* (binase) e antiviral toxicity have no toxic effect on human epithelial cells. The pretreatment of viral particles with binase at approximately a 1 µg/mL concentration caused a significant (up to tenfold) decrease in virus infectivity and suppressed the development of the virus-induced cytopathic effect in a A549 human lung cell line at various multiplicity of infections both during single-cycle and multi-cycle virus reproduction. Fine-tuned mechanisms of antiviral activity need further examination, although it is conceivable that they include both the charge–charge interaction between cation binase and the negatively charged hemagglutinin receptors on the surface of a host cell and catalytic cleavage of the viral RNA inside cells. The data confirm the applicability of binase as an effective antiviral agent against the pandemic influenza A (H1N1). ●

The authors are grateful to Prof. S. Pleshka from the Yustus Liebig University (Giessen, Germany) for the opportunity to conduct a number of experiments in his laboratory, and to V.I.Vershina and V.V.Ulyanova, the staff members of the Microbiology Chair of the Kazan Federal University, for fruitful discussions.

The work was also funded by the subsidy of the Russian Government to support the Program of competitive growth of Kazan Federal University among world class academic centers and universities.

This work was supported by the Russian Foundation for Basic Research (grant no. 12-04-01226a), the Yevgeniy Zavoyskiy Program (DAAD together with the Ministry of Education and Science of the Tatarstan Republic), and the federal target-oriented program “Scientific and Scientific-Pedagogical Personnel of Innovative Russia for 2009-2013” (State Contract no. 16.740.11.0611).

REFERENCES

- Makarov A.A., Ilinskaya O.N. // FEBS Lett. 2003. V. 540. № 1–3. P. 15–20.
- Makarov A.A., Kolchinsky A., Ilinskaya O.N. // Bioessays. 2008. V. 30. № 8. P. 781–790.
- Ardelt W., Ardel B., Darzynkiewicz Z. // Eur. J. Pharmacol. 2009. V. 625. № 1–3. P. 181–189.
- Youle R.J., Wu Y.N., Mikulski S.M., Shogen K., Hamilton R.S., Newton D., D'Alessio G., Gravell M. // Proc. Natl. Acad. Sci. 1994. V. 91. № 13. P. 6012–6016.
- Gribencha S.V., Potselueva L.A., Barinskij I.F., Balandin T.G., Deev S.M., Leshchinskaia I.B. // Vopr. Virusol. 2004. V. 49. № 6. P. 38–41.
- Sharipova M.R., Toimentseva A.A., Sabirova A.R., Mukhametzianova A.D., Akhmetova A.I., Mardanova A.M., Balaban N.P. // Mikrobiologiya. 2011. V. 80. № 3. P. 424–426.
- Leland P.A., Raines R.T. // Chem. Biol. 2001. V. 8. № 5. P. 405–413.
- Gribencha S.V., Potselueva L.A., Barinskii I.F., Deev S.M., Balandin T.G., Leshchinskaia I.B. // Vopr. Virusol. 2006. V. 51. № 5. P. 41–43.
- Ilinskaya O.N., Zelenikhin P.V., Petrushanko I.Y., Mitkevich V.A., Prassolov V.S., Makarov A.A. // Biochem. Biophys. Res. Commun. 2007. V. 361. № 4. P. 1000–1005.
- Schneider M.A., Shtil'bans E.B., Kuprianov-Ashin E.G., Potselueva L.A., Zaikonnikova I.V., Kurinenko B.M. // Antibiot. Khimioter. 1990. V. 35. № 3. P. 27–31.
- Schulga A., Kurbanov F., Kirpichnikov M., Protasevich I.,

RESEARCH ARTICLES

- Lobachev V., Ranjbar B., Chekhov V., Polyakov K., Engelborghs Y., Makarov A. // *Protein Eng.* 1998. V.11. № 9. P. 775–782.
12. Yakovlev G.I., Moiseyev G.P., Struminskaya N.K., Borzykh O.A., Kipenskaya L.V., Znamenskaya L.V., Le-schinskaya I.B. Chernokalskaya E.B., Hartley R.W. // *FEBS Lett.* 1994. V. 354. № 3. P. 305–306.
13. Ilinskaya O.N., Karamova N.S., Ivanchenko O.B., Kipenskaya L.V. // *Mutat. Res.* 1996. V. 354. № 2. P. 203–209.
14. Mosmann T. // *J. Immunol. Methods.* 1983. V. 65. № 1–2. P. 55–63.
15. Anfinsen C.B., Redfield R.R., Choate W.I., Page J., Carrol W.R. // *J. Biol. Chem.* 1954. V. 207. P. 201–210.
16. Wegmann T.G., Smithies O. // *Transfusion.* 1966. V. 6. № 1. P. 67–73.
17. Pleschka S., Stein M., Schoop R., Hudson J.B. // *Viol. J.* 2009. V. 6. № 197. (doi:10.1186/1743-422X-6-197)
18. Payne A.F., Binduga-Gajewska I., Kauffman E.B., Kramer L.D. // *J. Virol. Meth.* 2006. V. 134. № 1–2. P. 183–189.
19. Cabrera-Fuentes H.A., Zelenikhin P.V., Kolpakov A.I., Ilinskaya O.N. // *J. CTTE.* 2012. V. 7. № 3. P. 72–76.
20. Cabrera-Fuentes H.A., Zelenikhin P.V., Kolpakov A.I., Preissner K.T., Ilinskaya O.N. // *Proceedings of Kazan State University. Science series.* 2010. V. 152. № 1. P. 121–126.
21. Rosenberg H.F., Domachowske J.B. // *J. Leukoc. Biol.* 2001. V. 70. № 5. P. 691–698.
22. Rosenberg H.F., Domachowske J.B. // *Curr. Pharm. Biotechnol.* 2008. V. 9. № 3. P. 135–140.
23. Liang S.L., Quirk D., Zhou A. // *IUBMB Life.* 2006. V. 58. № 9. P. 508–514.
24. Domachowske J.B., Dyer K.D., Adams A.G., Leto T.L., Rosenberg H.F. // *Nucleic Acids Res.* 1998. V. 26. № 14 P. 3358–3363.
25. Saxena S.K., Gravell M., Wu Y.N., Mikulski S.M., Shogen K., Ardelt W., Youle R.J. // *J. Biol. Chem.* 1996. V. 271. № 34. P. 20783–20788.
26. Lee Y.H., Wei C.W., Wang J.J., Chiou C.T. // *Antiviral Res.* 2011. V. 89. № 3 P. 193–198.
27. Cabrera-Fuentes H.A., Zelenikhin P.V., Kolpakov A.I., Preissner K., Ilinskaya O.N. Comparative toxicity of binase towards tumor and normal cell. *Toxicol.* 2013. (doi 10.1016/j.toxicol.2013.03.015).
28. Mitkevich V.A., Tchurikov N.A., Zelenikhin P.V., Petrushanko I.Y., Makarov A.A., Ilinskaya O.N. // *FEBS J.* 2010. V. 277. P.186–196.
29. Arinaminpathy N., Grenfell B. // *PLoS One.* 2010. V. 5. № 12. P. e15674 (doi: 10.1371/journal.pone.0015674).
30. Kobayashi Y., Suzuki Y. // *PLoS One.* 2012. V. 7. № 7. P. e40422 (doi: 10.1371/journal.pone.0040422).
31. Ulyanova V., Vershinina V., Ilinskaya O. // *FEBS J.* 2011. V. 278. № 19. P. 3633–3643.
32. Alekseeva I.I., Kurinenko B.M., Kleiner G.I., Skuia A.Zh., Penzikova G.A. // *Antibiotiki.* 1981. V. 26. № 7. P. 527–532.

Competition within Introns: Splicing Wins over Polyadenylation via a General Mechanism

M. Tikhonov, P. Georgiev*, O. Maksimenko*

Department of the Control of Genetic Processes, Institute of Gene Biology, Russian Academy of Sciences, 34/5 Vavilova Str., Moscow, Russia, 119334

*E-mail: mog@genebiology.ru, georgiev_p@mail.ru

Received 17.06.2013

Copyright © 2013 Park-media, Ltd. This is an open access article distributed under the Creative Commons Attribution License, which permits unrestricted use, distribution, and reproduction in any medium, provided the original work is properly cited.

ABSTRACT Most eukaryotic messenger RNAs are capped, spliced, and polyadenylated via co-transcriptional processes that are coupled to each other and to the transcription machinery. Coordination of these processes ensures correct RNA maturation and provides for the diversity of the transcribed isoforms. Thus, RNA processing is a chain of events in which the completion of one event is coupled to the initiation of the next one. In this context, the relationship between splicing and polyadenylation is an important aspect of gene regulation. We have found that cryptic polyadenylation signals are widely distributed over the intron sequences of *Drosophila melanogaster*. As shown by analyzing the distribution of genes arranged in a nested pattern, where one gene is fully located within an intron of another gene, overlapping of putative polyadenylation signals is a fairly common event affecting about 17% of all genes. Here we show that polyadenylation signals are silenced within introns: the poly(A) signal is utilized in the exonic but not in the intronic regions of the transcript. The transcription does not end within the introns, either in a transient reporter system or in the genomic context, while deletion of the 5'-splice site restores their functionality. According to a full *Drosophila* transcriptome analysis, utilization of intronic polyadenylation signals occurs very rarely and such events are likely to be inducible. These results confirm that the transcription apparatus ignores premature polyadenylation signals for as long as they are intronic.

KEYWORDS transcription termination; splicing; polyadenylation signals; exon; intron.

INTRODUCTION

During maturation, eukaryotic messenger RNAs undergo capping, splicing, and polyadenylation, and the molecular machineries responsible for these modifications are coupled both to each other and to the transcriptional apparatus [1–5]. Collaboration between these machineries is confirmed by the existence of splicing proteins and the cleavage and polyadenylation proteins that can be recruited to RNA polymerase II (RNAP II) *in vitro* prior to transcription and then transferred to the RNA [6, 7]. The process of terminal exon definition is another example of such collaboration. It has been shown that recognition of the 3'-splice site (3'SS) of the gene's last intron strongly improves the efficiency of the downstream polyadenylation site [8–10] and that the 3'-SS-associated factor U2AF enhances the function of the polyadenylation site by direct molecular contacts with poly(A) polymerase [11]. Similarly, the protein components of U2snRNP that associate with the 3'SS and nearby lariat branch point help to enhance downstream 3'-end processing through interactions with CPSF (cleavage and polyadenylation

specificity factor) [12]. U2AF65 (splicing factor U2AF 65 kDa subunit) stimulates pre-mRNA 3'-end processing via the interaction of its arginine/serine-rich region with an RS-like alternating charge domain of the 59 kDa subunit of the human cleavage factor I (CF Im) [13]. It is likely that poly(A) site cleavage is followed by polyadenylation of the 3'-end and, finally, by splicing of the last intron [14], and that poly(A) addition triggers RNA release from the polymerase only after being licensed by splicing [15]. Another relevant fact is that U1 snRNP, an essential component in defining the 5'-splice site, interacts with mammalian polyadenylation cleavage factor I (CF Im) [16]. These data provide evidence for the interrelation of all processes involved in gene transcription, including its initiation, transcript elongation, splicing, and polyadenylation.

Polyadenylation signals (PASs) are not complex, and it appears that these elements are not confined to the 3'-UTRs of genes but occur throughout the genome, including the 5'-UTRs [17]. Premature PAS utilization may result in gene dysfunction and, therefore, must be prevented. It has been discovered that PASs become

functionally silent when they are positioned close to transcription start sites in either *Drosophila* or human cells [17]. PAS were also found upstream of 5' splice sites, and point-mutated splice donor activates an upstream cryptic polyadenylation (CpA) site [18]. In the bovine papilloma virus, utilization of the late PAS at earlier stages of infection is prevented by the presence of a closely positioned, upstream 5'SS. Recognition of this 5'SS by U1snRNP blocks poly(A) polymerase activity at the late PAS by direct interaction with the 70K protein component of U1snRNP [19]. A recent whole genome study on the effect of functional U1 snRNP knockdown in HeLa cells has revealed cases of premature cleavage and polyadenylation in numerous pre-mRNAs at cryptic PASs, frequently in introns near the transcription start site [20]. Based on the fact of polyadenylation silencing by U1 snRNP it was suggested that recruiting of U1 snRNP to the target pre-mRNA inhibits poly(A)-tail addition, causing degradation of such RNA species in the nucleus [21, 22]. Quantitative analysis of a number of mRNA variants generated by intronic PASs suggests that the intronic polyadenylation activity can vary under different cellular conditions [23]. For example, the level of U1 snRNP defines the length of the transcript and the ability to utilize premature PAS within introns and in distal 3'UTRs [24]. In view of the abovementioned data, it is likely that splicing and polyadenylation within introns interact in a competitive manner.

In this study, we focus on the relationships between splicing and polyadenylation in cases of intronic location of PASs in the *Drosophila* genome. Our results confirm the wide distributions of these signals within the introns of genes and show that PASs are silenced within introns in a transient reporter system, as well as in the genomic context. Meanwhile, deletion of 5'SS restores polyadenylation activity. Analysis of RNA-seq data for different cell lines and development stages of *Drosophila* provides evidence of a switch between synthesized isoforms in case of alternative 3'-exon-inclusion transcripts.

EXPERIMENTAL

Bioinformatic poly(A) signal prediction

The PolyA_SVM program was used to identify putative polyadenylation sites [25]. This program was previously shown to be suitable for site prediction in *Drosophila* [17]. The program searches for poly(A) signals by using a window-based scoring scheme to evaluate the fitness of 15 *cis*-elements identified from known human poly(A) signals [25]. The whole data set of *D. melanogaster* annotated introns is available from FlyBase [26]. The probability for an element to be a poly(A) signal is character-

ized by the E-value (the lower the value, the higher the probability). The output was programmatically sorted into three categories: "site is present," "site is not found," and "input sequence is too short."

Search for nested genes

Drosophila melanogaster genome annotation data from FlyBase [26] were used to parse the coordinates of genes and introns. A gene was considered to be nested if its start coordinate was greater than the start coordinate of the corresponding intron and its end coordinate was smaller than the end coordinate of the intron.

Construction of plasmid reporter system

The bicistronic plasmid constructs were generated in pAc5.1/V5-His B (Invitrogen). The firefly and *Renilla* luciferase sequences were taken from the pGL3Basic and pRL-CMV vectors (Promega), respectively. The *reaper* gene IRES was amplified from genomic DNA and cloned upstream of the firefly luciferase sequence. The SV40 terminator sequence was taken from the pAc5.1/V5-His B vector. The intron and terminator of the *yellow* gene were taken from a 8-kb gene fragment kindly provided by P. Geyer. The polyadenylation signals of the *nop5* and *eIF6* genes were amplified from genomic DNA. To produce the artificial intron (AI), oligonucleotides containing the desired sites were synthesized. The *lacZ* CDS region was taken as a linker sequence between the donor and acceptor splicing sites.

Cell culture, transfection, RNA purification, and dual luciferase assay

Drosophila S2 cells were grown in a SFX medium (HyClone) at 25°C. Transfection of plasmids was performed with the Cellfectin II reagent (Invitrogen) according to the manufacturer's instructions. Typically, cells were transfected in six-well plates and grown for 24 to 48 h before harvesting.

Total RNA was extracted from the transfected cells using the TRI reagent (Ambion) according to the manufacturer's instructions. To fractionate nuclear and cytoplasmic RNAs, S2 cells collected from a 100 mm dish were washed with PBS, pelleted, and re-suspended in 100 µl of TD (0.8% NaCl, 0.028M KCl, 0.01% Na₂HPO₄, 0.3% Tris-HCl; pH 7.4–7.5). The mixture was supplemented with 100 µl of TD with 1% NP-40 and SUPERase-In (Ambion) and kept on ice for 5 min. The sample was then centrifuged, and the supernatant fluid was used to isolate the cytoplasmic RNA fraction with the TRI reagent (Ambion). The nuclear pellet was re-suspended in 200 µl of TD with 0.5% NP-40 and SUPERase-In, incubated on ice, and centrifuged again. The nuclear RNA fraction was isolated from the pellet using the TRI reagent.

The dual luciferase assay was performed with the Firefly & Renilla Luciferase Assay Kit (Biotium).

RNA analysis

For Northern analysis, 5–20 µg of total RNA was separated in 1% agarose gel in the presence of formaldehyde and blotted onto a positively charged nylon membrane (BrightStar-Plus, Ambion) in a Trans-Blot SD Semi-Dry Electrophoretic Transfer Cell (Bio-Rad), which was followed by cross-linking under UV light. The regions of interest were amplified and cloned under the T7 promoter. The membranes were hybridized with *in vitro* synthesized RNA probes (Ambion MEGAscript and MAXIscript kits) with biotin-16-UTP (Roche) inclusion and examined using a Chemiluminescent Nucleic Acid Detection Module (Thermo Scientific).

Real-time PCR experiments were performed with reverse transcription products. RNA was treated with two units of Turbo DNase I (Ambion) for 30 min at 37°C to eliminate genomic DNA. The synthesis of cDNA was performed using ArrayScript reverse transcriptase (Ambion) in a reaction mixture containing 5 µg of RNA and random hexamer primers. Specific cDNA fragments were quantitatively analyzed by real-time PCR using a CFX96 Thermal Cycler (Bio-Rad). At least three independent experiments with each primer set were performed for three independent RNA samples. Relative levels of mRNA expression were calculated using the cycle threshold method.

Analysis of isoform expression pattern based on RNA-seq data

All procedures were performed programmatically using Java language. We used the genome annotation data from FlyBase (release 5.40) to search for transcripts ending within an intron. These were transcripts with the last exon starting upstream of the donor splice site and the end of the transcript located between the splicing signals. The genes overlapping with each other were then excluded from consideration, and analysis was confined to the genes with transcripts of only two forms, the first being spliced and the second ending within an intron. SAM files with RNA-seq information were obtained from modENCODE for 30 development stages and 4 cell lines, and their reads were superimposed and matched up with the structural features of genes. The mean value of the read density for the 3'-exon was taken to reflect the level of the spliced form. The level of the intron-cleaved/polyadenylated isoform was calculated as the difference between the mean values of the read density for the region between the 5' splice site and the transcript end and for the region between the transcript end and the 3' splice site (probably corresponding to unspliced RNA). A heat

map was created to visualize the expression pattern of each isoform and the ratio of the intron-intron-cleaved/polyadenylated isoform to the sum of two forms.

RESULTS

PASs are widely present in *Drosophila* introns

As noted above, PASs appear to be widely distributed throughout the genome, and their premature utilization may result in gene dysfunction. Hence, there should be mechanisms for preventing utilization of inappropriate PASs. Previously, polyadenylation silencing was shown to take place in the 5'UTRs of genes [17]. The occurrence of any inappropriate signals in coding sequences is prevented by selection pressure, but non-coding intronic sequences are prone to change and can contain premature PASs. We checked how widely such signals are distributed within the intronic sequences of *Drosophila* genes. For this purpose, we used the PolyA_SVM program designed for the analysis and prediction of mRNA polyadenylation sites by a Support Vector Machine [25]. This program was previously shown to be suitable for site prediction in *Drosophila* [17].

The full set of 58 594 *Drosophila* intron sequences was taken from the FlyBase genome annotation database, release 5.34 [26]. Approximately 55% of these sequences were shorter than 120 bp, the minimum length necessary for running the above program (Figure 1A); two-thirds of the other sequences (about 30% of the total set) were predicted to contain one or more PAS copies. Thus, putative PASs were found to be widely distributed in *Drosophila* introns. There are two functional possibilities for such intronic PASs: they can be either silenced or utilized. In the first case, the signal has no effect on transcription and subsequent splicing; in the second case, transcription is untimely interrupted by the signal.

In this context, it was of interest to study the genes arranged in a nested pattern, where one ('nested') gene is located within an intron of another ('host') gene. In this case, a PAS from the nested gene should have no effect on the host gene transcription. The main difference (except in length) between the transcripts of the host and nested genes at the time of read-through of the PAS of the latter is that the host gene transcript contains the 5' splice site. We analyzed the distribution of such genes using the FlyBase data [26] (Fig. 1B). The coordinates of genes and introns were used for searching for cases where one gene is fully located within an intron of another gene. We determined 865 host genes that contained 1,651 nested genes within the introns on both strands. Among them, 727 nested genes had the same transcription direction as the host genes, and, therefore, their putative regulatory elements over-

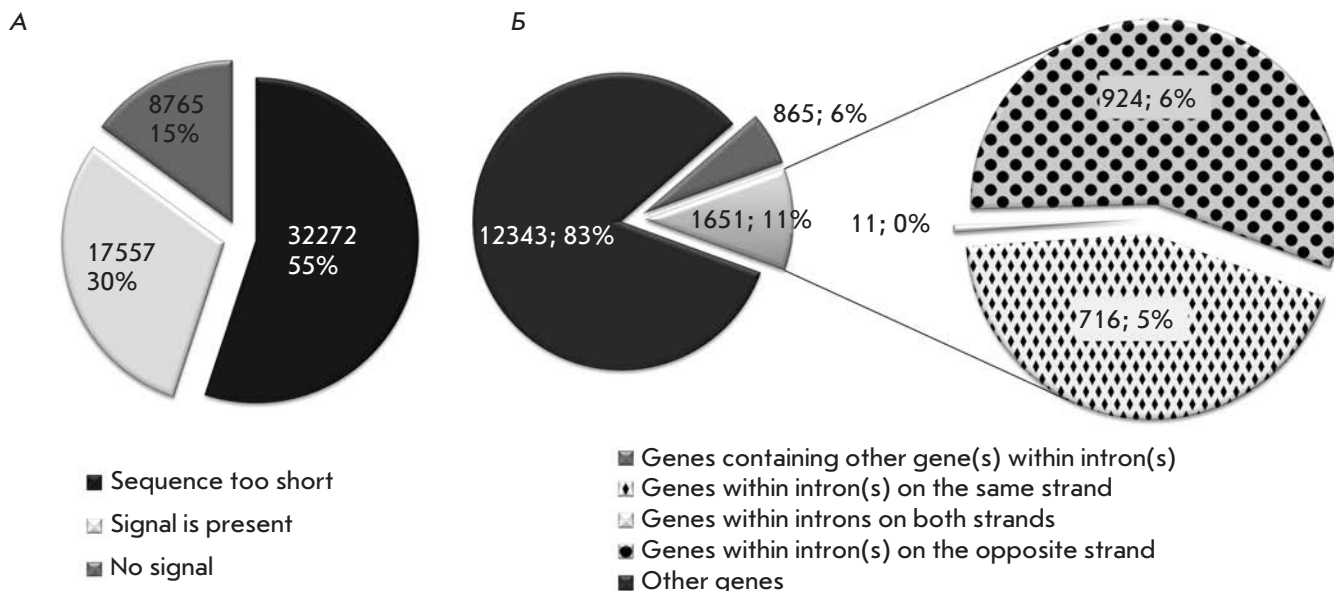


Fig. 1. Poly(A) signals are widely distributed in *Drosophila* introns. **A.** Pie chart showing the proportion of introns with or without poly(A) signals and of short introns as predicted by the PolyA_SVM program. **B.** Pie charts showing the proportions of the genes containing other gene(s) within introns (host genes) and of genes enclosed into introns (nested genes) divided into three groups according to their location on DNA strands

lapped with those of the latter. Thus, we found that PASs are widely distributed over the intron sequences and that overlapping of putative PASs signals is a fairly common event affecting about 17% of genes.

Experimental evidence for PAS utilization in exonic, but not intronic, transcript regions

As shown above, the transcription machinery frequently stumbles due to untimely PASs within introns. If these intronic PASs are indeed utilized, this could be shown on the pairs of nested and host genes. To test whether the PAS from the nested gene influences the transcription of the host gene, we performed a RT-PCR analysis for two gene pairs, *ytr-eIF6* and *xl6-nop5* (Fig. 2). The main criterion for selecting these genes was the high expression level of both nested and host genes in the *Drosophila* S2 cell line. The expression profiles were obtained from the modENCODE RNA-seq database [27, 28]. The analysis was performed with nuclear and cytoplasmic RNA samples using probes for sequences located in the gene regions shown in Fig. 2. While the cytoplasmic fraction contained fully processed mRNA, the nuclear fraction additionally included intermediates and decay products, and its analysis allowed us to detect transcripts that had not been processed to their mature form and released into the cytoplasm.

In cytoplasmic samples, the RT-PCR analysis revealed high RNA levels only for the exonic regions of

the test genes (Fig. 2; probes 1, 4, 6), while intronic regions were expressed at the background level (Fig. 2; probes 3, 5). In nuclear samples, however, RNA levels for the intronic are detectable, indicating the presence of long, unspliced *ytr* (Fig. 2A) or *xl6* transcripts (Fig. 2B). The absence of significant variations between intronic regions (points 3 and 5) and the last exon (point 6) is evidence that no premature cleavage/polyadenylation of *ytr* or *xl6* occurred within the intron and that the respective *eIF6* or *nop5* transcripts were processed at their own PASs. Notably it recognizes only its own polyadenylation signal for each transcript.

We simultaneously performed a Northern blot analysis for the *xl6-nop5* pair to reveal bands recognized by all exonic and one intronic probes within the *xl6/nop5* gene span (Fig. 2B). In the nuclear fraction, all probes detected the presence of long RNA (at the detection limit), which corresponded to an unspliced read-through *xl6* gene product. In both nuclear and cytoplasmic fractions, we also observed signals from exonic probes, which corresponded to the processed forms of *xl6* (probes 1 and 6) and *nop5* (probe 4). It should be noted that the Northern blot analysis did not reveal the form of *xl6* transcript cleaved/polyadenylated at the *nop5* PAS, which is located in the intronic region of the nascent *xl6* transcript. The *xl6* transcript was only cleaved/polyadenylated at its own PAS located in the corresponding exonic sequence.

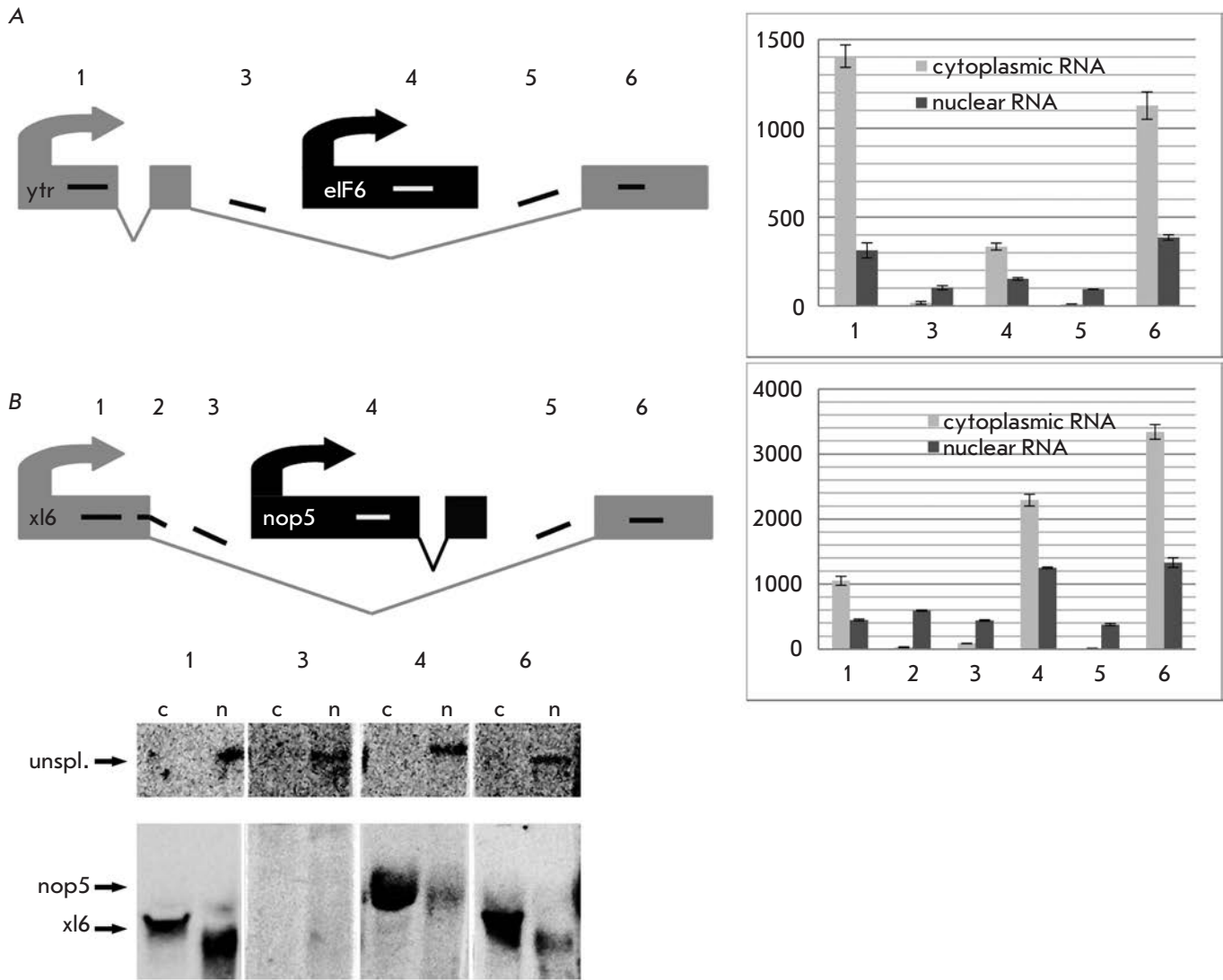


Fig. 2. Poly(A) signals are utilized in exonic, but not intronic transcript regions. In schemes of experiments with (A) *ytr-elf6* and (B) *xl6-nop5* gene pairs, exons and introns are shown as boxes and angles (V), respectively; short numbered lines indicate the regions recognized by probes. Histograms show the levels of nuclear and cytoplasmic RNAs in these regions. Error bars represent s.d. (n=3). Northern-blot analysis of nuclear (n) and cytoplasmic (c) RNAs isolated from S2 cells and hybridized with probes to the *xl6-nop5* gene pair is shown at the bottom

Summarizing the results of Northern blotting and RT-PCR allows us to conclude that the transcription machinery of the host gene ignores the intronic PAS, whereas that of the nested gene successfully utilizes the same signal, which in this case is exonic.

PAS inserted in an intron is functionally disabled

Analysis of endogenous cleavage/polyadenylation events characterizes gene functioning “as is” and does not provide enough freedom for making alterations in this process. Therefore, we turned to the plasmid reporter system to analyze PAS functioning in the *Dro-*

sophila S2 cell line. This bicistronic system was based on the *Renilla* luciferase (Rluc) and firefly luciferase (Fluc) coding sequences driven by the single *Drosophila actin 5C* promoter, with the IRES sequence from the *Drosophila reaper* gene [29] being inserted between the luciferase sequences (Fig. 3).

We expected that if the test PAS was functional, a monocistronic Rluc mRNA would be produced; if this PAS was nonfunctional or weakly functional, a longer mRNA would be generated, extending to the SV40 PAS located downstream of the Fluc sequence. The plasmid constructs were transfected into *Drosophila* S2 cells

and analyzed 24 to 48 h after transfection by means of dual luciferase assay. The amount of long bicistronic mRNA relative to the total mRNA from the construct was estimated from the Fluc/Rluc ratio.

In the first set of constructs, which was used to measure the basal cleavage/polyadenylation activity, the late PAS from the SV40 virus (tSV40) and PASs from the *nop5* (tnop5), *eIF6* (teIF6), *yellow* (ty) genes were inserted downstream of the first cistron. The basic construct without insertion and the construct with the linker sequence (without PAS) of the same length as the PASs were used as controls. All the above-mentioned PASs proved to reduce the Fluc/Rluc ratio, indicating that the transcripts were cleaved/polyadenylated after the first luciferase (Rluc) (Fig. 3A). For basic and ty constructs, we performed a Northern blot analysis of isolated total RNA with probes R and F recognizing the Rluc and Fluc sequences, respectively. The results confirmed that the ty construct generated shorter transcripts: as detected with probe R, 1.7 kb vs. 3.8 kb in the basic construct (Fig. 3).

The second set of constructs was aimed at measuring the cleavage/polyadenylation activity in the intronic sequence from the *Drosophila yellow* gene. It included plasmids with this intron and with the ty PAS inserted in the intron. The dual luciferase assay showed that intron insertion reduced the Fluc/Rluc ratio, compared to the basic construct (Fig. 3A). We attributed this observation to the change in the efficiency of IRES-dependent translation initiation. Meanwhile, the ty insertion in the *yellow* intron did not change the ratio characteristic of the intron construct without this insertion. The Northern blot analysis for these constructs was performed with probes to both luciferases (Fig. 3). Probe F generated signals for long bicistronic transcripts. Signals were obtained for basic and two intron-containing constructs, with the transcript length of intron-containing constructs corresponding to a spliced variant (4.2 kb). Probe R generated a signal for all RNA transcribed from the construct promoter. For the ty construct, a short form of monocistronic transcript was only detected (1.7 kb). For basic and intron-containing constructs, the bands obtained with probe R were the same as those detected with probe F. Remarkably, there were no short forms of transcripts from the construct with the ty insertion within the intron.

Thus, we showed that the transcript was processed in all constructs where a PAS was placed in the exonic sequence. PAS insertion in the *yellow* intron did not interrupt transcription, and only a spliced form of RNA was detected.

The intron from the *yellow* gene, a long sequence, could contain unknown putative regulatory elements having an effect on transcription. Therefore, we con-

structed an artificial intron (AI) that contained no other regulatory elements except the minimum set of splicing signals: the donor site, acceptor site, branch point, and poly(T/C) region. A fragment of the *lacZ* CDS was used as a linker between the splicing signals. Based on the basic bicistronic reporter, we designed constructs containing different PASs or the linker sequence within the AI. Four PASs were tested in this way: ty, tSV40, tnop5, and teIF6 (Fig. 3B). As negative controls, ty, tnop5, and teIF6 were cloned at the same position in reverse orientation. Since SV40 poly(A) is functional in both orientations, a *lacZ* CDS fragment of equal length was taken as a negative control in this case. The Fluc/Rluc ratio in constructs containing polyadenylation signals in the direct orientation was not changed significantly compared to that in the control constructs with these signals in the reverse orientation or with the *lacZ* linker (Fig. 3B). Thus, no events of intronic-PAS utilization were observed in this case, as well as in the experiments with the endogenous gene pairs and the model system based on the *yellow* gene intron.

To confirm cleavage/polyadenylation silencing within the intronic sequence, we performed a similar experiment with AI variants of ty and tSV40 constructs in which the donor splice site was deleted. Expectedly, if this deletion turned the AI into exon extension, then PAS would be utilized. As shown in Fig. 3B, the Fluc/Rluc ratios for PAS-containing plasmids were lower. Therefore, in the absence of the donor splice site, a short monocistronic transcript isoform is generated due to the functioning of the first PAS. A reverse experiment, where mutation creates a functional 5' splice site and that its recognition by the spliceosomal component U1 snRNP causes suppression of 3' end formation, was also described [30, 31].

PAS utilization within intron is a rare event in the genome and appears to be inducible

We found that polyadenylation occurs within introns neither in the genome nor in transgenic constructs. It is known, however, that in case of alternative 3'-exon inclusion the transcript should be interrupted within an intron (Fig. 4A, B). Using the FlyBase genome annotation data [26], we checked how often the annotated transcripts ended within the introns of another transcript isoform and found 403 genes organized in this way. To analyze the expression pattern of isoforms, we used RNA-seq data on different cell lines and developmental stages that are available from the modENCODE project [27, 28]. We excluded 170 genes whose transcripts overlapped with each other at their boundaries, because in this case it was impossible to determine the gene from which a given sequence was transcribed. Then we chose 70 genes with transcripts of

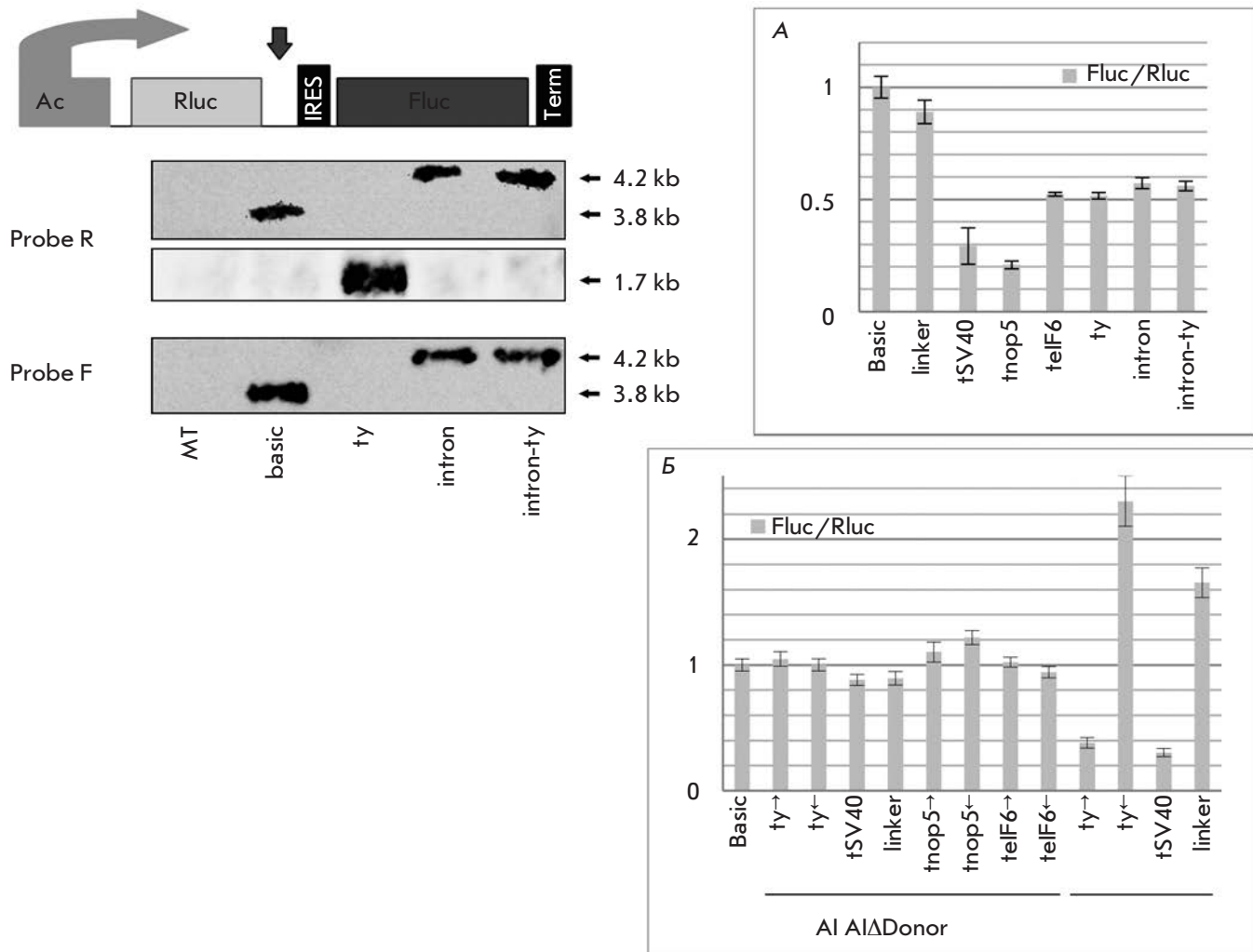


Fig. 3. Plasmid reporter system confirms that poly(A) signal inserted in an intron is functionally disabled. This bicistronic reporter system is based on *Renilla* luciferase (Rluc) and *Firefly* luciferase (Fluc) coding sequences driven by the single *Drosophila actin* 5C promoter, with the IRES sequence inserted between the luciferase sequences. The arrow shows the site of insertion of the late SV40 PAS (tSV40) and PASs from genes *nop5* (tnop5), *eIF6* (telF6), and *yellow* (ty). The intron from the *yellow* gene and this intron with a ty insertion were cloned at the same position. The Fluc/Rluc ratios for these constructs are shown in histogram **A**. Error bars represent s.d. (n=5). Northern blot analysis of total RNA from mock-treated (MT) and transfected S2 cells with probes to both luciferases confirms the results of luciferase assay. Histogram **B** shows the Fluc/Rluc ratios for artificial intron (AI)-based constructs containing the complete AI and AI with donor site deletion (AI ΔDonor). Error bars represent s.d. (n=3)

only two forms, the first being spliced and the second ending within an intron (Fig. 4A). The proportion of the intron-cleaved/polyadenylated form was estimated as the ratio between its level and the sum of the two RNA forms.

According to the calculated levels and ratios, we sorted the chosen genes into several groups. The first major group consisted of 20 genes in which transcripts utilizing PAS within introns were not detected or their level was close to the baseline noise. It may well be that

such genes do not produce intron-cleaved/polyadenylated transcripts or produce a very small amount of them. The second group included six genes showing no detectable splicing events and impugning the existence of 3'-exons. The third group consisted of 16 genes with transcriptional switching between the isoforms, which is likely to be inducible (Fig. 4C). The level of each isoform and the ratio between them change during development or in different cell lines. In addition, we sorted out a group of genes with apparently erroneous anno-

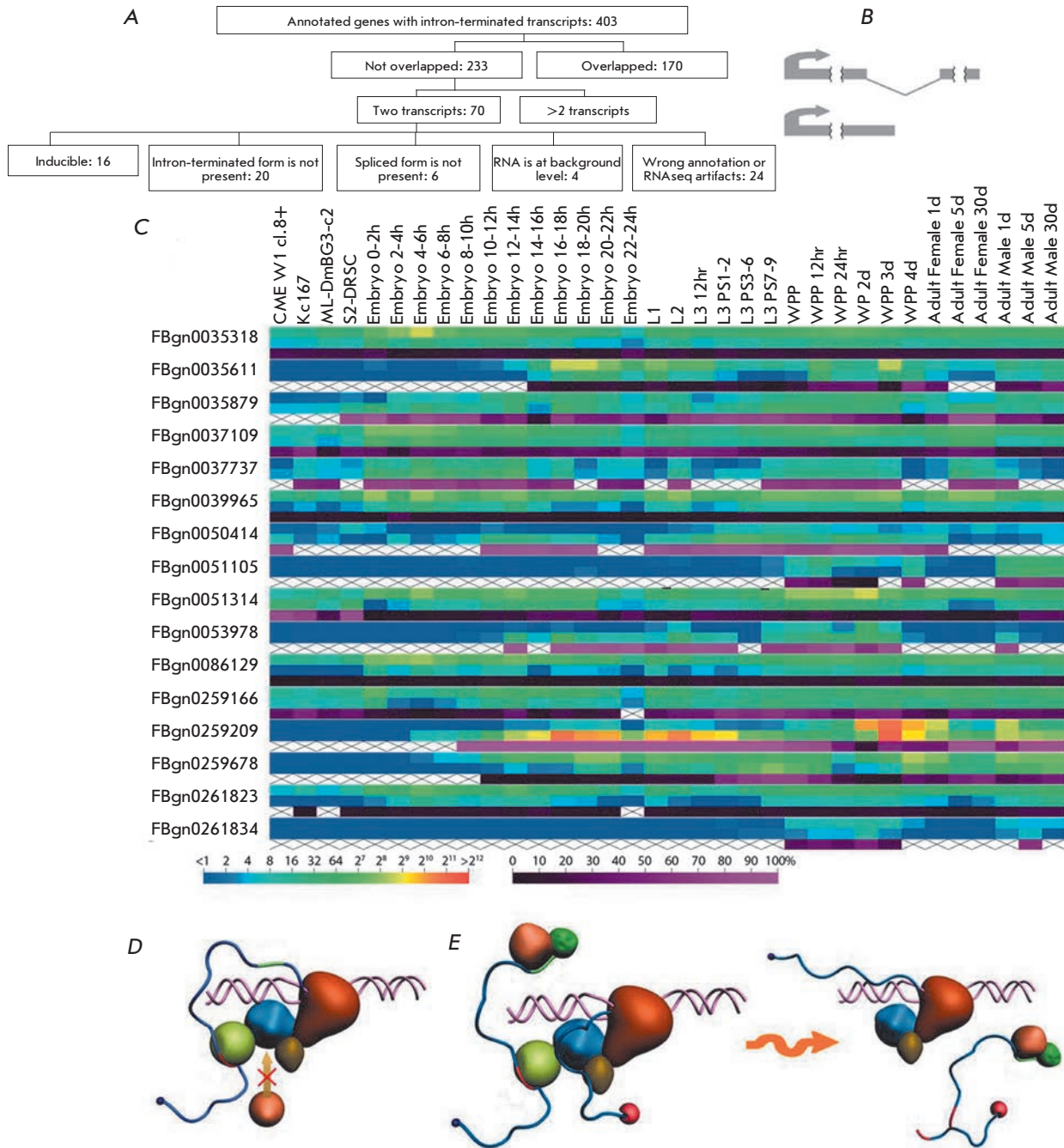


Fig. 4. Cleavage/polyadenylation within an intron is a rare event in the genome and appears to be inducible. **A.** Scheme of searching for genes with intron-cleaved/polyadenylated transcript isoforms. **B.** Scheme of selected genes transcripts, with one isoform cleaved/polyadenylated within the intron of the other isoform. **C.** Heat map illustrating the expression patterns of the two transcript isoforms from 15 genes in 4 cell lines and at 30 development stages. For each gene, the top line refers to the spliced form; the middle line, to the intron-terminated isoform; and the bottom line, to the ratio between the intron-terminated isoform and the total gene mRNA. Color scales at the bottom characterize the level of isoform expression in RNA-seq read density units (on the left) and the proportion of the intron-terminated isoform (on the right). **D-E.** Two potential models for intronic PAS bypassing. **D.** In the "antitermination" model, PAS is inaccessible to cleavage/polyadenylation proteins due to competitive binding of splicing and termination components to the elongation complex, in which splicing wins over polyadenylation because of its earlier functional readiness during transcription. **E.** In the "kinetic model," PAS is accessible, but moving polymerase reaches the 3' splice site quickly enough to initiate the splicing reaction; an introduced break remains in the cut-out intermediate and does not allow exonuclease-based transcription termination

tation. Thus, our observations show that PAS utilization within introns is a very rare occurrence. According to the genome annotation data, only 403 genes possibly have transcripts ending within introns. In fact, only 20 out of the 70 genes included in the analysis produced such transcripts at a near-baseline level and only 16 genes produced both transcript isoforms, with their levels and ratio changing during development or in different cell lines.

DISCUSSION

Our premise in this study was that inappropriate PASs in the intronic sequences of genes are prevented from utilization. This phenomenon was described earlier as finding functional cryptic PASs in introns after U1 snRNP knockdown in HeLa cells [20]. To begin with, we checked the occurrence frequency of such signals in *Drosophila* and found cryptic PASs to be widely distributed over the introns (about 30% of all introns). We then turned our attention to the cases where one gene is located within an intron of another gene and, therefore, the transcription machinery of the latter needs to read through premature PASs from the gene nested in its intron. Our experiments showed that such gene architecture does not result in the functional overlap of PASs and that the transcription machinery of the host gene takes no notice of intronic PASs from the nested gene. Furthermore, we did not observe transcript generated at intronic polyadenylation sites in experiments with the plasmid reporter system containing either an endogenous intron from the *yellow* gene or an artificially constructed intron. It is noteworthy that deletion of the donor splice site in this reporter system proved to restore the functionality of PAS. Finally, the full transcriptome analysis showed that transcripts of the isoform resulting from intronic PAS utilization are rarely expressed in *Drosophila* and that the ratio between these isoforms and the spliced ones varies during development.

Summarizing our findings and the previously obtained [19, 20] data, we can draw a conclusion that transcription is generally not interrupted at intronic PASs. Exceptions to this rule are rare, which confirms its validity and indicates that there should be some additional conditions for the activation of PASs within introns. It is noteworthy that, among genes with alternative 3'-exon inclusion transcripts, we found only 16 genes producing two transcript isoforms at the same time, one spliced and the other ending within an intron. In our opinion, inducible switching between the two isoforms takes place in this case.

There are two models that can potentially explain this phenomenon. The first one, the “antitermination” model, is based on the recent data on coupling between

the splicing machinery and the cleavage/polyadenylation complex [14, 19, 20]. It is possible that splicing and polyadenylation events interact in a competitive manner, with the former prevailing over the latter (Fig. 4D). The effect may be mediated by direct protein–protein interactions: for example, by competitive binding of splicing and cleavage/polyadenylation components to the CTD of RNAP II or inactivation of cleavage/polyadenylation components by splicing factors. For example, snRNP inhibits PAP through a direct interaction between U1 70K and PAP [19]. After recognition of the donor splice site by U1snRNP, the elongation complex of RNAP II becomes inaccessible to the C/P components. Splicing wins over polyadenylation because the components of its machinery are assembled into a functional complex at earlier stages of the transcription process. Meanwhile, utilization of PAS within introns may be induced in some cases by the general mechanisms involved in the regulation of alternative splicing (such as masking of the donor splicing site by a regulatory protein or complementary RNA binding, changes in chromatin status) or by the level of U1 snRNP as described in [24].

The second one, the “kinetic model,” is based on the assumption that RNAP II continues to move after stumbling on a PAS [32, 33]; as a result, it successfully arrives to the acceptor splice site, initiating the splicing reaction with lariat formation (Fig. 4E). In this variant, cleavage and polyadenylation reactions take place but do not affect mRNA maturation, since the lariat intermediate is cut out. As shown in [34], the exons flanking the intron that has been engineered to be a co-transcriptional self-cleavage site (CoTC) are accurately and efficiently spliced together. So we may assume that PASs within introns act in a similar way to CoTC. In this model, the “choice” of the transcript isoform can be regulated not only by masking the donor splice site but also by changes in the rate of RNAP II movement depending on CpG methylation and chromatin status. In the general case, RNAP II moving at a high rate manages to reach the acceptor splice site before being displaced by 5'-3'-exonuclease, which is recruited onto nascent RNA after cleavage events at the intronic PAS. If RNAP II is paused or slowed down, then transcription is terminated, which results in short isoform production.

Another possibility of the products obtained utilizing intronic PAS is degradation. However, no products generated on PAS within introns were detected in our study. Hence, if these events occur, either degradation is very quick or the amount of produced RNA is extremely low.

The observed phenomenon contributes to the understanding of the transcription logic, indicating that

transcript 3'-end formation takes place only at appropriate positions. The molecular mechanisms of PAS skipping or, on the contrary, rare activation require special study. ●

We are grateful to N.A. Gorgolyuk for his assistance in preparing the manuscript. Experiments were performed using the equipment of IGB RAS facilities supported by the Ministry of Science and Education of the Russian Federation (grant no. 16.552.11.7067).

This study was supported by the Molecular and Cell Biology Program of the Russian Academy of Sciences (to P.G.); the Russian Foundation for Basic Research, grant no. 10.04.00341-a (to P.G.); the President's Stipendy SP-1960.2012.4 (to O.M.); the Ministry of Science and Education of the Russian Federation, grant no. P1165 (to O.M.); and by the OPTEC grant (to O.M.).

REFERENCES

1. Auboeuf D., Dowhan D.H., Dutertre M., Martin N., Berget S.M., O'Malley B.W. // *Mol Cell Biol.* 2005. V. 25. P. 5307–5316.
2. Bentley D.L. // *Curr Opin Cell Biol.* 2005. V. 17. P. 251–256.
3. Calvo O., Manley J.L. // *Genes Dev.* 2003. V. 17. P. 1321–1327.
4. Kornblihtt A.R., de la Mata M., Fededa J.P., Munoz M.J., Nogues G. // *RNA.* 2004. V. 10. P. 1489–1498.
5. Maniatis T., Reed R. // *Nature.* 2002. V. 416. P. 499–506.
6. Dantonel J.C., Murthy K.G., Manley J.L., Tora L. // *Nature.* 1997. V. 389. P. 399–402.
7. Ujvári A., Luse D.S. // *J Biol Chem.* 2004. V. 279. P. 49773–49779.
8. Niwa M., Rose S.D., Berget S.M. // *Genes Dev.* 1990. V. 4. P. 1552–1559.
9. Niwa M., Berget S.M. // *Genes Dev.* 1991. V. 5. P. 2086–2095.
10. Dye M.J., Proudfoot N.J. // *Mol Cell.* 1999. V. 3. P. 371–378.
11. Vagner S., Vagner C.C., Mattaj I.W. // *Genes Dev.* 2000. V. 14. P. 403–413.
12. Kyburz A., Friedlein A., Langen H., Keller W. // *Mol Cell.* 2006. V. 23. P. 195–205.
13. Millevoi S., Loulergue C., Dettwiler S., Karaa S.Z., Keller W., Antoniou M., Vagner S. // *EMBO J.* 2006. V. 25. P. 4854–4864.
14. Rigo F., Martinson H.G. // *Mol Cell Biol.* 2008. V. 28. P. 849–862.
15. Rigo F., Martinson H.G. // *RNA.* 2009. V. 15. P. 823–836.
16. Awasthi S., Alwine J.C. // *RNA.* 2003. V. 9. P. 1400–1409.
17. Guo J., Garrett M., Micklem G., Brogna S. // *Mol Cell Biol.* 2011. V. 31. P. 639–651.
18. Andersen P.K., Lykke-Andersen S., Jensen T.H. // *Genes Dev.* 2012. V. 26. P. 2169–79.
19. Gunderson S.I., Polycarpou-Schwarz M., Mattaj I.W. // *Mol Cell.* 1998. V. 1. P. 255–264.
20. Kaida D., Berg M.G., Younis I., Kasim M., Singh L.N., Wan L., Dreyfuss G. // *Nature.* 2010. V. 468. P. 664–668.
21. Goraczniak R., Behlke M.A., Gunderson S.I. // *Nat Biotechnol.* 2009. V. 27. P. 257–263.
22. Abad X., Vera M., Jung S.P., Oswald E., Romero I., Amin V., Fortes P., Gunderson S.I. // *Nucleic Acids Res.* 2008. V. 36. P. 2338–2352.
23. Tian B., Pan Z., Lee J.Y. // *Genome Res.* 2007. V. 17. P. 156–165.
24. Berg M.G., Singh L.N., Younis I., Liu Q., Pinto A.M., Kaida D., Zhang Z., Cho S., Sherrill-Mix S., Wan L., Dreyfuss G. // *Cell.* 2012. V. 150. P. 53–64.
25. Cheng Y., Miura R.M., Tian B. // *Bioinformatics.* 2006. V. 22. P. 2320–2325.
26. McQuilton P., St Pierre S.E., Thurmond J. // *Nucleic Acids Res.* 2012. V. 40. P. D706–D714.
27. Graveley B.R., Brooks A.N., Carlson J.W., Duff M.O., Landolin J.M., Yang L., Artieri C.G., van Baren M.J., Boley N., Booth B.W., et al. // *Nature.* 2011. V. 471. P. 473–479.
28. Celniker S.E., Dillon L.A., Gerstein M.B., Gunsalus K.C., Henikoff S., Karpen G.H., Kellis M., Lai E.C., Lieb J.D., MacAlpine D.M., et al. // *Nature.* 2009. V. 459. P. 927–930.
29. Hernandez G., Vazquez-Pianzola P., Sierra J.M., Rivera-Pomar R. // *RNA.* 2004. V. 10. P. 1783–1797.
30. Langemeier J., Radtke M., Bohne J. // *RNA Biol.* 2013. V. 10. P. 180–184.
31. Langemeier J., Schrom E.M., Rabner A., Radtke M., Zychlinski D., Saborowski A., Bohn G., Mandel-Gutfreund Y., Bodem J., Klein C., Bohne J. // *EMBO J.* 2012. V. 31. P. 4035–44.
32. West S., Gromak N., Proudfoot N.J. // *Nature.* 2004. V. 432. P. 522–525.
33. Luo W., Johnson A.W., Bentley D.L. // *Genes Dev.* 2006. V. 20. P. 954–965.
34. Dye M.J., Gromak N., Proudfoot N.J. // *Mol Cell.* 2006. V. 21. P. 849–59.

3D Structure Modeling of Alpha-Amino Acid Ester Hydrolase from *Xanthomonas rubrilineans*

S.A. Zarubina^{1,2}, I.V. Uporov¹, E.A. Fedorchuk^{1,2}, V.V. Fedorchuk^{1,2}, A.V. Sklyarenko⁴, S.V. Yarotsky⁴, V.I. Tishkov^{1,2,3*}

¹Department of Chemical Enzymology, Faculty of Chemistry, M.V. Lomonosov Moscow State University; Leninskie gory, 1/3, Moscow, Russian Federation, 119991

²Innovations and High Technologies MSU Ltd, Tsimlyanskaya Str., 16, office 96, Moscow, Russian Federation, 109559

³A.N. Bach Institute of Biochemistry, Russian Academy of Sciences, Leninskiy prospect, 33/2, Moscow, Russian Federation, 119071

⁴State Research Institute for Genetics and Selection of Industrial Microorganisms (GosNIIGenetika), 1-st Dorozhniy pr., 1, Moscow, Russian Federation, 117545

*E-mail: vitishkov@gmail.com

Received 11.06.2013

Copyright © 2013 Park-media, Ltd. This is an open access article distributed under the Creative Commons Attribution License, which permits unrestricted use, distribution, and reproduction in any medium, provided the original work is properly cited.

ABSTRACT Alpha-amino acid ester hydrolase (EC 3.1.1.43, AEH) is a promising biocatalyst for the production of semi-synthetic β -lactam antibiotics, penicillins and cephalosporins. The AEH gene from *Xanthomonas rubrilineans* (XrAEH) was recently cloned in this laboratory. The three-dimensional structure of XrAEH was simulated using the homology modeling method for rational design experiments. The analysis of the active site was performed, and its structure was specified. The key amino acid residues in the active site – the catalytic triad (Ser175, His341 and Asp308), oxyanion hole (Tyr83 and Tyr176), and carboxylate cluster (carboxylate groups of Asp209, Glu310 and Asp311) – were identified. It was shown that the optimal configuration of residues in the active site occurs with a negative net charge -1 in the carboxylate cluster. Docking of different substrates in the AEH active site was carried out, which allowed us to obtain structures of XrAEH complexes with the ampicillin, amoxicillin, cephalexin, *D*-phenylglycine, and 4-hydroxy-*D*-phenylglycine methyl ester. Modeling of XrAEH enzyme complexes with various substrates was used to show the structures for whose synthesis this enzyme will show the highest efficiency.

KEYWORDS alpha-amino acid ester hydrolase; *Xanthomonas rubrilineans*; computer simulation; docking; enzymatic synthesis of antibiotics, protein engineering.

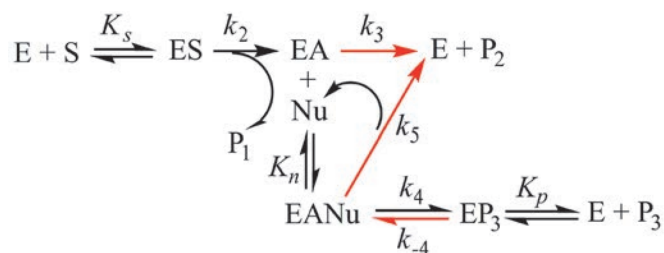
ABBREVIATIONS AEH – alpha-amino acid ester hydrolase; PA – penicillin acylase; XrAEH, XcAEH, ActAEH – alpha-amino acid ester hydrolase from *Xanthomonas rubrilineans*, *Xanthomonas citri*, *Acetobacter turbidans*, respectively; Met-DPG – *D*-phenylglycine methyl ester; DPG – *D*-phenylglycine.

INTRODUCTION

Semi-synthetic β -lactam antibiotics are widely used to treat pathogens and make up more than half of the world market of antibacterial drugs [1]. These antibiotics are currently produced using the penicillin acylase (PA) enzyme, which catalyzes the reaction of acyl group transfer from the corresponding amide to the β -lactam nucleus (*Scheme*) [2, 3]. In the case of PA, the role of acyl moiety donors is played by amides, which are less reactive than the corresponding ethers. Therefore, the formation of an acyl-enzyme (stage with constant k_2) can proceed much faster when the corresponding ester is used as a source of the acyl group, but this requires

using a hydrolase instead of an amidase, such as PA. Hydrolase is more active with ethers, amide being the target product. Hence, the rate of the hydrolytic side reaction (stage with constant k_5) catalyzed by hydrolase is lower compared to that of hydrolysis by amidase. This should increase the ratio between the synthesis and hydrolysis reaction rates. Thus, the use of hydrolase instead of amidase improves the efficiency of antibiotics synthesis in both steps.

One such is hydrolase specific to α -amino acids esters (AEH, [EC 3.1.1.43]). Penicillin acylases have been isolated from various sources and well characterized; however, the data on AEH are scarce. Some data is available on AEH isolated from bacteria *Acetobacter*



Scheme 1. The common kinetic scheme of β -lactam antibiotic synthesis [2]. E – enzyme; S – substrate, donor of acyl moiety; ES – enzyme-substrate complex; EA – acyl-enzyme; P_1 and P_2 – products of substrate S hydrolysis; Nu – nucleophile; EANu – complex of acyl-enzyme with nucleophile; EP_3 – complex of enzyme with target antibiotic; P_3 – target antibiotic. K_s – dissociation constant of the enzyme-substrate complex; K_n – dissociation constant of complex of acyl-enzyme with nucleophile; K_p – dissociation constant of enzyme with antibiotic synthesis product; k_2 – rate constant of acyl-enzyme formation; k_3 – rate constant of acyl-enzyme hydrolysis; k_4 , k_{-4} – forward and reverse rate constants of the chemical formation stage and target antibiotic hydrolysis, respectively; k_5 – hydrolysis rate constant of the complex of acyl-enzyme with nucleophile

turbidans ATCC 9325 (ActAEH) [4, 5] and *Xanthomonas citri* IF0 3835 (XcAEH) [6], *X. campestris pv. campestris* ATCC 33913 [7], and a number of other sources. The Protein Data Bank (PDB) contains three-dimensional structures of only two enzymes that exhibit the highest activity in antibiotics synthesis – ActAEH and XcAEH. Only a structure of holo-form is available for XcAEH (PDB ID: 1MPX, resolution 1.9 Å) [6]. In the case of ActAEH, there are structures of both, holo-form of wild type enzyme (PDB ID: 2B9V, resolution 2.0 Å), and its complex with D-phenylglycine (PDB ID: 2B4K, 3.3 Å), as well as structures of the mutant ActAEH Y206A (PDB ID: 1RYY, resolution 2.8 Å) and complex of an inactive mutant ActAEH S205A with ampicillin (PDB ID: 1NX9, resolution 2.2 Å) [5].

We recently cloned the AEH gene from bacteria *X. rubrilineans* (XrAEH). This strain was discovered at the State Scientific Center for Antibiotics. The enzyme has been successfully expressed in *Escherichia coli* cells; preliminary experiments have confirmed the high efficacy of recombinant XrAEH in the synthesis of several antibiotics. However, additional experiments on XrAEH engineering are required to ensure efficient practical use of the enzyme. The experiments should be focused on improving the enzyme's properties with specified substrates. The rational design method is one of the most efficient approaches in pro-

tein engineering. This method involves introducing point amino acid substitutions into a protein globule, which are selected according to data obtained by analyzing the enzyme 3D structure. This method requires the availability of the structure of the enzyme under study, which can be obtained either experimentally (XRD or NMR) or through a computer simulation. The latter approach is now being used increasingly frequently thanks to the development of computer simulation methods and the continuous increase in the number of experimentally determined structures in the PDB data bank.

The purpose of this study was to build a model structure of XrAEH of holo-form of enzyme as well as complexes with the key compounds used for the synthesis of β -lactam antibiotics.

EXPERIMENTAL

The amino acid sequences of XrAEH and known AEH structures were aligned using the BioEdit Sequence Alignment Editor ClustalW Multiple Alignment program [8].

A computer model of the three-dimensional structure of XrAEH was obtained with the homology modeling method using the Insight II software package. The structure of AEH from *X. citri* (XcAEH), available in the PDB database, code 1MPX (resolution of 1.9 Å) [6], was used as a reference structure. The structure was further optimized using the molecular mechanics method (Discover_3 module of the Insight II software package, 300 steps of minimization, CVFF force field [9]) to relieve the potential conformational strains of the structure. The structure was finally optimized using molecular dynamics (5 ps at 298 K). Docking of the substrates and products into the active site of the model structure XrAEH was performed with the Monte Carlo method using the Docking module of the Insight II software package. The structure was further optimized using 300 minimization steps (CVFF force field) and molecular dynamics (1 ps at 298 K).

The Accelrys Discovery Studio 2.5 software package [10] was used to obtain the images of the protein globule and its complexes with the substrates.

RESULTS AND DISCUSSION

This study included the following steps:

- multiple alignment of the XrAEH amino acid sequence with known AEH sequences to identify conserved regions (primarily the active site residues) and to select the optimal structure to be used as a reference;
- building of the three-dimensional structure of XrAEH with the homology modeling method using the reference enzyme selected at the preceding step;

Fig. 1. The multiple alignment of the amino acid sequences of XrAEH, AEH from *X. citri*, *X. campestris* pv. *campestris*, *X. oryzae*, and *A. turbidans* in the active site area. The catalytic triad residues, two Tyr residues from the oxyanion hole and three residues of the carboxylate cluster, are shown in red, purple, and green, respectively

	65	75	85	95	105	115
<i>X. rubrilineans</i>	LHTVIVLPKG	AHGAPILLTR	TPYDASGRAS	RLA-SPHMRD	LLPQGDEVFV	DGGYIRVFQD
<i>X. citri</i>	LHTVIVLPKG	AKNAPIVLTR	TPYDASGRTE	RLA-SPHMKD	LLSAGDDVFV	EGGYIRVFQD
<i>X. oryzae</i>	LHTVIVLPKG	AKNAPIVLTR	TPYDASGRTE	RLA-SPHMKD	LLSAGDDVFV	EGGYIRVFQD
<i>X. campestris</i>	LHTVIVLPKG	ARNAPIVLTR	TPYDASGRTE	RLA-SPHMKD	LLSAGDDVFV	EGGYIRVFQD
<i>A. turbidans</i>	LYTVIVIPKN	ARNAPILLTR	TPYNAKGRAN	RVPNALTMRE	VLPQGDDEVFV	EGGYIRVFQD
	125	135	145	155	165	175
<i>X. rubrilineans</i>	IRGKYGSEGD	YVTRPLRGP	LNPTKVDHAT	DAWDTIDWL	KHVPESNGKV	GMIGSSYEGF
<i>X. citri</i>	VRGKYGSEGD	YVMTRPLRGP	LNPSVDHAT	DAWDTIDWL	KNVSESNGKV	GMIGSSYEGF
<i>X. oryzae</i>	VRGKYGSEGD	YVMTRPLRGP	LNPSKVDHAT	DAWDTIDWL	KNVKESNGKV	GMIGSSYEGF
<i>X. campestris</i>	VRGKYGSEGE	YVMTRPLRGA	LNPSVDHAT	DAWDTIDWL	KNLKESNGKV	GMIGSSYEGF
<i>A. turbidans</i>	IRGKYGSQGD	YVMTRPPHGP	LNPTKTDETT	DAWDTVDWL	HNVPESENGRV	GMTGSSYEGF
	185	195	205	215	225	235
<i>X. rubrilineans</i>	TVVMALADPH	PALKVAAPES	PMIDGWMGDD	WLNYGAFRQV	NLDYFTGQMT	RRGKGEIPIR
<i>X. citri</i>	TVVMALTNPH	PALKVAAPES	PMIDGWMGDD	WFNYGAFRQV	NFDYFTGQLS	KRGKGAGIAR
<i>X. oryzae</i>	TVVMALTNPH	PALKVAAPES	PMVDGWMGDD	WFNDGAFRQV	NFDYFTAQLS	KRGKGAGIPIR
<i>X. campestris</i>	TVVMALTNPH	PALKVAAPES	PMIDGWMGDD	WFNYGAFRQV	NFDYFTGQLS	KRGKGAGIPIR
<i>A. turbidans</i>	TVVMALLDPH	PALKVAAPES	PMVDGWMGDD	WFHYGAFRQV	AFDYFVSQMT	ARGGGNDIPIR
	245	255	265	275	285	295
<i>X. rubrilineans</i>	QGDDYSNFL	RAGSAGDYAK	AAGLEQLPWW	HKLTEHPAYD	AFWQEALDK	VMARTPLKVP
<i>X. citri</i>	QGHDDYSNFL	QAGSAGDFAK	AAGLEQLPWW	HKLTEHAAYD	AFWQEALDK	VMARTPLKVP
<i>X. oryzae</i>	QGDDYSNFL	QAGSAGDFAK	AAGLEQLPWW	HKLTEHAAYD	AFWQEALDK	VMARTPLKVP
<i>X. campestris</i>	QGHDDYSNFL	QAGSAGDFAK	AAGLEQLPWW	HKLTEHAAYD	AFWQEALDK	VMARTPLKVP
<i>A. turbidans</i>	RDADDYTNFL	KAGSAGSFAT	QAGLDQYFPW	QRMHAHPAYD	AFWQQALDK	ILAQRKPTVP
	305	315	325	335	345	355
<i>X. rubrilineans</i>	TMWLQGLWDQ	EDMWGAIHSY	EAMEPRDTGN	DKNYLVMGPW	RHSQVNYEGA	SLGALQFDGD
<i>X. citri</i>	TMWLQGLWDQ	EDMWGAIHSY	AAMEPRDKRN	TLNYLVMGPW	RHSQVNYDGS	ALGALNFEFGD
<i>X. oryzae</i>	TMWLQGLWDQ	EDMWGAIHSY	AAMEPRDKSN	TLNYLVMGPW	RHSQVNYDGS	ALGALSFEFGD
<i>X. campestris</i>	TMWLQGLWDQ	EDMWGAIHSY	AAMEPRDKSN	KLNYLVMGPW	RHSQVNSDAS	SLGALNFDGD
<i>A. turbidans</i>	MLWEQGLWDQ	EDMWGAIHAW	QALKDADVKA	P-NTLVMGPW	RHSGVNYNGS	TLGPLEFEFGD

- refinement of the determined XrAEH enzyme structure; and
- docking of various substrates and products of the enzymatic reaction into the model structure of XrAEH.

Alignment of amino acid sequences of AEH from different sources

It is known that accuracy in modeling is primarily impacted by two factors: the degree of homology between the modeled and the reference enzymes that are used as standard structures, and the resolution of the reference structure. Furthermore, even provided that homology is high, the modeling accuracy highly depends on the number and length of the gaps/insertions in the amino acid sequence alignment of the modeled and reference enzymes. The fewer the gaps/insertions, the higher the simulation accuracy will be. Therefore, in order to select the reference structure, we carried out the alignment of the amino acid sequence of the enzyme under study and two AEH sequences with known structures:

from *X. citri* (XcAEH) and *A. turbidans* (ActAEH), as well as two highly homologous AEH from *X. campestris* pv. *campestris* and *X. campestris oryzae*. Note that the data on AEH from *A. pasteurianus* (which is completely identical to ActAEH in terms of the amino acid sequence) have been published; for this reason it was left out in the alignment.

The alignment results are shown in Fig. 1. The alignment data analysis shows that XcAEH shows the highest homology to XrAEH (84%). The homology of AEH from *X. campestris* pv. *campestris* and *X. campestris oryzae* is slightly lower (83%). The homology between XrAEH and ActAEH is much lower (62%). Moreover, Fig. 1 shows that the alignment of the amino acid sequences of the enzyme under study and other AEH from *Xanthomonas* bacteria has no deletions or insertions, while there is one deletion and one insertion of an amino acid residue in the case of ActAEH.

Thus, based on the results of the alignment of two experimentally determined structures (ActAEH and

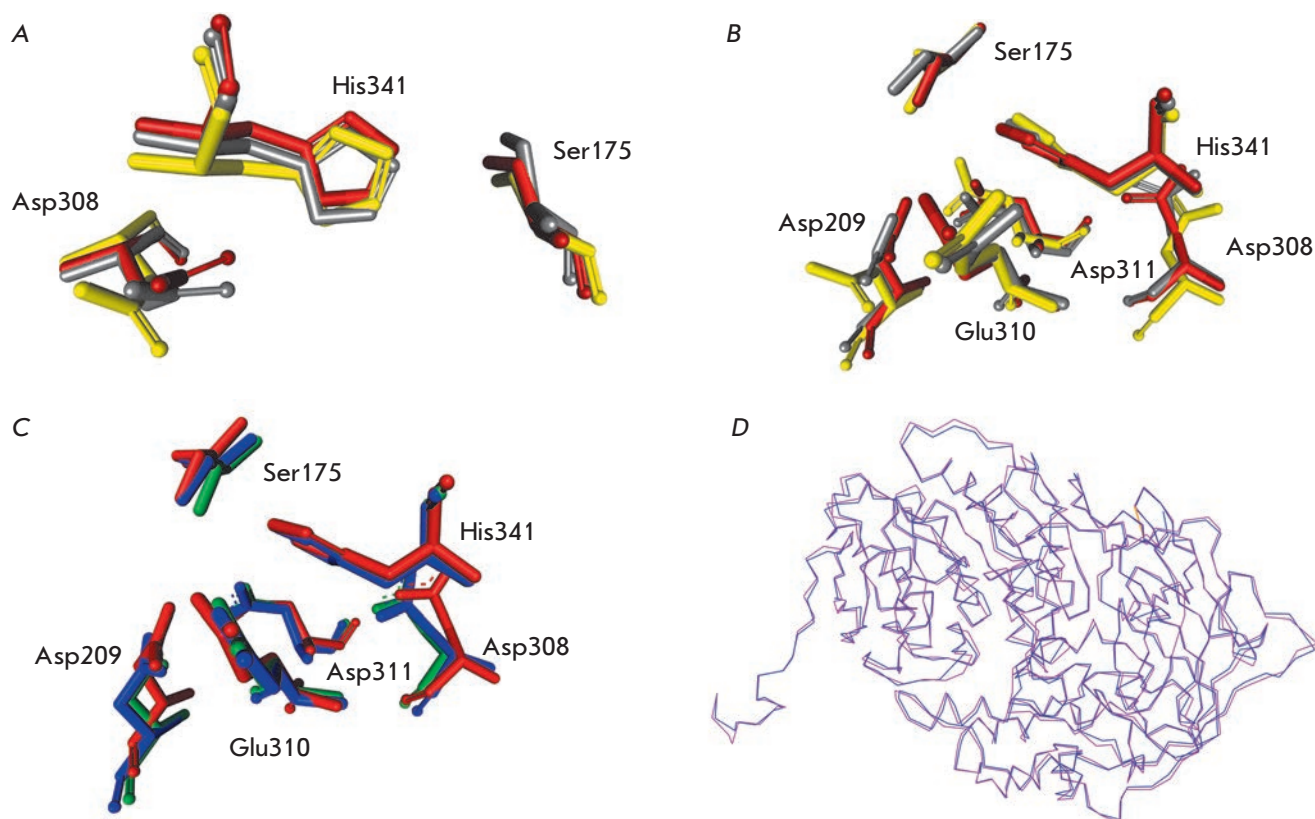


Fig. 2. A and B – optimization of the active site structure in the model structure of XrAEH. The mutual orientation of the catalytic triad residues only and that of both the catalytic triad and carboxylate cluster residues are shown in Figs. A and B, respectively. Residues in structures with a negative net charge -3 , -2 , and -1 in the carboxylate cluster are shown in yellow, grey, and red, respectively. C – superimposition of the active site and carboxylate cluster residues in the model XrAEH structure (shown in red) and the experimental XcAEH and ActAEH structures (shown in green and blue, respectively). D – superimposition of C α -atoms of the XrAEH and XcAEH structures (shown in purple and blue, respectively). The residue numbering is given according to the XrAEH sequence

XcAEH), the structure of the XcAEH enzyme (PDB ID: 1MPX [6]) was chosen as the reference one. In addition, the selected XcAEH 1MPX structure had a slightly higher resolution than that of the unbound ActAEH 2B9V (1.9 and 2.0 Å, respectively).

Analysis of the active site of XrAEH

The data on the alignment of the amino acid sequences enable to determine the functionally important residues of the active site of XrAEH. Unlike penicillin G acylase (PA), which consists of two different subunits, XrAEH is a homotetramer of four identical subunits with the active site located inside each subunit. According to X-ray diffraction analysis data [4–7], the presence of three types of key amino acid residues is a characteristic feature of α -amino ester hydrolase:

1) The proton relay system to activate the catalytic serine residue. This is the typical catalytic triad of serine hydrolases; in XrAEH enzyme, it consists of Ser175, His341, and Asp308 residues (Fig. 1);

2) An oxyanion center consisting of two Tyr83 and Tyr176 residues in the XrAEH enzyme; it is required to stabilize the negative charge on the catalytic Ser175 residue; and

3) A carboxylate cluster consisting of three carboxyl groups of two aspartic acid residues (Asp311, Asp209) and a glutamic acid residue (Glu310). The negatively charged carboxylate cluster is involved in the binding of the positively charged amino-group of the acyl moiety of the substrate at the α -position; this binding ensures the high specificity of XrAEH to α -amino acids.

Furthermore, the Tyr223 residue is functionally important as it is involved in the binding of the phenyl moiety of the substrate due to the stacking interaction contributing to the correct orientation of the substrate in the active site of the enzyme.

Computer modeling of the XrAEH structure

The 3D structure of XrAEH was built in two steps. First, the preliminary structure of the tetrameric en-

zyme XrAEH [11] was obtained using the homology modeling method with the SWISS-MODEL server. This structure was further optimized by relaxing the structure to relieve potential conformational strains using 300 steps of minimization with the Discover_3 module of the Insight II software package. An analysis of the active site structure in the model XrAEH structure obtained at this step showed that the mutual orientation of the Ser175, His341, and Asp308 residues constituting the catalytic triad is not optimal for ensuring a catalytic function (Fig. 2A, B, residues are shown in yellow). Figure 2 demonstrates that the carboxyl group of the Asp308 residue faces away from the imidazole ring of His341. It has been suggested that this non-optimal orientation can be associated with the too-high negative charge assigned to the negatively charged carboxylate cluster consisting of carboxyl groups of the Asp209, Glu310, and Asp311 residues during the simulation. The negative charge was initially assigned to all the carboxyl groups in the residues of the carboxylate cluster of the original structure, thereby resulting in a net charge of -3 . It is known that close positioning of the carboxyl groups in polymers typically prevents complete dissociation of all these groups. Therefore, we performed an additional optimization of the structure assuming that the net charge on the carboxylate cluster was equal to -2 (Fig. 2A, B, residues are shown in gray) and -1 (Figs. 2A, B, residues are shown in red). Figures 2A, B show that along with a decrease in the total negative charge of the carboxylate cluster the orientation of the carboxyl group of the Asp308 residue in the catalytic triad with respect to the imidazole ring of His341 becomes closer to a correct orientation. Along with this, the OH-groups of the catalytic Ser175 residue move towards the imidazole ring of His341 (Fig. 2A). As a result, configuration of all the residues of the catalytic triad is optimal for the reaction. In addition, the negative charge of -1 at the carboxylate cluster is sufficient for the binding of the positively charged amino group of the substrate. After binding, the carboxylate cluster has no negative charge, thus suppressing the dissociation of the OH group of the catalytic residue Ser175.

Figure 2C shows the results of overlapping of the catalytic triad and carboxylate cluster residues of the optimized model of the XrAEH structure with respect to the same residues in the ActAEH and XrAEH structures determined through an X-ray diffraction analysis (PDB ID: 2B9V [5] and 1MPX [6], respectively). Figure 2C clearly shows that the spatial arrangement of the active site residues is almost identical in all three structures: the catalytic residues Ser175 and His341 and the carboxylate cluster occupy the same positions, while only a subtle deviation in the conformation of Asp308 is observed.

Figure 2D shows overlapping of the C_{α} -atoms positions in the XrAEH and XcAEH structures. The figure also shows that the overall folding of the overlapping enzymes is almost identical, with the smallest deviation observed in the vicinity of the active site and the largest one observed at the periphery of the protein globule. The standard deviation of the positions of C_{α} -atoms in the model XrAEH structure and the reference XcAEH structure was just 0.7 \AA . In the case of overlapping between the XrAEH and ActAEH structures, the standard deviation was 1.1 \AA , as could be expected considering the lower homology between these enzymes.

A comparative analysis of the resulting model structure was carried out to identify residues with a non-optimal configuration. Ramachandran maps were constructed for the model XrAEH structure and the experimental XcAEH structure (Figs. 3A, B, respectively). Figure 3 clearly shows that most residues in both structures localize in the areas of the optimal ψ and ϕ values. In fact, Asp84 in XrAEH and Asp83 in XcAEH are the only residues with non-optimal conformations. However, the ψ and ϕ values in these residues in the model and experimental structures are very close. This residue is located near the entrance to the active site in the vicinity of the bend between α -helix and β -strand (Fig. 4A). This fact means that there is a degree of strain between these subunits. The reason for such a deviation from the optimal angles is unclear. However, it should be noted that such deviations are often encountered in residues located exactly at the bends connecting secondary structure elements. For example, the same values of the ψ and ϕ angles are observed in the Ala198 residue in the wild-type formate dehydrogenase from bacterium *Pseudomonas sp.101* [PDB 2NAC].

Thus, these data suggest that the model structure XrAEH is reliable and has high precision; it is also in good agreement with the structure of the reference enzyme XcAEH, as well as with that of ActAEH. Figure 4 shows the structures of the monomeric and tetrameric enzyme XrAEH. This structure was further used for the docking of substrates and products into the active site of the enzyme.

Docking of substrates and products in the active site of XrAEH

The next step was to fit a series of substrates and products into the active site of XrAEH. The docking procedure is described in the Experimental section. The bank of three-dimensional structures provides only data on the unbound apo-enzyme of hydrolase XcAEH, which is the structurally closest homolog of our enzyme. For this reason, the structures of the XrAEH complexes resulting from docking were com-

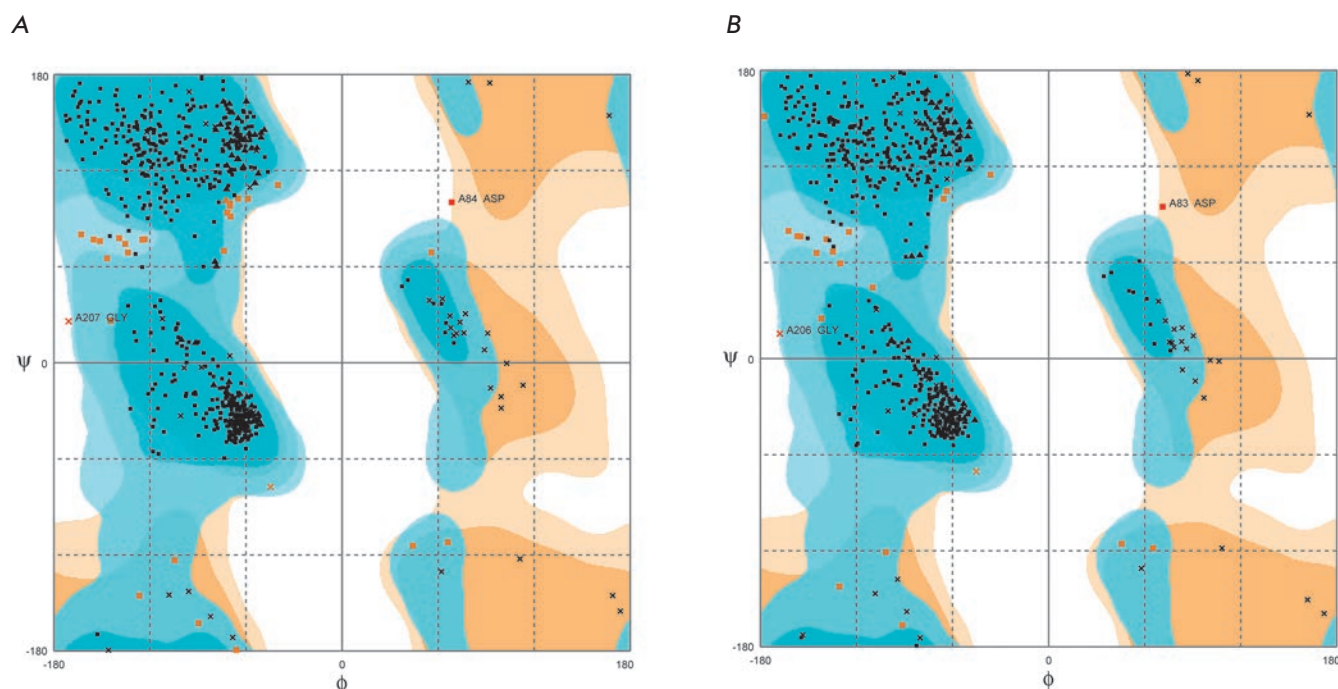


Fig. 3. The Ramachandran plot for the model XrAEH (A) and experimental apo-XcAEH (PDB 1MPX) structures (B). The difference in the residue numbering is due to the presence of the Met residue at the N-termini in the XrAEH sequence, while the starting Met residue is not included in the amino acid sequence of XcAEH [6]

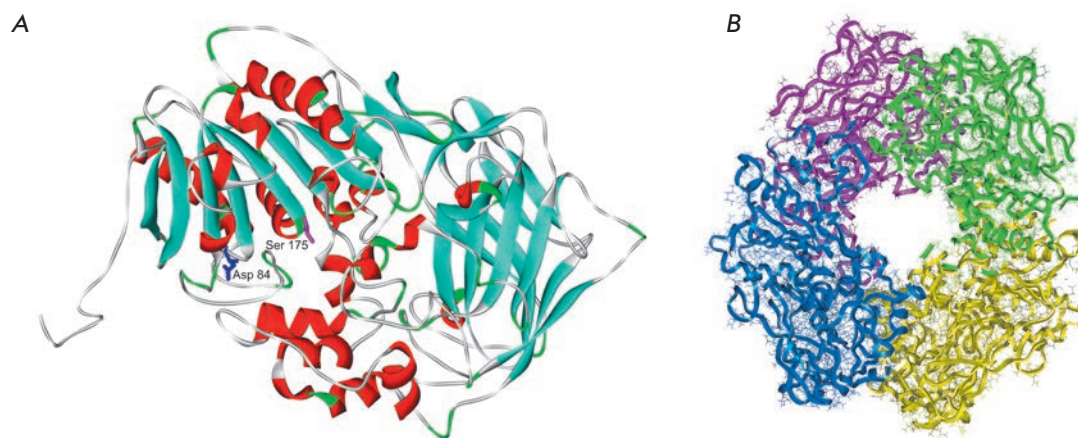


Fig. 4. General view of one subunit (A) and the XrAEH tetramer (B)

pared to the same or similar ActAEH structures determined experimentally.

The structure of the ActAEH complex with *D*-phenylglycine (DPG) is available in the PDB (PDB ID: 2B4K [5]). However, in the case of XrAEH, the structure of its complex with *D*-phenylglycine methyl ester (Met-DPG), which is used as an acylating agent in a AEH-catalyzed synthesis of ampicillin, is of greater interest. Figure 5A shows the overlap between the obtained structure and the 2B4K structure. It can be seen that the overall folding of the structures of binary complexes is very similar; the standard deviation of C_{α} -atoms for the entire protein

globule is 1.1 Å (note that the standard deviation for all C_{α} -atoms of the protein globules of the unbound XrAEH and ActAEH enzymes was also 1.1 Å). Apart from the general folding, almost complete match of the conformations of several active site residues is observed (i.e. imidazole ring of His341 residue and carboxyl group of Asp308 residue of the catalytic triad, the carboxyl groups of the Glu310 and Asp311 residues in the carboxylate center). However, the results of the overlay show noticeable differences in the conformation of other residues. Primarily, these include the hydroxyl group of the catalytic residue Ser175 and the phenolic group of the Tyr83 resi-

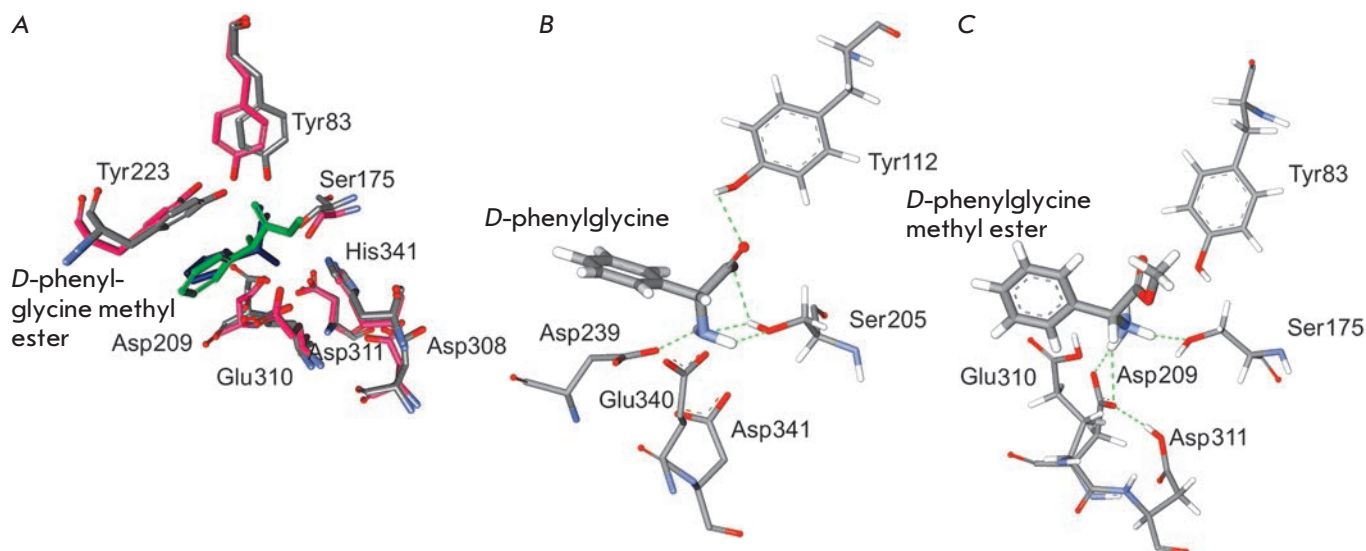


Fig. 5. A – superimposition of the structures of the Met-DPG complex with XrAEH and the DPG complex with ActAEH. ActAEH, XrAEH, Met-DPG, and DPG are shown in pink, grey, green, and blue, respectively. The residue numbering is given according to the XrAEH sequence. B and C – interaction of active site residues with the bound ligand in the ActAEH complex with DPG and the XrAEH complex with Met-DPG

due at the oxyanion center, as well as the amino group of the Met-DPG substrate. A thorough analysis of the experimental and model structures (Figs. 5B, C) with the hydrogen atoms shown provides an explanation for these differences. In the experimental 2B4K structure (Fig. 5B), there is a ActAEH complex with the reaction product. In this complex, the active site residues Ser205 and Tyr112 (Ser175 and Tyr83 in XrAEH, respectively) are positioned extremely improperly for catalysis; i.e., the hydrogen atom of the hydroxyl group of the Tyr112 phenolic ring forms a hydrogen bond with the oxygen atom of the DPG carboxyl group. As a result, the phenolic ring is fixed far away from the oxy group of the catalytic Ser205 and, therefore, cannot act as an oxyanion center in this conformation. In turn, the oxy group of the catalytic Ser205 participates in the formation of three hydrogen bonds, wherein the hydrogen atom is rotated towards the imidazole ring of the His residue due to the formation of two hydrogen bonds. The above His residue accepts this proton to produce a negatively charged oxygen atom at the Ser residue, which is required for the catalysis. In addition, the amino group of DPG is also turned away from the carboxylate center due to the formation of two hydrogen bonds with the hydroxyl group of the catalytic Ser205. As a result, only one carboxyl group of the Asp239 residue (Asp209 in XrAEH) interacts with the amino group of DPG (Fig. 5B).

A totally different picture is observed in the model structure of the XrAEH complex with the Met-DPG substrate (Fig. 5C). Figure 5C clearly shows that the

phenol group of the Tyr83 residue has an optimal conformation to act as an oxyanion center; the oxygen atom of the hydroxyl group of the Ser175 catalytic residue forms only one hydrogen bond, and the hydrogen atom of this group is rotated towards the imidazole ring of the His341 residue belonging to the proton transfer system. The distance between the O γ atom of Ser175 and the attacked carbon atom in the substrate is just 2.9 Å, and the angle of attack is 115.1°, which is close to the value of 109.5° optimal for the tetrahedral conformation. Thus, the resulting model of the XrAEH complex with Met-DPG is optimal for catalysis in terms of configuration. A somewhat different picture is observed for the XrAEH complex with 4-hydroxy-D-phenylglycine methyl ester, which is used as an acyl group donor in the synthesis of amoxicillin (Fig. 6A). The additional hydroxyl group in the aromatic ring of this substrate causes some steric hindrance when it is built into the active site of the enzyme. As a result, the angle of attack between the carbon atom of the carboxyl group and the O γ atom of Ser175 increases to 128.4° (Table), which is certainly worse than that in the case of Met-DPG, but still enough for the reaction to proceed efficiently.

We have also modeled the structures of the XrAEH complexes with the desired products of antibiotics synthesis reactions: ampicillin and amoxicillin (penicillin group) and cephalexin (cephalosporin group). The docking results are shown in Figs. 6B-D. According to overlay of the structures of the ampicillin and amoxi-

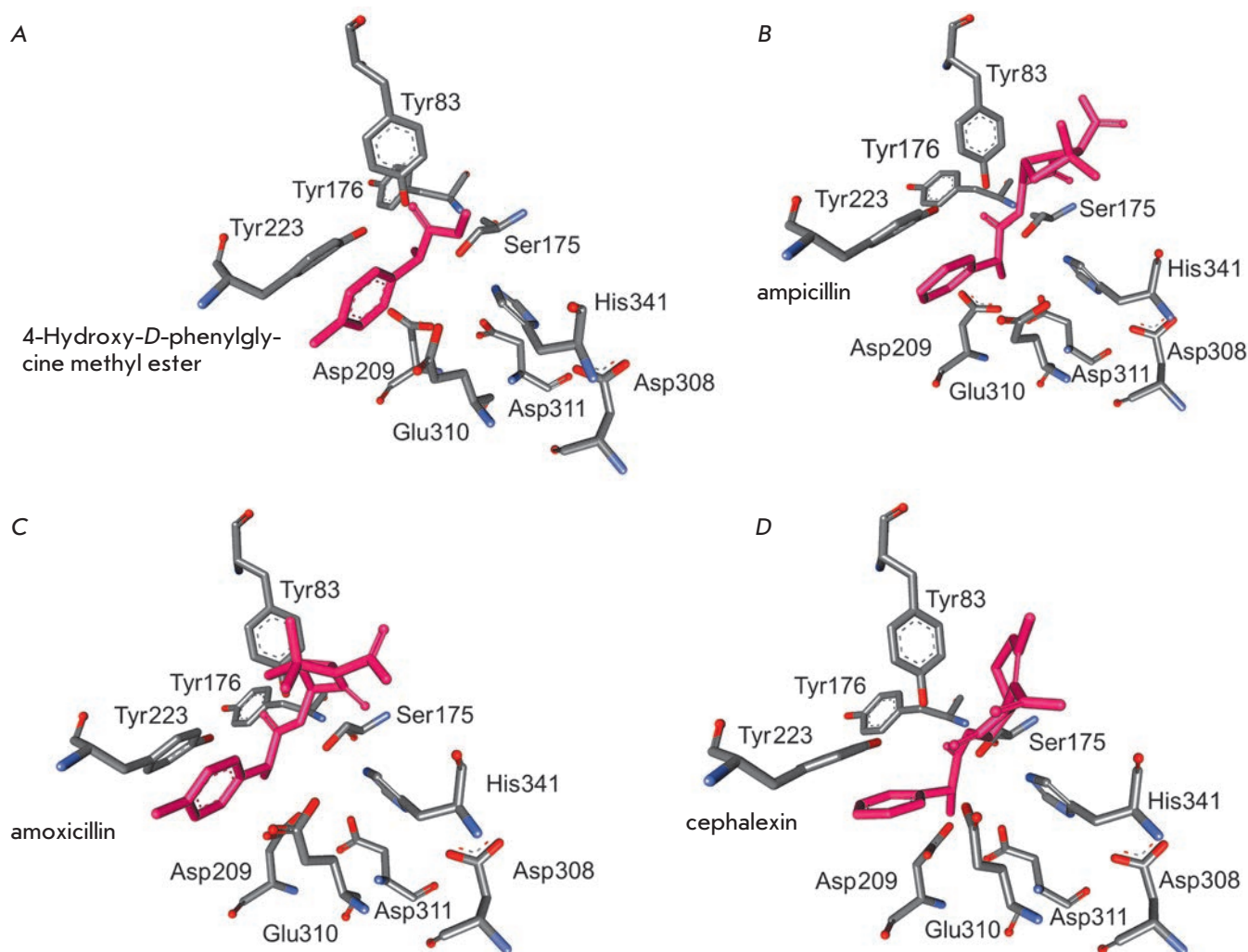


Fig. 6. A–D –docking of 4-hydroxy-*D*-phenylglycine methyl ester, ampicillin, amoxicillin, and cephalixin in the active site of XraEH, respectively

cillin complexes with XraEH, the standard deviation of C_{α} -atoms for the entire protein globule is just 0.005 Å; however, the conformations of the antibiotics bound to the active site are different. Identically to the case of substrates (acyl moiety donors), the distance between the O_{γ} atom of the catalytic residue Ser175 of the enzyme and the carbon atom of the amide group of the product (or carboxyl carbon in the substrate) is 2.7, 3.0, and 2.9 Å for ampicillin, amoxicillin, and cephalixin, respectively, but the angles differ sharply. For ampicillin, the angle is 80.9°, which is much less than the optimal value of 109.5°. For cephalixin (the angle is 73.0°), this difference is even greater. Thus, the probability that these two antibiotics are hydrolyzed in the active site of XraEH is very low. This is not the case for amoxicillin with an attack angle of 103.2°, which is close to the opti-

Table. The numerical results of the binding of substrates and products of the enzyme reaction in the active site of the model XraEH structure

Embedded molecule	Distance from O_{γ} Ser175, Å	Angle of attack of atom O_{γ} Ser175, deg.
<i>D</i> -phenylglycine methyl ester	2.9	115.1°
Ampicillin	2.7	80.9°
4-hydroxy- <i>D</i> -phenylglycine methyl ester	2.9	128.4°
Amoxicillin	3.0	103.2°
Cephalixin	2.9	73.0°

mal value. This fact means that in the case of amoxicillin, the ratio between the synthesis and hydrolysis rates (and, consequently, the yield of the target product) will be lower as compared to that of ampicillin, which is in close agreement with the experimental data [12] obtained by studying the efficacy of the recombinant enzyme in the synthesis of these antibiotics. However, note that the absolute efficacy of recombinant XrAEH in the synthesis of amoxicillin was higher than that of penicillin acylase from *E. coli*.

Thus, we have modeled the structure of a new α -amino acid ester hydrolase from *X. rubrilineans* in the present study. In addition, the model structures of the complexes of this enzyme with a series of substrates and products have been obtained. The analysis of these structures showed good agreement with the experimental data for this enzyme, as well as for other AEHs, which is indicative of high-precision modeling. We believe that the most interesting data are the results of modeling of the structure of the XrAEH com-

plex with amoxicillin, which is a far more efficient (and more expensive) antibacterial drug than ampicillin. For this reason, amoxicillin is used in combination with clavulanic acid, an inhibitor of β -lactamase (trade names "Augmentin", "Clavamox" and other). As mentioned above, the penicillin acylase used today is an efficient biocatalyst for ampicillin synthesis, but it shows much lower efficiency in the synthesis of amoxicillin. Therefore, searching for and designing new biocatalysts for amoxicillin synthesis are topical tasks for the pharmaceutical industry. Availability of a model structure of the XrAEH complex with amoxicillin offers an opportunity for increasing XrAEH efficacy in the synthesis of amoxicillin using the rational design, one of the most efficient methods for protein engineering. ●

This study was supported by the Ministry of Education and Sciences of the Russian Federation (State contract № 14.512.11.0066) and the Russian Foundation for Basic Research (grant number 11-04-00962-a).

REFERENCES

1. Elander R.P. // Appl. Microbiol. Biotechnol. 2003. V. 61. № 5–6. P. 385–392.
2. Youshko M.I., Moody H.M., Bukhanov A.L., Boosten W.H.J., Švedas V.K. // Biotechnol. Bioeng. 2004. V. 85. № 3. P. 323–329.
3. Tishkov V.I., Savin S.S., Yasnaya A.S. // Acta Naturae. 2010. V. 2. № 3(6). P. 47–61.
4. Barends Th.R.M., Polderman-Tijmes J.J., Jekel P.A., Williams Ch., Wybenga G., Janssen D.B., Dijkstra B.W. // J. Biol. Chem. 2006. V. 281. № 9. P. 5804–5810.
5. Polderman-Tijmes J.J., Jekel P.A., Jeronimus-Stratingh C.M., Bruins A.P., van der Laan J.-M., Sonke Th., Janssen D.B. // J. Biol. Chem. 2002. V. 277. № 32. P. 28474–28482.
6. Barends Th.R.M., Polderman-Tijmes J.J., Jekel P.A., Hensgens C.M.H., de Vries E.J., Janssen D.B., Dijkstra B.W. // J. Biol. Chem. 2003. V. 278. № 25. P. 23076–23084.
7. Blum J.K., Bommarius A.S. // J. Mol. Catal. B: Enzym. 2010. V. 67. № 1–2. P. 21–28.
8. Hall Th.A. // Nucl. Acids Symp. Ser. 1999. V. 41. № 1. P. 95–98.
9. Dauber-Osguthorpe P., Roberts V.A., Osguthorpe D.J., Wolff J., Genest M., Hagler A.T. // Proteins: Struct. Funct. Genet. 1988. V. 4. № 1. P. 31–47.
10. Discovery Studio 2.5 // <http://accelrys.com/products/discovery-studio/>
11. Kiefer F., Arnold K., Künzli M., Bordoli L., Schwede T. // Nucl. Acids Res. 2009. V. 37. Suppl. 1. P. D387–D392.
12. Yarotsky S.V., Sklyarenko A.V. // Proc. VII Moscow Intern. Congress «Biotechnology: State of the Art and Prospects Development», March 19–22, 2013. Moscow. Russia. Part 2. P. 142–143.

Neolactoferrin As a Stimulator of Innate and Adaptive Immunity

A.D. Chernousov^{1,2}, M.F. Nikonova¹, N.I. Sharova¹, A.N. Mitin¹, M.M. Litvina¹, P.E. Sadchikov¹, I.L. Goldman², A.A. Yarilin¹, E.R. Sadchikova^{2,*}

¹Institute of Immunology, Federal Medical and Biological Agency, Kashirskoe shosse, 24/2, Moscow, Russia, 115478

²Institute of Gene Biology, Russian Academy of Sciences, Vavilova Str., 34/5, Moscow, Russia, 119334

*E-mail: e.r.sadchikova@gmail.com

Received 07.05.2013

Copyright © 2013 Park-media, Ltd. This is an open access article distributed under the Creative Commons Attribution License, which permits unrestricted use, distribution, and reproduction in any medium, provided the original work is properly cited.

ABSTRACT The effect of the innovative product Neolactoferrin, a natural combination of recombinant human lactoferrin (90%) and goat lactoferrin (10%) isolated from the milk of transgenic goats carrying the full-length human lactoferrin gene, on human immune system cells was studied. Neolactoferrin enhanced the production of IL-1 β . Neolactoferrin saturated with iron ions increased the synthesis of pro-inflammatory cytokine TNF α . It determined the direction of the differentiation of precursor dendrite cells. Under the action of T cells, Neolactoferrin amplified the expression of the transcription factors responsible for the differentiation of Th- and Treg-cells and stimulated the production of both IFN γ and IL-4. The results suggest that Neolactoferrin exhibits an immunotropic activity and hinders the development of immune inflammatory processes. Iron saturation of Neolactoferrin increases its pro-inflammatory activity.

KEYWORDS Recombinant human lactoferrin; Neolactoferrin; immunity; inflammation; cytokines; transcription factors.

INTRODUCTION

Lactoferrin (LF) is the key bactericidal protein in human milk that protects neonates against infections. LF exhibits antimicrobial [1–3], antiviral [4–6], and antifungal [7, 8] activities. LF has also been shown to affect the antibiotic-resistant microflora, while microorganisms can manage no genetic adaptation to it [9, 10]. When used together with antibiotics, LF enhances their effect [11, 12]. Despite its strong antimicrobial properties, LF does not suppress the vital activity of the normal microflora of the gastrointestinal tract [13, 14]. Furthermore, it stimulates the growth of bifidobacteria by supplying the iron ions required to ensure their vital activity [15]. The other biological activities of LF include immunomodulation [9, 16], antioxidation [17, 18], and anti-inflammatory [19] activity. LF and its derivatives (lactoferricins) have been found to suppress the progression of tumors and metastases in experimental animals [20–22].

The mechanism behind the biological activities of LF has been well studied [23–25]. The bactericidal effect of LF was found to be caused both by its direct action on pathogenic microorganisms and by its ability to activate the immune system of the organism via the stimulation of innate immunity, as well as activation and differentiation of immune-competent cells [26]. Researchers

endeavored to isolate pure human lactoferrin (hLF) in an attempt to use it as a component of functional feed products or various biologically safe new-generation drugs. Researchers at the Herzen Moscow Oncological Research Institute have verified the feasibility of using hLF in such a way: they used hLF isolated from human breast milk to design high-efficiency drugs with a broad therapeutic effect [27–30], including injection forms [31]. Unfortunately, the demand for hLF cannot be met because of the problems associated with breast milk supply.

Lactoferrin isolated from bovine milk (bovine lactoferrin, bLF) with biological activity largely similar to that of hLF has been widely used over the past decade [32, 33]. However, despite the success in using bLF [34], a decision was made to use recombinant human lactoferrin (rhLF) instead of the “alien” bLF as it is done for some other biologically active animal proteins. There is only 67% homology between the amino acid sequences of hLF and bLF [35]. The differences in the primary structure cause differences in the secondary and tertiary structures of these proteins, which may determine their functional features. Certain differences in the structure of hLF and bLF in various human organs and tissues have already been revealed [36]. Thus, the receptor of small intestine cells was found to show higher

specificity to hLF than to bLF; this difference can be to a significant extent attributed to the hLF structure [37]. The hLF receptor is believed to participate in iron absorption in the small intestine in humans [38]. Iron is typically transported through the apical membrane of the small intestine by the divalent metal transporter-1 (DMT-1). Iron bound to hLF cannot penetrate into the cell via DMT-1; the hLF receptor performs that function. Once hLF is inside the cell, it binds to the nucleus, where it is believed to act as a transcription factor and induce the biosynthesis of signaling proteins, such as caspase-1 and interleukin-18. These proteins subsequently enter circulation as a systemic signal. This pathway is considered to be the minor one; only ~10% of hLF is transported via this pathway. The main pathway of hLF penetration into epithelial cells results in the degradation of ~90% of the protein and iron release.

hLF receptors similar to the small intestinal receptor have been found in salivary glands, the heart, skeletal muscles, adrenal glands, and the pancreas [39]. Two other types of receptors were detected in the liver: the low-density lipoprotein receptor-related protein (LFR) and the asialoglycoprotein receptor (ASGPR).

Degradation of bLF and hLF yields the so-called lactoferricins denoted by the symbols B [40] and H [41], respectively. These lactoferricins differ in terms of both the amino acid sequence and their biological activity.

Immunologists believe that full biological safety of bLF for humans can be ensured only if this protein is used as a component of food products, whereas hLF can also be used as a component of the injection form of drugs.

rhLF has been produced in different countries by modern bioengineering methods using plants [42, 43], microscopic fungi [44], and animals [45, 46] as producers.

In Russia, rhLF has been produced as a component of goat milk within the framework of the Belarus–Russia Union State program [47]. Its physicochemical parameters and biological activity correspond to those of natural hLF [48, 49]. This protein was used to produce an innovative product, Neolactoferrin (Neolact), a combination of rhLF and goat lactoferrin (gLF) in transgenic goat milk at a 90 : 10 rhLF : gLF ratio.

Goat lactoferrin was experimentally found to enhance the expression of the *NF-κB* gene and synthesis of the tumor necrosis factor (TNFα), which is extremely important for the activation of innate immunity; however, it has no effect on the activation of interleukin-1 (IL-1) synthesis.

This study is focused on the joint effect of rhLF and gLF on innate immunity indicators in humans. The ability of Neolact with different iron contents (4% (Fe-) and 16% (Fe+)) to induce innate immunity, to enhance the

presentation capacity of dendritic cells, to determine the direction of differentiation of T-cell precursors, and to boost the synthesis of major adaptive immune response cytokines (interferon-γ (IFNγ) and IL-4) was studied.

EXPERIMENTAL

The activity of Neolact samples was assessed in a concentration range from 0.1 to 100 μg/ml under incubation with the tested cells for 18 h at 37°C.

Mononuclear cells (mostly lymphocytes) were isolated from human whole blood via centrifugation using the one-step ficoll-verographin density gradient (density of 1.077 g/ml). The fraction was obtained by incubating blood mononuclear cells in 24-well plates (Costar, USA) for 1 h at 37°C.

The human dendritic cell line HTSC.IL-10 was cultured and stored at the Lymphocyte Differentiation Laboratory (Institute of Immunology, Russia) [50].

The expression level of membrane molecules on the cell surface was assessed by flow cytometry (BD FACSCanto II analyzer) using monoclonal antibodies labeled with fluorescein isothiocyanate (anti-CD80, anti-CD123) or phycoerythrin (anti-HLA-DR, anti-CD86) (Caltag, USA).

The cytokine concentration in the culture media was determined by ELISA using the proper test kits (OAO Cytokine, St. Petersburg, Russia).

Intracellular cytokines were determined in mononuclear cells activated by a mixture of 4-phorbol 12-myristate 13-acetate (PMA) and ionomycin (iono) in the presence of BD GolgiStop (Becton Dickinson, USA) and permeabilized using the BD Cytotfix/Cetoperm Fixation/Permeabilization Kit on a flow cytometer using labeled anti-cytokine monoclonal antibodies [51].

The expression levels of the transcription factor genes (*NF-κB*, *GATA-3*, *Tbet*, *FOXP3* and *RORc*) were determined by a real-time reverse-transcription polymerase chain reaction. The TaqMan One-Step RT-PCR Master Mix Reagents Kit and TaqMan Gene Expression Assays (Applied Biosystems, USA) were used [52]. The mRNA expression level was determined with respect to the expression mRNA level in the house-keeping gene of β2-microglobulin (B2M) according to the formula:

$$\Delta\Delta Ct = 2^{-((Ct_{ic}^{B2M} - Ct_{B2M}) - (Ct_{geneX} - Ct_{geneX}))}$$

where Ct is the threshold cycle determined in the exponential portion of the DNA accumulation curve and IC is the internal control.

The results were statistically processed using non-parametrical methods for data analysis. The indices were represented as Me (L–H), where Me is the median

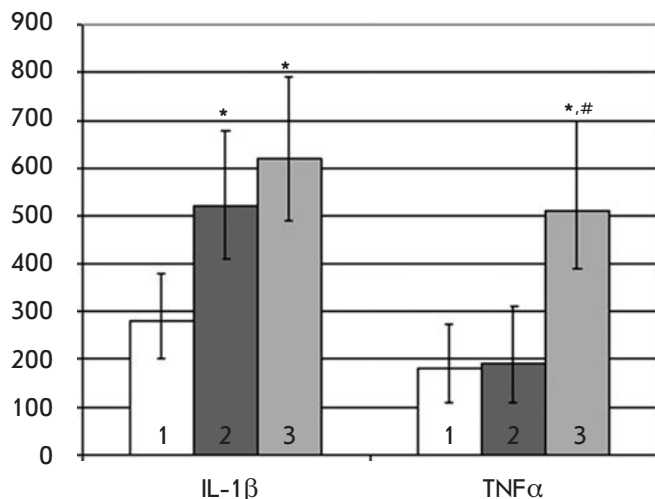


Fig. 1. The effect of Neolact (2) and Neolact enriched in iron (3) on the monocyte secretion of cytokines IL-1 β and TNF α . 1 – cytokine secretion level in the control. Y axis: cytokine concentrations (pg/ml) in the culture medium of monocytes. Medians * $p < 0.05$ regarding the control are presented; # – the same regarding Neolact. The concentration of Neolact and Neolact enriched in iron is 10 $\mu\text{g/ml}$

value and L and H are the lower and higher quartiles, respectively. The Mann–Witney U-test was used to compare the indicators.

RESULTS AND DISCUSSION

Neolact was found to activate innate immunity: at concentrations of 10 and 100 $\mu\text{g/ml}$, Neolact significantly boosted the secretion of IL-1 β by human blood monocytes, while having no effect on TNF α secretion.

The enrichment of Neolact in iron ions induced the ability to boost TNF α secretion (Fig. 1). Thus, the pro-inflammatory activity of Neolact was limited by an increase in IL-1 β secretion by blood monocytes, while its enrichment in iron ions activated the innate immunity and enhanced the manifestation of pro-inflammatory effects to a significant extent.

Figure 2 shows the effect of Neolact on the expression of the membrane molecules that play a crucial role in antigen presentation, which was determined for HTSC.IL-10 dendritic cells. Neolact at three tested doses significantly reduced the number of cells expressing major histocompatibility complex class II (HLA-DR) molecules and the costimulatory molecule CD86, which were originally present in almost all cells in this cell line, and increased the number of cells carrying another costimulatory molecule (CD80), which was originally contained in a small number of cells in this cell line. Neolact actually induced the replacement of costimulatory molecules on the surface of dendritic

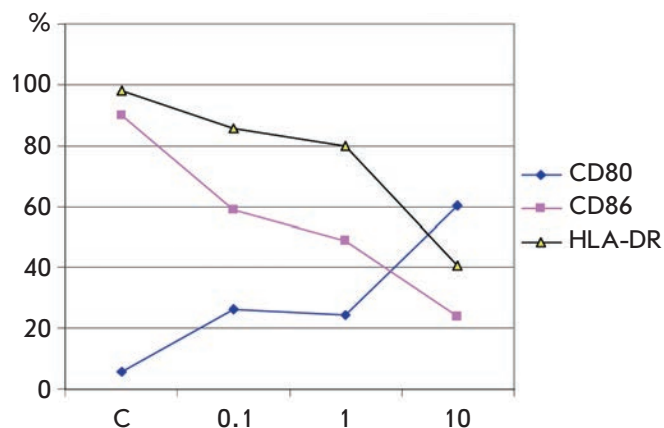


Fig. 2. The effect of Neolact on the expression of the costimulatory molecules HLA-DR, CD80, and CD86 by HTSC. IL10 dendritic cells. The mean values of three experimental runs are shown. X axis – Neolact concentration, $\mu\text{g/ml}$, Y axis – percentage of cells carrying a marker. C – original expression of costimulatory molecules without adding Neolact

cells. Meanwhile, the density of HLA-DR molecules on each individual cell increased under the action of Neolact. These effects were eliminated by enriching the drug in iron ions. The decrease in the percentage of dendritic cells carrying HLA-DR molecules can be considered as evidence of the fact that Neolact limits the antigen-presenting ability of a dendritic cell population. Neolact causes no quantitative changes in T-cell activation dependent on the expression of costimulatory molecules, since attenuation of the expression of one costimulatory molecule is accompanied by the enhancement of the expression of another molecule performing the same function. Meanwhile, Neolact exhibits the activity of a dendritic cell differentiation factor: this can be seen from the expression of the marker for plasmacytoid dendritic cells (CD123), which is an IL-3 receptor (Fig. 3). The induction of CD123 expression, which can be interpreted as a sign of the conversion of the dendritic cell phenotype from myeloid to plasmacytoid [53], determines the Th2-type immune response and attenuates the more aggressive response of T cells (Th1 and Th17) that causes immune inflammation. It should be mentioned that the differentiating ability of gLF is pronounced to a much lesser extent (Fig. 3).

The choice of the differentiation direction of T-helper cells eventually determines the direction of the immune response, whether it is pro- or anti-inflammatory, the ability to promote the development of various forms of immune pathology, etc. Th1- and

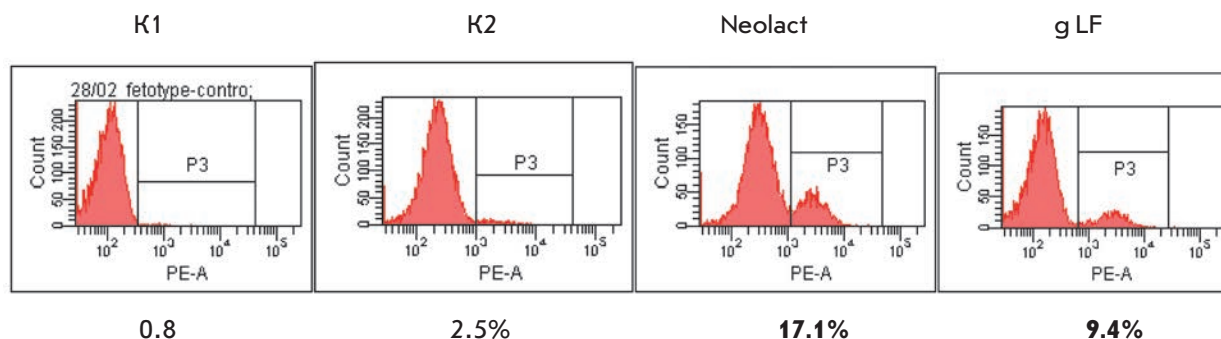


Fig. 3. The effect of Neolact and goat lactoferrin on the expression of CD123 molecules on HTSC.IL10 dendritic cells in one-day-old cultures. Histograms of two-color staining with monoclonal antibodies. K1 – without anti-CD123-PE staining; K2 – without incubation with Neolact. Values that differ from the control at least twofold are shown in bold. The concentrations of Neolact and goat lactoferrin were 10 µg /ml

Effect of Neolact on the expression of the genes of the transcription factors that control the differentiation of CD4⁺ T-lymphocytes

Neolact, µg/ml	Transcription factor genes			
	GATA3	TBX21	RORC	FOXP3
Nonactivated lymphocytes				
0 (control)	0.718 (0.527–0.974)	0.010 (0.005–0.018)	0.260 (0.199–0.292)	0.569 (0.306–0.818)
1.0	1.173* (0.815–1.690)	0.014 (0.002–0.016)	0.266 (0.159–0.272)	0.834* (0.811–1.120)
10.0	0.727 (0.481–2.587)	0.018 (0.001–0.028)	0.172 (0.043–0.409)	0.767 (0.246–0.774)
Phytohemagglutinin-activated lymphocytes				
0 (control)	0.613 (0.483–0.894)	0.010 (0.005–0.017)	0.649 (0.433–1.013)	0.805 (0.047–1.101)
1.0	1.228* (0.705–1.815)	0.014 (0.007–0.018)	0.487 (0.399–0.802)	1.018 (0.759–2.446)
10.0	0.675 (0.399–0.807)	0.011 (0.008–0.013)	0.743 (0.483–1.576)	0.678 (0.361–1.069)

**p* < 0.05.

Note. Medians are presented (the lower and upper quartiles are shown in brackets).

Th17 cells can be conventionally classified as pro-inflammatory cells, while Th2 and Treg can be classified as anti-inflammatory ones. Of note, Th2 cells are typically regarded as proallergic cells. The differentiation direction and stabilization of the cell phenotype is determined by the expression of the GATA-3 (for Th2 cells), Tbet (for Th1), RORc (for Th17), and FOXP3 (for Treg) transcription factors, which are encoded by the *GATA3*, *TBX21*, *RORC*, and *FOXP3* genes, respectively. In this context, the range of expression of the specified genes by blood T cells significantly predetermines the

hereditary or induced tendency of the organism to develop certain types of the immune response and various forms of immune pathology.

The effect of Neolact on the development of various T-helper cells was assessed according to their effect on the expression of the transcription factor genes that regulate CD4⁺ T-cell differentiation (Table). Neolact and its iron-enriched derivative at concentrations as low as 1 µg/ml enhanced the expression of the *GATA3* gene responsible for the development of Th2 cells, anti-parasite protection, and pro-allergic orientation of the

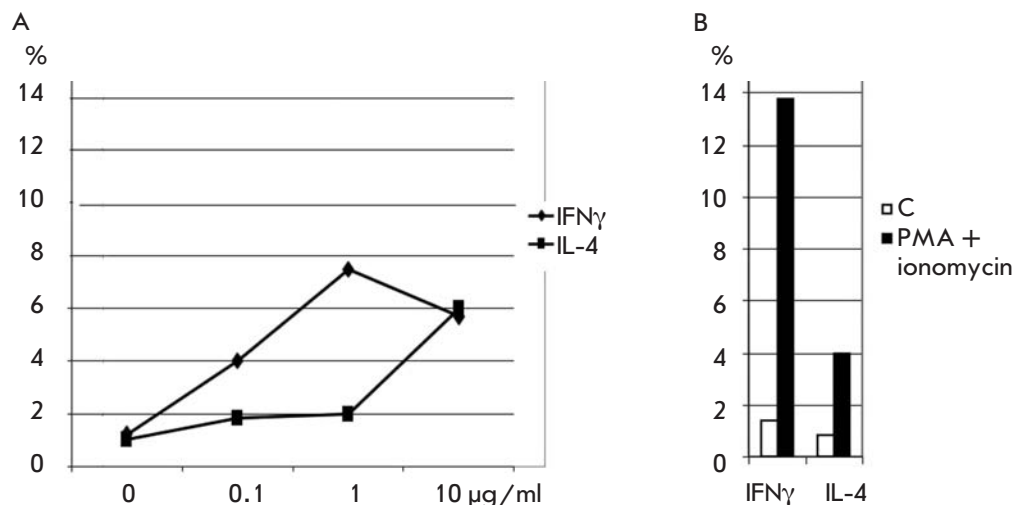


Fig. 4. (A) The effect of Neolact on the induction of the T cells forming IFN γ and IL-4 ($n=3$). (B) positive control of the specified cytokines by T cells under optimal stimulation with PMA/ionomycin (100 nM/2 μ M, respectively). X-axis – rhLF concentration (A); Y-axis – the percentage of cells producing the specified cytokines (A, B)

immune processes. The effect of Neolact could be seen for both resting and activated T cells. No significant effect on the expression of the “pro-inflammatory” genes *TBX21* (encodes the Tbet factor of Th1 cells) and *RORC* (encodes the RORc factor of Th17 cells) have been detected. Neolact enhanced the expression of the *FOXP3* gene responsible for the development of regulatory T cells, which limit the intensity and duration of the immune response. Neolact does not induce expression in the dendritic cells of the gene of the IL-12 beta chain, which is responsible for Th1 cell differentiation.

Thus, Neolact exhibited no ability to stimulate the expression of the factors contributing to the development of immune inflammation in this series of tests. Instead, it had the opposite effect as it stimulated the expression of the genes responsible for the development of Th2 and Treg cells.

The assessment of the effect of Neolact on the differentiation of Th1 and Th2 cells (Th1 and Th2 cells were determined according to the number of cells producing their key cytokines, IFN γ and IL-4, respectively) has demonstrated that Neolact enhances the secretion of both cytokines. Neolact at a concentration of 1 μ g/ml increases IFN γ secretion to a greater extent than IL-4 secretion. The secretion of both cytokines becomes identical at a Neolact concentration of 10 μ g/ml (Fig. 4). However, the number of cells producing IFN γ remains much lower event at a Neolact concentration of 1 μ g/ml than it is when cells are activated with a PMA-iono-

mycin mixture. The number of IL-4-producing cells is higher than this level. In other words, stimulation of Th2 cells with Neolact corresponds to the physiological level of their involvement in the immune response, whereas stimulation of Th1 cells remains below this level, which is consistent with data obtained by assessing the effect of rhLF on the expression of the genes of the transcription factor regulating the differentiation of T-helper cell subtypes.

CONCLUSIONS

Summarizing the results of the assessment of the effect of Neolact on certain manifestations of the immune system activity, one can draw a conclusion that the agent exhibits immunotropic activity and that its effect is associated with either inhibition of immune processes or their development via the Th2-dependent pathway to a certain extent. Meanwhile, according to its effect on the formation of the cells producing IFN γ - and IL-4, the agent does not cause a strong polarization of the immune response, which could have resulted in the development of allergic or autoimmune processes. Neolact enriched in iron ions is characterized by an enhanced pro-inflammatory activity and lacks a number of the effects that are typical of original Neolact. ●

This work was supported by the Ministry of Education and Science of the Russian Federation (State contract № 01.916.12.0001).

REFERENCES

1. Farnaud S., Evans R.W. // *Mol. Immunol.* 2003. V. 40. P. 395–405.
2. Brock J.H. // *Biochem. Cell Biol.* 2012. V. 90. P. 245–251.
3. Sallmann F.R., Baveye-Descamps S., Pattus F., Stivense K.J. // *J. Biol. Chem.* 1999. V. 274. P. 16107–16114.
4. Van Hooijdonk A.C., Kustndrager K.D., Steijns J.M. // *Br. J. Nutr.* 2000. V. 84. P. 127–134.

5. Ikeda M., Nozaki A., Sugiyama K., Shiita J., Sato T. // *Virus Res.* 2000. V. 66. P. 51–63.
6. Pietrantonio A., Ammendolia M.G., Superti F. // *Biochem. Cell Biol.* 2012. V. 90. P. 442–448.
7. Andersson Y., Lindquist S., Lagerqvist C., Hernell O. // *Early. Hum. Dev.* 2000. V. 59. P. 95–105.
8. Giels S., Czuprynski C. // *Microb. Pathog.* 2002. V. 32. P. 87–97.
9. Kruzel M.L., Zimecki M. // *Arch. Immunol. Ther.* 2002. V. 50. P. 339–410.
10. Leitch E.C., Willcox M.D. // *Int. J. Antimicrob. Agents.* 2001. V. 18. P. 399–402.
11. Naidu A.S., Arnold R.R. // *Diagn. Microbiol. Infect. Dis.* 1994. V. 20. P. 69–75.
12. Fowler C.E., Soothill J.S., Oakes L. // *J. Antimicrob. Chemother.* 1997. V. 40. P. 877–879.
13. Reiter B. // *Ann. Rech. Vet.* 1978. V. 9. P. 205–224.
14. Petschow B.M., Talbott R.D., Batema R.P. // *J. Med. Microbiol.* 1999. V. 48. P. 541–546.
15. Kim W.S., Ohashi M., Tanaka T., Nozaki A., Sugiyama K. // *Biomaterials.* 2004. V. 17. P. 279–283.
16. Yamauchi K., Wakabayashi H., Shin K., Takase M. // *Biochem. Cell Biol.* 2006. V. 84. P. 291–296.
17. Tomita M., Wakabayashi H., Shin K., Kuwata H., Yip T.T., Yamauchi K., Teraguchi S., Hayasawa H. // *Biochimie.* 2009. V. 91. P. 52–57.
18. Mulder A.M., Connellan P.A., Oliver C.J., Morris C.A., Stevenson L.M. // *Nutr. Res.* 2008. V. 28. P. 583–589.
29. Kulics J., Kijstra A. // *Immunol. Lett.* 1986/1987. V. 14. P. 349.
20. Furlong S.J., Mader J.S., Hoskin D.W. // *Exp. Mol. Pathol.* 2010. V. 88. P. 371–375.
21. Mader J.S., Salsman J., Conrad D.M., Hoskin D.W. // *Mol. Cancer Ther.* 2005. V. 4. P. 612–624.
22. Bezault J., Bhimani R., Wiprovnick J. // *Cancer Res.* 1994. V. 54. P. 2310–2312.
23. Murphy M.E., Kariwa H., Mizutani T., Yoshimatsu K., Arikawa J., Takashima I. // *Arch. Virol.* 2000. V. 145. P. 1571–1582.
24. Buharin O.V., Valishev A.V., Valisheva I.V. // *Uspehi Sovremennoy Biologii (Biology Bulletin Reviews).* 2011. V. 131. P. 135–144.
25. Lonnerdal B., Iyer S. // *Annu. Rev. Nutr.* 1995. V. 15. P. 93–110.
26. Spadaro M., Caorsi C., Ceruti P., Varadhachary A., Forini G., Pericle F., Giovarelli M. // *FASEB J.* 2008. V. 22. P. 2747–2757.
27. Nemtsova E.R., Ivanova L.M., Yakubovskaya R.I., // *Bio-medical chemistry.* 1995. V. 3. P. 58–61.
28. Edeleva N.V., Sergeeva T.V., Nemtsova E.R., Tsherbitskaya I. Ya., Yakubovskaya R.I., Osipova N.A. // *Anesteziology and reanimatology.* 2001. V. 5. P. 61–64.
29. Nemtsova E.R., Edeleva N.V., Osipova N.A., Yakubovskaya R.I., Chissov V.I. // *Russian oncology.* 2006. V.4. P.29–33
30. Edeleva N.V., Nemtsova E.R., Yakubovskaya R.I., Osipova N.A. // *Russian oncology.* 2005. V. 6. P. 25–28
31. Chissov V.I., Yakubovskaya R.I., Boyko A.V. Pat. № 2165789.04.27.2001.R.I.
32. Spik G., Burnet B., Mazurier-Dehaine C., Fontaine G., Montreuil J. // *Acta Paediatr. Scand.* 1982. V. 71. P. 979–985.
33. Cirioni O., Giacometti A., Barchiesi F., Scalise G. // *J. Antimicrob. Chemother.* 2000. V. 46. P. 577–582.
34. Valenti P., Berlutti F., Conte M.P., Longhi C., Seganti L. // *J. Clin. Gastroenterol.* 2004. V. 38. P. 127–129.
35. Magnuson J.S., Henry J.F., Yip T.T., Hutchens T.W. // *Pediatr. Res.* 1990. V. 28. P. 176–181.
36. Kawakami H., Lonnerdal B. // *Am. J. Physiol.* 1991. V. 261. P. 841–846.
37. Suzuki Y.A., Shin K., Lonnerdal B. // *Biochemistry.* 2001. V. 40. P. 15771–15779.
38. Baker E.N., Baker H.M. // *Cell Mol. Life Sci.* 2005. V. 62. P. 2531–2539.
39. Suzuki Y.A., Lopez V., Lonnerdal B. // *Cell. Mol. Life Sci.* 2005. V. 62. P. 2560–2575.
40. Bellamy W., Takase M., Wakabayashi H., Kawase K., Tomita M. // *J. Appl. Bacteriol.* 1992. V. 73. P. 472–479.
41. Odell E.W., Sarra R., Foxworthy M., Chapple D.S., Evans R.W. // *FEBS Lett.* 1996. V. 382. P. 175–178.
42. Conesa C., Calvo M., Sánchez L. // *Biotechnol. Adv.* 2010. V. 28. P. 831–838.
43. Lonnerdal B. // *J. Am. Coll. Nutr.* 2002. V. 21. P. 218S–221S.
44. Andersen J.H. // *Curr. Opin. Mol. Ther.* 2004. V. 6. P. 344–349.
45. Van Berkel P.H., Welling M.M., Geerts M., van Veen H.A., Ravensbergen B., Salaheddine M., Pauwels E.K., Pieper F., Nuijens J.H., Nibbering P.H. // *Nat. Biotechnol.* 2002. V. 20. P. 484–487.
46. Zhang J., Li L., Cai Y., Xu X., Chen J., Wu Y., Yu H., Yu G., Liu S., Zhang A., et al. // *Protein. Expr. Purif.* 2008. V. 57. P. 127–135.
47. Goldman I.L., Georgieva S.G., Gurskiy Y.G., Krasnov A.N., Deykin A.V., Popov A.N., Ermolkevich T.G., Budzevich A.I., Chernousov A.D., Sadchikova E.R. // *Biochem. Cell Biol.* 2012. V. 90. P. 512–519.
48. Sokolov A.V., Pulina M.O., Kristiyan A.V., Zaharova E.T., Runova O.L., Vasilev V.B., Gurskiy Y.G., Minashkin M.M., Krasnov A.N., Kadulin C.G., et al. // *DAS.* 2006. V. 411. № 2. P. 267–270.
49. Goldman I., Chernousov A., Sadchikova E. // *Recent Adv. Clin. Med.* 2010. P. 315–321.
50. Sharova N.I., Litvina M.M., Yarilin A.A. // *Russian Immunology.* 2010. V. 31. P. 181–185.
51. Jung T., Schauer U., Heusser C., Neumann C., Rieger C. // *J. Immunol. Meth.* 1993. V. 159. P. 197–207.
52. Donetskova A.D., Nikonova M.F., Yarilin A.A. // *Russian Immunology.* 2011. V. 32. P. 184–188.
53. Schmitt N., Cumont M.C., Nugeyre M.T., Hurtrel B., Barré-Sinoussi F., Scott-Algara D., Israël N. // *Immunobiology.* 2007. V. 212. P. 167–177.

Depolarization-Induced Calcium-Independent Synaptic Vesicle Exo- and Endocytosis at Frog Motor Nerve Terminals

M.M. Abdrakhmanov, A.M. Petrov*, P.N. Grigoryev, A.L. Zefirov
Kazan State Medical University, Butlerov str., 49, Kazan, Russia, 420012

*E-mail: fysio@rambler.ru

Received 04.04.2013

Copyright © 2013 Park-media, Ltd. This is an open access article distributed under the Creative Commons Attribution License, which permits unrestricted use, distribution, and reproduction in any medium, provided the original work is properly cited.

ABSTRACT The transmitter release and synaptic vesicle exo- and endocytosis induced by constant current depolarization of nerve terminals were studied by microelectrode extracellular recording of miniature endplate currents and fluorescent microscopy (FM 1-43 styryl dye). Depolarization of the plasma membrane of nerve terminals in the control specimen was shown to significantly increase the MEPC frequency (quantal transmitter release) and exocytotic rate (FM 1-43 unloading from the synaptic vesicles preliminarily stained with the dye), which was caused by a rise in the intracellular Ca^{2+} concentration due to opening of voltage-gated Ca channels. A slight increase in the MEPC frequency and in the rate of synaptic vesicle exocytosis was observed under depolarization in case of blockade of Ca channels and chelating of intracellular Ca^{2+} ions (cooperative action of Cd^{2+} and EGTA-AM). The processes of synaptic vesicle endocytosis (FM 1-43 loading) were proportional to the number of synaptic vesicles that had undergone exocytosis both in the control and in case of cooperative action of Cd^{2+} and EGTA-AM. A hypothesis has been put forward that Ca-independent synaptic vesicle exo- and endocytosis that can be induced directly by depolarization of the membrane exists in the frog motor terminal in addition to the conventional Ca-dependent process.

KEYWORDS motor nerve terminals; exocytosis; endocytosis; calcium; constant depolarization current; cadmium.

ABBREVIATIONS EGTA-AM – ethylene glycol-O, O'-bis(2-aminoethyl)-N, N, N', N'-tetraacetic acid acetoxymethyl ester; MEPC – miniature end plate currents.

INTRODUCTION

Transmitter release via synaptic vesicle exocytosis is the main function of presynaptic nerve terminals in a chemical synapse. Exocytosis is accompanied by processes of endocytosis (i.e., by the formation of new vesicles that are filled with the neurotransmitter and can participate in the transmitter release again) [1, 2]. It is believed that the exo- and endocytotic processes are induced under natural conditions due to an increase in the intracellular Ca^{2+} concentration as the voltage-gated Ca channels in the plasma membrane open [3–5].

Ca-dependence of the voltage-gated action of synaptic vesicle exocytosis is associated with specialized proteins, synaptotagmins I, II, IX, which are the main candidates as calcium ion sensors [6]. Spontaneous (asynchronous) exocytosis is also Ca^{2+} -dependent and is determined by the action of intracellular Ca^{2+} on synaptotagmin I and Doc2b [7, 8]. The effect of calcium ions

on endocytosis is more complex [9, 10]. An increase in the intracellular Ca^{2+} concentration can either induce/accelerate endocytosis [11] or inhibit it [3, 9]. Calcium ion regulation of endocytosis can be mediated by calcineurin, Ca^{2+} /calmodulin-dependent phosphatase, and calcium binding to synaptotagmin [12, 13].

However, there is a hypothesis that transmitter release can be controlled directly by changes in the membrane voltage of the nerve terminal without entry of Ca^{2+} [14, 15]. In ganglionic neurons, depolarization enhances exocytosis in a Ca-independent manner [16], while the subsequent endocytosis is independent of an increase in the intracellular Ca^{2+} concentration and shows a rapid dynamics [17].

The role of depolarization in transmitter release and synaptic vesicle exo- and endocytosis in a motor nerve terminal was studied in this work by electrophysiological and fluorescent methods.

EXPERIMENTAL

Study object, solutions

Isolated nerve and muscle preparation from the cutaneous pectoris muscle of the frog *Rana ridibunda* in the winter season (December through February) were used for the experiments. The frogs were refrigerated at 5°C and transferred to the laboratory 2 h before the experiment. The work was carried out in compliance with international guidelines for the proper conduct of animal experiments.

The standard Ringer's solution (115.0 mM NaCl, 2.5 mM KCl, 1.8 mM CaCl₂, 2.4 mM NaHCO₃) was used; a pH of 7.2–7.4 and temperature of 20°C were maintained. All the experiments were conducted only for the nerve terminals on the surface. In order to block the nerve terminal action potential, 1 μM tetrodotoxin was added to the perfusion solution. In some cases, Ringer's solution supplemented with Cd²⁺ ions (0.2 mM) was used for blockage of the Ca²⁺ channels of the nerve terminal. To ensure binding of intracellular Ca²⁺ ions, the preparation was treated with the membrane-permeable form of EGTA calcium chelator (EGTA-AM) (50 μM) for 1 h. All the reagents used were purchased from Sigma (USA). The experiments were conducted at a constant perfusion rate of 5 ml/min; bath volume was 10 ml.

Electrophysiology

Miniature end plate currents (MEPC) were recorded using extracellular glass microelectrodes filled with a 2 M NaCl solution (~1 μm tip end; resistance of 1–5 MΩ). The electrode was applied to a nerve terminal at a distance of 20–40 μm from the final myelin segment. The signals were amplified using an extracellular amplifier and digitized using L-CARD 1250. The MEPC frequency was determined from the average time between two successive signals (impulses/s).

Fluorescent microscopy

A 6 μM FM1-43 fluorescent dye (SynaptoGreen C4, Invitrogen, USA) was used for the experiments. The marker was bound reversibly to the presynaptic membrane and became trapped inside the newly formed synaptic vesicles during endocytosis (was “loaded” into a nerve terminal) [18]. Fluorescence images were obtained using an Orca II CCD video camera (Hamamatsu, Japan) and an Olympus BX51 motorized microscope (Germany, CellP software) equipped with the DSU confocal system and an Olympus LUMPLFL 60xw lens. Terminal fluorescence in the central and distal portions of the nerve terminal was analyzed. The ImagePro program was used to assess the fluorescence intensity as relative fluorescence units of a pixel minus the background fluorescence. The background fluorescence

was determined as the mean fluorescence intensity in a 50 × 50 pixel square in an image area showing no nerve terminal [19].

Depolarization of the nerve terminal

Two glass micropipettes with a 2–5 μm tip diameter filled with a 2 M NaCl solution were used to depolarize the nerve terminal. One (depolarizing) pipette was applied to the preterminal portion of the nerve terminal under visual control, while the second one was applied to the muscle fiber containing the nerve terminal at a distance of 1 mm from the first pipette. The stimulating pipettes were connected to a DS3 stimulator (Digitimer Ltd.) that was used as a current source. The current in the circuit was controlled with a microamperometer.

The statistical analysis was performed using the Origin Pro software. The quantitative results are presented as a mean ± standard error, *n* is the number of independent runs. Statistical significance was determined using the Student's *t*- and ANOVA tests.

RESULTS

Electrophysiology. Transmitter release under depolarization of nerve terminals

At an extracellular Ca²⁺ concentration of 1.8 mM, the MEPC frequency was 0.23 ± 0.03 impulses/s (*n* = 25). Constant current depolarization of the membrane resulted in a rapid increase in the MEPC frequency (Fig. 1A), which was retained during the entire time that the current was applied (up to 40–50 min). The increase in the MEPC frequency depended on the current (Fig. 1B). Thus, the MEPC frequency increased to 2.9 ± 0.3 impulses/s (*n* = 10, *p* < 0.01) under a direct current (2 μA), while increasing to 6.1 ± 0.4 (*n* = 10, *p* < 0.01) and 12.9 ± 0.5 impulses/s (*n* = 10, *p* < 0.01) at 4 and 6 μA, respectively (Fig. 1A,B).

Supplementation of the perfusion solution with Cd²⁺ ions (0.2 mM) increased the MEPC frequency to 2.22 ± 0.04 impulses/s (*n* = 20, *p* < 0.01). A weaker effect of depolarization on the MEPC frequency was observed in this case (Fig. 1A,B). Thus, when a depolarizing current (2, 4 and 6 μA) was applied, the MEPC frequency reached 2.8 ± 0.3 (*n* = 10, *p* < 0.05), 3.8 ± 0.4 (*n* = 10, *p* < 0.01), and 5.2 ± 0.4 (*n* = 10, *p* < 0.01) impulses/s, respectively (Fig. 1A,B).

An hour-long exposure to EGTA-AM caused no significant changes in the MEPC frequency, which was 0.20 ± 0.03 impulses/s (*n* = 16, *p* > 0.05) in this case. The preliminary treatment of the nerve-muscle preparation with EGTA-AM (see the Experimental section) eliminated the stimulating effect of Cd²⁺ ions (0.2 mM) on the MEPC frequency (Fig. 1A,B). The MEPC frequency under these conditions (0.21 ± 0.02 impulses/s (*n* = 20,

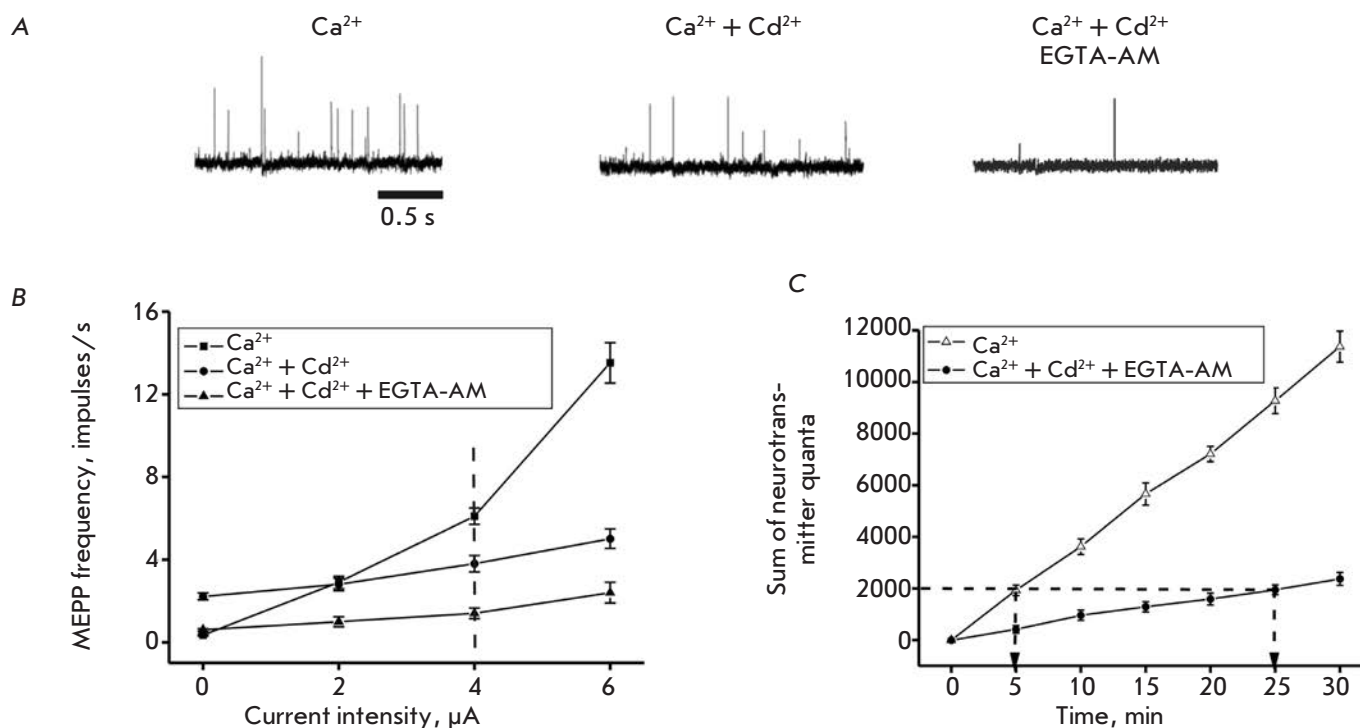


Fig. 1. Effect of the depolarizing current on neurotransmitter release. **A** — MEPC frequency during the action of the depolarizing current (4 μA) in the control; Cd²⁺ ions were added, both EGTA-AM and Cd²⁺ were used. **B** — MEPC frequency as a function of the intensity of the depolarizing current. The dashed line indicates the MEPC frequency under a depolarizing current of 4 μA. **C** — Cumulative curves of transmitter release during the action of a depolarizing current of 4 μA. Y axis shows the sum of neurotransmitter quanta, X axis shows the time elapsed since the beginning of depolarization, min. The dashed line indicates the coordinates of the points corresponding to an identical sum of neurotransmitter quanta

$p > 0.05$) was identical to that for the control specimens. However, the stimulating effect of depolarization on the MEPC frequency was still observed, although it was weaker than that in the control or against the action of Cd²⁺ (Fig. 1B). A depolarizing current of 2, 4, and 6 μA increased the MEPC frequency to 0.9 ± 0.2 ($n = 10$, $p < 0.05$), 1.5 ± 0.2 ($n = 10$, $p < 0.01$), and 2.8 ± 0.3 ($n = 10$, $p < 0.01$) impulses/s, respectively.

The rate and time dependence of transmitter secretion under constant current depolarization of the nerve terminal was analyzed using cumulative curves (Fig. 1C). In this case, the sum of all the MEPC that had emerged vs. polarization time was plotted. Figure 1B shows the cumulative curves of transmitter release under depolarization of the nerve terminal (current of 4 μA) for 30 min. The number of quanta of neurotransmitter released from the nerve terminals in the control after a 5-min depolarization is equal to that released after a 25-min depolarization of a nerve terminal treated with EGTA-AM and in the presence of Cd²⁺ ions in an ambient environment (Fig. 1C).

Fluorescent microscopy. Depolarization of the nerve terminal and processes of synaptic vesicle endocytosis

The incubation of a nerve-muscle preparation in the standard Ringer's solution with FM1-43 (5–40 min) caused nonspecific fluorescence of the nerve terminal (Fig. 2A) due to dye binding to the membrane [18–20]. The mean fluorescence intensity of the nerve terminal was 0.075 ± 0.005 rel. units ($n = 32$) (Fig. 2B). Intensely fluorescent spots along the nerve terminal could be seen after constant current depolarization (4 μA) of the nerve terminal for 5 min in the standard Ringer's solution with FM1-43. These spots are an aggregation of vesicles that had undergone the exocytosis–endocytosis cycle and entrapped the fluorescent dye (Fig. 2A). In this case, the mean fluorescence intensity was 0.16 ± 0.01 rel. units ($n = 27$, $p < 0.05$) (Fig. 2B). When EGTA-AM and Cd²⁺ exerted a joint effect in addition to constant current depolarization of the membrane (4 μA) for 5 min, the dye was not loaded into the nerve terminal (nonspecific fluorescence of nerve terminal 0.08 ± 0.004 rel. units, $n = 30$, $p > 0.01$) (Fig. 2A,B).

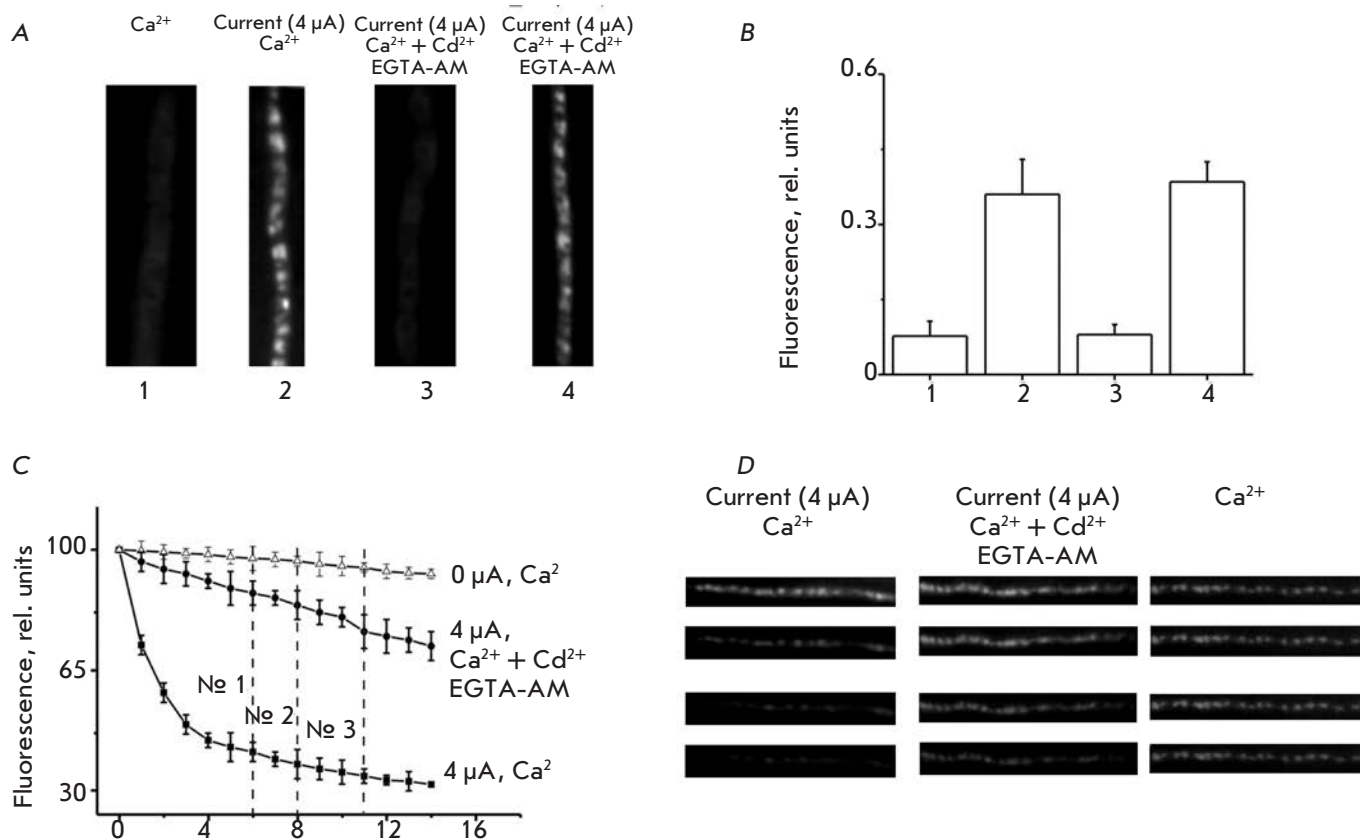


Fig. 2. Synaptic vesicle exo- and endocytosis induced by depolarization of the nerve terminal membrane. **A** — Images of FM 1-43 fluorescence in the nerve terminal after application of FM 1-43 (25 min) at rest (1), under the depolarizing current for 5 min (2), and use of both EGTA-AM and Cd²⁺ during 5 (3) and 25 (4) min. **B** — Fluorescence intensity of the nerve terminals preliminarily stained with FM 1-43 according to different protocols: 1, 2, 3, 4. Y axis shows the fluorescence intensity (rel. units). **C** — Average fluorescent de-staining profiles during depolarization in the control (4 μA, Ca²⁺) and when using EGTA-AM and Cd²⁺ (4 μA, Ca²⁺+Cd²⁺+ EGTA-AM). The curve (0 μA, Ca²⁺) representing the changes in the fluorescence intensity at rest without depolarization is shown on the graph. Y axis shows fluorescent intensity, % (100% — fluorescent intensity before depolarization), X axis shows the time elapsed since the beginning of depolarization, min. **D** — Images of the FM 1-43 fluorescence of the nerve terminal at the times 0, №1, №2, and №3. The dashed lines (№1, №2, №3) designate fluorescence levels corresponding to times of 6, 8, and 11 min

However, a longer constant current exposure (25 min) gave rise to fluorescent spots along the nerve terminal (0.17 ± 0.01 rel. units, $n = 25$, $p < 0.05$), attesting to the fact that endocytosis was occurring (Fig. 1A,B).

Dynamics of synaptic vesicle exocytosis under depolarization of nerve terminals

In order to assess the synaptic vesicle exocytosis, we analyzed the dynamics of the decrease in the fluorescence intensity of nerve terminals that had been pre-loaded with a marker [18–20]. First, FM1-43 was loaded under a depolarization current (4 μA) for 5 min. After a rest period (1 h), a depolarization current (4 μA) was applied on the stained nerve terminals again, resulting in the release of the dye (through exocytosis) from synaptic

vesicles and in a decrease in the fluorescence intensity of nerve terminals (Fig. 2C,D). It should be mentioned that the fluorescent spots were observed in the standard Ringer's solution for a long time (Fig. 2C,D). An appreciably rapid and sharp decrease in the fluorescence of the preliminarily loaded nerve terminals was observed under constant current depolarization (4 μA) (Fig. 2C,D). By the time the depolarization current had been applied for 2 min, the fluorescence intensity had fallen to $58 \pm 3\%$ ($n = 10$, $p < 0.01$), while 12–15 min later it became as low as ~30% of the initial level. If the preparations were treated with EGTA-AM prior to the loading of the dye and the nerve terminal membrane was subsequently subjected to constant current depolarization in the presence of Cd²⁺, the fluorescence intensity

of a nerve terminal (unloading) occurred much slower (Fig. 2C,D). Thus, the fluorescence intensity dropped to $95 \pm 2\%$ ($n = 10$, $p < 0.01$) after depolarization for 2 min, while the fluorescence intensity of the spots 12–15 min after remained at the level of $\sim 70\%$ of the initial one.

DISCUSSION

In most studies focused on exo- and endocytosis, depolarization of the membrane was induced using a solution with an increased content of potassium ions [1, 20, 21]. However, the use of the solution changes the equilibrium potential for K^+ and all the processes associated with the transport of K^+ ions (e.g., function of Na/K-ATPase) and can also inhibit synaptic vesicle endocytosis [22]. Constant-current depolarization of the nerve terminal membrane, which does not have the side effects described above, was used in this study to assess the role of the membrane potential in synaptic vesicle exo- and endocytosis.

Ca-independent exocytosis

The experiments have demonstrated that constant current depolarization of the nerve terminal membrane at an extracellular concentration of calcium ions of 1.8 mM results in an increase of quantal transmitter release (MEPC frequency) and an appreciably rapid and well-pronounced unloading of FM1-43 (Fig. 1B, 2C). All these facts attest to the fact that depolarization of the nerve terminal membrane induces synaptic vesicle exocytosis due to the opening of the potential-gated Ca^{2+} channels, entry of Ca^{2+} ions into the nerve terminals, and activation of the fusion mechanism [1, 6, 23].

The next task was to assess the Ca^{2+} ion values in depolarization-induced synaptic vesicle exocytosis. One could attempt to stimulate exocytosis in a calcium-free medium by depolarization; however, the removal of extracellular Ca^{2+} is fraught with the disturbance of the architecture of exocytic sites, the phase state of the membrane, the structure of membrane proteins and blocks synaptic vesicle endocytosis [10, 24]. Hence, all the experiments were conducted at a normal extracellular concentration of Ca^{2+} ions.

Cd^{2+} ions at a concentration of 0.2 mM are efficient and universal blockers of voltage-dependent Ca^{2+} channels of all (L-, N-, P/Q-, R-, and T-) types [25]. It has been demonstrated in experiments using Cd^{2+} that depolarization increases the MEPC frequency, although this rise is not as significant as that in the control (Fig. 1B). It is an interesting fact that Cd^{2+} ions increase transmitter release to a certain extent (Fig. 1B), which is also typical of other bi- and trivalent cations [27]. Cd^{2+} can affect the Ca^{2+} -sensitive metabotropic receptor, whose activation induces the phospholipase C signaling pathway. Diacylglycerol (stimulating protein

kinase C and exocytosis protein Munc13) and inositol trisphosphate (increasing the intracellular concentration of Ca^{2+} due to the release from the endoplasmic reticulum) are eventually formed in the nerve terminal [28]. It can be assumed that cadmium ions penetrate into a nerve terminal and cause an increase in the cytosolic calcium level due to its release from the calcium depot [29].

We have previously demonstrated that two buffers binding the intracellular Ca^{2+} ions – EGTA-AM and BAPTA-AM (1,2-bis(2-aminophenoxy) ethane-N,N,N',N'-ethylenediamine tetraacetic acid tetra(acetoxymethyl ester)) – suppress the increase in the MEPC frequency induced by a hyperpotassium solution (suppress the increase in the MEPC frequency induced by a solution with an increased content of potassium ions) to an identical extent, thus attesting to similar efficiencies in the chelating of the cytosolic Ca^{2+} [30]. EGTA-AM was used to eliminate the aforementioned effect of Cd^{2+} . Indeed, there was no stimulating effect of Cd^{2+} ions on the MEPC frequency against chelating of intracellular Ca^{2+} (Fig. 1B). Meanwhile, in the presence of EGTA-AM and blockage of Ca^{2+} entry into the extracellular environment, the depolarizing current caused a slight (but statistically significant) increase in the MEPC frequency (Fig. 1B). The efficiency of a direct current (4 μ A) in inducing synaptic vesicle exocytosis was also detected under these conditions by fluorescent microscopy, which could be observed as reduced fluorescence of the preliminarily loaded nerve terminals (Fig. 2C). All these observations indicate that in addition to the conventional Ca^{2+} -dependent exocytosis, an extracellular Ca^{2+} -independent synaptic vesicle exocytosis also exists. This type of exocytosis is presumably induced by membrane depolarization under presynaptic voltage and is a component of the induced transmitter release.

Ca-independent endocytosis

Exo- and endocytosis processes are tightly coupled and occur at a 1:1 ratio; thus, the endocytosis intensity should be assessed only for an identical exocytosis intensity. According to the resulting data, we found that the number of quanta released from a nerve terminal in the control under depolarization for 5 min and current intensity of 4 μ A is equal to that released during depolarization of the nerve terminal preliminarily treated with EGTA-AM for 30 min with Cd^{2+} ions added to the medium (Fig. 1C). These findings were also confirmed by the results of experiments using a FM1-43 endocytic marker. Fluorescent spots of intensity almost identical to those in the control emerged in the nerve terminals under these conditions (Fig. 2A,B). A hypothesis can be put forward that compensatory endocytosis can be

induced both by an increase in the intracellular Ca^{2+} concentration when the voltage-gated calcium channels of the plasma membrane open [12, 13] and directly via depolarization of the nerve terminal membrane.

CONCLUSIONS

The revealed dependence of exo- and endocytosis on the membrane voltage of a nerve terminal provides some additional potentialities for regulating transmitter release and synaptic transmission. No molecular targets for a direct effect of depolarization on synaptic vesicle exo- and endocytosis have been identified yet. However, recent studies have revealed the dependence on voltage in a large number of signaling molecules (protein kinases A and C, phosphatase of phosphoinositides conjugated to presynaptic autoreceptor G-proteins) af-

fecting the mechanism of synaptic vesicle exo- and endocytosis [17, 31–33]. It is also possible that Ca^{2+} channels of the plasmatic membrane, which can transduce the depolarization signal to the SNARE complex and endocytosis proteins, are sensors that detect changes in the membrane voltage [14, 34]. ●

This work was supported by the Russian Foundation for Basic Research (grants № 11-04-00568_a, 12-04-31550_mol_a, №12-04-33195_mol_a_ved), the Ministry of Education of Science of the Russian Federation (NSh-4670.2012.4, MK-108.2013.4) and the State contract of the Ministry of Education and Science of the Russian Federation (Federal target-oriented program).

REFERENCES

- Zefirov A.L., Petrov A.M. Synaptic vesicle and mechanism of neurotransmitter release (exo-endocytosis vesicular cycle). Kazan: Art-café, 2010. 356p.
- Heuser J.E., Reese T.S. // *J. Cell Biol.* 1973. V. 57. № 2. P. 315–344.
- Zefirov A.L., Abdrakhmanov M.M., Grigor'ev P.N. // *Russ. Fiziol. Zh. Im. I.M. Sechenova.* 2005. V. 91. № 7. P. 821–831.
- Ceccarelli B., Hurlbut W.P. // *J. Cell Biol.* 1980. V. 87. № 1. P. 297–303.
- Ramaswami M., Krishnan K.S., Kelly R.B. // *Neuron.* 1994. V. 13. № 2. P. 363–375.
- Pang, Z.P., Sudhof T.C. // *Curr. Opin. Cell Biol.* 2010. V. 22. P. 496–505.
- Xu J., Pang Z.P., Shin O.H., Südhof T.C. // *Nat. Neurosci.* 2009. V. 12. № 6. P. 759–766.
- Groffen A.J., Martens S., Díez Arazola R., Cornelisse L.N., Lozovaya N., de Jong A.P., Goriounova N.A., Habets R.L., Takai Y., Borst J.G., et al. // *Science.* 2010. V. 327. P. 1614–1618.
- Cousin M.A., Robinson P.J. // *Trends Neurosci.* 2001. V. 24. P. 659–665.
- Zefirov A.L., Abdrakhmanov M.M., Mukhamedyarov M.A., Grigoryev P.N. // *Neuroscience.* 2006. V. 143. № 4. P. 905–910.
- Balaji J., Armbruster M., Ryan T.A. // *J. Neurosci.* 2008. V. 28. P. 6742–6749.
- Wu X.S., McNeil B.D., Xu J., Fan J., Xue L., Melicoff E., Adachi R., Bai L., Wu L.G. // *Nat. Neurosci.* 2009. V. 12. P. 1003–1010.
- Yao J., Kwon S.E., Gaffaney J.D., Dunning F.M., Chapman E.R. // *Nat. Neurosci.* 2011. V. 15. P. 243–249.
- Parnas H., Segel L., Dudel J., Parnas I. // *Trends Neurosci.* 2000. V. 23. № 2. P. 60–68.
- Silinsky E.M., Watanabe M., Redman R.S., Qiu R., Hirsh J.K., Hunt J.M., Solsona C.S., Alford S., MacDonald R.C. // *J. Physiol.* 1995. V. 1. № 482. P. 511–520.
- Zhang C., Zhou Z. // *Nat. Neurosci.* 2002. V. 5. № 5. P. 425–430.
- Zhang C., Xiong W., Zheng H., Wang L., Lu B., Zhou Z. // *Neuron.* 2004. V. 42. № 2. P. 225–236.
- Betz W.J., Bewick G.S., Ridge R.M. // *Neuron.* 1992. V. 9. № 5. P. 805–813.
- Petrov A.M., Naumenko N.V., Uzinskaya K.V., Giniatul'lin A.R., Urazaev A.K., Zefirov A.L. // *Neuroscience.* 2011. V. 186. P. 1–12.
- Zefirov A.L., Grigor'ev P.N., Petrov A.M., Minlebaev M.G., Sitdikova G.F. // *Tsitologiya.* 2003. V. 45. № 12. P. 1163–1171.
- Ramirez D.M., Kavalali E.T. // *Curr. Opin. Neurobiol.* 2011. V. 21. № 2. P. 275–282.
- Zefirov A.L., Abdrakhmanov M.M., Grigor'ev P.N., Petrov A.M. // *Tsitologiya.* 2006. V. 48. № 1. P. 34–41.
- Angleson J.K., Betz W.J. // *J. Neurophysiol.* 2001. V. 85. № 1. P. 287–294.
- Zefirov A.L., Mukhamedzianov R.D., Minlebaev M.G., Cheranov S.Iu., Abdrakhmanov M.M., Grigor'ev P.N. // *Russ. Fiziol. Zh. Im. I.M. Sechenova.* 2002. V. 88. P. 191–204.
- Zheng N., Raman I.M. // *J. Neurosci.* 2009. V. 29. № 31. P. 9826–9838.
- Nurullin L.F., Tsentssevitsky A.N., Malomouzh A.I., Nikolsky E.E. // *Dokl. Biol. Sci.* 2013. V. 449. № 3. P. 360–363.
- Van der Kloot W., Molgó J. // *Physiol. Rev.* 1994. V. 74. № 4. P. 899–991.
- Vyleta N.P., Smith S.M. // *J. Neurosci.* 2011. V. 31. № 12. P. 4593–4606.
- Braga M.F., Rowan E.G. // *Gen. Pharmacol.* 1994. V. 25. № 8. P. 1729–1739.
- Zefirov A.L., Grigor'ev P.N. // *Bull. Exp. Biol. Med.* 2008. V. 146. № 12. P. 608–612.
- Chen X., Zhang X., Jia C., Xu J., Gao H., Zhang G., Du X., Zhang H. // *J. Biol. Chem.* 2011. V. 286. № 46. P. 39760–39767.
- Dekel N., Priest M.F., Parnas H., Parnas I., Bezanilla F. // *Proc. Natl. Acad. Sci. USA.* 2012. V. 109. № 1. P. 285–290.
- Murata Y., Okamura Y. // *J. Physiol.* 2007. V. 583. P. 875–989.
- Zheng H., Fan J., Xiong W., Zhang C., Wang X., Liu T., Liu H., Sun L., Wang Y., Zheng L., et al. // *Biophys. J.* 2009. V. 96. P. 2449–2456.

Alu- and 7SL RNA Analogues Suppress MCF-7 Cell Viability through Modulating the Transcription of Endoplasmic Reticulum Stress Response Genes

D.N. Baryakin^{1*}, D.V. Semenov¹, A.V. Savelyeva^{1,2}, O.A. Koval¹, I.V. Rabinov¹, E.V. Kuligina¹, V.A. Richter¹

¹Institute of Chemical Biology and Fundamental Medicine, Siberian Branch of the Russian Academy of Sciences, Lavrentiev Ave., 8, Novosibirsk, Russia, 630090

²Novosibirsk State University, Pirogova Str., 2, Novosibirsk, Russia, 630090

*E-mail: baryakindn@niboch.nsc.ru

Received 14.08.2013

Copyright © 2013 Park-media, Ltd. This is an open access article distributed under the Creative Commons Attribution License, which permits unrestricted use, distribution, and reproduction in any medium, provided the original work is properly cited.

ABSTRACT 11% of the human genome is composed of Alu-retrotransposons, whose transcription by RNA polymerase III (Pol III) leads to the accumulation of several hundreds to thousands of Alu-RNA copies in the cytoplasm. Expression of Alu-RNA Pol III is significantly increased at various levels of stress, and the increase in the Alu-RNA level is accompanied by a suppression of proliferation, a decrease in viability, and induction of apoptotic processes in human cells. However, the question about the biological functions of Pol III Alu-transcripts, as well as their mechanism of action, remains open. In this work, analogues of Alu-RNA and its evolutionary ancestor, 7SL RNA, were synthesized. Transfection of human breast adenocarcinoma MCF-7 cells with the Alu-RNA and 7SL RNA analogues is accompanied by a decrease in viability and by induction of proapoptotic changes in these cells. The analysis of the combined action of these analogues and actinomycin D or tamoxifen revealed that the decreased viability of MCF-7 cells transfected with Alu-RNA and 7SL RNA was due to the modulation of transcription. A whole transcriptome analysis of gene expression revealed that increased gene expression of the transcription regulator *NUPR1* (p8), as well as the transcription factor *DDIT3* (CHOP), occurs under the action of both the Alu- and 7SL RNA analogues on MCF-7 cells. It has been concluded that induction of proapoptotic changes in human cells under the influence of the Alu-RNA and 7SL RNA analogues is related to the transcriptional activation of the genes of cellular stress factors, including the endoplasmic reticulum stress response factors.

KEYWORDS Alu-repeats; Alu-RNA; 7SL RNA; MCF-7 human breast adenocarcinoma cells.

ABBREVIATIONS FITC – fluorescein-5-isothiocyanate; ER – endoplasmic reticulum; MTT – 3-(4,5-dimethyl-2-thiazolyl)-2,5-diphenyl-2H-tetrazolium bromide; JC-1 – 5,5',6,6'-tetrachloro-1,1',3,3'-tetraethylbenzimidazolium carbocyanine iodide; SRP – signal recognition particle.

INTRODUCTION

45% of the human genome is composed of mobile elements, of which Alu-repeats are the most numerous, ~ 1.1×10^6 copies, which accounts for 10.6 % of nuclear DNA [1, 2]. In a variety of Alu-repeats of primates, several subfamilies are identified and classified into three main groups: AluJ, AluS, and AluY [3]. The copy number of representatives of evolutionarily ancient AluJ-repeats, which emerged in the genome about 80 million years ago, and intermediate AluS subfamilies (about 40 million years ago), has not increased in the human genome. AluY subfamily repeats (> 20 million years ago) still remain transpositionally active [4].

It is known that the formation of new copies of Alu- and related SINE-repeats in the genome of mammals occurs by a retrotransposition mechanism, which

comprises a step for the production of RNA copies of SINE-DNA. Evolutionarily significant variations in the genome occur due to the “successful” events of retrotransposition of repeats in germ cells [5, 6].

However, it is known that RNA copies of genomic Alu-repeats (Alu-RNA) are present both in germ and in somatic human cells [7]. Alu-RNAs are synthesized by RNA polymerase III (Pol III) [8] and are a set of RNA copies of the “ancient,” transpositionally inactive Alu-repeats of the subfamilies J and S, and transpositionally active AluY [7, 9, 10]. Alu-RNAs, as well as their evolutionary ancestor, 7SL RNA, are synthesized in the nucleus and are then transported into the cytoplasm. Some Alu-transcripts undergo 3'-endonuclease processing to yield the truncated forms, scAlu-RNAs, represented by the “left” Alu monomers (Fig. 1A). Along with the

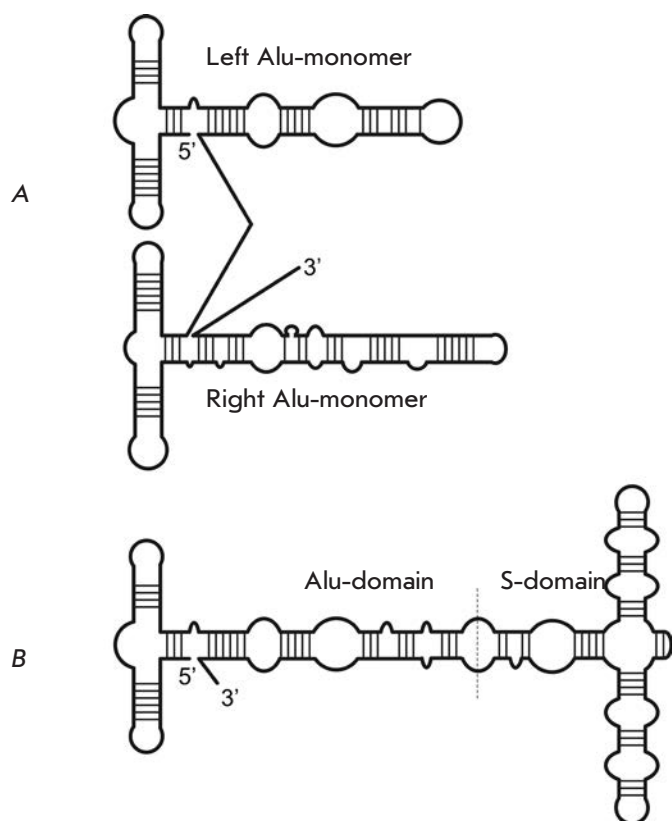


Fig. 1. A schematic representation of the secondary structure of Alu-RNA (A) and 7SL RNA (B) according to [12]

truncated Alu-transcripts, unprocessed forms are determined in cells. The latter are represented by Alu-RNA, which includes the “left” and “right” monomers, and the 3'-terminal poly-A-sequence (Fig. 1A) [10, 11]. The number of full-length Pol III Alu-transcripts is $\sim 10^2$ – 10^3 molecules per cell. Regulation of Alu-RNA expression in human cells differs from that of other Pol III-transcripts. Thus, a translation inhibitor, cycloheximide, and heat shock increase the expression of Alu-RNA to a greater extent compared with the expression of other Pol III-transcripts, such as 7SL, 7SK, 5S and U6 RNAs [8]. The permanent presence of full-length Alu transcripts in the cytoplasm, as well as an increase in the expression of these RNAs under stress, on one hand, indicates that Alu-RNA is a closely controlled endogenous factor of mutagenesis and, on the other hand, makes it possible to suggest that Alu-RNAs are regulators of vital cellular processes [12].

Earlier K. Sakamoto *et al.* [13] demonstrated that transfection of HeLa cells with DNA constructs containing transcriptionally active Alu-repeats, as well as with constructs encoding 7SL RNA, causes suppression of DNA replication, inhibits translation, and provides

an antiproliferative effect. It was found that transfection of human embryonic kidney HEK 293 cells with DNA encoding Alu-repeats leads to specific activation of the expression of the reporter genes, presumably due to direct inhibition of the dsRNA-activated protein kinase PKR by Alu-RNA [14]. It was shown later [15] that activation of reporter gene expression in the presence of Alu-RNA was induced by a decrease in the lag period of translation of newly synthesized mRNAs and was not associated with inhibition of PKR. However, a new molecular mechanism, by which Alu-RNA might affect the translation initiation of newly synthesized mRNAs, was not proposed.

J. Häsler and K. Strub assumed that the participation of Pol III Alu-transcripts in cellular processes was related to their structural similarity with 7SL RNA (Fig. 1) [12, 16]. Like 7SL RNA, Alu-RNA interacts with the proteins of the signal recognition particle (SRP) [17, 18]. The ability of Alu-RNA to modulate translation is attributed to its interaction with SRP9/14 proteins: it has been shown that Alu-RNA activates translation, but Alu-RNA in complex with SRP9/14 inhibits the *in vitro* translation of total mRNA in HeLa cells in wheat germ extracts [16].

It has been demonstrated *in vitro* that Alu-RNA directly interacts with the catalytic subunit of human RNA polymerase II (Pol II) and inhibits the activity of the complex Pol II-TBP-TFIIB-TFIIF at a step of transcription initiation [19, 20]. These data suggest that Alu-RNA is a nonspecific regulator of mRNA transcription in human cells [19].

Recently, in a study on the molecular and cellular mechanisms of the geographic atrophy of the retina (one of the main reasons for a decrease in visual acuity and blindness in people older than 50 years) it was found that retinal pigment epithelial cell death is accompanied by a decrease in the *DICER1* gene expression and by the accumulation of the Pol III AluSc-transcript in these cells [21]. It was shown that the key enzyme in post-transcriptional microRNA processing, Dicer1 RNase, hydrolyzes Alu-RNA *in vitro*. A decreased expression of *DICER1* leads to the accumulation of AluSc-RNA, which in turn suppresses the viability and induces the apoptotic death of the epithelial cells of the retina [21]. A molecular mechanism for the cytotoxic action of Alu-RNA in pigmented epithelial cells has been suggested. It includes the generation of reactive oxygen species by mitochondria, activation of NLRP3-inflammasomes, as well as activation of the MyD88-signaling cascade [22]. Thus, it is the increase in the Alu-RNA expression level that is considered as the main cause of cell death in the geographic atrophy of the retina. However, the question as to why Alu-RNA causes reactive oxygen species formation remains open [21, 22].

In this work, the AluYa5-RNA and 7SL RNA analogues were synthesized and a comparative analysis of their effect on the viability and activation of proapoptotic processes in MCF-7 human breast adenocarcinoma cells was performed. The effect of the Alu-RNA and 7SL RNA analogues, along with cytostatics (inhibitors of replication, transcription, translation, and cellular transport), on MCF-7 cells was also analyzed. It has been established that the proapoptotic processes induced in MCF-7 cells by the Alu-RNA and 7SL RNA analogues are modulated by tamoxifen and actinomycin D. The results of the whole transcriptome analysis of gene expression variation in cells transfected with the Alu-RNA and 7SL RNA analogues allow us to put forward a new mechanism of the cytotoxic action of these RNAs based on the activation of the ER stress response genes *NUPR1*, *DDIT3*, *FOXRED2*, and *ASNS*.

EXPERIMENTAL

Reagents

The following reagents were used in this work: MTT – 3-(4,5-dimethylthiazol-2-yl)-2,5-diphenyl -2H-tetrazolium bromide (Sigma, USA); Trizol, Lipofectamine 2000 (Invitrogen, USA); Taq-polymerase, T7-RNA-polymerase (Fermentas, USA); propidium iodide, JC-1 indicator, staurosporine (Sigma, USA); annexin V-FITC conjugate (BD Pharmingen, USA); cisplatin (LENS-Farm, Russia); cycloheximide, actinomycin D (AppliChem, Germany); interferon α (Microgen, Russia); methotrexate, monensin (Sigma, USA); tamoxifen (Veropharm, Russia), the human recombinant tumor necrosis factor α (State Research Center of Virology and Biotechnology VECTOR, Novosibirsk, Russia), reverse transcriptase MoMLV, ribonucleoside triphosphates, deoxyribonucleoside triphosphates, and T4-polynucleotide kinase (Biosan, Novosibirsk, Russia). Deoxyribooligonucleotides were synthesized in the Laboratory of Medicinal Chemistry, Institute of Chemical Biology and Fundamental Medicine (SB RAS).

Synthesis of the Alu- and 7SL RNA analogues

To obtain DNA templates, which are PCR products encoding the Alu- and 7SL RNA analogues under the T7 phage RNA polymerase promoter, genomic DNA of MCF-7 cells was amplified with the following primer pairs (T7-RNA polymerase promoter is shown with lowercase letters): AluYa5, chr6:104,183,151-104,183,559: 5'-ATTTGATTGCGTTATTTCCAAGA-3', 5'-atgcagctaatacactactataggGAGAGTCTCAGCTACAGAAATTGAA-3'; 7SL, chr14:50,329,268- 50,329,585: 5'-AAGAGACGGGGTCTCGCTAT-3', 5'-atgcagctaatacactactatagg-TTCGACGCTCTCCGACC-3'.

DNA templates were purified by electrophoresis in a 10% polyacrylamide gel (PAGE) under native conditions. DNA was eluted from the gel in the presence of 100 mM NaAc and then re-precipitated with 70% ethanol.

The human AluYa5-RNA and 7SL RNA analogues were synthesized in a buffer containing 40 mM Tris-HCl (pH 8.0), 6 mM MgCl₂, 10 mM DTT, 10 mM NaCl, 2 mM spermidine, 2 mM NTP, and 30 units T7 phage RNA polymerase at 37 °C for 2 hrs. DNA templates were digested in the presence of 1 unit DNase I at 37 °C for 40 min, and then DNase I was inactivated by incubation at 65 °C for 15 min.

Purification of the AluYa5-RNA and 7SL RNA analogues was performed on a MiLiChrom A-02 chromatography system (EcoNova, Russia) with re-precipitation with 70% ethanol in the presence of 100 mM NaAc. The primary structure of the analogues was confirmed by RNA reverse transcription, cDNA amplification, and sequencing by the Sanger method on an automatic sequencer, ABI 3730XL Genetic Analyzer (SB RAS Genomics Core Facility).

Analysis of the viability of MCF-7 cells transfected with the Alu- and 7SL RNA analogues

Human breast adenocarcinoma cells were cultured in a IMDM medium supplemented with 10 mM L-glutamine, 100 u/ml penicillin, 0.1 mg/ml streptomycin, 0.25 μ g/ml amphotericin, and a 10% fetal bovine serum at 37 °C in a 5% CO₂ atmosphere. The cell number was counted in the Goryaev chamber.

MCF-7 cells were cultured in a 96-well plate until a 60-70% confluent monolayer was formed. The cells were transfected with 1 μ g/ml RNA in a complex with Lipofectamine (Invitrogen, USA) according to the manufacturer's protocol and were incubated for 24 or 72 hrs as indicated in the legends to Tables. The medium was added with MTT to a final concentration of 0.7 mg/ml and was incubated at 37 °C for 45 min. The medium was removed, MTT formazan was dissolved in isopropyl alcohol, and the solution's optical density was determined by absorbance at $\lambda=570$ nm with the control at $\lambda=620$ nm using an Apollo LB 912 8 multichannel spectrophotometer (Berthold Technologies).

Analysis of proapoptotic changes in MCF-7 cells by flow cytometry

MCF-7 cells transfected with the Alu- and 7SL RNA analogues and the control cells incubated in the medium with Lipofectamine without RNA were washed three times with PBS and were incubated in the presence of 0.1 mg/ml trypsin at 37 °C for 5 min. To analyze cell membrane changes, a cell suspension was incubated in the presence of 4.5 μ g/ml propidium iodide and annexin V – FITC conjugate according to the manufac-

turer's protocol (BD Pharmingen, USA). A cell suspension was incubated with 2.5 µg/ml JC-1 to analyze the changes in the mitochondrial transmembrane potential ($\delta\Psi$). Preparations were analyzed by flow cytometry on a Beckman Coulter FC 500 device according to the method described in [23]. MCF-7 cell preparations incubated with a 5 µg/ml tumor necrosis factor α or with 1 µM staurosporine for 24 hrs were used as a positive control of the proapoptotic changes.

Analysis of variations in the transcriptome of MCF-7 cells using Illumina chips

MCF-7 cells were transfected with 1 µg/ml Alu-RNA or with 1 µg/ml 7SL RNA and incubated at 37 °C in a 5% CO₂ atmosphere for 24 hrs. Cells incubated with Lipofectamine without RNA under the same conditions were used as a control. Hybridization of the total RNA of MCF-7 cells on HT-12 Illumina chips was performed on the basis of Genoanalytika, CJSC (Moscow). The differential analysis of the variations in gene expression was performed using the Illumina custom algorithm with data normalization by the rank invariant method. The parameter *Detection_Pval* < 0.05 was used to interpret the results of the differential analysis of gene expression variations. Upon interpretation of the data on an increase in the gene expression under the influence of Alu-RNA, transcripts for which the structure of hybridization probes (Illumina PROBE_SEQUENCE) contained direct sequences of Alu-repeats were excluded from consideration.

Sampling verification of the whole transcriptome analysis results was performed with the real-time RT-PCR method using the following primer pairs:

PSPH - 5'-ATGATTGGAGATGGTGCCAC-3',
5'-CAGTGATATACCATTTGGCG-3';
DDIT3 - 5'-GACCTGCAAGAGGTCCTGTC-3',
5'-AAGCAGGGTCAAGAGTGTTG-3';
MTHFD - 5'-TGTAGGACGAATGTGTTTGG-3',
5'-AACATTGCAATGGGCATTCC-3';
TDP1 - 5'-CTCATCAGTTACTTGGATGGC-3',
5'-TGACTTCCTTGAAAAGCGTCC-3';
ZNF682 - 5'-AAGCCAGAACTGATTAGCCG-3',
5'-AAGGTCTTCAGTGTAATGAG-3';
CEBPG - 5'-CGCTCGGAGTGAGGCCGCC-3',
5'-CAGGGTGATCAATGGTTTCC-3'.

GAPDH and *HPRT* mRNAs were used as normalization control [24].

RESULTS AND DISCUSSION

Influence of the Alu- and 7SL RNA analogues on the viability of human breast adenocarcinoma MCF-7 cells

The action of Alu-RNA and its evolutionary ancestor, 7SL RNA, on human cells was analyzed using an ana-

logue of Alu-RNA, a transcript of human genomic repeat AluYa5, as well as using an analogue of 7SL RNA.

It was found that transfection of MCF-7 human breast adenocarcinoma cells with the Alu- and 7SL RNA analogues caused substantial morphological changes: condensation of the cytoplasm and nucleus, degradation of membrane contacts, and cell detachment from the plastic scaffold. The Alu- and 7SL RNA analogues induced morphological changes in approximately 20–30% of the cells by the 72nd h of incubation. Moreover, incubation in the medium with total MCF-7 RNA or with a L1-RNA moiety analogue or with Lipofectamine without RNA caused condensation and detachment from the scaffold of less than 5% of the MCF-7 cells.

The cells were incubated with the Alu- and 7SL RNA analogues, and their viability was analyzed using the MTT test to determine whether the morphological changes observed under the action of these analogues were caused by antiproliferative and proapoptotic processes.

The data presented in Table 1 demonstrate that the Alu-RNA and 7SL RNA analogues cause a statistically significant reduction in MCF-7 cell viability upon transfection with Lipofectamine ($p < 0.05$). The observed morphological changes in conjunction with the reduction in viability under the action of the Alu- and 7SL RNA analogues indicate that transfection with these RNAs leads to proapoptotic changes in cells.

We analyzed the changes in the mitochondrial transmembrane potential ($\delta\Psi$) using the JC-1 indicator to evaluate, by an independent method, induction of the proapoptotic processes in MCF-7 cells under the influence of Alu- and 7SL RNAs. The indicator JC-1 forms aggregates in the mitochondria of viable cells, with the fluorescence spectrum shifted to the longer wavelengths ($\lambda_{\max} = 590$ nm). Dissipation of the mitochondrial transmembrane potential $\delta\Psi$ is accompanied by a shift in the fluorescence spectrum maximum of the indicator to the green region ($\lambda_{\max} = 527$ nm). The analysis of cell preparations by flow cytometry in the presence of the JC-1 indicator made it possible to estimate the relative contribution of a cell population to proapoptotic changes the mitochondrial membrane [23, 25].

It was found that the reduction in MCF-7 cell viability under the action of the 7SL RNA analogue is accompanied by a reduction in the transmembrane potential $\delta\Psi$ in approximately 17% of the cells (Table 1). However, the action of 7SL RNA was not different from that of the Alu-RNA analogue ($p > 0.05$). Therefore, the data on the changes in the mitochondrial potential $\delta\Psi$ are consistent with the results of the viability analysis obtained using the MTT test, and with the evaluation of the depth of the morphological changes in the cells.

Transfection of cells with the Alu- and 7SL RNA analogues leads to the formation of cell-like structures exposing phosphatidylserine on the outer surface, as well as structures whose membrane is permeable to propidium iodide (apoptotic and secondary necrotic bodies). The overall contribution of the apoptotic and secondary necrotic bodies to the total population of cells transfected with the Alu-RNA analogue or 7SL RNA analogue was about 31% (Table 1).

It is known that the emergence of phosphatidylserine on the outer surface of the cytoplasmic membrane, detected by staining with annexin V, is one of the earliest biochemical signs of apoptosis [26]. Meanwhile, a decrease in the activity of mitochondrial and cytoplasmic oxidoreductases and a change in the NADH/NADPH level, detectable using the MTT test [27], are characteristic of the late stages of apoptosis. Therefore, the differences in the cytotoxic action of Alu- and 7SL RNAs, estimated from the reduction of the MTT-index (~ 15–19%) and from the induction of apoptotic processes by phosphatidylserine exposure and by plasma membrane permeability (~ 31%), can be attributed to the greater sensitivity of the approach using the annexin V/PI system.

Over all, these results suggest that analogues of both Alu-RNA and 7SL RNA reduce viability and induce proapoptotic changes in a MCF-7 cell subpopulation and that the effect of the Alu-RNA analogues is not significantly different from that of 7SL RNA at the level of the changes in the activity of cytoplasmic and mi-

tochondrial dehydrogenases (MTT test), dissipation of the mitochondrial transmembrane potential $\delta\Psi$, and by assessment of the depth of the morphological changes.

Effect of Alu-RNA and RNA 7SL along with cytostatics on MCF-7 cell viability

Key processes, the inhibition or activation of which occurs upon transfection of cells with the Alu-RNA and 7SL RNA analogues, were characterized by a change in the MCF-7 viability upon the combined action of the analogues and a series of cytostatic agents (Table 2). The combined action of RNAs and cellular process inhibitors was analyzed using such a cytostatic concentration in a culture medium at which MCF-7 cell viability was reduced by 40% (IC_{40}) by the 72nd h of incubation.

It is seen from the data in Table 2 that transfection of cells with the Alu- and 7SL RNA analogues enhances the cytotoxic action: for cisplatin by ~ 25 and 20%; for cycloheximide by ~ 18 and 15%; for interferon α by ~ 18 and 27%, respectively ($p < 0.05$). Therefore, transfection with the Alu- and 7SL RNA analogues caused an unidirectional and comparable magnitude effect on MCF-7 cells for this set of effectors.

The formation of unrepairable DNA crosslinks and suppression of replication and mitosis underlay the cytotoxic effect of cisplatin [28]. The additivity of cisplatin and Alu-RNA or 7SL RNA (Table 2) clearly indicates that the cytotoxic effects of this cytostatic agent and Alu-RNA or RNA 7SL are independent processes and the effects of these RNAs are related directly neither

Table 1. The effect of Alu-RNA and 7SL RNA analogues on the viability, asymmetry, cell membrane permeability, and mitochondrial transmembrane potential of MCF-7 cells

RNA*	Decrease in viability (MTT-index \pm SD, %)**	Proapoptotic changes in membrane***			Mitochondrial transmembrane potential $\delta\Psi$ ****, % of cells	
		Ann V-/PI-	Ann V+/PI-	Ann V+/PI+	without dissipation	with dissipation
		Viable cells, %	Apoptotic bodies, %	Secondary necrotic cells, %		
7SL RNA	19.0 \pm 4.8	69.2	19.3	11.5	83.4	16.6
Alu-RNA	15.3 \pm 6.5	68.7	13.8	17.5	85.6	14.4
RNA MCF-7	-2.8 \pm 8.2	85.2	7.4	7.3	97.9	2.1
Lipofectamine	0 \pm 2.5	89.9	6.8	3.3	99.7	0.3

* Cells were transfected with 1 μ g/ml RNA in a complex with Lipofectamine.

** Viability of cells incubated in the medium with Lipofectamine without RNA was taken as 100%.

*** Changes in the cell membrane were analyzed by flow cytometry using annexin V (AnnV) conjugated to FITC and propidium iodide (PI).

**** Dissipation of the mitochondrial transmembrane potential was evaluated using flow cytometry of cells stained with the mitochondrial dye JC-1 [23].

Table 2. Effect of Alu-RNA and 7SL RNA analogues on MCF-7 cell viability in the presence of cytostatic agents

Effector (IC ₄₀ *)	Alu(+)-RNA		7SL(+)-RNA	
	MTT-index \pm SD, %**	p***	MTT-index \pm SD, %**	p***
Cisplatin (9.5 μ M)	25.7 \pm 7.7	0.004	20.0 \pm 3.5	0.001
Cycloheximide (0.56 μ M)	17.9 \pm 6.7	0.010	14.9 \pm 7.5	0.026
Interferon α (400 U/ml)	17.8 \pm 7.6	0.022	26.5 \pm 7.9	0.009
Methotrexate (33.3 μ M)	11.5 \pm 10.2	0.171	26.5 \pm 8.4	0.011
Monensin (2.5 pM)	3.8 \pm 6.3	0.352	10.8 \pm 5.1	0.021
Tamoxifen (450 μ M)	-1.2 \pm 12.7	0.897	-12.1 \pm 12.6	0.244
Actinomycin D (5.6 nM)	21.5 \pm 21.2	0.232	-57.7 \pm 22.6	0.031

* The empirically obtained effector concentrations are indicated at which cell viability decreased by 40% after incubation (with Lipofectamine) for 72 hrs.

** Additional decrease in the MTT-index in cells by the 72nd h after transfection with RNA. Viability of cells incubated in the medium with Lipofectamine, with an effector at the indicated concentration, and without RNA was taken as 0%.

*** *p* value for the Student's *t*-test.

to DNA replication nor to the activation of repair processes in MCF-7 cells.

The action of interferon α is based on the receptor-mediated transcriptional activation of interferon-induced genes, including the protein kinase PKR gene. PKR, in turn, is activated upon interaction with double-stranded RNA or with RNA comprising elongated hairpins, and it inhibits protein synthesis in the cell by phosphorylation of the translation initiation factor eIF2 [29]. Therefore, the additive action of the Alu- or 7SL RNA analogues and interferon α can be attributed to the fact that these RNAs, having a developed secondary structure (Fig. 1), induce the PKR-dependent suppression of translation in cells treated with interferon α : on the other hand, PKR activation by double-stranded RNA serves as a signal for the induction of innate immune cell response cascades and, as a consequence, as an interferonogenic stimulus [29]. Therefore, the PKR-dependent mechanism of the Alu- and 7SL RNA action provides manifold enhancement of the action of interferon α . At the same time, both Alu- and 7SL RNA cause the additive reduction of the MTT-index in interferon-stimulated cells, which is comparable to the reduction of viability upon combination of Alu- or 7SL RNA with cycloheximide or to the action of the RNAs without interferon α (Table 1, 2). Moreover, a number of studies have shown that the action of Alu-RNA on different processes in mammalian cells is directly connected neither to the developed secondary structure of these RNAs nor to the PKR activation [15, 21, 22]. Therefore, the PKR-dependent mechanism of action of structured RNAs and the interferonogenic activity of such RNAs only partially explain the induction of proa-

poptotic Alu- and 7SL RNA processes in MCF-7 cells.

7SL RNA, along with methotrexate and monensin, caused a significant decrease in the MTT-index ($p < 0.05$), but the variation of cell viability upon transfection with Alu-RNA, along with these cytostatic agents, was not statistically significant (Table 2). However, the decrease in the MTT-index of 7SL RNA in the presence of methotrexate or monensin was different from that induced by Alu-RNA along with these cytostatics ($p < 0.05$). These data demonstrate that the dihydrofolate reductase inhibitor methotrexate and ionophore monensin partially inhibit the cytotoxic effect of Alu- RNA, but not that of 7SL RNA.

An additional statistically significant reduction of viability ($p > 0.05$) in preparations of cells incubated in the medium with tamoxifen was not observed upon transfection with Alu-RNA or 7SL RNA (Table 2). Therefore, a conclusion can be drawn that tamoxifen partially suppresses the cytotoxic effect of both Alu-RNA and 7SL RNA on MCF-7 cells.

It is known that tamoxifen inhibits estrogen receptors, and that its effect on MCF-7 cells is due to a change in the transcription of estrogen-dependent genes. Tamoxifen is also an effective modulator of interferon action. The combined effect of interferon and tamoxifen synergistically reduces MCF-7 cell viability and induces their massive death both in culture and in a xenograft model [30, 31]. Thus, the partial inhibition of the cytotoxic effect of the Alu- and 7SL RNA analogues on MCF-7 cells by tamoxifen confirms the assumption that the influence of these RNAs on cell viability is not related to the potential interferonogenic properties of these structured RNAs.

Actinomycin D, a DNA intercalator and an inhibitor of transcription and replication, completely inhibited the cytotoxic effect of the 7SL RNA analogue, while Alu-RNA, along with this cytostatic, caused no additional significant reduction of viability (Table 2). Taking into account that inhibition of replication with cisplatin did not reduce the effect of Alu- and 7SL RNA, it is possible to conclude that partial (in the case of Alu-RNA) and total (in the case of 7SL RNA) cessation of their cytotoxic action by actinomycin D is caused by the influence of these RNAs on transcription in human cells. The data on the compensation of the Alu- and 7SL RNA cytotoxic effect by the transcription modulator tamoxifen (Table 2) support the conclusion that the modulation of nuclear DNA transcription is the key element of the action mechanism of both Alu-RNA and its closest homologue, 7SL RNA, on MCF-7 cell viability.

Analysis of the variation in gene expression in MCF-7 cells under the influence of Alu- and 7SL RNA analogues

Genes whose expression varies under the action of the Alu- and 7SL RNA analogues were determined by the whole transcriptome analysis of MCF-7 cell RNA using Illumina HT-12 microarrays. Cells incubated in the medium with Lipofectamine without RNA were used as a control.

It was found that transfection of MCF-7 cells with Alu-RNA results in an increase in the expression of 68 transcripts by 3 and more times and in a decrease in the expression of 87 transcripts. Transfection of cells with 7SL RNA increased the level of 45 genes by 3 and more times and lowered the level of 74 genes. Thirteen transcripts common to Alu- and 7SL RNA were revealed in groups of transcripts with increased expression. Twenty-five transcripts common to Alu- and 7SL RNA were detected in the groups with lowered expression. These data demonstrate that Alu-RNA and 7SL RNA cause variations in differing sets of transcripts, and they suggest that there are also differences in the specificity of the influence and, possibly, in the induction mechanisms of the pro-apoptotic processes in human cells. However, a detailed analysis of the variation in the expression of the pro- and anti-apoptotic factors allowed us to determine a number of key processes common to cells transfected with both Alu-RNA and 7SL RNA.

It is seen from the data presented in Tables 3 and 4 that products of interferon-inducible genes such as *OAS*, *ISG*, *IFIT*, or *STAT1* are almost absent from the list of transcripts whose expression is increased to the greatest extent [32]. Moreover, the analysis of GO-annotations in a group of 68 transcripts induced with Alu-RNA and in a group of 45 transcripts induced with 7SL RNA revealed no statistically significant ($p < 10^{-4}$)

increase in the contribution of groups of the interferon response genes and innate immune response genes (data not shown). These results, again, confirm the conclusion that induction of proapoptotic processes in human cells with the Alu-RNA and 7SL RNA analogues cannot be explained by the activation of PKR, the interaction with TLR-receptors, or by another mechanism associated with the interferonogenic action of these RNAs.

Among the genes whose expression is increased under the action of both Alu-RNA and 7SL RNA (Tables 3, 4), *NUPR1* stands out. It is known that the expression of the transcriptional regulator gene *NUPR1* (encodes protein p8) is enhanced in response to various stress factors and results in cell resistance to chemotherapeutic agents, while a decrease in *NUPR1* expression is accompanied by a suppression of cancer cell growth *in vitro* and *in vivo* [33, 34]. However, an increase in the level of *NUPR1* mRNA also accompanies apoptotic changes in cancer cells [35].

The *DDIT3* gene product, a CHOP transcription factor, is a key mediator of cell death in response to endoplasmic reticulum stress. Increased expression of this gene or microinjections of the CHOP protein cause dissipation of the mitochondrial transmembrane potential ($\delta\Psi$), generation of reactive oxygen species, and apoptotic cell death (a detailed consideration is provided in the review [36]). Therefore, the observed increase in the expression of the *DDIT3* gene in MCF-7 cells under the action of the Alu- and 7SL RNA analogues (Tables 3, 4) is an essential proapoptotic stimulus. The increase in the expression of *DDIT3* (CHOP) and induction of apoptosis in response to endoplasmic reticulum stress can be directly induced by *NUPR1* (p8) gene activation, as has been shown in the case of the cannabinoid-induced apoptosis of astrocytoma cells U87MG [35].

It should be mentioned that an increase in the level of *DDIT3* mRNA, as well as *PSPH* and *MTHFD2* mRNAs, in MCF-7 cells under the influence of Alu-RNA or 7SL RNA (Tables 3, 4) was confirmed by random inspection of the results of a whole transcriptome analysis performed with the independent RT-PCR method (data not shown).

Expression of the *FOXRED2* gene is reduced under the action of both Alu- and 7SL RNA (Tables 3, 4). The *FOXRED2* gene product flavoprotein ERFAD participates in the transport of proteins from the endoplasmic reticulum into the cytoplasm. A reduction in the expression of this gene is associated with activation of proteotoxic stress in the endoplasmic reticulum [37]. Another sign of activation of the endoplasmic reticulum stress response is an increase in asparagine synthetase *ASNS* gene expression, whose transcription is activated by the CCAAT/enhancer binding protein CHOP [38].

Table 3. MCF-7 cell transcripts whose level varies under the action of the Alu-RNA analogue

Transcript*	Identifier	Relative change in expression**	Annotation
Increase in expression			
<i>NUPR1</i>	NM_001042483	5.3	Nuclear protein, transcriptional regulator
<i>PER3</i>	NM_016831	5.1	Period homolog 3 (Drosophila)
<i>TXNIP</i>	NM_006472	4.7	Thioredoxin interacting protein
<i>ASNS</i>	NM_133436	4.5	Asparagine synthetase, transcript variant 1
<i>ZNF773</i>	NM_198542	4.3	Zinc finger protein 773
<i>FAM119A</i>	NM_001127395	4.1	Family with sequence similarity 119, member
<i>ZNF750</i>	NM_024702	4.1	Zinc finger protein 750
<i>PRRT2</i>	NM_145239	4.0	Proline-rich transmembrane protein 2
<i>KCNE4</i>	NM_080671	3.9	Potassium voltage-gated channel
<i>C6ORF48</i>	NM_001040437	3.9	Chromosome 6 open reading frame 48
<i>AUH</i>	NM_001698	3.8	AU RNA binding protein
<i>DDIT3</i>	NM_004083	3.8	DNA-damage-inducible transcript 3
<i>KRT81</i>	NM_002281	3.7	Keratin 81
<i>RNASE4</i>	NM_194430	3.6	Ribonuclease, RNase A family 4
<i>FBXO15</i>	NM_152676	3.6	F-box protein 15
<i>FLJ45244***</i>	NM_207443	3.6	<i>DICER1</i> antisense RNA 1 non-coding RNA
<i>MTHFD2</i>	NM_001040409	3.5	Methylenetetrahydrofolate dehydrogenase
Decrease in expression			
<i>FOXRED2</i>	NM_024955	0.15	FAD-dependent oxidoreductase domain containing 2
<i>PPRC1</i>	NM_015062	0.19	Peroxisome proliferator-activated receptor gamma, coactivator-related 1
<i>CHP</i>	NM_007236	0.21	Calcium binding protein P22
<i>PHLDA2</i>	NM_003311	0.21	Pleckstrin homology-like domain, family A, member 2
<i>TMEM158</i>	NM_015444	0.21	Transmembrane protein 158
<i>ATN1</i>	NM_001007026	0.22	Atrophin 1 (ATN1)
<i>DLK2</i>	NM_206539	0.23	Delta-like 2 homolog (Drosophila)
<i>HPS1</i>	NM_182639	0.23	Hermansky-Pudlak syndrome 1
<i>TMEM214</i>	NM_017727	0.23	Transmembrane protein 214
<i>MED24</i>	NM_014815	0.24	Mediator complex subunit 24
<i>PLEC1</i>	NM_000445	0.24	Plectin 1, intermediate filament binding protein 500 kDa
<i>ZYX</i>	NM_003461	0.24	Zyxin
<i>ACD</i>	NM_022914	0.25	Adrenocortical dysplasia homolog (mouse)
<i>PCDH7</i>	NM_002589	0.25	Protocadherin 7 (PCDH7)
<i>RDH10</i>	NM_172037	0.25	Retinol dehydrogenase 10 (all-trans)
<i>GPX2</i>	NM_002083	0.26	Glutathione peroxidase 2 (gastrointestinal)

* Transcripts annotated in the RefSeq database (accessions NM, NR). The transcripts whose expression changed under the action of both Alu-RNA and 7SL RNA are shown in grey.

** Variation in the transcript amount in cells treated with Alu-RNA relative to the control cells treated with Lipofectamine.

*** The Illumina HT-12 probe sequence for the *FLJ45244* gene coincides with the *DICER-AS1* sequence (NR_015415).

Table 4. MCF-7 cell transcripts whose level varies under the action of the 7SL RNA analogue

Transcript*	Identifier	Relative change in expression**	Annotation
Increase in expression			
<i>NUPR1</i>	NM_001042483	4.5	Nuclear protein, transcriptional regulator
<i>TXNIP</i>	NM_006472	4.3	Thioredoxin interacting protein
<i>PRRT2</i>	NM_145239	4.3	Proline-rich transmembrane protein 2
<i>PSPH</i>	NM_004577	4.2	Phosphoserine phosphatase
<i>ASNS</i>	NM_133436	3.8	Asparagine synthetase, transcript variant 1
<i>KY</i>	NM_178554	3.8	Kyphoscoliosis peptidase
<i>FABP6</i>	NM_001445	3.7	Fatty acid binding protein 6, ileal
<i>DDIT3</i>	NM_004083	3.6	DNA-damage-inducible transcript 3
<i>CTSK</i>	NM_000396	3.6	Cathepsin K
<i>KRT81</i>	NM_002281	3.6	Keratin 81
<i>PFAAP5</i>	NM_014887	3.4	Phosphonoformate immuno-associated protein 5
<i>NT5E</i>	NM_002526	3.4	5'-Nucleotidase, ecto (CD73)
<i>ARL3</i>	NM_004311	3.4	ADP-ribosylation factor-like 3
<i>ULBP1</i>	NM_025218	3.4	UL16 binding protein 1
<i>BACE2</i>	NM_138992	3.4	Beta-site APP-cleaving enzyme 2
<i>RNASE4</i>	NM_194431	3.3	Ribonuclease, RNase A family 4
Decrease in expression			
<i>FOXRED2</i>	NM_024955	0.16	FAD-dependent oxidoreductase domain containing 2
<i>GPX2</i>	NM_002083	0.16	Glutathione peroxidase 2 (gastrointestinal)
<i>TUBB2A</i>	NM_001069	0.17	Tubulin, beta 2A
<i>PLEC1</i>	NM_000445	0.19	Plectin 1, intermediate filament binding protein
<i>ZC3HAV1</i>	NM_024625	0.20	Zinc finger CCCH-type, antiviral 1
<i>SLC35C1</i>	NM_018389	0.21	Solute carrier family 35, member C1
<i>NCOR2</i>	NM_001077261	0.21	Nuclear receptor co-repressor 2
<i>PIGW</i>	NM_178517	0.22	Phosphatidylinositol glycan anchor biosynthesis, class W
<i>MUC1</i>	NM_001044391	0.22	Mucin 1, cell surface associated
<i>OPA3</i>	NM_025136	0.23	Optic atrophy 3 (autosomal recessive, with chorea and spastic paraplegia)
<i>PDPK1</i>	NM_002613	0.23	3-Phosphoinositide dependent protein kinase-1
<i>SLC29A3</i>	NM_018344	0.23	Solute carrier family 29 (nucleoside transporters), member 3
<i>HCFC1</i>	NM_005334	0.24	Host cell factor C1 (VP16-accessory protein)
<i>FAHD1</i>	NM_001018104	0.24	Fumarylacetoacetate hydrolase domain containing 1 (FAHD1)
<i>PARP12</i>	NM_022750	0.24	poly (ADP-ribose) polymerase family, member 12
<i>LRRC14</i>	NM_014665	0.25	Leucine rich repeat containing 14

*Transcripts annotated in the RefSeq database (accessions NM, NR). The transcripts whose expression changed under the action of both Alu-RNA and 7SL RNA are shown in grey.

**Variation in the transcript amount in cells treated with Alu-RNA relative to the control cells treated with Lipofectamine.

Therefore, the decrease in *FOXRED2* expression, observed simultaneously with an increase in the level of *NUPR1* (p8), *DDIT3* (CHOP), and *ASNS*, suggests that induction of the proapoptotic processes in MCF-7 cells under the influence of Alu- and 7SL RNAs is associated with modulation of the transcription of the key cellular factors of the endoplasmic reticulum stress response.

A new mechanism for the development of geographic atrophy of the retina has recently been proposed, which is based on a decrease in *DICER1* expression in the epithelial cells and enhanced expression of Alu-RNA [21]. Subretinal transfection of cells with a construct encoding 7SL RNA, as well as with a 7SL RNA analogue, did not lead to degeneration of the retinal pigment epithelium in mice in contrast to transfection with Alu-RNA [21, 22]. It has been suggested that the cytotoxic effect of Alu-RNA on retinal pigment epithelial cells is associated with unidentified properties of Alu-RNA, and that the mechanism of action is associated with the generation of reactive oxygen species by mitochondria [22].

Our data demonstrate that both Alu- and 7SL RNAs cause comparable changes in the mitochondrial transmembrane potential of MCF-7 cells (Table 1). Consequently, both Alu-RNA and 7SL RNAs induce similar changes in the mitochondrial membrane at least in MCF-7 cells. The analysis of the action of Alu- and 7SL RNAs, along with actinomycin D and tamoxifen, on MCF-7 cell viability revealed that the cytotoxic effect of these RNAs was caused by transcription modulation. The data on the variation of gene expression (Tables 3, 4) demonstrate that transfection of cells with Alu-RNA or 7SL RNA analogues is accompanied not only by a nonspecific response to exogenous RNA, an increase in the levels of *RNASE4* ribonuclease mRNA and *NT5E* 5'-ectonucleotidase mRNA, but also by the emergence of proapoptotic stimuli: *NUPR1*, *DDIT3*, *FOXRED2*. While *NUPR1* gene expression is induced in response to a wide range of stress factors, *DDIT3* and *FOXRED2* are specifically related to the endoplasmic reticulum stress response. The *DDIT3* gene product, the CHOP protein, is the key apoptosis inducer in the proteotoxic ER stress response. The obtained data suggest a mechanism of Alu- and 7SL RNA proapoptotic action which includes activation of the transcription of the *NUPR1* (p8) and proapoptotic *DDIT3* genes. The product of the latter, CHOP, induces apoptosis through the mitochondrial pathway in a MCF-7 cell subpopulation (Fig. 2).

Since 7SL RNA is a component of the signal recognition particle and Alu-RNA is capable of interacting with the proteins SRP9/14, it can be assumed that activation of the endoplasmic reticulum stress response with Alu- and 7SL RNA analogues is caused by a mal-

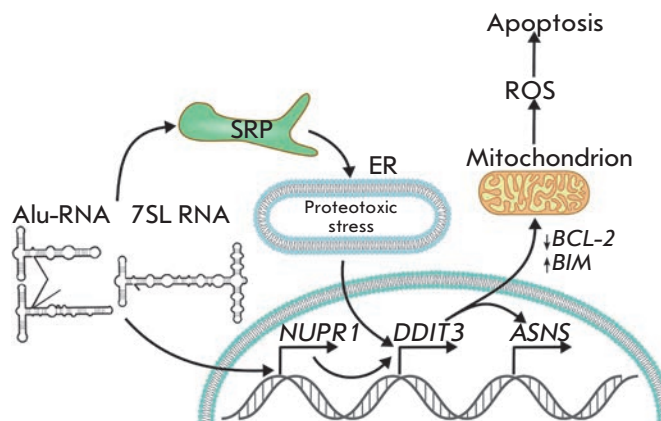


Fig. 2. A scheme of the supposed mechanism of induction of proapoptotic processes in MCF-7 cells transfected with Alu- and 7SL RNA analogues. Transfection of cells with Alu- and 7SL RNA analogues is accompanied by an increase in the expression of the *NUPR1* (p8) transcription regulator gene which activates the transcription of *DDIT3* (CHOP) [35]. The increase in the *DDIT3* transcription factor expression causes apoptotic changes in the mitochondrial outer membrane through a mechanism including a reduction in the *BCL-2* transcription and activation of *BIM* transcription. CHOP (*DDIT3*)-induced apoptosis is accompanied by the generation of reactive oxygen species (ROS) [36]. The increase in *DDIT3* expression can occur as a response to the endoplasmic reticulum stress caused by the interaction of Alu- and 7SL RNAs with SRP proteins – failure in the protein transport through the ER membrane. Endoplasmic reticulum stress is accompanied by an increase in the expression of the asparagine synthetase (*ASNS*) gene, whose transcription is activated by CHOP [38]

function of this very component translational machinery of human cells.

CONCLUSIONS

It was found previously that an increase in the expression of Alu-RNA in human cells causes the suppression of DNA replication, inhibits translation, and exerts an antiproliferative effect. Our data indicate that nuclear DNA transcription is the key process that mediates the decrease in the viability of MCF-7 human adenocarcinoma cells under the action of both Alu-RNA and 7SL RNA analogues. However, no activation of the expression of interferon-inducible genes is observed. Meanwhile, transfection of MCF-7 cells with Alu-RNA or 7SL RNA is accompanied by changes in the expression of a number of genes, including *NUPR1*, *DDIT3*, *FOXRED2*, and *ASNS*. Variation in the transcription of these genes is known to be associated with the complex cell response to ER stress, which is capable of inducing the formation of reactive oxygen species and cell death

through the mitochondrial apoptosis pathway. Activation of the ER stress response under the influence of Alu- and 7SL RNA analogues is presumably associated with SRP malfunction in cells.

On the whole, our results and published data indicate that Alu-RNA is not only a marker, but also a mediator of cell stress signals. ●

This work was supported by the Russian Foundation for Basic Research (grant № 13-04-01058), and by the interdisciplinary integration project of the Presidium of the Siberian Branch of RAS № 84 (2012–2014).

REFERENCES

1. International Human Genome Sequencing Consortium // *Nature*. 2001. V. 409. № 6822. P. 860–921.
2. Deininger P.L., Batzer M.A. // *Genome Res.* 2002. V. 12. № 10. P. 1455–1465.
3. Batzer M.A., Deininger P.L., Hellmann-Blumberg U., Jurka J., Labuda D., Rubin C.M., Schmid C.W., Zietkiewicz E., Zuckerkandl E. // *J. Mol. Evol.* 1996. V. 42. № 1. P. 3–6.
4. Jurka J., Krnjajic M., Kapitonov V.V., Stenger J.E., Kokhanyy O. // *Theor. Popul. Biol.* 2002. V. 61. № 4. P. 519–530.
5. Dewannieux M., Esnault C., Heidmann T. // *Nat. Genet.* 2003. V. 35. № 1. P. 41–48.
6. Batzer M.A., Deininger P.L. // *Nat. Rev. Genet.* 2002. V. 3. № 5. P. 370–379.
7. Liu W.M., Maraia R.J., Rubin C.M., Schmid C.W. // *Nucleic Acids Res.* 1994. V. 22. № 6. P. 1087–1095.
8. Liu W.M., Chu W.M., Choudary P.V., Schmid C.W. // *Nucleic Acids Res.* 1995. V. 23. № 10. P. 1758–1765.
9. Shaikh T.H., Roy A.M., Kim J., Batzer M.A., Deininger P.L. // *J. Mol. Biol.* 1997. V. 271. № 2. P. 222–234.
10. Maraia R.J., Driscoll C.T., Bilyeu T., Hsu K., Darlington G.J. // *Mol. Cell Biol.* 1993. V. 13. № 7. P. 4233–4241.
11. Sarrowa J., Chang D.Y., Maraia R.J. // *Mol. Cell Biol.* 1997. V. 17. № 3. P. 1144–1151.
12. Häslér J., Strub K. // *Nucleic Acids Res.* 2006. V. 34. № 19. P. 5491–5497.
13. Sakamoto K., Fordis C.M., Corsico C.D., Howard T.H., Howard B.H. // *J. Biol. Chem.* 1991. V. 266. № 5. P. 3031–3038.
14. Chu W.M., Ballard R., Carpick B.W., Williams B.R., Schmid C.W. // *Mol. Cell Biol.* 1998. V. 18. № 1. P. 58–68.
15. Rubin C.M., Kimura R.H., Schmid C.W. // *Nucleic Acids Res.* 2002. V. 30. № 14. P. 3253–3261.
16. Hasler J., Strub K. // *Nucleic Acids Res.* 2006. V. 34. № 8. P. 2374–2385.
17. Bovia F., Wolff N., Ryser S., Strub K. // *Nucleic Acids Res.* 1997. V. 25. № 2. P. 318–326.
18. Chang D.Y., Hsu K., Maraia R.J. // *Nucleic Acids Res.* 1996. V. 24. № 21. P. 4165–4170.
19. Mariner P.D., Walters R.D., Espinoza C.A., Drullinger L.F., Wagner S.D., Kugel J.F., Goodrich J.A. // *Mol. Cell.* 2008. V. 29. № 4. P. 499–509.
20. Yakovchuk P., Goodrich J.A., Kugel J.F. // *Proc. Natl. Acad. Sci. USA.* 2009. V. 106. № 14. P. 5569–5574.
21. Kaneko H., Dridi S., Tarallo V., Gelfand B.D., Fowler B.J., Cho W.G., Kleinman M.E., Ponicsan S.L., Hauswirth W.W., Chiodo V.A., et al. // *Nature*. 2011. V. 471. № 7338. P. 325–330.
22. Tarallo V., Hirano Y., Gelfand B.D., Dridi S., Kerur N., Kim Y., Cho W.G., Kaneko H., Fowler B.J., Bogdanovich S., et al. // *Cell*. 2012. V. 149. № 4. P. 847–859.
23. Galluzzi L., Vitale I., Kepp O., Seror C., Hangen E., Perfettini J.L., Modjtahedi N., Kroemer G. // *Methods Enzymol.* 2008. V. 442. P. 355–374.
24. Stepanov G.A., Semenov D.V., Savelyeva A.V., Kuligina E.V., Koval O.A., Rabinov I.V., Richter V.A. // *Biomed. Res. Int.* 2013. P. 656158.
25. Kroemer G., Galluzzi L., Brenner C. // *Physiol. Rev.* 2007. V. 87. № 1. P. 99–163.
26. Demchenko A.P. // *Exp. Oncol.* 2012. V. 34. № 3. P. 263–268.
27. Berridge M.V., Herst P.M., Tan A.S. // *Biotechnol. Annu. Rev.* 2005. V. 11. P. 127–152.
28. Siddik Z.H. // *Oncogene*. 2003. V. 22. № 47. P. 7265–7279.
29. Balachandran S., Barber G.N. // *Meth. Mol. Biol.* 2007. V. 383. P. 277–301.
30. Lindner D.J., Kolla V., Kalvakolanu D.V., Borden E.C. // *Mol. Cell Biochem.* 1997. V. 167. № 1–2. P. 169–177.
31. Iacopino F., Robustelli della Cuna G., Sica G. // *Int. J. Cancer*. 1997. V. 71. № 6. P. 1103–1108.
32. Der S.D., Zhou A., Williams B.R., Silverman R.H. // *Proc. Natl. Acad. Sci. USA.* 1998. V. 95. № 26. P. 15623–15628.
33. Goruppi S., Iovanna J.L. // *J. Biol. Chem.* 2010. V. 285. № 3. P. 1577–1581.
34. Guo X., Wang W., Hu J., Feng K., Pan Y., Zhang L., Feng Y. // *Anat. Rec. (Hoboken)*. 2012. V. 295. № 12. P. 2114–2121.
35. Carracedo A., Lorente M., Egia A., Blázquez C., García S., Giroux V., Malicet C., Villuendas R., Gironella M., González-Feria L., et al. // *Cancer Cell*. 2006. V. 9. № 4. P. 301–312.
36. Tabas I., Ron D. // *Nat. Cell Biol.* 2011. V. 13. № 3. P. 184–190.
37. Riemer J., Appenzeller-Herzog C., Johansson L., Bodenmiller B., Hartmann-Petersen R., Ellgaard L. // *Proc. Natl. Acad. Sci. USA.* 2009. V. 106. № 35. P. 14831–14836.
38. Siu F., Chen C., Zhong C., Kilberg M.S. // *J. Biol. Chem.* 2001. V. 276. № 51. P. 48100–48107.

Polyreactive Monoclonal Autoantibodies in Multiple Sclerosis: Functional Selection from Phage Display Library and Characterization by Deep Sequencing Analysis

Y. A. Lomakin¹, M. Yu. Zakharova¹, A. A. Belogurov^{1,2}, N. A. Bykova^{3,4}, M. A. Dronina¹, A. E. Tupikin^{5,6}, V. D. Knorre¹, A. N. Boyko^{7,8}, A. V. Favorov^{9,10,11}, M. R. Kabilov^{5,6}, N. A. Ponomarenko¹, A. G. Gabibov^{1,2,12}

¹Shemyakin–Ovchinnikov Institute of Bioorganic Chemistry, Russian Academy of Sciences, 117997, Moscow, Russia

²Institute of Gene Biology, Russian Academy of Sciences, 119334, Moscow, Russia

³Kharkevich Institute for Information Transmission Problems, Russian Academy of Sciences, 127994, Moscow, Russia

⁴Faculty of Bioengineering and Bioinformatics, Lomonosov Moscow State University, 119991, Moscow, Russia

⁵Institute of Chemical Biology and Fundamental Medicine, Siberian Branch, Russian Academy of Sciences, 630090, Novosibirsk, Russia

⁶Genomics Core Facility, Siberian Branch, Russian Academy of Sciences, 630090, Novosibirsk, Russia

⁷Moscow Multiple Sclerosis Center at the City Hospital #11, 127018, Moscow, Russia

⁸Pirogov Russian National Research Medical University, Department of Fundamental and Clinical Neurology and Neurosurgery, 117997, Moscow, Russia

⁹Vavilov Institute of General Genetics, Russian Academy of Sciences, 119991, Moscow, Russia

¹⁰Department of Oncology, Division of Biostatistics and Bioinformatics, Johns Hopkins University School of Medicine, 21218, Baltimore, Maryland, USA

¹¹State Research Institute of Genetics and Selection of Industrial Microorganisms GosNII Genetika, 117545, Moscow, Russia

¹²Faculty of Chemistry, Lomonosov Moscow State University, 119991, Moscow, Russia

E-mail: yasha.l@bk.ru

Received 01.09.2013

Copyright © 2013 Park-media, Ltd. This is an open access article distributed under the Creative Commons Attribution License, which permits unrestricted use, distribution, and reproduction in any medium, provided the original work is properly cited.

ABSTRACT Multiple Sclerosis (MS) is a chronic inflammatory demyelinating disease of the central nervous system that primarily affects young and middle-aged people. It is widely accepted that B lymphocyte activation is required for MS progression. Despite the fact that the exact triggering mechanisms of MS remain enigmatic, one may suggest that MS can be induced by viral or bacterial infection in combination with specific genetic and environmental factors. Using deep sequencing and functional selection methodologies we characterized clones of poly- and cross-reactive antibodies that are capable of simultaneous recognition of viral proteins and autoantigens. The latter, in turn, possibly may trigger MS progression through molecular mimicry. It was identified that two cross-reactive antigens are probably recognized by light or heavy chains individually. According to the high structural homology between selected autoantibodies and a number of various antiviral IgGs, we suggest that a wide range of pathogens, instead of a single virus, be regarded as possible triggers of MS.

KEYWORDS Multiple sclerosis, deep sequencing, cross-reactivity, autoreactive B cells, myelin basic protein, viral triggers.

ABBREVIATIONS MS – multiple sclerosis; EBV – Epstein-Barr virus; MBP – myelin basic protein; LMP-1 – latent membrane protein 1; MOG – myelin oligodendrocyte glycoprotein; ELISA – enzyme-linked immunosorbent assay; CNS – central nervous system; CSF – cerebrospinal fluid; BBB – blood-brain barrier.

INTRODUCTION

Multiple sclerosis (MS) is a chronic inflammatory demyelinating disease of the central nervous system that affects mainly young and middle-aged people at a rate of 3: 10,000. There are more than 2.5 million people with MS all over the world [1]. Thus, MS is the most common demyelinating neuroinflammatory disorder wherein the immune system of a body destroys the myelin sheath of axons for reasons that remain unclear [2]. Social and economic factors are of great importance in this disease due to severe symptoms, including optic neuritis, loss of bowel and bladder control, severe paralysis, and also long duration of the chronic period. In 80% of cases, the disease begins as a relapsing-remitting form, which eventually morphs into the secondary progressive course. Much less frequently (in 20% of cases), the primary progressive form of MS occurs from the very onset [3].

Despite the numerous studies on the etiology of MS, neither the exact cause of its development nor a potential pathogen capable of inducing the disease is known thus far. It is believed that the development of MS requires a predisposition; i.e. the chronic activation of immune cells leading to neuronal damage is possible only under a certain combination of genetic and environmental factors. Genetic screening has identified several candidate genes. *HLA* (human leukocyte antigen) is considered to be the most important of them, since it is associated with the MS region to the greatest extent. Unfortunately, no unambiguous correlations have been identified in this case. Thus, in Northern Europe association between the disease and *HLA-DR2* or *HLA-DRB1*15* has been historically established [4, 5], while in other parts of Europe (e.g., Sardinia) the strongest association was determined with *HLA-DRB1*0301*, *HLA-DRB1*0405*, and *HLA-DRB1*1303* [6]. According to other sources, new haplotypes (*HLA-DRB1*03*, *HLA-DRB1*01*, *HLA-DRB1*10*, *HLA-DRB1*11*, *HLA-DRB1*14* and *HLA-DRB1*08*) have also been found, correlating with the pathology both negatively and positively, but the strength of the effect varied from case to case [7–10]. Nevertheless, increased risk of MS development by the relatives of MS patients was unambiguously identified [11–14]. The risk of MS in first-degree relatives was about 10–25 times higher compared to that of a normal population sample. Association between the *CD40* gene (rs6074022) and MS has also been identified [15]. A significant genetic determinism of individual response to treatment with many drugs may be evidence of genetic predisposition. For example, the pharmacogenomic studies of MS have revealed a significant role for a number of polymorphic variants of genes (*CCR5*, *DRB1*, *IFNG*, *TGFB1*, *IFNAR1*, *IL7RA*, and possibly, *TNF* and *CTLA4*) in re-

sponse to the administration of Copaxone [16]. Epidemiological studies, in turn, have identified several risk factors for MS, including bacterial and viral infections, climatic conditions, and smoking.

Although the cause of MS remains unknown, the disease is always accompanied by similar processes, such as activation and increase in immune cell number in the CNS, which further leads to demyelination, axonic/neuronal damage, and death of oligodendrocytes; these are significant symptoms of MS [17]. At the initial stages of studying MS, the major role in the development of the disease was attributed to T lymphocytes. But now we can confidently assert that activation of B cells is required for pathology development. In addition to producing pathogenic autoantibodies, B lymphocytes are also active antigen-presenting (APC) and cytokine-producing cells [18]. The list of potential autoantigens in MS is constantly expanding and includes various proteins associated with the oligodendrocyte membrane. The emphasis is on the myelin basic protein (MBP), proteolipid protein (PLP1), and myelin-oligodendrocyte glycoprotein (MOG). Moreover, the catalytic antibodies to MBP, which not only bind but also hydrolyze it, were found in the serum of MS patients and SJL mice with experimental autoimmune encephalomyelitis (MS model) [19–21].

Thus, detection of a foreign (e.g., viral) antigen capable of inducing the production of autoantibodies to components of the myelin sheath, and analysis of the structure of these antibodies may be extremely promising for understanding the mechanisms of the disease and developing new approaches to MS treatment and diagnostics.

To date, there is no medical protocol that would allow complete curing of MS patients. Betaferon, which lowers the inflammation level in the CNS [22], and Copaxone, which also reduces the exacerbation frequency [23], are the most commonly used agents in MS patients. Vaccines aimed at eliminating autoreactive B cells are being designed; the already certified drug product Rituximab (a monoclonal antibody that eliminates all B cells) is the best known among them. There are also pilot projects focused on specific elimination [24] or suppression [25] of autoreactive B cells that are precisely known to be pathogenic.

A scFv phage display library has been constructed in our laboratory on the basis of genetic material from MS patients [26]. A series of monoclonal antibodies binding MBP have been selected and characterized. *In vitro* cross-reactivity between MBP and latent membrane protein 1 (LMP-1 protein) of the Epstein-Barr virus (EBV) has been shown for one of these antibodies. A series of papers on the possible viral induction of the disease by molecular mimicry have recently been

published [27–29]; the results were further evidence of the triggering role of EBV. In this work, we set out to determine how unique the formation of cross-reactive autoantibodies to MBP and LMP-1 is. To do this, we purposefully obtained cross-reactive clones by successive enrichment of the library on these two antigens. An analysis of their structure and germlines revealed the high diversity of these cross-reactive clones, which have the potential of inducing MS. It is interesting to note that most of the obtained antibodies are highly homologous to the antibodies to proteins of other pathogens, which may be regarded as an extension of the list of potential MS triggers.

EXPERIMENTAL

Reagents

Agar, tryptone, yeast extract (Difco, UK), mono- and dibasic sodium phosphate, sodium chloride, bovine serum albumin, fraction V (BSA), ethidium bromide, β -mercaptoethanol (Sigma, USA), acrylamide, N,N'-methylenebisacrylamide, sodium dodecyl sulfate (SDS), urea, Hybond C extra nitrocellulose membrane (Amersham, USA), NP-40 surfactant glycine, isopropyl- β -D-thiogalactopyranoside (IPTG) (Fermentas, Lithuania), TMB (tetramethylbenzidine) solution (ZAO "NBO Immunotech", Russia) were used. The other reagents were produced in Russia and were of ultrapure grade.

Enzymes

Thermostable DNA-dependent DNA polymerase, alkaline phosphatase, Rapid DNA Ligation kit (Fermentas, Lithuania), restriction endonucleases and the corresponding standard buffer solutions (Fermentas, Lithuania), deoxyribonuclease I (Biozyme Laboratories Ltd., USA), trypsin, lysozyme (Merck, Germany) DNA fragment size markers and molecular weight markers: GeneRuler™ 50 bp DNA Ladder GeneRuler™ 1 kb DNA Ladder, Protein Molecular Weight Marker 14.4–116.0 kDa, Prestained Protein Molecular Weight Marker 19.0–118.0 kDa (Fermentas, Lithuania) low molecular weight marker 2.5–16.9 kDa (Amersham, USA).

Antibodies

Antibodies to c-myc epitope produced by C-MYC hybridoma antibodies to 3-flag epitope conjugated to horseradish peroxidase (Sigma, USA) antibodies to M13 phage envelope protein conjugated and non-conjugated to horseradish peroxidase (GE Healthcare, USA).

Protein expression and purification

Preparations of purified bovine MBP and recombinant human MOG (30–147 a.a.) were done according

to the previously published procedure [21]. Recombinant LMP-1 was expressed in HEK293 eukaryotic cells. HEK293 cells were transfected with pBudCE1.4/EF/LMP1-FLAG-His-Strep plasmid using unifactin-56. Cells were lysed in a RIPA buffer with 1 M urea and inhibitor cocktail (Roche, Germany) overnight at 4°C under continuous stirring. LMP-1 was purified from the lysate using anti-FLAG agarose in agreement with the protocol. The N- and C-terminal domains of LMP-1 were purified using affinity chromatography on Talon resin (Clontech, USA) and then using the MonoQ sepharose column (Amersham).

Enrichment of the library

The scFv phage display library derived from the peripheral blood lymphocytes of MS patients was described previously [26]. The enrichment was carried out according to the procedure (Tomlison protocol; Source BioScience, <http://www.lifesciences.sourcebioscience.com>) with minor modifications. 10 μ g/ml of antigen (MBP, MOG, LMP-1) was absorbed on immuno tubes (Immuno Tubes maxisorp, Nunc, Germany) in a carbonate buffer (pH 9.2). Two rounds of biopanning were carried out for each antigen. Two additional rounds using MBP as an antigen were conducted in the case of double enrichment for LMP-1/MBP.

ELISA

Antigen diluted in a 0.1 M carbonate buffer to a concentration of 5 μ g/ml was adsorbed on polystyrene plates (MaxiSorp, Denmark) overnight at 4°C. The next day, after removal of the antigen, the wells were washed 3 times with a PBS buffer with 0.1% Tween 20. Nonspecific binding regions were blocked with a 3% BSA solution in PBS, pH 7.2 (37°C, 1 h). Thereafter, the wells were washed thrice with the PBS buffer with 0.1% Tween 20 again and then incubated for 1 h at 37°C with the second layer reactants in the PBS buffer with 0.1% Tween 20. Washing with the PBS buffer with 0.1% Tween 20 was performed three times after each incubation. The antibodies of the last layer were conjugated to horseradish peroxidase. Development was conducted using the proprietary reagent TMB (ZAO "NBO Immunotech", Russia); the reaction was quenched with 10% H_3PO_4 . The absorbance (A_{450}) was measured using a Varioscan Flash microplate reader (Thermo Scientific, USA).

Deep sequencing of genes of the V_H/V_L variable regions from phage display libraries

The original MS phage display library and four sub-libraries enriched for different antigens (MBP, MOG, LMP-1, double enrichment for LMP-1/MBP) were amplified in the TG-1 cells of *Escherichia coli*. PCR was

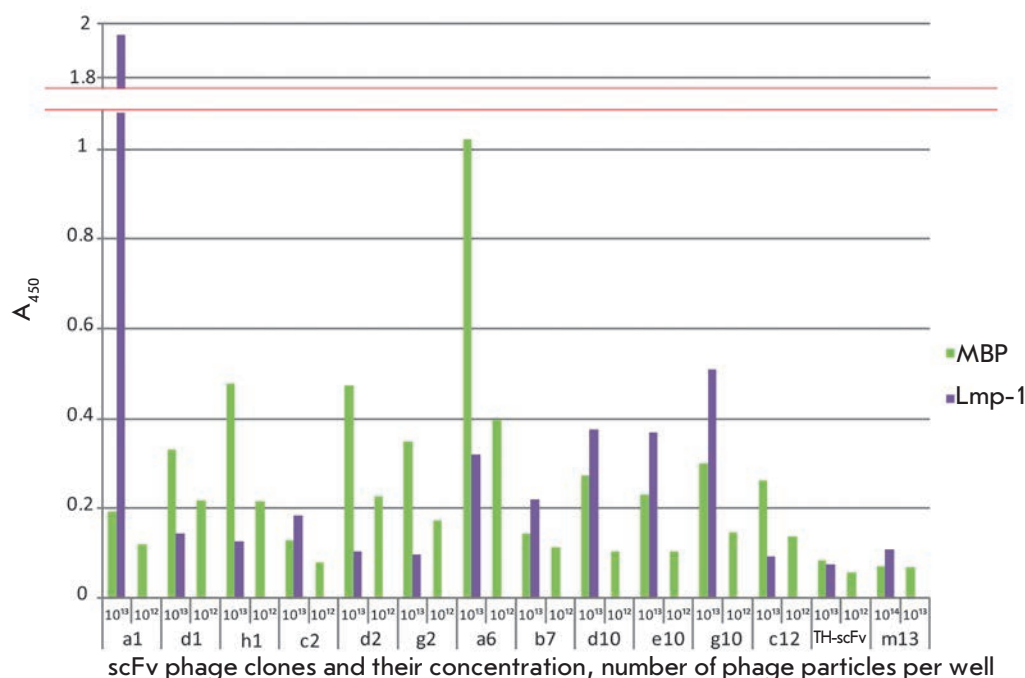


Fig. 1. Monoclonal phage ELISA of MBP (green bars) and Lmp1 (violet bars) binding by the antibodies under study. The bacteriophage M13K07 (m13) and bacteriophage exposing on its surface scFv towards thyroglobulin (TH-scFv) were used as negative controls

performed using Phusion Hot Start II High-Fidelity DNA Polymerase (Fermentas, Lithuania). The reaction mixture contained 5 ng of DNA plasmid as a template and 10 pmol of the flanking primers. PCR products were purified using a GeneJET Gel Extraction Kit (Thermo Scientific, USA) and ligated with NEBNext Multiplex Oligos adapters (New England Biolabs, UK) using the NEBNext Ultra DNA Library Prep Kit for Illumina (New England Biolabs, UK). After the samples had been prepared, the libraries were analyzed both quantitatively using Qubit (Invitrogen) and qualitatively using the 2100 Bioanalyzer (Agilent Technologies). The libraries were normalized to a concentration of 10 nM based on counting and mixed at an equimolar ratio. Amplification of the samples was carried out according to the protocol (Illumina) using MiSeq with the Reagent Kit v2 (2 × 250). Merging and alignment of the related readings was carried out based on GW CLC Bio. The characteristics of the antibodies were determined immediately after the deep sequencing using the IMGT/HighV-QUEST online resource [30].

Filter parameters for analyzing the occurrence of the hypervariable regions

The results of the alignment of the sequences obtained using deep sequencing after the analysis using the IMGT/V-QUEST software [31] were filtered by the following criteria: the “Functionality” field of the alignment should be “productive” (the antibody sequence should be evaluated by the program as productive); the

identity of V-gene alleles and germline from the IMGT database should be 70 % or higher; and the sequences of the light chains identified by the IMGT/V-QUEST program as heavy chains were not considered.

RESULTS AND DISCUSSION

We analyzed the structures and representation of the antibodies selected for the major MS autoantigens – MBP and MOG, as well as viral protein LMP-1, which was previously shown to be a potential trigger of MS [26]. To this end, two rounds of enrichment for MOG and LMP-1 (the enrichment for MBP was conducted previously [26]), and two consecutive rounds of biopanning for LMP-1 and then two rounds for MBP to find cross-reactive antibodies, were conducted. All of the enrichment was carried out under the control of polyclonal ELISA. After the selection, the resulting scFvs as a component of phage particles were analyzed using monoclonal ELISA. A clone was considered positive if the signal of its binding to one or two antigens in ELISA exceeded by threefold the signal of the M13K07 phage used as a negative control (a titer of 10^{13} phage particles/well). The ELISA results for the most promising clones capable of binding both MBP and LMP-1 are shown in Fig. 1. The ability of these phage clones to bind both antigens was confirmed by at least three independent ELISA tests.

As a result, several phage clones carrying scFvs, which most efficiently bound to LMP-1 or LMP-1/MBP, were selected. The Table lists the data on

Table. ELISA of scFvs selected after two rounds of biopanning for respective antigens as indicated. NoFe. LL in the scFv name indicates that this clone was selected upon enrichment of library for LMP-1. Relative binding was calculated as a ratio between the observed signal demonstrated by selected scFv phage clone divided by the signal of the negative control (M13K07 phage) added at the same amount. Symbols: exceedence over background signal more than 1.5-fold (\pm), threefold (+), sixfold (++), ninefold (+++), not determined (ND). All experiments were performed in triplicates.

Clone	Selection for LMP-1 / MBP										Binding to LMP-1	Binding to MBP
	V _h	D _h	J _h	H-CDR3	V _L	J _L	L-CDR3					
b7	IGHV1-2*04	IGHD1-26*01	IGHJ4*02	VRGSTYSPSGYFEY	IGKV5-2*01	IGKJ2*01	LQHDNFP				+	++
g10	IGHV1-3*01	IGHD6-13*01	IGHJ4*02	ARIFEGLSGIAAPFDY	IGKV4-1*01	IGKJ4*01	QQYFSSPLT				+	\pm
h1	IGHV1-8*01	IGHD4-17*01	IGHJ6*03	AREVSDYSDYGDVYYMDV	IGKV3-20*01	IGKJ5*01	QQYCCSPIT				\pm	\pm
e11	IGHV1-8*01	IGHD4-17*01	IGHJ6*03	AREVSDYSDYGDVYYMDV	IGLV1-44*01	IGLJ3*02	AAWDGSLNGP				\pm	\pm
h11	IGHV1-18*04	IGHD3-3*02	IGHJ2*01	ARREGLYTTSPGYFGV	IGLV3-21*03	IGLJ7*02	RVWDKQTVSRSG				\pm	+
e12	IGHV1-46*01	IGHD4-11*01	IGHJ6*02	ARRGFDY	IGKV1-33*01	IGKJ1*01	LQFYEFPYT				\pm	\pm
c11	IGHV1-46*03	IGHD5-12*01	IGHJ6*03	AKDLRPRDIGDMDV	IGKV1-39*01	IGKJ5*01	QQSYSSP				\pm	+
c12	IGHV1-69*06	IGHD1-26*01	IGHJ6*02	ARCGILRSHYFYGMVDV	IGLV1-47*01	IGLJ7*01	AAWDDSLSG				\pm	+
a6	IGHV3-7*01	IGHD4-11*01	IGHJ6*02	VRGGLGAGADY	IGLV4-69*01	IGLJ7*01	QTWGTGI				+	++
c3	IGHV4-b*01	IGHD2-21*01	IGHJ5*01	AGLTQSSHNDAN	IGKV2-30*01	IGKJ1*01	MQATHWP				\pm	+
f11 (=e1 LL)	-	-	-	-	IGLV1-47*01	IGLJ3*02	VAWDDNLSG				\pm	\pm
c2	-	-	-	-	IGLV3-1*01	IGLJ7*01	AAWDDSLNGPV				\pm	\pm
d1	-	-	-	-	IGLV6-57*01	IGLJ7*01	QSYNTSTLI				\pm	\pm
a1	-	-	-	-	IGLV10-54*01	IGLJ3*02	SVWDDSSLSA				\pm	\pm
Selection for LMP-1												
h4 LL	IGHV3-23*01	IGHD6-13*01	IGHJ2*01	AKDIAAAATTPFY	IGKV3-11*01	IGKJ5*01	QQRSNWPPT				+++	ND
c12 LL	IGHV5-51*01	IGHD4-17*01	IGHJ4*03	ARFYDSTGSCDY	IGKV1D-33*01	IGKJ2*02	SIQXKFFPLXC				+++	ND
d4 LL, g3 LL, b3 LL	-	-	-	-	IGLV1-47*01	IGLJ7*01	AAWDDSLSG				+++	ND
e1 LL (=f11)	-	-	-	-	IGLV1-47*01	IGLJ3*02	VAWDDNLSG				+++	ND
d2 LL (=a1)	-	-	-	-	IGLV10-54*01	IGLJ3*02	SVWDDSSLSA				+++	ND

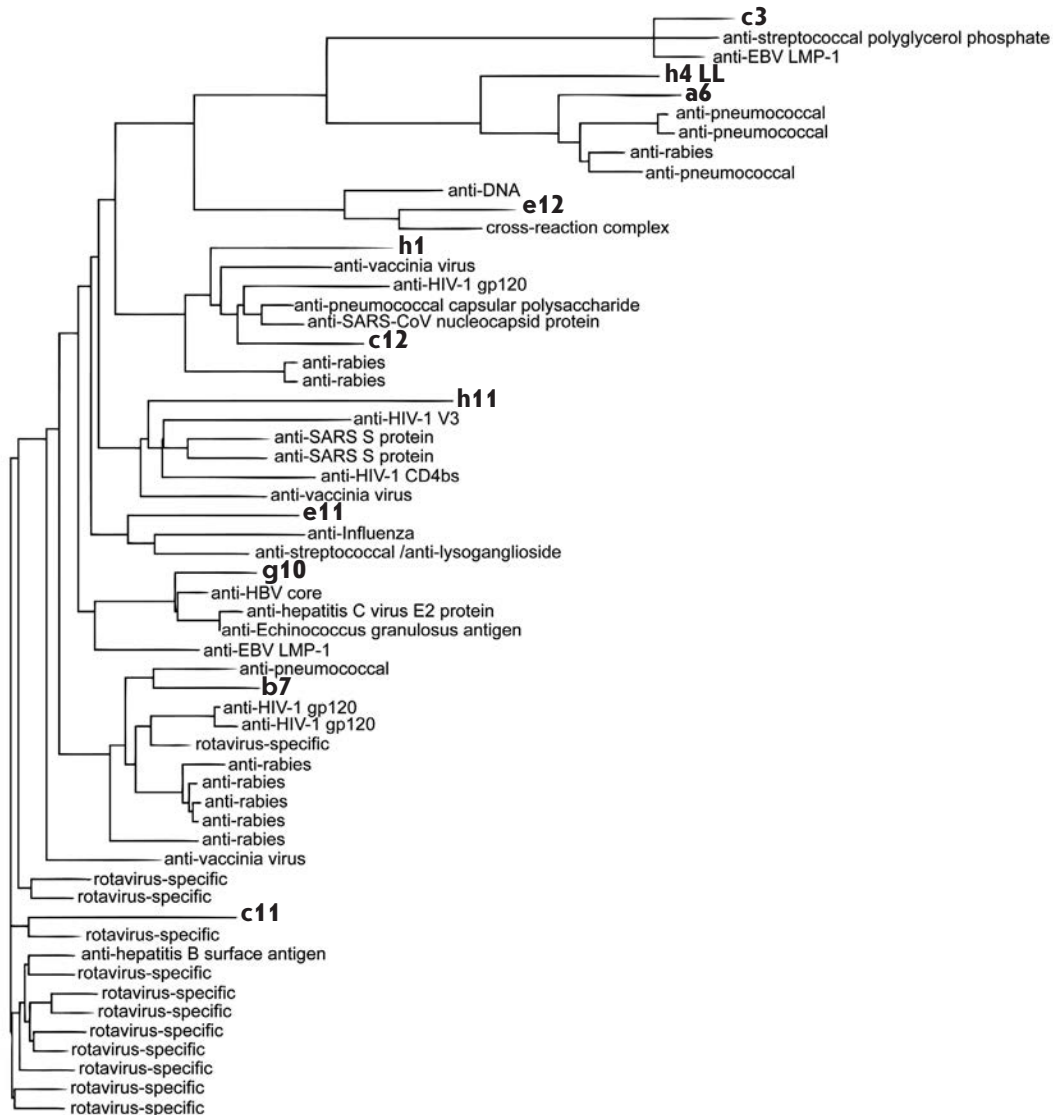


Fig. 2. Homology of the selected heavy chains with anti-viral antibodies as indicated. The scFvs selected in the current study are shown in bold

the relative strength of binding of phage clones to the analyzed antigens, as well as the amino acid sequences of their hypervariable regions and related germlines. Several interesting patterns can be noticed by comparing the structures of the resulting scFvs: (1) multiple selection of individual light chains both on LMP-1 and on two antigens; (2) occurrence of identical light chains both in free form and as part of scFv – c12 and b3 LL, g3 LL, d4 LL clones. Selection of specific light chains both in free form for the selection on LMP-1 (b3 LL, g3 LL, d4 LL) and as part of scFv in obtaining cross-reactive clones (c12) may indicate their essential role in LMP-1 binding, which has been used as the first antigen in double selection. Meanwhile, their combination with a heavy chain is probably a necessity for further binding of MBP; i.e., in this case binding to two antigens and potential cross-reactivity is determined by

recognition of the related antigen by heavy and light chains separately. Another interesting fact is that the relative strength of binding of anti-LMP-1-antibodies to the related antigen is much higher than that of binding to both antigens of potentially cross-reactive anti-LMP-1/-anti-MBP-antibodies (Table). These observations may reflect the natural situation occurring during the development of MS, when the primarily formed antibodies to some pathogen (e.g. EBV) can later interact with MBP as they enter the central nervous system (if the blood-brain barrier (BBB) is damaged), causing degradation of the myelin sheath. Apparently, the ability of these antibodies to exhibit potential poly-reactivity, albeit at weak binding, is preferable over high specificity with strong affinity.

Homology search among the selected monoclonal antibodies was performed for the amino acid sequences

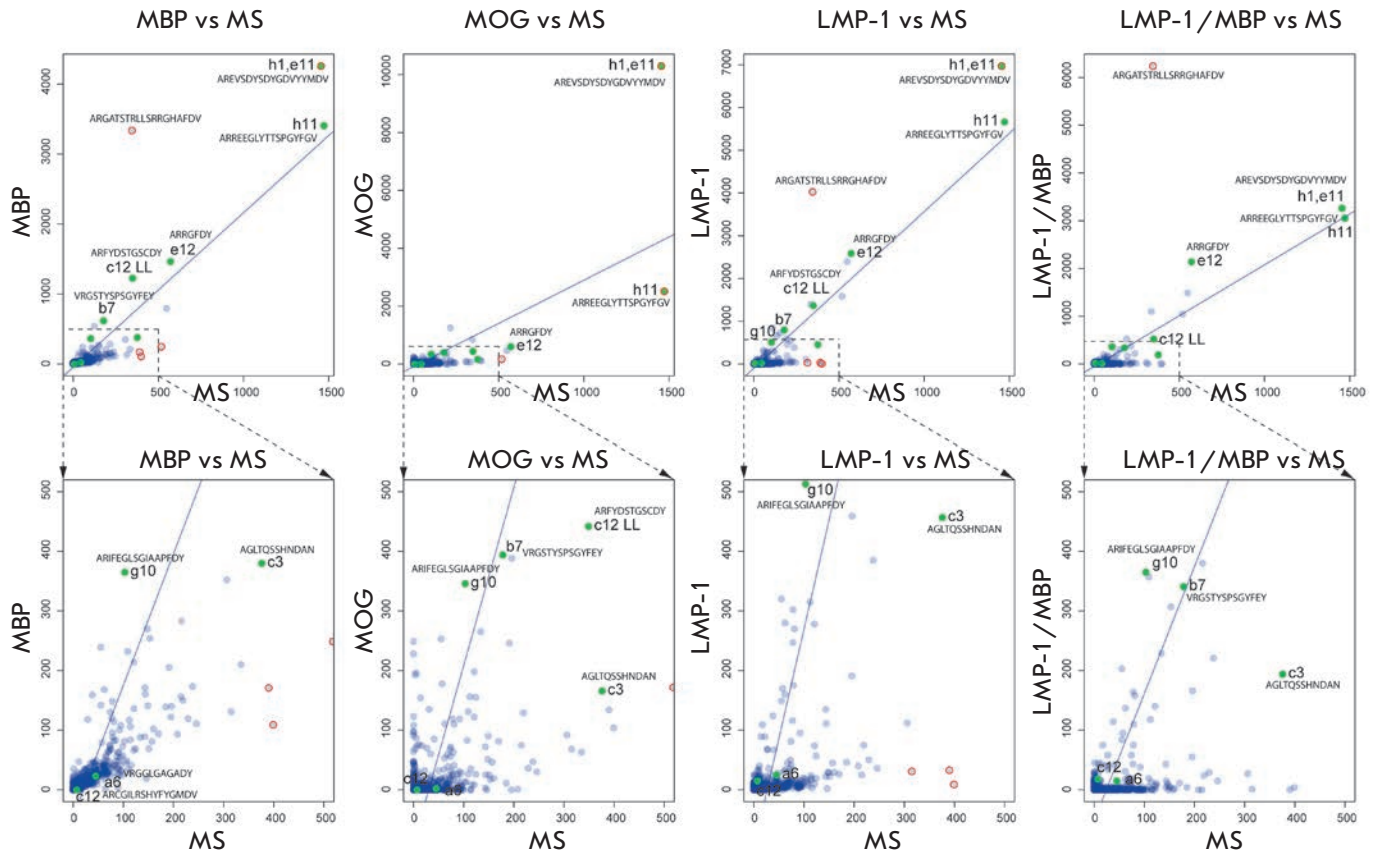


Fig. 4. Occurrence of the CDR3 of heavy chain in enriched sublibraries as compared to the initial MS library. Each circle indicates unique CDR3 with the number of reads for this CDR3 in MS library (X axis) and in respective enriched sublibrary (Y axis). For each pair of libraries, the regression and the outlier analysis were done using ‘car’ R package (outliers are colored in red). The functionally selected monoclones are shown in green with indication of their code according to the Table. Sequences of the H-CDR3 for the most interesting clones are indicated

using the Protein Data Bank (pdb), UniProtKB / Swiss-Prot (swissprot) databases and protein BLAST software. Figures 2 and 3 show data on the relative homology between the structures of the resulting antibodies and immunoglobulins specific to different viral and bacterial proteins. A high level of similarity between the obtained antibodies and a series of pathogen-specific antibodies (against the influenza virus, West Nile virus, rabies virus, rotavirus, pneumococcus, streptococcus, etc.) was revealed both for heavy and light chains. There is also a high level of structural similarity between the obtained antibodies and antibodies from CSF in MS, anti-MOG, anti-CD152 (cytotoxic lymphocyte antigen 4), and antibodies to the Bence-Jones protein. The data on the homology of the heavy chain structures of cross-reactive c3 antibody and the anti-LMP-1 antibody (gb | ABA55010.1 – 91% homology), as well as cross-reactive g10 and anti-LMP-1 antibody (gb | ABA55014.1 – 86% homology), are of special interest, because it possibly confirms the accuracy of the per-

formed biopanning. As for the light chains, the high homology of the b7 antibody and MOG-specific antibody (gb | AAY15116.1 – 90% homology) may be indicative of the polyreactivity of the selected antibody, while the similarity of a6 and the antibody from the CSF of a MS patient (gb | AAS21063.1 – 94% homology) may confirm the autoimmune nature of the selected antibody. In our opinion, the high proviral homology of the antibodies capable of MBP binding indicates that many viral proteins can act as the primary target for these antibodies. Thus, along with genetic and environmental factors, for MS induction and activation of pathogenic B cells, not a single specific exogenous pathogen is essential, but rather the ability of this pathogen to recruit the immune cells into the central nervous system along with its own penetration, which eventually causes “multiple and disorderly” activation of such cells. In other words, the antibody-secreting cells activated in the peripheral lymph nodes migrate through the damaged BBB. Thus, the primary antibodies to viral antigens interact with

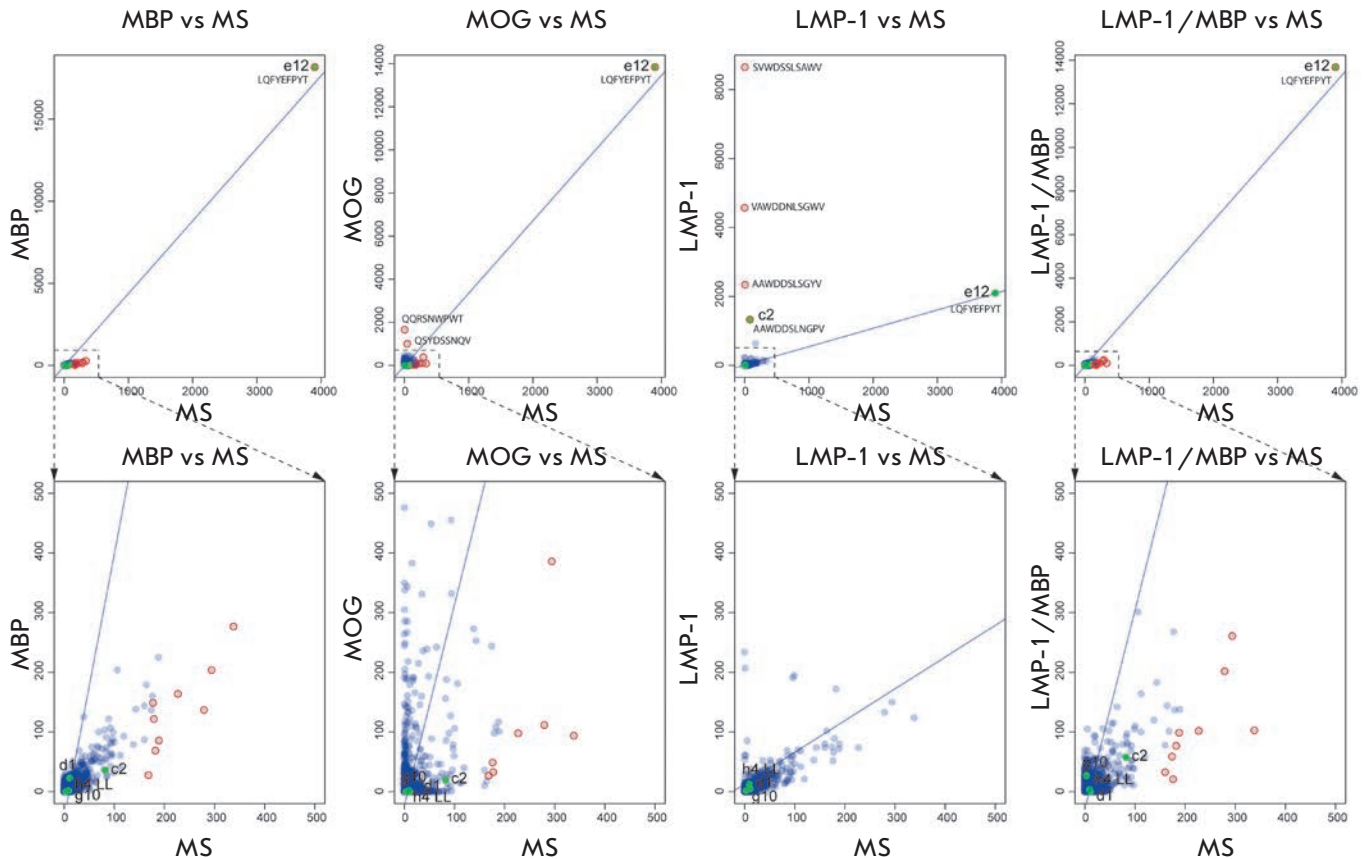


Fig. 5. Occurrence of the CDR3 of light chain in enriched sublibraries as compared to the initial MS library. Each circle indicates a unique CDR3 with the number of reads for this CDR3 in MS library (X axis) and in the respective enriched sublibrary (Y axis). For each pair of libraries, the regression and the outlier analysis were done using the 'car' R package (outliers are colored in red). The functionally selected monoclones are shown in green with indication of their code according to the Table. Sequences of the L-CDR3 for the most interesting clones are indicated

their own cross-reactive auto-antigens in the CNS, causing local inflammation and further development of the disease.

Deep sequencing of enriched libraries was carried out to evaluate the results of the selection of antibodies to the desired antigens. About 100,000 sequences from each library (50,000 for heavy and light chains, respectively) were identified using the Illumina MiSeq equipment. Further analysis of the heavy and light chains of the selected antibodies for the occurrence of CDR3 was carried out; the relative charges of the most effectively selected CDR3 were determined. To that end, the sequences obtained using deep sequencing were aligned with those of antibodies from the IMGT database [32] using the IMGT/V-QUEST software [31]. The results of the alignments were then filtered to get rid of artifacts. Only the filtered sequencing results were further analyzed. A comparative analysis was applied to the representation of different CDR3 in the enriched

libraries as compared to the initial MS library; the total number of sequences carrying CDR3 was regarded as a measure of CDR3 representation (Figs. 4, 5). Figures 4, 5 also show the representation of CDR3 antibodies obtained using functional selection (Table). The outlier points located above the regression line correspond to positive selection on the given CDR3 (it predominates in this selection compared to the other CDR3), while the outlier points below the line correspond to negative selection. We were primarily interested in the positive outliers, since they were the first candidates for functionally important CDR3 in each selection. As expected, most clones selected after the functional selection using monoclonal phage ELISA were predominant among the CDR3 that were prevailing according to their occurrence. Moreover, it is clear that clones h1 and e11 carry a heavy-chain CDR3 with increased polyreactivity, since the frequency of its occurrence is increased in all four enriched libraries compared to the original one.

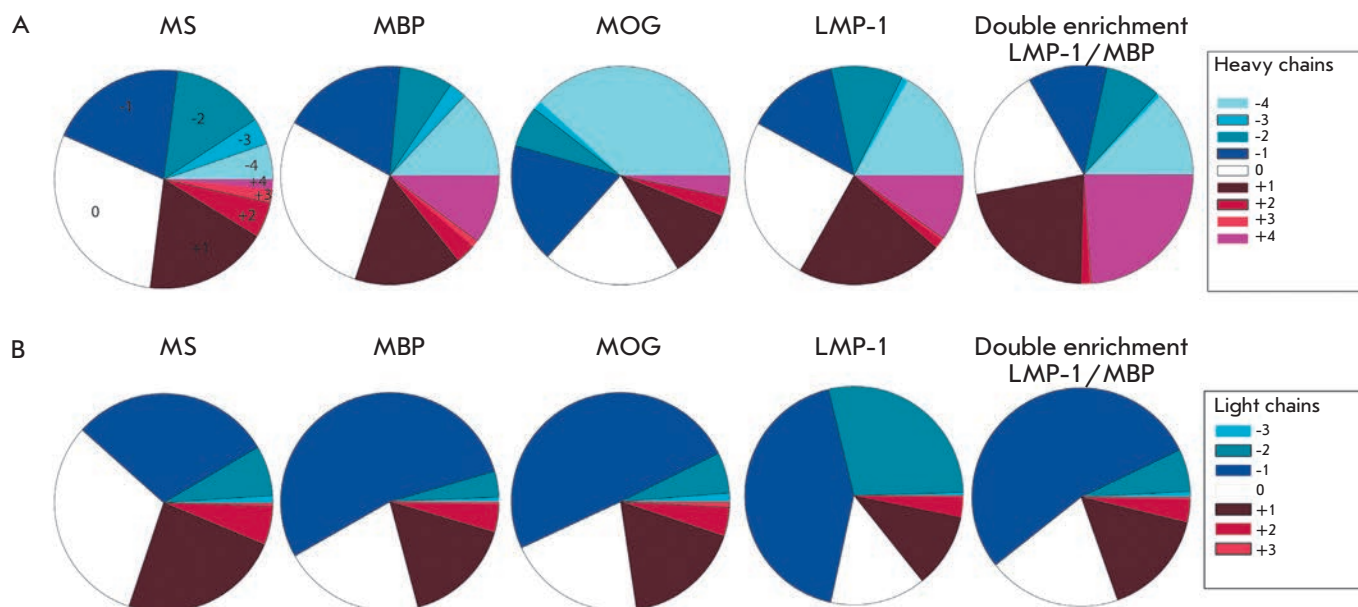


Fig. 6. Distribution of the CDR3 net charge in sublibraries enriched for different antigens for heavy (A) and light (B) chains

CDR3 of clone h11 was amplified in the MBP, LMP-1, and LMP-1/MBP libraries, which can characterize it as part of the cross-reactive paratope for two common epitopes in MBP and LMP-1. On the other hand, an unusual situation occurred when the ARGATSTRLL-SRRGHAFDV sequence underwent explicit selection for binding of MBP and LMP-1 in the analysis of the occurrence of H-CDR3, but no antibodies with such CDR3 were obtained using monoclonal phage ELISA. This fact could be attributed to the limited number of clones analyzed by phage ELISA. This situation may also result from the low affinity of the specific phage clone for two antigens in monoclonal ELISA, whereby this clone was not selected for further analysis. However, in reality it quantitatively passed selection for two antigens. In any case, further analysis of clones with similar hypervariable regions may help clarify the cross-reactivity problem. Among the light chains, scFv e12 had potentially increased cross-reactivity between MBP and MOG. It was also effectively selected in the LMP-1/MBP library after enrichment for MBP, although no effective selection for this CDR3 was observed upon enrichment for LMP-1.

Interaction between two proteins occurs largely due to the charge in the contact area. Since CDR3 plays the most important role in the formation of an antibody binding site, we decided to evaluate the contribution of electrostatic interactions in this region to the binding specificity in the selection on different antigens, as well as in the selection of cross-reactive clones. We determined the occurrence frequency of CDR3 with differ-

ent charges for heavy and light chains (Fig. 6), taking into account the number of readings for each sequence. It may be noted that in the library enriched for MOG, the amount of neutrally charged CDR3 of the heavy chain fell almost by a third, and the total amount of CDR3 with a high negative net charge (-4 and higher) increased sevenfold. This is mainly due to the reduction in the positive charge ($+1$). A shift of the net charge to a higher charge, either positive ($+4$) or negative (-4), was observed in the case of selection for the other antigens. For the light chains, a decrease in the amount of neutral and an increase in the amount of weakly negative CDR3 (-1 for MBP, MOG and double enrichment LMP-1/MBP and $-1-2$ for LMP-1) was observed. Thus, a conclusion can be drawn that although the library of antibodies of MS patients (MS in Fig. 6), which to some extent represents the distribution of the antibodies in the patient's body, is originally dominated by immunoglobulins with a neutral CDR3, the tendency to be autoreactive is mainly characteristic of antibodies with charged residues in the antigen binding sites. Notably, heavy chains demonstrated a more significant charge shift towards the extreme values in absolute magnitude, both positive and negative, compared to light chains. This may be indicative of the more active participation of the heavy chain in the formation of a binding site.

CONCLUSIONS

We obtained a panel of antibodies to several autoantigens in MS patients, as well as a set of cross-reactive antibod-

ies binding both to the Epstein-Barr virus protein and to the structural unit of the myelin sheath (MBP). The high homology of the antibodies to selected autoantigens and viral or bacterial pathogens may attest to the participation of several viruses in the development of MS. Poly-reactivity of autoantibodies in MS patients can be due to the combination of two chains, a heavy and light one, each of them being largely responsible for binding to its own antigen. In the case of sequential selection for LMP-1 and MBP conducted in this work, the antibody light chain is probably responsible for the binding to LMP-1, whereas combination with the heavy chain leads to the formation of a full-featured cross-reactive antibody binding both to LMP-1 and MBP. An increase in charged CDR3 is typical of autoantibodies specific for the studied

MS autoantigens (MBP, MOG) and a potential viral MS trigger (LMP-1). ●

This work was supported by the Russian Foundation for Basic Research (grant № 12-04-01609-a, 12-04-33258, 12-04-92428-EMBL-a, 13-04-40277-H, 09-04-12128-ofi_m), Skolkovo grant “Personalized Therapy of Autoimmune Diseases and Cancer”, Programs of the Presidium of the Russian Academy of Sciences “Fundamental Sciences to Medicine” and program № 27 “Fundamental Research in Nanotechnology and Nanomaterials”, NSH-2046.2012.4, grant of the President of Russian Federation SP 2445.2013.4.

REFERENCES

- Hauser S.L., Oksenberg J.R. // *Neuron*. 2006. V. 52. № 1. P. 61–76.
- Hemmer B., Nessler S., Zhou D., Kieseier B., Hartung H.P. // *Nat. Clin. Practice Neurol.* 2006. V. 2. № 4. P. 201–211.
- Compston A., Coles A. // *Lancet*. 2008. V. 372. № 9648. P. 1502–1517.
- Jersild C., Fog T., Hansen G.S., Thomsen M., Svejgaard A., Dupont B. // *Lancet*. 1973. V. 2. № 7840. P. 1221–1225.
- Barcellos L.F., Oksenberg J.R., Begovich A.B., Martin E.R., Schmidt S., Vittinghoff E., Goodin D.S., Pelletier D., Lincoln R.R., Bucher P., et al. // *Am. J. Hum. Genet.* 2003. V. 72. № 3. P. 710–716.
- Marrosu M.G., Murru R., Murru M.R., Costa G., Zavattari P., Whalen M., Cocco E., Mancosu C., Schirru L., Solla E., et al. // *Hum. Mol. Genet.* 2001. V. 10. № 25. P. 2907–2916.
- Dyment D.A., Herrera B.M., Cader M.Z., Willer C.J., Lincoln M.R., Sadovnick A.D., Risch N., Ebers G.C. // *Hum. Mol. Genet.* 2005. V. 14. № 14. P. 2019–2026.
- Masterman T., Ligiers A., Olsson T., Andersson M., Olerup O., Hillert J. // *Ann. Neurol.* 2000. V. 48. № 2. P. 211–219.
- Barcellos L.F., Sawcer S., Ramsay P.P., Baranzini S.E., Thomson G., Briggs F., Cree B.C., Begovich A.B., Villoslada P., Montalban X., et al. // *Hum. Mol. Genet.* 2006. V. 15. № 18. P. 2813–2824.
- Ramagopalan S.V., Morris A.P., Dyment D.A., Herrera B.M., DeLuca G.C., Lincoln M.R., Orton S.M., Chao M.J., Sadovnick A.D., Ebers G.C. // *PLoS Genet.* 2007. V. 3. № 9. P. 1607–1613.
- Robertson N.P., Fraser M., Deans J., Clayton D., Walker N., Compston D.A. // *Brain*. 1996. V. 119. P. 449–455.
- Sadovnick A.D., Baird P.A., Ward R.H. // *Am. J. Med. Genet.* 1988. V. 29. № 3. P. 533–541.
- Willer C.J., Dyment D.A., Risch N.J., Sadovnick A.D., Ebers G.C. // *Proc. Natl. Acad. Sci. USA*. 2003. V. 100. № 22. P. 12877–12882.
- Ebers G.C., Sadovnick A.D., Dyment D.A., Yee I.M., Willer C.J., Risch N. // *Lancet*. 2004. V. 363. № 9423. P. 1773–1774.
- Sokolova E.A., Malkova N.A., Korobko D.S., Rozhdestvenskii A.S., Kakulya A.V., Khanokh E.V., Delov R.A., Platonov F.A., Popova T.Y., Aref'eva E.G., et al. // *PLoS One*. 2013. V. 8. № 4. P. e61032.
- Tsareva E.Yu., Kulakova O.G., Makarycheva O.Yu., Boyko A.N., Shchur S.G., Lashch N., Popova N.F., Gusev E.I., Bashinskaya V.V., Lvov D.V. et al. // *Mol Biol (Mosk)*. 2011. V. 45. № 6. P. 886–893.
- Yong V.W., Marks S. // *Neurology*. 2010. V. 74. Suppl 1. P. S9–S16.
- Lund F.E., Randall T.D. // *Nat. Rev. Immunol.* 2010. V. 10. № 4. P. 236–247.
- Ponomarenko N.A., Durova O.M., Vorobiev I.I., Aleksandrova E.S., Telegin G.B., Chamborant O.G., Sidorik L.L., Suchkov S.V., Alekberova Z.S., Gnuchev N.V., et al. // *J. Immunol. Meth.* 2002. V. 269. № 1–2. P. 197–211.
- Ponomarenko N.A., Durova O.M., Vorobiev I.I., Belogurov A.A., Telegin G.B., Suchkov S.V., Misikov V.K., Morse H.C., Gabibov A.G. // *Immunol. Lett.* 2006. V. 103. № 1. P. 45–50.
- Ponomarenko N.A., Durova O.M., Vorobiev I.I., Belogurov A.A. Jr., Kurkova I.N., Petrenko A.G., Telegin G.B., Suchkov S.V., Kiselev S.L., Lagarkova M.A., et al. // *Proc. Natl. Acad. Sci. USA*. 2006. V. 103. № 2. P. 281–286.
- Paty D.W., Li D.K. // *Neurology*. 1993. V. 43. № 4. P. 662–667.
- Sela M. // *Rejuvenation Res.* 2006. V. 9. № 1. P. 126–133.
- Stepanov A.V., Belogurov A.A. Jr., Ponomarenko N.A., Stremovskiy O.A., Kozlov L.V., Bichucher A.M., Dmitriev S.E., Smirnov I.V., Shamborant O.G., Balabashin D.S., et al. // *PLoS One*. 2011. V. 6. № 6. P. e20991.
- Belogurov A.A. Jr., Stepanov A.V., Smirnov I.V., Melamed D., Bacon A., Mamedov A.E., Boitsov V.M., Sashchenko L.P., Ponomarenko N.A., Sharanova S.N., et al. // *FASEB J.* 2013. V. 27. № 1. P. 222–231.
- Gabibov A.G., Belogurov A.A. Jr., Lomakin Y.A., Zakharova M.Y., Avakyan M.E., Dubrovskaya V.V., Smirnov I.V., Ivanov A.S., Molnar A.A., Gurtsevitch V.E., et al. // *FASEB J.* 2011. V. 25. № 12. P. 4211–4221.
- Wekerle H., Hohlfield R. // *N. Eng. J. Med.* 2003. V. 349. № 2. P. 185–186.
- Lunemann J.D., Jelcic I., Roberts S., Lutterotti A., Tackenberg B., Martin R., Munz C. // *J. Exp. Med.* 2008. V. 205. № 8. P. 1763–1773.
- Chastain E.M., Miller S.D. // *Immunol. Rev.* 2012. V. 245. № 1. P. 227–238.
- Alamyar E., Giudicelli V., Li S., Duroux P., Lefranc M.P. // *Immunome Res.* 2012. V. 8. № 1. P. 26.
- Brochet X., Lefranc M.P., Giudicelli V. // *Nucl. Acids Res.* 2008. V. 36. P. W503–508.
- Lefranc M.P., Giudicelli V., Ginestoux C., Jabado-Michaloud J., Folch G., Bellahcene F., Wu Y., Gemrot E., Brochet X., Lane J., et al. // *Nucl. Acids Res.* 2009. V. 37. P. D1006–1012.

Antidepressant Effect of Dimeric Dipeptide GSB-106, an Original Low-Molecular-Weight Mimetic of BDNF

S.B. Seredenin, T.A. Voronina, T.A. Gudasheva, T.L. Garibova*, G.M. Molodavkin, S.A. Litvinova, E.A. Elizarova, V.I. Poseva
V.V. Zakusov Institute of Pharmacology, Russian Academy of Medical Sciences, Baltiyskaya Str., 8, Moscow, Russia, 125315

*E-mail: t_garibova@mail.ru

Received 13.03.2013

Copyright © 2013 Park-media, Ltd. This is an open access article distributed under the Creative Commons Attribution License, which permits unrestricted use, distribution, and reproduction in any medium, provided the original work is properly cited.

ABSTRACT A large amount of clinical and experimental data suggest the involvement of neurotrophins, in particular the brain-derived neurotrophic factor (BDNF), in depression pathogenesis. However, the therapeutic use of BDNF is limited because of its instability in biological fluids, poor blood-brain barrier (BBB) permeability, and the presence of side effects. A low-molecular-weight mimetic GSB-106, which is a substituted dimeric dipeptide *bis*(N-monosuccinyl-L-seryl-L-lysine)hexamethylenediamide, was designed and synthesized based on the BDNF fourth loop structure at the V.V. Zakusov Institute of Pharmacology (RAMS). GSB-106 was found to exhibit an antidepressant activity in various models of depressive-like state when administered intraperitoneally to outbred mice and rats. An effect for the substance, when administered daily for 4–5 days, was detected in the Porsolt forced swimming test (0.1 and 1.0 mg/kg) and in the tail suspension test in mice (1.0 and 1.5 mg/kg). An effect for GSB-106 at doses of 0.1 and 0.5 mg/kg was observed after a single application in experiments on rats in the Nomura water wheel test. The obtained evidence supports the hypothesis on the involvement of BDNF in the pathogenesis of various depression conditions, thus opening prospects for searching for new original antidepressants.

KEYWORDS BDNF, mimetic, GSB-106, antidepressant activity, forced swimming test, tail suspension test.

ABBREVIATIONS MAO – monoamine oxidase; BDNF – brain-derived neurotrophic factor, GSB-106 – *bis*(N-monosuccinyl-L-seryl-L-lysine)hexamethylenediamide; TrkB – tropomyosin-related receptor kinase B; AKT – serine/threonine protein kinase; CREB – cAMP response element binding protein; ERK – extracellular signal-regulated kinase.

INTRODUCTION

According to the WHO, 4–5% of the world population suffers from depression and depressions could become the most prevalent disease by 2030 [1, 2]. Even now about 20% of mental patients in economically developed countries suffer from endogenous and psychogenic depressive disorders [3].

Disregulation of the major monoaminergic systems of the brain, including the serotonergic, noradrenergic, and dopaminergic ones, has for a long time been regarded as the primary pathophysiological mechanism for the development of depressive disorders. The application of virtually all antidepressants that are being currently used, which are either monoamine oxidase (MAO) or monoamine reuptake inhibitors, does not always yield the desired clinical results.

A large body of evidence for the important role of the changes in the neurotrophin level, BDNF especial-

ly, in depression pathogenesis has been accumulated over the past decades [4–6]. Clinical studies have shown that the BDNF blood content in patients with severe depression is significantly reduced and recovers after the administration of antidepressants [7, 8].

Based on depression models, BDNF has been shown to exhibit a pronounced antidepressant effect upon central administration [9, 10]. The high resistance of transgenic mice with elevated levels of this neurotrophin to depression also provides evidence of the antidepressant properties of BDNF [11]. In addition, positive feedback between BDNF and serotonin was found in [12].

The therapeutic use of BDNF is limited by its instability in biological fluids, poor blood-brain barrier permeability, the risk of a reaction, and side effects due to its pleiotropy.

In connection with this, the strategy to develop new compounds on the basis of low-molecular-weight mi-

metics of BDNF, which would possess an antidepressant activity when administered systemically and would have none of the side effects typical of the original neurotrophin, seems rather promising. A series of low-molecular-weight mimetics of BDNF has been described. Thus, a group of Australian researchers have designed bicyclic and tricyclic dimeric peptides with agonistic activity on the basis of the second loop [13]. A group of American scientists [14] have obtained seven non-peptide compounds on the basis of the second loop, as well. However, no data have been reported regarding an antidepressant activity for the described mimetics of BDNF.

A low-molecular-weight mimetic GSB-106 [15, 16], which is a substituted dimeric dipeptide bis(N-mono-succinyl-L-seryl-L-lysine)hexamethylenediamide, was designed and synthesized based on the BDNF fourth loop structure at the V.V. Zakusov Institute of Pharmacology (RAMS). GSB-106 was selected in the course of pharmacological screening of four compounds, mimetics of the first and fourth loops of BDNF, as a dimeric dipeptide exhibiting antidepressant activity in the Balb/c mouse line upon single administration in the Porsolt forced swimming test [16].

In vitro studies of GSB-106 on a culture of immortalized NT22 mouse hippocampal cells demonstrated that this compound at concentrations ranging from 10^{-5} to 10^{-8} M exhibits a neuroprotective activity in models of oxidative stress and glutamate toxicity. The neuroprotective activity of GSB-106 was also detected in cultured SH-SY5Y human neuroblastoma cells when treated with neurotoxin 6-hydroxidopamine [17].

The aim of the present work was to study GSB-106 antidepressant properties on various depressive state models in outbred mice and rats upon single and subchronic administration.

EXPERIMENTAL

GSB-106 was studied on white outbred male rats (2–2.5 months old, weighing 270–290 g) and male mice weighing 22–25 g received from the “Stolbovaya” Central Laboratory for Animal Breeding (Moscow Region, Russia). Animal husbandry activities were performed in compliance with good laboratory practices regulations and sanitary rules for the maintenance of experimental biological clinics (vivarium). The study was conducted in accordance with Order of the Ministry of Health Care and Social Development of the Russian Federation № 708n of 23.08.2010 “Approval of the Rules of Good Laboratory Practice.” GSB-106 synthesized at the V.V. Zakusov Institute of Pharmacology of RAMS was used in the study.

The antidepressant activity of the compounds was evaluated in the Porsolt forced swimming test [18], the

Nomura water wheel test [19], and the tail suspension test in mice [20].

The experimental setup for creating the Porsolt depression-like state (behavioral despair) in mice consisted of a cylindrical vessel (10 cm in diameter and 30 cm high). The vessel was filled with water to a height of 18 cm, and its temperature was maintained at 27°C. Preliminarily, one day prior to testing, each animal was immersed in a container with water for 5–6 min for adaptation. On the day of the experiment, the animal was placed in the vessel with water so that it neither could escape from the vessel nor could find a support within. Once in water, the animals began to show violent motor activity aimed at finding a way out of the aversive stress situation, but then they gave up and hung in the water in a characteristic pose, remaining completely motionless or making the small movements necessary to keep their head above water. This behavior is considered as a sign of desperation, despondency, and a depressive-like state [18]. A measure of the severity of the depressive-like state in this test is immobility duration, i.e. the sum of immobility episodes over 6 min of observation for each animal. A statistically significant reduction in the immobilization duration is considered to be the antidepressant activity criterion.

A four-channel setup designed at the V.V. Zakusov Institute of Pharmacology (RAMS) [21] was used to model a depressive-like state in rats by the method of Nomura [19] in a vessel with water and freely rotating wheels. The setup consisted of a 64 x 30 x 42 cm vessel divided into four equal compartments. Each compartment comprised a 11 cm wide wheel with 12 blades (2 cm wide each); the outer diameter of the wheel was 10 cm. Magnets were anchored on the edges of each wheel, and reed switches were located over the wheels and responded each time when a magnet passed under them. The automatic detection of wheel rotation was carried out in this manner and served as objective measure of animal activity. The vessel was filled with water at 25°C until it reached the midline of the wheel. Rats were placed in each compartment, with their heads oriented away from the wheel, and the wheel rotation speed was recorded for 10 min with electromechanical counters.

The animals' tails were tied to a horizontal crossbar in the tail suspension test [20]. First, the animals placed into stressful situations began to show motor activity aimed at finding a way out of the aversive conditions, but then they stopped this activity and hung on the crossbar remaining almost completely immobile.

Dipeptide GSB-106 was dissolved in distilled water and administered to the animals intraperitoneally at doses of 0.01, 0.1, 0.5, 1.0, and 1.5 mg/kg 30 min prior

to testing once or repeatedly once a day for 4–5 days. The control animals received normal saline in the same regimen.

Statistical processing of the results was carried out with the Biostatistics III program using the Student's and Mann–Whitney tests.

RESULTS AND DISCUSSION

Antidepressant activity of GSB-106 in the Porsolt forced swimming test in mice

It was found that immobilization for 238–278 s in different groups of control mice was observed after a period of activity (Table 1). GSB-106, when administered once at doses of 0.1 and 1.0 mg/kg, showed a tendency to reduce the immobilization time (Table 1).

GSB-106, when administrated subchronically at a dose of 0.1 mg/kg for five days or at a dose of 1.0 mg/kg for four days, corrected the animal's behavior in the forced swimming test, significantly reducing the duration of immobilization episodes compared to the control group: by 1.2 times using GSB-106 at a dose of 0.1 mg/kg and by 1.3 times when GSB-106 was administered at a dose of 1.0 mg/kg (Table 1).

Therefore, GSB-106 at doses of 0.1 and 1.0 mg/kg upon repeated administration for 4–5 days exhibited an antidepressant effect in the Porsolt behavioral despair test, which manifested itself in a statistically significant decrease in the immobilization time of the animals. An increase in the antidepressant effect of BDNF

upon repeated administration was also described. Thus, BDNF (0.25–1.0 μg) when bilaterally injected once into the hippocampus reduced the immobilization duration twofold [10], and when infused in the midbrain of rats for 4–5 days at a dose of 12–24 $\mu\text{g}/\text{day}$ it reduced the immobilization duration threefold in the Porsolt forced swimming test [9].

Antidepressant effect of GSB-106 in the Nomura depressive-like state test in rats

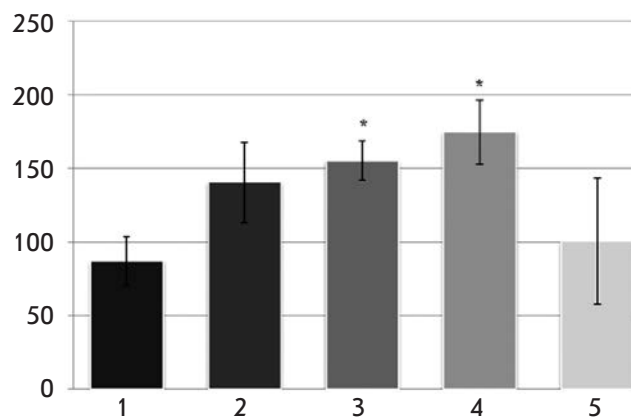
The rats in the control group were found to make on average 87 wheel turns during 5 min of registration (Figure). GSB-106 at a dose of 0.01 mg/kg did not cause any increase in the number of wheel turns, but when administered at a higher dose (0.1 mg/kg), the compound showed a distinct antidepressant activity as evidenced by a statistically significant increase (1.8 times) in the number of wheel turns made by the rats compared to the parameters of the control animals (Figure). The antidepressant effect of GSB-106 at a dose of 0.5 mg/kg was stronger, and the number of wheel turns made by the rats increased twofold. However, with a further increase in the dose of GSB-106 to 1.0 mg/kg its antidepressant effect decreased and the number of wheel turns remained the same as that in the control animals (Figure).

Hence, GSB-106 at doses of 0.1 and 0.5 mg/kg produced a distinct antidepressant effect in the Nomura forced swimming test. The plot of the effect *vs* dose of GSB-106 is bell-shaped.

Table 1. Antidepressant effect of GSB-106 in mice (by Porslot)

Dose of GSB-106 administered intraperitoneally, mg/kg, once a day	Administration frequency	Immobilization time, s (M \pm SEM)
Control (saline)	1	255.61 \pm 25.07
0.1	1	206.29 \pm 33.35
1.0	1	204.83 \pm 26.67
Control (saline)	5	278.38 \pm 12.02
0.1	5	231.41 \pm 11.22*
Control (saline)	4	271.73 \pm 13.37
1.0	4	205.76 \pm 11.02*
Control (saline)	1	238.50 \pm 15.37
Amitriptyline, 10.0 mg/kg	1	134.62 \pm 23.42*

* $p < 0.05$ – statistical significance of the differences with the Mann-Whitney U test compared to the control group.



Antidepressant effect of GSB-106 in the Nomura depressive-like state test. Dose of intraperitoneal administration of GSB-106, mg/kg: 1 – control; 2 – 0.01; 3 – 0.1; 4 – 0.5; 5 – 1.0. Y-direction: the number of wheel turns * $p < 0.05$ statistical significance of the deviation from the control group with the Mann-Whitney U-test

Antidepressant activity of GSB-106 in the depressive-like state test caused by suspending mice by the tail

It was found that the average immobilization time upon suspension by the tail in the control group of animals was 174 and 148 s for different groups. GSB-106, when administered subchronically (4 days) and intraperitoneally at doses of 0.1 and 0.5 mg/kg, did not alter the animal's immobilization duration in this test compared to the control. However, GSB-106 had a clear antidepressant effect at higher doses. GSB-106 at doses of 1.0 and 1.5 mg/kg (4 days, intraperitoneally) significantly ($p=0.04$) decreased (1.3 times) the immobilization time in mice in the tail suspension test (Table 2).

Thus, the antidepressant effect of the GSB-106 dipeptide was clearly revealed under conditions of three validated methods for modeling the depressive-like state: in the Porsolt behavioral despair test (0.1 and 1.0 mg/kg, 4–5 days), in the Nomura water wheel test (0.1 and 0.5 mg/kg, single dose), and in the Steru tail suspension test in mice (1.0 and 1.5 mg/kg, 4 days).

It is important that the antidepressant effect of GSB-106 was observed upon systemic intraperitoneal administration to outbred mice and rats both as a single dose and as repeated daily doses in the range of 0.1–1.5 mg/kg. It appears that the stronger pronounced effect of GSB-106 in rats is related to species differences and to the methodological features of the evaluation.

As mentioned above, according to the neurotrophin theory of depression development, low BDNF levels in the central nervous system damage brain structures and cause the development of depressive states; however, the use of antidepressants or administration of BDNF to animals corrects these disorders. The antidepressant effect of GSB-106 attained in the present work is similar to that of BDNF upon intraventricular infusion or upon administration of the latter to the brain regions of an animal responsible for depression [8–10]. In the study by Schmidt and Duman [22], systemic (subcutaneous) administration of recombinant BDNF to mice caused an antidepressant effect characterized by a 1.5-fold decrease in the immobilization duration in the forced swimming test. However, this effect of BDNF was only observed when used at doses 6–7 times higher than those of GSB-106, and only after

Table 2. Antidepressant effect of GSB-106 upon subchronic (4 days) administration in the depressive-like state test in mice caused by tail suspension

Dose of GSB-106 administered intraperitoneally, mg/kg	Immobilization time, s (M ± SEM)
Control (saline)	174.00 ± 10.4
0.1	145.20 ± 15.81
1.0	135.50 ± 12.85*
Control (saline)	148.25 ± 6.38
0.5	126.22 ± 9.89
1.5	120.13 ± 10.53*

*Statistical significance of the deviation from the control, $p \leq 0.05$ (Student's *t*-test).

long-term administration (for 7–14 days). Induction of neurogenesis in the hippocampus and midbrain was a functional consequence of the antidepressant action of recombinant BDNF; the authors attributed its mechanism to the increased BDNF level and to the increased level of activation/phosphorylation of ERK and CREB in the downstream targets of the BDNF-TrkB signaling pathways [22]. Previously, we found that GSB-106, the mimetic of BDNF, activates TrkB and its ERK and the AKT signaling pathways [23] involved in neuronal survival and this fact could presumably underly its antidepressant effect. Moreover, the ability of the GSB-106 dipeptide dimer to phosphorylate TrkB was selective, since no neuroprotective activity of GSB-106 was found in aPC12 cell line not expressing the full-length TrkB but expressing other neurotrophin receptors [23].

On one hand, the resulting data on the antidepressant activity of GSB-106, the low molecular weight mimetic of BDNF, support the hypothesis regarding the involvement of BDNF in the pathogenesis of various depressive states, while on the other hand opening prospects for designing a novel antidepressant (original in its structure and mechanism of action) based on the newly synthesized compound. ●

REFERENCES

- WHO Bulletin. 10 facts about the global burden of disease. 2008. http://www.who.int/features/factfiles/global_burden/ru/index.html.
- Sartorius N. // *Med. Res.* 2001. V. 1. P. 20–21.
- Wittchen H.U. // *V.M. Bekhterev Review of Psychiatry and Medical Psychology.* 2005. № 4. P. 42–46.
- Angelucci F., Mathe A.A., Aloe L. // *Progress in Brain Research.* 2004. V. 146. P. 151–165.
- Yu H., Chen Z.Y. // *Acta Pharmacologica Sinica.* 2011. V. 32. P. 3–11.
- Neto F.L., Borges G., Torres-Sanchez S., Mico J.A., Berrocoso E. // *Current Neuropharmacology.* 2011. № 9. P. 530–552.
- Karege F., Perret G., Bondolfi G., Schwald M., Bertschy G., Aubry J.M. // *Psychiatry Res.* 2002. V. 109. P. 143–148.
- Chen B., Dowlatshahi D., MacQueen G.M., Wang J.F., Young L.T. // *Biol. Psychiatry.* 2001. V. 50. P. 260–265.

RESEARCH ARTICLES

9. Siuciak J.A., Lewis D.R., Wiegand S.J., Lindsay R.M. // *Pharmacol. Biochem. Behav.* 1997. V. 56. P. 131–137.
10. Shirayama J., Chen A.C., Nakagawa S., Russel R.S., Duman R.S. // *J. Neurosci.* 2002. V. 22. P. 3251–3261.
11. Govindarajan A., Rao B.S.S., Nair D., Trinh M., Mawjee N., Tonegawa S., Chattarji S. // *Proc. Natl. Acad. Sci. USA.* 2006. P. 13208–13213.
12. Siuciak J.A., Altar C.A., Wiegand S.J., Lindsay R.M. // *Brain Res.* 1994. V. 663. P. 326–330.
13. O'Leary P.D., Huges R.A. // *J. Biol. Chem.* 2003. V. 278. P. 25738–25744
14. Massa S.M., Yang T., Xie Y., Shi J., Bilgen M., Joyce J.N., Nehama D., Rajadas J., Longo F.M. // *J. Clin. Investigation.* 2010. V. 120. P. 1774–1785.
15. Seredenin S.B., Gudasheva T.A. // Patent RUS № 2410392 of 16.02.2009 priority. 2011.
16. Gudasheva T.A., Tarasyuk A.V., Pomogaybo S.V., Logvinov I.O., Povarnina P.Y., Antipova T.A., Seredenin S.B. // *Bioorganic Chemistry.* 2012. V. 38. P. 280–290.
17. Logvinov I.O., Antipova T.A., Gudasheva T.A., Tarasyuk A.V., Antipov P.I., Seredenin S.B. // *Bull. Exp. Biol. Med.* 2013. In press.
18. Porsolt B.D., Bertin A., Jalfre M. // *Europ. J. Pharmacol.* 1978. V. 51. P. 291–294.
19. Nomura S., Shimizu J., Kinjo M., Kametani H., Nakazawa T. // *Eur. J. Pharmacol.*, 1982. V. 83. P. 171–175.
20. Steru L., Chermat R., Thierry B., Simon P. // *Psychopharmacology.* 1985. V. 85. P. 367–370.
21. Molodavkin G.M., Voronina T.A., Md zinarishvili A.L. // *Exp. Cl. Pharm.* 1994. V. 1. P. 3–5.
22. Schmidt H.D., Duman R.S. // *Neuropsychopharmacology.* 2010. V. 35. P. 2378–2391.
23. Gudasheva T.A., Logvinov I.O., Antipova T.A., Seredenin S.B. // *DAS.* 2013. V. 451. № 5. P. 577–583.

Three-Dimensional Model of Mouse Epidermis for Experimental Studies of Psoriasis

A.G. Soboleva, V.V. Sobolev, S.A. Bruskin, A.V. Mezentsev*

Federal Non-profit Research Institute of Russian Academy of Sciences, N.I. Vavilov Institute of General Genetics, Moscow 119991, Russia

*E-mail: mesentsev@vigg.ru

Received 27.02.2013

Copyright © 2013 Park-media, Ltd. This is an open access article distributed under the Creative Commons Attribution License, which permits unrestricted use, distribution, and reproduction in any medium, provided the original work is properly cited.

ABSTRACT Three-dimensional models of skin and epidermis imitate the structure of real tissues and provide accurate information about certain skin conditions, such as psoriasis. A three-dimensional model of mouse epidermis was generated from the epidermal keratinocytes of newborn mice and treated with cytokines. The aim of this study was to evaluate this model as an experimental model of psoriasis and to assess the changes occurring in its structure and gene expression after the exposure to proinflammatory cytokines. Treatment of the three-dimensional model with either interleukin 17 or a combination of tumor necrosis factor and interferon γ was shown to produce morphological changes, which were similar to acanthosis in psoriatic skin. The observed changes in gene expression of metalloproteinases and certain psoriasis biomarkers, such as *mki67*, *krt16* and *fosl1*, were similar to the changes in patients' skin. Notably, changes caused by interleukin 17 were less evident than those caused by the combination of interferon γ and tumor necrosis factor. On the contrary, HaCaT cells exhibited no significant changes in the expression of *fosl1* and had decreased levels of *mki67* after being treated with a combination of TNF and IFNG. Moreover, treatment with IL17 had no significant effect on *krt16* and *mki67* expression and even reduced the *fosl1* levels. The findings suggest that artificially generated three-dimensional models of murine skin can be used to study psoriasis.

KEYWORDS acanthosis; cell culturing; psoriasis; cornification; qPCR; three-dimensional modeling.

ABBREVIATIONS TNF – tumor necrosis factor; IL1 – interleukin 1; IL17 – interleukin 17; IFNG – interferon γ ; TMME – three-dimensional model of mouse epidermis; MMP1 – interstitial collagenase (EC 3.4.24.7).

INTRODUCTION

Recently, three-dimensional models of skin and epidermis have begun to be used very frequently to test cosmetic products, as well as to treat chronic wounds and burns [1–3]. The use of these models complies with the existing European regulations that encourage researchers to minimize their animal experimentations and demand proof of the innocuousness and effectiveness of their experimental procedures [4, 5]. With respect to other existing experimental models, three-dimensional models of skin and epidermis are of great interest in simultaneously testing the effectiveness of multiple compounds, taking into consideration the metabolic changes that occur during the terminal differentiation of keratinocytes. Moreover, these models can be used to study tissue remodeling in pathological conditions.

Compared to the conventional monolayered cell cultures where cells as presumed are the same, the existing organoleptic tissue models mimic both the

intercellular contacts and interactions of cells with the extracellular matrix. They also reproduce the changes in gene expression that occur in real tissues and organs. Thus, 3D models of skin and epidermis can potentially provide more accurate information regarding certain pathological conditions, such as psoriasis. This makes them an irreplaceable tool for experimental studies. Taking into account the fact that many basic researchers have limited access to donor skin, we would like to develop a new experimental approach to assess changes in the proliferation and differentiation of skin cells in psoriatic epidermis. This new approach does not involve human cells.

It is believed that psoriatic skin lesions are developed due to the action of the immune cells that infiltrate a patient's skin. These cells secrete certain proinflammatory cytokines, such as TNF, IFNG, and IL17 [6]. In turn, the secreted cytokines activate the epidermal keratinocytes, thus causing sufficient changes in their terminal differentiation program and accelerating their

proliferation. Taking into consideration this point, we treated an original three-dimensional model of mouse epidermis with either IL17 or a combination of INF γ and TNF to detect the changes in the model structure and gene expression that occurred thereafter. Thus, the aim of this study was to verify whether the model was able to exhibit certain morphological changes similar to those occurring in psoriatic plaques and to assess its potential for further experimental studies of psoriasis.

EXPERIMENTAL

Collection of skin biopsies

Samples were taken under local anesthesia using a 4 mm dermatological puncher. Patients selected for this study did not receive any systemic or PUVA/UV therapy for at least one month prior the study. Full skin biopsies from the patients diagnosed with common psoriasis, *psoriasis vulgaris*, were obtained from psoriatic plaques as well as from their uninvolved skin at least 3–4 cm away from any skin lesion. The samples designated for RNA purification were quickly frozen in liquid nitrogen and transported to the laboratory. Weighted skin samples were homogenized using a mortar and pestle avoiding their thawing. The samples were then subjected to RNA purification and qPCR. Samples designated for histology analysis were fixed in formalin. This protocol was approved to study human subjects by the ethics committee at the N.I. Vavilov Institute of General Genetics and complies with the principles of the Declaration of Helsinki and National regulations on research to study human subjects.

Preparation of primary keratinocytes from newborn mice

Corpses of newborn mice designated for the experiment were decontaminated in betadine and consequently washed with 70% ethanol, gentamycin, and an isotonic phosphate buffered saline (PBS). Each skin was then peeled, flattened on the bottom of a Petri dish, and incubated with 0.25% trypsin (PanEco, Russia) overnight. Next day, the epidermis was mechanically separated from the dermis and cut with scissors into small pieces. The cut tissue was incubated in KSF μ M medium (Life Technologies, USA) under moderate stirring for 30 min at 37°C. The cell suspension was then filtered through 70 μ m cell strainers (Sigma-Aldrich, USA) and centrifuged at 250 g for 5 min. The precipitated cells were counted and plated at a density of 1.1×10^4 cells/cm 2 into 25cm 2 flasks covered with collagen (Sigma-Aldrich, USA). The cells were cultured in KSF μ M medium supplemented with S7 supplement (Life Technologies, USA). The calcium concentration in the medium was maintained at 60 μ M to prevent cells from entering the

terminal differentiation program. The next morning after plating, unattached cells were removed. This protocol was approved for working with laboratory animals by the Ethics Committee of the N.I. Vavilov Institute of General Genetics. It also complies with the national regulations on research involving laboratory animals.

Cell culturing

HaCaT cells were cultured in DMEM supplemented with L-glutamin, 10% FBS (PanEco, Russia), and 5% antibiotic-antimycotic solution (Life Technologies, USA).

Preparation of murine skin equivalents

Mouse three-dimensional skin models were generated from acellular dermis and primary mouse keratinocytes. Deepidermized dermis was prepared by thermoinactivation of skin samples in PBS (56°C; 10 min). After thermoinactivation, the epidermis was peeled off the dermis [7]. Prior to the experiment, glass rings were installed on the deepidermized dermis. Rings were pressed firmly to form isolated compartments for culturing the cells. Cells were then seeded (3×10^5 cells/cm 2) and cultured for three days in a freshly prepared medium. The following medium was used to culture the cells: DMEM and F12 that were mixed at a 3:1 ratio, 5% FBS, 1% antibiotic-antimycotic, 4 mM L-glutamin (PanEco, Russia), adenine (25 μ g/mL), ascorbic acid (50 μ g/mL), triiodothyronine (1 μ g/mL), 1 μ M hydrocortisone (Sigma-Aldrich, USA), and 0.2 μ M recombinant mouse insulin and 10 ng/mL epidermal growth factor (R&D Systems, USA). EGF (R&D Systems, USA) was added to the medium after 24 h. The medium was changed every other day. On the third day, the rings were removed and the samples were submerged in the medium. On the sixth day, culturing was continued at the air-liquid interface to ensure that the upper surface of each sample was in contact with air. For this step of culturing, the medium was enriched with L-serine (1 mg/mL), L-carnitine (2 μ g/mL), 7 μ M arachidonic acid, and 15 μ M linoleic acid (Sigma-Aldrich, USA). Moreover, vitamin E (Sigma-Aldrich, USA) was added prior to changing the medium to the final concentration of 0.5 μ g/mL. The following proinflammatory cytokines (R&D Systems, USA) were used: TNF (25 ng/mL), IFN γ (25 ng/mL), and IL17A (50 ng/mL). The cytokines were added to the medium every other day for four days starting from day 10.

Purification and analysis of total RNA

RNA was purified using the TRIZOL method as described earlier [8]. Samples were repurified using the RNeasy kit (Qiagen, Germany) if the absorption ratio, A_{260}/A_{280} , in at least one TRIZOL purified sample was

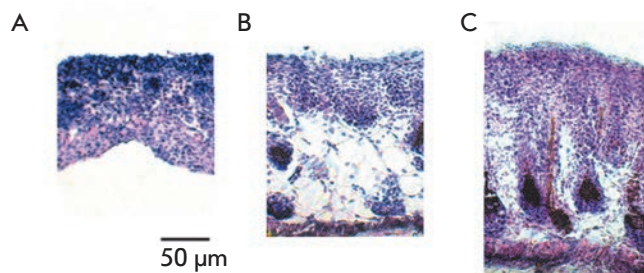


Fig. 1. The histological analysis of the most representative TMME samples after treatment with proinflammatory cytokines. TMME samples were cultured for two weeks and treated with proinflammatory cytokines starting from the 10th day of culturing: **A** – untreated control; **B** – sample treated with a combination of TNF and IFNG; **C** – sample treated with IL17 (n=6). Harvested samples were embedded in paraffin and stained with hematoxylin and eosin. See the Experimental section for the details

lower than 2.0. The integrity of the purified RNA was assessed electrophoretically in 1.5% agarose gel under non-denaturing conditions.

qPCR

The obtained RNA samples were converted to cDNA using the MMLV RT kit (Evrogen, Russia). These samples were subjected to qPCR with pre-designed commercial gene expression assays (Life technologies, USA) on an Eco PCR life cycler (Illumina, USA). The results were analyzed with the Eco software supplied by the manufacturer.

Histology

For histology analysis, the samples were processed into paraffin blocks. Hematoxylin- and eosin- (H + E) stained sections were assessed to evaluate the histopathological changes.

Statistical analysis

Data were represented as means \pm SE. The statistical differences between the means were assessed by a one-way analysis of variances and Student's t test. If *p*-values were less than 0.05, means were considered to be significantly different.

RESULTS

The resulting three-dimensional model of murine skin, TMME (Fig. 1A), exhibited a weakly differentiated structure. Unlike healthy human epidermis, TMME was missing the granular layer. Moreover, the transition from the basal layer to the suprabasal layer was

not clearly seen. Cornification was also weak, and a suggestion of the corny layer included 2–3 top rows of cells. In uninvolved psoriatic epidermis (Fig. 2A), the basal layer of cells was directly attached to the basal membrane. This cell layer should be the only cell layer where cells are able to proliferate. Starting from the suprabasal layer, keratinocytes gradually changed their shape as they entered the terminal differentiation program. In uninvolved skin, the granular layer separated the cornified anuclear cells and the living nucleated cells of the suprabasal layer (Fig. 2B). In turn, lesional psoriatic epidermis (Fig. 2C) was thickened because of cell proliferation in the suprabasal layer. The evident structural changes attested to certain alterations in the terminal differentiation of cells, such as a delay in the formation of cytoplasmic keratohyalin granules, the degradation of cell nuclei and desmosomes, as well as synthesis of certain biomarkers. Notably, our experimental model exhibited more structural similarities with psoriatic epidermis than normal skin even prior the treatment with proinflammatory cytokines.

In TMME, the expression of epidermal cytokeratins (*krt1*, *krt5* and *krt14*) and the expression of *lor*, which is a marker of the terminal differentiation of epidermal keratinocytes, did not change significantly compared to the skin of newborn mice (Fig. 3). Contrariwise, the expression of *krt10*, *krt18* and *ivl* was significantly different. The *krt10* and *krt18* levels were higher in the skin of newborn mice, while the expression of *ivl* was higher in TMME.

The treatment of TMME with a combination of proinflammatory cytokines TNF and IFNG increased the total thickness of the cell layers composed of living cells by a factor of 1.5 (Fig. 4) compared to the untreated samples. Moreover, the treatment prevented cornification in the top cell layers (Fig. 1B) and lowered the cell density in the inner cell layers. Overall, the structure of treated TMME became too fragile compared to the untreated control. The latter complicated the integrity of the generated TMME sections, which were to perform the histological analysis. Notably, the treatment with IL17 produced fewer changes in the total thickness than the treatment with a combination of TNF and IFNG (Fig. 1C and Fig. 4). Meanwhile, the total thickness of the model treated with IL17 significantly exceeded the same parameters in the control samples. Thus, TMME exhibited sensitivity to proinflammatory cytokines, such as TNF, IFNG, and IL17 in the same way as the psoriatic epidermis; treatment with a combination of TNF and IFNG produced a stronger response.

At the transcriptional level, TMME also exhibited significant changes. These changes were similar to those observed when comparing the lesional and unin-

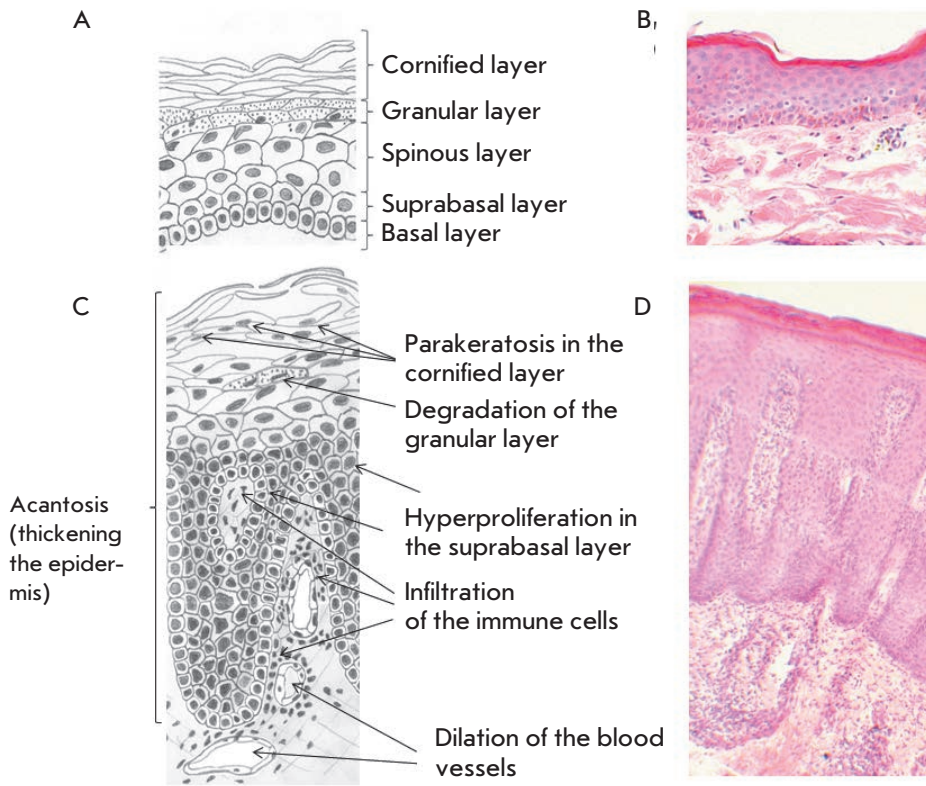


Fig. 2. Schematic representation and histological analysis of the psoriatic epidermis. The collected tissue samples were embedded in paraffin and stained with hematoxylin and eosin as described in the Experimental section: *A* – schematic representation of uninvolved psoriatic epidermis; *B* – uninvolved psoriatic epidermis stained with eosin and hematoxylin; *C* – schematic representation of a psoriatic skin lesion; *D* – psoriatic skin lesion stained with eosin and hematoxylin

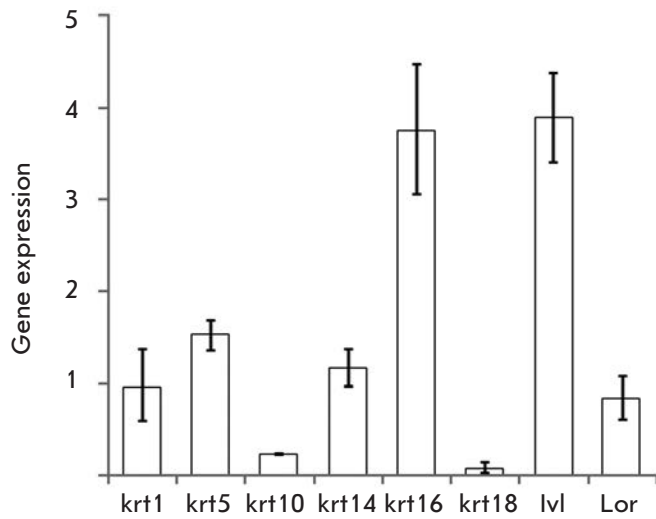


Fig. 3. Gene expression of selected cytokkeratins and markers of terminal differentiation of the epidermal keratinocytes. The gene expression was assessed by qPCR as described in the Experimental section. Gene expression in TMME was compared to gene expression in the skin of newborn mice (n=3). In untreated control, gene expression levels were considered to be equal to 1

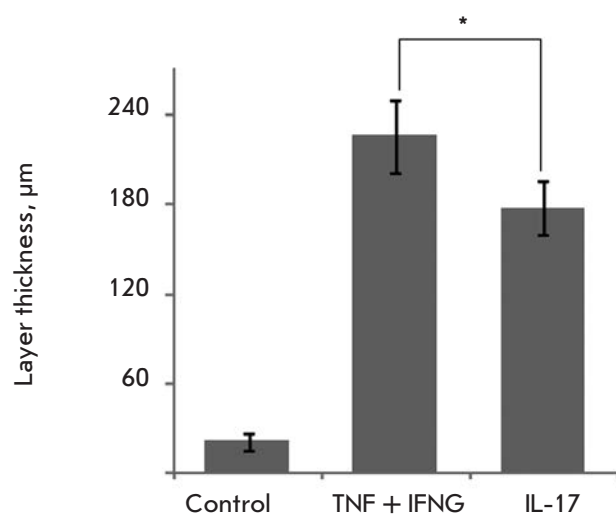


Fig. 4. Influence of proinflammatory cytokines on TMME total thicknesses. TMME samples were cultured for two weeks and treated with proinflammatory cytokines starting from the 10th day of culturing as described in the Experimental section

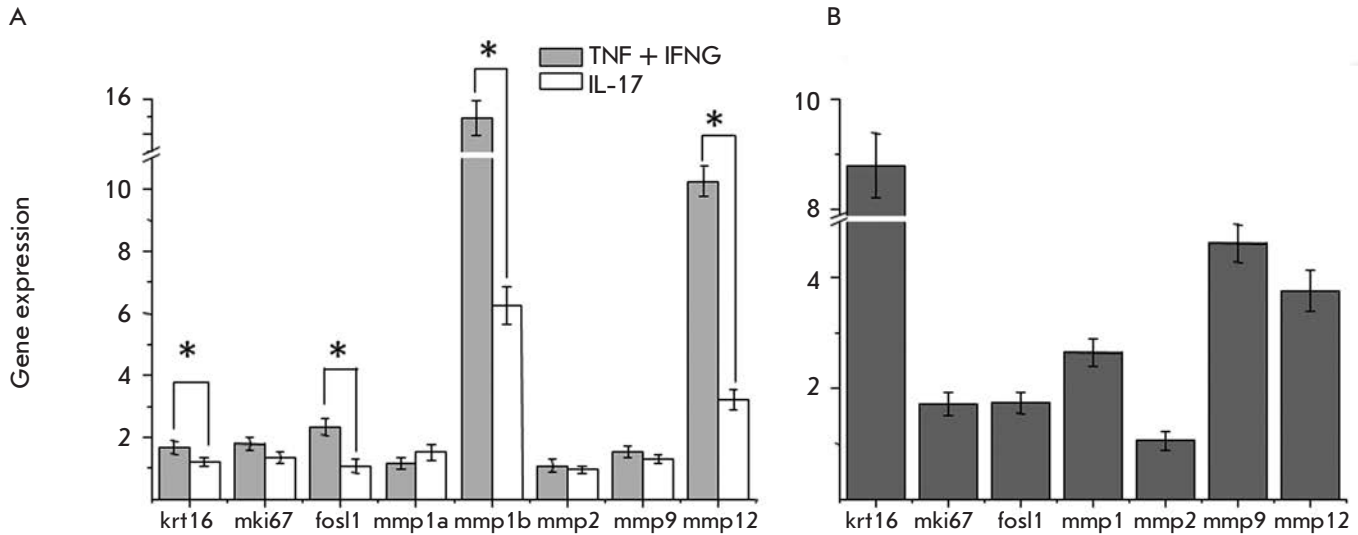


Fig. 5. Gene expression observed in TMME treated with proinflammatory cytokines (A) and patients' skin (B). TMME was treated with either a combination of TNF and IFNG or IL17. All samples were subjected to RNA purification, reverse transcription and qPCR analysis as described in the Experimental section. Gene expression in the treated TMME samples was compared to that in the untreated control (n=3)

involved psoriatic skin. The levels of certain biomarkers, such as *krt16* and *fosl1* as well as the hyperproliferation marker *mki67* were elevated after the treatment with TNF and IFNG (Fig. 5A). Moreover, TMME also reproduced the expression pattern of metalloproteinases, which included four genes: *mmp1*, *mmp2*, *mmp9*, and *mmp12*. In our previous study [9], we showed that this pattern was highly reproducible in lesional skin. Notably, the changes in the expression of *mki67*, *fosl1*, and *krt16* induced by the treatment of TMME with IL17 were less evident and did not differ significantly from the control (Fig. 5B). Thus, the combined treatment with TNF and IFNG could be a more significant contributor to the activation of keratinocytes in both psoriasis and TMME.

We have previously demonstrated that treatment of HaCaT cells with proinflammatory cytokines, such as a combination of TNF and IFNG, reproduced the expression patterns of metalloproteinases characteristic of psoriatic lesional skin [10]. The data generated in the present study suggested that TMME treated with TNF and IFNG exhibits similar changes in metalloproteinases expressions (Fig. 5A). Here, we also found that HaCaT cells as a proposed experimental model of psoriasis had sufficient differences with TMME. These differences should be taken into account in further experimental studies involving this type of cells. In particular, *krt16* was induced in HaCaT cells after treatment with a combination of TNF and IFNG

(Fig. 6A). However, these cells failed to induce *krt16* after treatment with IL17 (Fig. 6B). Moreover, neither treatment of HaCaT cells increased *mki67* and *fosl1* expression as compared to the untreated control (Fig. 6A and B).

DISCUSSION

Psoriatic skin lesions emerge through a complex multi-stage process that involves many signaling mechanisms and requires several kinds of cells. The imitation of pathological skin changes that occur in psoriasis will help to encircle the molecular processes playing an active role in the pathogenesis of this disease. It will also help to clarify the connections between these processes and the clinical symptoms of psoriasis. A number of recent publications have been devoted to the development of new three-dimensional models of human skin and epidermis for different practical needs; their number still continues to grow. The main reason behind the rising scientific interest in three-dimensional models is the ability of an artificial skin to heal severe skin damages. Several three-dimensional models, including the model that uses an endogenous carcass [11] and other models that use natural and biodegradable polymeric materials, such as chitin and chitosan [12], polylactate [13], a combination of amorphous poly (*D*, *L*-lactide) and polyethylene glycol [14], etc. have been developed in Russia. These inventions are helpful in healing burns [11] and venous stasis ulcers [3].

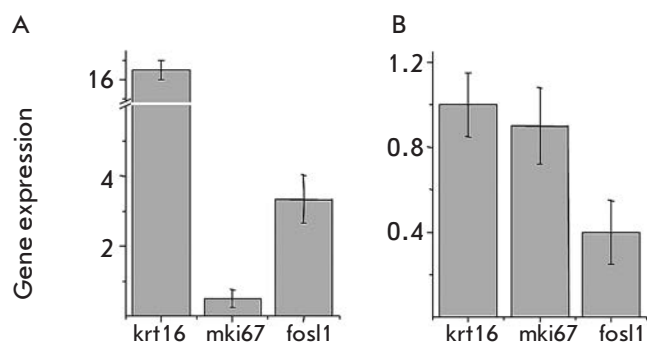


Fig. 6. Influence of proinflammatory cytokines on gene expression in HaCaT cells. HaCaT cells were grown to 70% confluence and treated with either a combination of TNF and IFNG (A) or IL17 (B). The cells were subjected to RNA purification, reverse transcription and qPCR analysis as described in the Experimental section. Gene expression in the treated samples was compared to that in the untreated control (n=3)

In the most frequently used experimental three-dimensional models of skin and epidermis designated for basic research, human epidermal keratinocytes are cultured on a support, such as deepidermized dermis or collagen gel with embedded fibroblasts. In these three-dimensional skin models, either mouse or human cell lines serve as the main source of fibroblasts. Prior to being embedded into the gel, these cells are usually treated with either γ -irradiation or mitomycin C to suppress cell division. In turn, leftovers of cosmetic surgery and circumcision are used as a main source of keratinocytes. Depending on the objectives of a study; three-dimensional skin models may also include macrophages [15], melanocytes [16], and dendritic cells [17]. Thus, the TMME that we are proposing in this study is made of mouse keratinocytes; thus, this model does not rely on any human tissue material or cells.

The use of keratinocytes and deepithelized mouse dermis in three-dimensional models can be beneficial for several reasons. The domestic mouse is the most frequently used laboratory animal. Mice are easy to hold and breed in captivity. Their high fertility and the relatively short gestation period allow one to minimize the external supplies of donor skin. An average litter of mice is typically 6–8 pups and their gestation period lasts only 18.5 days. The use of cells of newborn pups to construct TMME increases the cell yield because of the following rapid decline in the epidermal thickness during the first days of the pups' terrestrial life.

Several kinds of genetically modified mice, such as transgenic mice [18] and mice with deletions in certain genes [19], can serve as animal models to study psoria-

sis. In other mouse models of psoriasis, the diseased skin phenotype can be caused by either spontaneous mutations in the genome [20, 21] or by treating wild-type mice with certain chemical agents [22]. The development of these models made some of them very close in details to the clinical features of human psoriasis [18, 22].

Design and development of TMME is in line with European regulations that encourage researchers to minimize their needs in laboratory animals and to develop animal-free models, such as cell cultures and tissue equivalents [4, 5]. In the obtained model, we detected *krt1*, *krt5*, and *krt14*, which contribute to the terminal differentiation of epidermal keratinocytes. Moreover, their expression in TMME and the skin of newborn mice were comparable (Fig. 3). In addition to the cytokeratin genes, we also detected an expression of *ivl* and *lor* in the model, whose expression precedes the cornification process. The elevated *ivl* and *krt16* expression levels, as well as the lower *krt10* levels, in TMME suggest that certain changes in the differentiation of epidermal keratinocytes occurred during the culturing. On the contrary, lower *krt18* levels suggest that unlike the skin of newborn mice, TMME is predominantly composed of a single cell type, and these cells are epidermal keratinocytes.

The results presented in this paper also demonstrate that TMME exhibits certain important similarities with psoriatic plaques. Primarily, TMME was responsive to treatment with proinflammatory cytokines. Treatment with these cytokines thickened the populated cell areas (Fig. 4). Furthermore, this treatment prevented cornification in the upper cellular layers compared to the untreated control (Fig. 1A–C). In addition, treatment with these cytokines also caused certain changes in the expression of metalloproteinases, *krt16*, *mki67*, and *fosl1* (Fig. 5A). Notably, the observed changes in the TMME appearance (Fig. 1A–C) remind of acanthosis in psoriatic epidermis (Fig. 2B), while the changes in the expression of metalloproteinases, *mki67*, cytokeratin *krt16*, and nuclear protein *fosl1* in TMME (Fig. 5A), which are specific psoriasis biomarkers, were similar to those observed in psoriatic epidermis (Fig. 5B).

To characterize TMME at the transcriptional level, we selected the genes whose role in the pathogenesis of psoriasis had already been determined. For instance, metalloproteinases MMP1, MMP9, and MMP12 participate in the structural re-arrangement that occurs in psoriatic epidermis [9]. Their activity is crucial for the maintenance of the extracellular matrix and basal membrane, angiogenesis and cell migration within the epidermis, such as the migration of the immune cells, which infiltrate lesional psoriatic epidermis. A shift

in the balance between the metalloproteinases in the skin coincides with an aggravation of psoriasis. In turn, an increase in the *mki67* level is indicative of hyperproliferation of keratinocytes [23]. An elevated *mki67* expression is an important characteristic of lesional psoriatic skin [24]. Cytokeratin *krt16* is specifically expressed in lesional psoriatic skin (Fig. 5B). Moreover, this cytokeratin is expressed in normal skin at a very low level [25]. *fosl1* was chosen because its expression correlated with exacerbation of psoriasis and dropped with the beginning of remission [26].

Notably, the treatment with IL17 produced no such evident changes in gene expression compared to the treatment with a combination of TNF and IFNG (Fig. 5A). While the expression of the two preselected genes *mmp1b* and *mmp12* remained significantly higher compared to the untreated control, the expressions of other genes, such as *krt16*, *mki67*, *fosl1*, *mmp1a*, *mmp2*, and *mmp9*, did not change significantly: i.e., did not exceed 50% of their expression in the control samples.

Unlike humans that have only one MMP1 isoform, mice have two different MMP1 isoforms (MMP1a and MMP1b). The coding genes of *mmp1a* and *mmp1b* localize in the same gene cluster on chromosome 9 [27]. These genes have high sequence homology with each other as well as human *mmp1*. Despite the fact that both genes were discovered more than ten years ago [27], their physiological differences remain unclear. Moreover, both murine *mmp1* respond similarly to treatment with cytokines and growth factors [28]. The inclusion of both isozymes in our gene selection to verify TMME allowed us to demonstrate that *mmp1a* was capable of producing a stronger response to proinflammatory cytokines. On the contrary, *mmp1b* expression could not exceed the control levels by a factor of 1.6 after either treatment (Fig. 5A).

As compared to TMME, expression of the same genes by HaCaT cells, which have been previously considered to be a conventional two-dimensional cellular model to study psoriasis, has not met our expectations (Fig. 5A and 6, respectively). For instance, the treatment with TNF and IFNG suppressed *mki67* expression (Fig. 6A). The different responses of HaCaT and TMME to this treatment can be explained by the deviation from the physiological optimum of HaCaT cells. Notably, the least expected changes in gene expression occurred after the treatment of HaCaT cells with IL17. The expression levels of the two selected genes (*krt16* and *mki67*) did not change significantly, and the expression of *fosl1* dropped to a lower level compared to the

untreated cells. Thus, a conclusion can be drawn that TMME is more adequate in simulating biomarker expression than a monolayered culture of HaCaT cells.

On the other hand, TMME still has certain differences compared to the other three-dimensional human skin models. In TMME, cell layers are not clearly separated from each other, cornification is insignificant, and cell distribution in middle layers is more diffused than can be expected. Moreover, TMME is missing the granular layer. Unfortunately, we cannot explain these structural ablations yet. However, we believe that they might be caused by fundamental differences in the development of the murine and human epidermis. For instance, the murine epidermis is not completely formed by the time a mouse is born, and certain changes in the content of the TMME cell culture medium will allow us to overcome it.

In order to stabilize the levels of epidermal growth factors we propose to supplement the model with an underlying layer of non-proliferating dermal fibroblasts. To prevent fibroblasts from proliferating, we will treat them with mitomycin C prior to embedding cells into the gel [29]. At early stages of tissue culturing, we will use the inhibitors of GSK3 kinase to slow down the terminal differentiation of epidermal keratinocytes. Previously, one of such agents was used to generate inducible stem cells from the epidermal keratinocytes [30]. At the later stages of culturing, we will add either IL1 or oncostatin M to the culture medium. According to the published data [31, 32], both IL1 and oncostatin M have the ability to induce *S100A* genes. IL1 also stimulates the expression of terminal differentiation markers, such as transglutaminase 1, *Tgm1*, and involucrin, *Ivl*. Thus, this supplementation is expected to improve cornification of the TMME upper cell layers.

CONCLUSION

The findings suggest that artificially generated three-dimensional models of mouse epidermis can be used to study psoriasis. These data also demonstrate that activation of mouse keratinocytes is more evident after treatment with a combination of IFNG and TNF rather than IL17. ●

This work was supported by the Russian Ministry of Education and Science (grant 16.512.11.2049), Russian Academy of Sciences via the Federal Program “From Fundamental Science to Medicine”, and special program of the Russian Ministry of Education and Science “Scientific and Educational Potential of Innovative Russia” (grant P1309).

REFERENCES

1. Kolbe L., Mann T., Gerwat W., Batzer J., Ahlheit S., Scherner C., Wenck H., Stab F. // *J. Eur. Acad. Dermatol. Venerol.* 2013. V. 27. S1. P. 19–23.
2. Vasil'ev A.V., Vorotelyak E.A., Kisilev I.V., Terskikh V.V. // *Vestn. Ross. akad. med. nauk (Annals of the Russian Academy of Medical Sciences)*. 2008. № 2. P. 45–53.
3. Mel'tsova A.Zh., Gritsenko V.V., Orlovskii P.I., Tomson V.V., Sabel'nikov V.V., Shulepova E.K., Prokopets A.I., Pinaev G.P., Blinova M.I., Iudintseva N.M. // *Vestn. Khir. Im. I. I. Grek.* 2007. V. 166. № 1. P. 72–77.
4. Kandarova H., Liebsch M., Genschow E., Gerner I., Traue D., Slawik B., Spielmann H. // *Altex.* 2004. V. 21. № 3. P. 107–114.
5. Mun G.C., Aardema M.J., Hu T., Barnett B., Kaluzhny Y., Klausner M., Karetsky V., Dahl E.L., Curren R.D. // *Mutat. Res.* 2009. V. 673. № 2. P. 92–99.
6. Johnson-Huang L.M., Lowes M.A., Krueger J.G. // *Dis. Model Mech.* 2012. V. 5. № 4. P. 423–433.
7. Tjabringa G., Bergers M., van Rens D., de Boer R., Lamme E., Schalkwijk J. // *Am. J. Pathol.* 2008. V. 173. № 3. P. 815–823.
8. Chomczynski P., Mackey K. // *BioTechniques* 1995. V. 19. № 6. P. 942–945.
9. Starodubtseva N.L., Sobolev V.V., Soboleva A.G., Nikolaev A.A., Bruskin S.A. // *Genetika.* 2011. V. 47. № 9. P. 1117–1123.
10. Starodubtseva N.L., Minnibaev M.T., Soboleva A.G., Korsunskaya I.M., Krivoshchapov L.G., Elkin A.M., Iakovenko G.T., Piruzyan A.L., Bruskin S.A., Sobolev V.V. // *Sovremennye problemy dermatovenerologii, immunologii i vrachebnoy kosmetologii (Modern problems of dermatovenerology, immunology, and clinical cosmetology)*. 2011. V. 2. № 15. P. 38–41.
11. Smirnov S.V., Kiselev I.V., Vasil'ev A.V., Terskikh V.V. // *Khirurgiia (Mosk)*. 2003. № 12. P. 58–62.
12. Panarin E.F., Nud'ga P.A., Petrova V.A., Bochek A.M., Goffman I.V., Baklagina Yu.G., Saprykina N.N., Blinova M.I., Yudintseva N.M., Spichkina O.G. et al. // *Cellular transplantation and tissue engineering*. 2010. V. 5. № 1. P. 65–73.
13. Shved Yu.A., Kukhareva L.V., Zorin I.M., Solov'ev A.Iu., Blinova M.I., Bilibin A.Iu., Pinaev G.P. // *Tsitologiya.* 2006. V. 48. № 2. P. 161–168.
14. Shved Yu.A., Zorin I.M., Pinaev G.P., Bilibin A.Iu. // *Fisiko-khimiya polimerov: sintez, svoystva i primeneniye* (Physical chemistry of polymers: synthesis, properties and applications). 2009. № 15. P. 175–179.
15. Linde N., Gutschalk C.M., Hoffmann C., Yilmaz D., Mueller M.M. // *PloS One.* 2012. V. 7. № 7. P. e40058.
16. Souto L.R., Vassallo J., Rehder J., Pinto G.A., Puzzi M.B. // *Sao Paulo Med. J.* 2009. V. 127. № 1. P. 28–33.
17. Uchino T., Takezawa T., Ikarashi Y. // *Toxicol. in vitro.* 2009. V. 23. № 2. P. 333–337.
18. Nakajima K., Kanda T., Takaishi M., Shiga T., Miyoshi K., Nakajima H., Kamijima R., Tarutani M., Benson J.M., Elloso M.M., et al. // *J. Immunol.* 2011. V. 186. № 7. P. 4481–4489.
19. Schonthaler H.B., Huggenberger R., Wculek S.K., Detmar M., Wagner E.F. // *Proc. Natl. Acad. Sci. USA.* 2009. V. 106. № 50. P. 21264–21269.
20. Liang Y. // *Patholog. Res. Int.* 2011. P. 936794.
21. Wang Z., Sokolovska A., Seymour R., Sundberg J.P., Hogenesch H. // *PloS One.* 2012. V. 7. № 2. P. e31809.
22. van der Fits L., Mourits S., Voerman J.S., Kant M., Boon L., Laman J.D., Cornelissen F., Mus A.M., Florencia E., Prens E.P., et al. // *J. Immunol.* 2009. V. 182. № 9. P. 5836–5845.
23. Fransson J., Hammar H. // *Arch. Dermatol. Res.* 1992. V. 284. № 6. P. 343–348.
24. Rikimaru K., Moles J.P., Watt F.M. // *Exp. Dermatol.* 1997. V. 6. № 5. P. 214–221.
25. Iizuka H., Takahashi H., Honma M., Ishida-Yamamoto A. // *J. Dermatol.* 2004. V. 31. № 4. P. 271–276.
26. Serov D.N., Sobolev V.V., Potekaev N.N., Piruzian E.S., Korsunskaya I.M., Abdeeva I.A., Soboleva A.G., Zolotarev A.D., Minnibaev M.T. // *Klinicheskaya dermatologia i venerologia (Clinical dermatology and venereology)*. 2010. № 4. P. 4–9.
27. Balbin M., Fueyo A., Knauper V., Lopez J. M., Alvarez J., Sanchez L.M., Quesada V., Bordallo J., Murphy G., Lopez-Otin C. // *J. Biol. Chem.* 2001. V. 276. № 13. P. 10253–10262.
28. Hyc A., Osiecka-Iwan A., Niderla-Bielinska J., Moskalewski S. // *Int. J. Mol. Med.* 2011. V. 27. № 1. P. 127–137.
29. Huang Y.C., Wang T.W., Sun J.S., Lin F.H. // *Artif. Organs.* 2006. V. 30. № 3. P. 150–159.
30. Li Z., Rana T.M. // *Nat. Commun.* 2012. V. 3. P. 1085.
31. Yano S., Banno T., Walsh R., Blumenberg M. // *J. Cell. Physiol.* 2008. V. 214. № 1. P. 1–13.
32. Gazel A., Rosdy M., Bertino B., Tornier C., Sahuc F., Blumenberg M. // *J. Invest. Dermatol.* 2006. V. 126. № 12. P. 2647–2657.

Intensity of Free Radical Processes in Rat Liver under Type 2 Diabetes and Introduction of Epifamin

T.N. Popova, A.A. Agarkov, A.N. Verevkin*

Voronezh State University, Universitetskaya pl., 1, Voronezh, Russia, 394006

*E-mail: wer.all@mail.ru

Received 25.04.2013

Copyright © 2013 Park-media, Ltd. This is an open access article distributed under the Creative Commons Attribution License, which permits unrestricted use, distribution, and reproduction in any medium, provided the original work is properly cited.

ABSTRACT The effect of epifamin on free radical processes, the activity of caspase-1 and -3, aconitate hydratase and citrate content in rat's liver at experimentally induced type 2 diabetes mellitus (T2DM) was studied. The action of epifamin at T2DM leads to a decrease in biochemiluminescence parameters, characterizing the intensity of free radical processes, and changes in aconitase activity and citrate level towards the control. Activities of caspase-1 and caspase-3 in the tissue decreased by a factor of 2.4 and 1.6 in comparison with the levels at the disease. Apparently, epifamin-mediated correction of the level of melatonin, providing a significant antioxidant effect, promotes positive action on the free radical homeostasis.

KEYWORDS type 2 diabetes mellitus, biochemiluminescence, aconitate hydratase, citrate, caspase, epifamin.

ABBREVIATIONS AH – aconitate hydratase, ROS – reactive oxygen species, BCL – biochemiluminescence, T2DM – type 2 diabetes mellitus.

INTRODUCTION

Diabetes mellitus is one of the existing socially significant diseases and remains a challenge both for fundamental medicine and for public health services. T2DM is responsible for over 90% of all of the cases of this pathology.

Free-radical oxidation of biomolecules plays a significant role in the pathogenesis of T2DM complications. The rate of free radical formation at T2DM depends on the rate of protein glycosylation and, therefore, on the degree of hyperglycemia, as well [1]. One of the reasons behind the enhancement of free-radical processes at T2DM may be associated with the activation of the polyol pathway, whose function is geared towards converting glucose to sorbitol with the participation of aldose reductase. Free radicals at hyperglycemia can also be formed via glucose autoxidation as the final glycosylation products are formed; in turn, these products participate in angiopathy pathogenesis, increase ischemia, and intensify the free-radical processes in tissues at T2DM [1]. Increased glycosylation of hemoglobin causes secondary tissue hypoxia [2].

The disruption of redox homeostasis at T2DM may be the reason behind the induced apoptosis, programmed cell death, which is characterized by the activation of a cascade of intracellular cysteine proteases (known as caspases). Caspases are a family of evolutionarily conserved proteases that are capable of cleaving proteins at specific sites after asparaginic acid residues [3]. In particular, caspase-3 participates in the proteolysis of

the inhibitor of the DNase responsible for DNA fragmentation (CAD). Furthermore, caspases induce the hydrolysis of the lamin proteins that reinforce the nuclear membrane, resulting in chromatin condensation. They participate in the disintegration of the proteins that maintain the structural and functional status of the cytoskeleton; in the inactivation and disruption of the regulation of the proteins involved in DNA reparation, mRNA splicing, and DNA replication. Caspase-3 (cpp32) is the key enzyme in the caspase family; assessing its activity is one of the main methods used to determine the level of apoptosis in tissue [4]. Activity of caspase-1 (ICE), which belongs to the group of cytokines (caspase activators), is another important parameter characterizing the apoptotic process.

Aconitate hydratase (AH), which plays the key role in the regulation of citrate accumulation, is known to be one of the sensitive targets of free radicals [5]. It was demonstrated that the regulation of AH activity is significantly changed by the activation of free-radical oxidation, resulting in the suppression of enzymatic activity and accumulation of citrate, which is a low-molecular-weight antioxidant due to its chelating properties for Fe^{2+} [6]. Fe^{2+} ions are known to exhibit a pro-oxidant activity, since they help produce a hydroxyl radical, one of the most aggressive and dangerous reactive oxygen species (ROS), via the Fenton and Haber–Weiss reactions [7].

The use of drugs that would reduce the intensity of free-radical processes in the organisms remains rather

topical. Epifamin is a peptide bioregulator that exhibits tropicity for the epithalamic-epiphysal area. It belongs to the family of cytomedins. In addition to having a positive effect on the immune system and normalizing the fat and carbohydrate metabolism, these peptides can also correct the endogenous melatonin level [8, 9]. The antioxidant mechanism is one of the main biochemical mechanisms used by melatonin to impact cells. Melatonin is an active electron donor and an efficient scavenger of radicals (OH^\cdot , OOH , O_2^\cdot , singlet oxygen, NO^\cdot , ONOO^-) [10]. Unlike most other intracellular antioxidants that localize primarily in certain cellular structures, the presence of melatonin and its antioxidant activity have been detected in all cellular structures, including the nucleus [11]. This fact attests to the universal nature of the antioxidant effect of melatonin and to the pronounced protective properties that ensure protection of DNA, proteins, and lipids against free radical damage.

This work was aimed at studying the effect of epifamin on the intensity of free-radical processes, activity of caspase-1 and 3 and aconitate hydratase, and on the citrate level in the liver of rats with experimental T2DM.

EXPERIMENTAL

White male rats (*Rattus rattus* L.; 150–200 g) were used for the experiments. All the procedures were performed in compliance with the Guidelines for Humane Care and Use of Laboratory Animals and the sanitary rules for maintenance of experimental biological clinics (vivarium). T2DM was induced via intramuscular injection of protamine sulfate during 3 weeks at a dose of 10 mg/kg b.w. (0.5 ml of 0.9% NaCl) thrice daily [12].

The animals were divided into three groups: group 1 ($n = 8$) consisted of the control animals; group 2 ($n = 8$) included the animals with T2DM; group 3 ($n = 8$) included the animals with T2DM, which intraperitoneally received the epifamin solution (in 1 ml of 0.9% NaCl solution) thrice daily at a dose of 2.5 mg/kg on day 15, 17, and 19. Three weeks after the induction of T2DM had started, the narcotized animals in all the experimental groups were euthanized and used for further analysis. The liver was removed as follows: anesthetized rats were subjected to laparotomy; a ligature was placed below the portal vein; the vein was incised, and a cannula was inserted 10 mm below the sinus. The anterior vena cava was cut in the diaphragm area; the liver was perfused with an ice-cold isotonic solution at a rate of 5 ml/min for 5 min. A weighed portion of tissue was homogenized by grinding it with quartz sand in a porcelain mortar with a 4-fold volume of a cold medium. The medium consisted of 0.1 M Tris-HCl buffer (pH 7.8), 1 mM EDTA, and 1% β -mercaptoethanol. The

homogenate was centrifuged at 10,000 g for 12 min. The supernatant fluid was used for further study.

The glucose level in the rat blood serum was determined by the glucose oxidase method using the GLUCOSE-12-VITAL reagent kit (OOO Vital Diagnostics, St. Petersburg, Russia). Blood samples were collected from the tail vein on days 15, 17, and 19 [13]. Serum was obtained by short-term centrifugation.

Induced biochemiluminescence (BCL) was used to determine the intensity of free-radical processes [14]. The BCL kinetic curve was recorded on a BCL-07 biochemiluminometer with software during 30 s, and the following parameters were determined: light sum (S) corresponding to the area below the chemiluminescence curve; the maximum flash intensity (I_{max}) – the maximum value on the biochemiluminescence curve characterizing the intensity of free-radical processes; and the slope of the tangent line to the BCL curve ($\text{tg}\alpha_2$), which characterizes the total antioxidant activity.

The medium used to determine the BCL intensity consisted of 0.4 ml of a 0.02 mM potassium phosphate buffer (pH 7.5), 0.4 ml of 0.01 mM FeSO_4 , and 0.2 ml of a 2% hydrogen peroxide solution (added immediately prior to the measurement). The analyzed material (0.1 ml) was introduced directly prior to the measurement before adding hydrogen peroxide.

Caspase-1 and 3 activities were determined using the Caspase 1 Assay Kit, Colorimetric and the Caspase 3 Assay Kit, Colorimetric, respectively (both kits were purchased from Sigma), on a Hitachi U1900 spectrophotometer with software. The colorimetric analysis of caspase activity is based on the hydrolysis of the peptide substrates acetyl-Tyr-Val-Ala-Asp-*p*-nitroanilide (Ac-YVAD-pNA) (for caspase-1) and acetyl-Asp-Glu-Val-Asp-*p*-nitroanilide (Ac-DEVD-pNA) (for caspase-3), yielding *p*-nitroaniline with the adsorption peak at 405 nm (molar extinction coefficient = 10.5). Caspase activity was expressed as picomoles of the product formed during 1 min calculated for 1 mg of the protein.

The AH activity was measured on a Hitachi U1900 spectrophotometer at 233 nm. The rate of citrate dehydration was assessed from the formation of a double bond in the *cis*-aconitate molecule. The AH activity was determined in a 50 mM Tris HCl buffer, pH 7.8, containing 0.15 mM citrate. A unit of enzyme activity (E) was defined as the amount of enzyme catalyzing the formation of 1 μmol of the reaction product during 1 min at 25°C.

The amount of citrate was determined using the Nattelson technique [15]. This method is based on bromination of citrate in the presence of potassium permanganate yielding pentabromoacetone, which reacts with thiourea to produce a colored complex. The color inten-

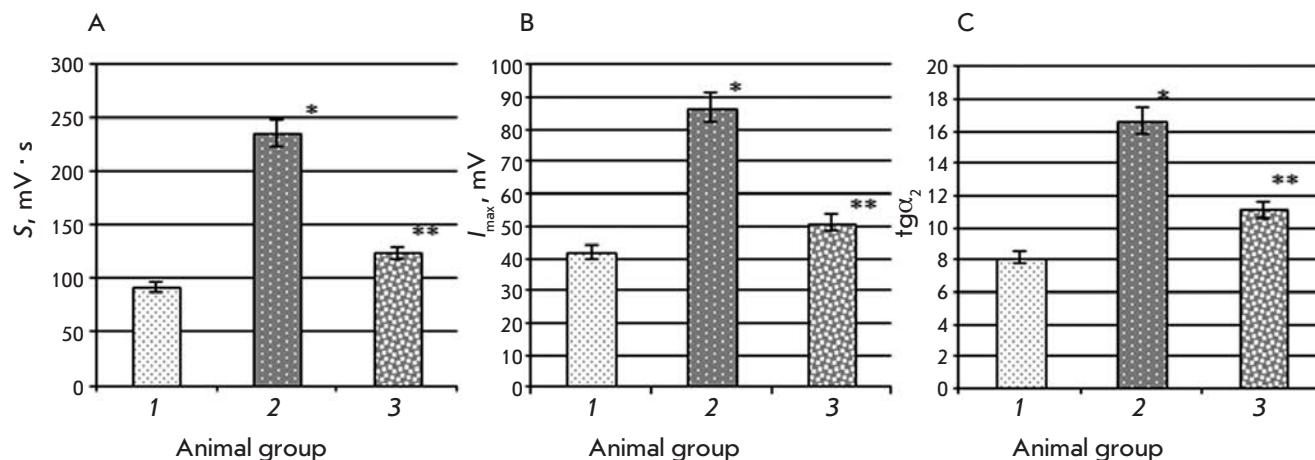


Fig. 1. Biochemiluminescence parameters: Light sum (S), $\text{mV} \cdot \text{c}$ (A), maximum flash intensity (I_{max}), mV (B), the slope of the tangent line to the kinetic curve ($\text{tg } \alpha_2$) (C) in rat liver in the control group (1), animals with type 2 diabetes mellitus (2), and after introduction of epifamin into animals with pathology (3)

Note. The differences are significant at $p \leq 0.05$: * – compared to the control group, ** – compared to the group of rats with T2DM.

Glucose concentration in rat blood serum in the experimental groups on days 15, 17, and 19 after the beginning of the experiment

Animal group	Glucose concentration, mM		
	day 15	day 17	day 19
1 (control)	5.00 ± 0.24	5.26 ± 0.23	5.5 ± 0.26
2	9.02 ± 0.41	9.72 ± 0.43	13.74 ± 0.64
3	8.18 ± 0.38	7.92 ± 0.36	7.71 ± 0.34

sity of this compound was measured spectrophotometrically at 430 nm on a Hitachi U1900 spectrophotometer. The calibration curve was used for calculations.

The total amount of protein was determined using the biuret test. The statistical significance of differences was assessed by Student's t -test. Differences at $p \leq 0.05$ were regarded as statistically significant.

RESULTS AND DISCUSSION

The introduction of protamine sulfate into experimental animals was found to increase the glucose level in blood serum. The use of epifamin as a protector reduced the hyperglycemia level in rats with experimentally induced T2DM: on day 19 after the experiment was started, the glucose blood level in animals with T2DM that received epifamin was lower 1.8-fold as compared to that in animals with T2DM that did not receive epifamin (Table). This can be attributed to the ability of epifamin to increase the melatonin level in the organ-

ism. It is a known fact that melatonin can stimulate glucose transport to skeletal muscles, thus activating the IRS-1/PI-3-kinase pathway and reducing the glucose concentration in the blood [16].

According to the resulting data, the light sum (S) and the maximum flash intensity (I_{max}) in the liver of rats with T2DM were 2.6- and 2.1-fold higher than the same parameters in the control animals (Fig. 1A, B), thus attesting to the fact that the intensity of free-radical oxidation increases. In accordance with the published data, the polyol pathway in which glucose is converted to sorbitol with the participation of aldose reductase takes place upon T2DM. Sorbitol dehydrogenase converts sorbitol to fructose, which is accompanied by an increase in the NADH/NAD⁺ ratio, similar to that during the development of tissue hypoxia. This condition has become known as “reductive stress” or “hyperglycemic pseudohypoxia” [2]. This condition may change the degree of reduction of the components of the elec-

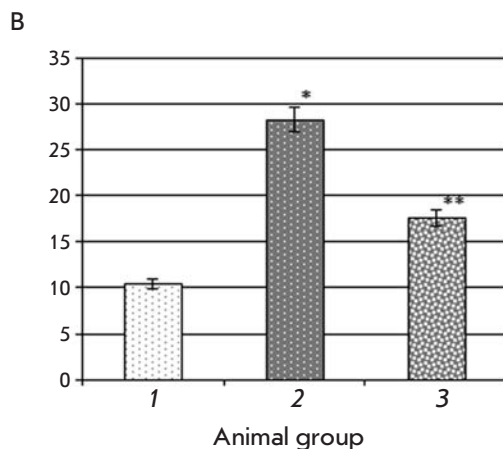
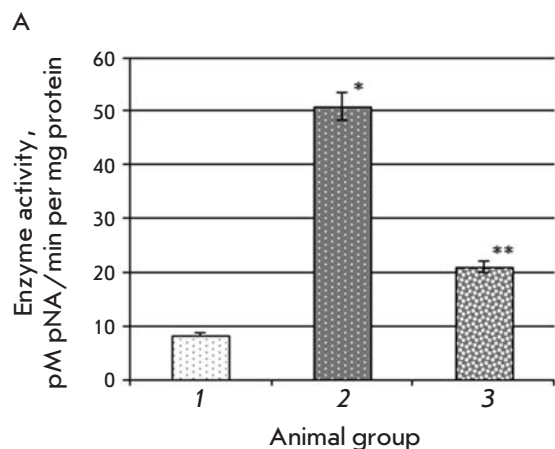


Fig. 2. Activity of caspase-1 (A) and caspase-3 (B) in rat liver in the control group (1), animals with type 2 diabetes mellitus (2), and after introduction of epifamin into animals with the pathology (3) Note. The differences are significant at $p \leq 0.05$: * – compared to the control group, ** – compared to the group of rats with T2DM.

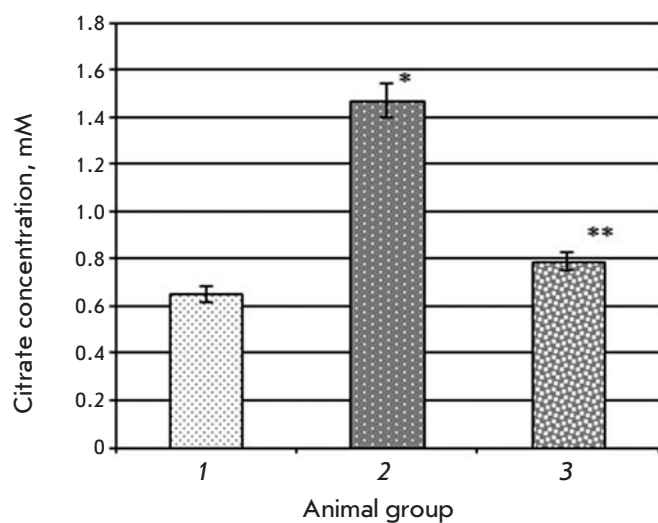


Fig. 3. Citrate concentration in rat liver in the control group (1), animals with type 2 diabetes mellitus (2), and after introduction of epifamin into animals with the pathology (3)

Note. The differences are significant at $p \leq 0.05$: * – compared to the control group, ** – compared to the group of rats with T2DM.

tron transport chain, thus increasing the probability of ROS formation.

A 2.1-fold increase in $tg\alpha_2$ (BCL parameter characterizing the total antioxidant activity) was also detected in the liver of animals with T2DM as compared to that in the control group (Fig. 1C). The introduction of epifamin into rats with T2DM reduced the S and I_{max} values by 1.9 and 1.7 times, respectively (Fig. 1A,B). The recorded decrease in the free-radical oxidation level may result from a manifestation of the antioxidant properties of melatonin, whose level can be controlled by epifamin. According to the published data, melatonin

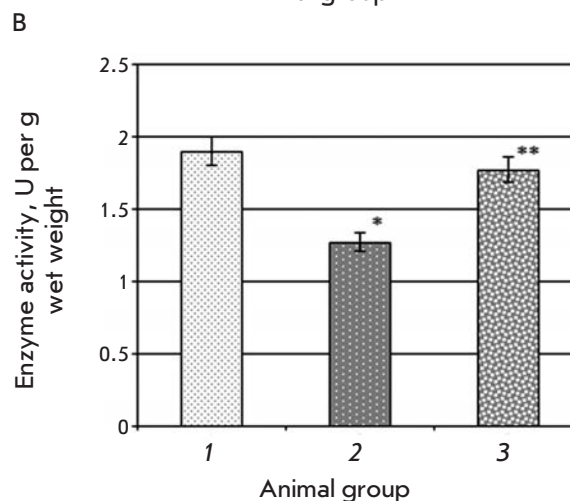
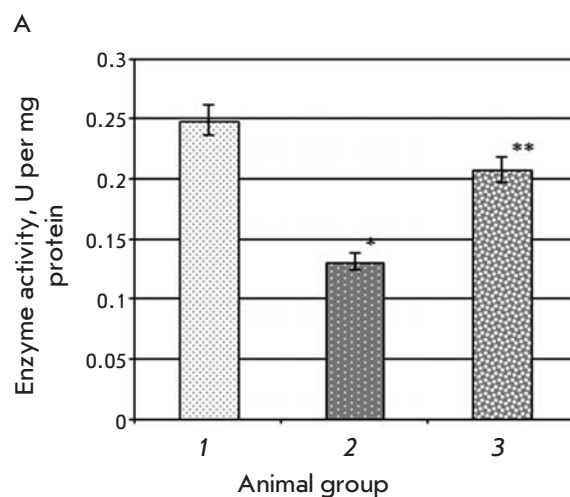


Fig. 4. Aconitate hydratase activity in U per mg protein (A) and U per g wet weight (B) in rat liver in the control group (1), animals with type 2 diabetes mellitus (2), and after introduction of epifamin into animals with pathology (3)

Note. The differences are significant at $p \leq 0.05$: * – compared to the control group, ** – compared to the group of rats with T2DM.

tonin can interact with a number of reactive oxygen metabolites and neutralize the hydroxyl radical, one of the most active ROS in particular [10, 17].

Furthermore, the $t\alpha_2$ values in animals with T2DM that received epifamin were 1.5-fold lower than those in animals with T2DM that did not receive the agent. This can be attributed to the decrease in the degree of mobilization of the antioxidant system due to inhibition of free-radical processes.

The specific activity of caspase-1 and 3 in the liver of rats with experimentally induced T2DM was found to increase 6.0- and 2.7-fold, respectively (Fig. 2). This is indicative of the enhancement of apoptotic processes in liver cells. An increased activity of caspase-3 in rat liver was also observed after the rats were exposed to carbon tetrachloride [18]. Introduction of epifamin into animals with T2DM reduced caspase-1 and -3 activities in liver 2.4- and 1.6-fold compared to the corresponding values in animals with T2DM that did not receive epifamin (Fig. 2).

Thus, the results demonstrate that epifamin reduces the level of apoptotic processes in the liver of rats with T2DM, which can presumably be attributed to the fact that the rate of free-radical processes decreases after the introduction of epifamin. It was shown that the citrate concentration in the liver of rats with T2DM increases 2.3-fold compared to the control values (Fig. 3). A 1.9-fold decrease in the specific activity of aconitase in the liver of animals with T2DM and a 1.5-fold decrease in activity (U/g dry weight) compared to the control were also observed (Fig. 4). It is well-known that the AH activity can be an oxidative stress marker, since the enzyme loses its activity under the action of ROS as

the active site is modified and an iron atom is released from the iron-sulfur cluster [5]. The data regarding the changes in the AH activity and citrate concentration in animals with T2DM show agreement with the results of measurements of the BCL parameters, which attest to the fact that the intensity of free-radical oxidation increases under conditions of developing T2DM.

Introduction of epifamin into rats with T2DM reduced the citrate concentration in liver 1.9-fold (Fig. 3) and increased specific AH activity 1.6-fold (Fig. 4A) compared to these parameters in animals with T2DM that did not receive epifamin. The AH activity expressed as U/g wet weight of the liver also increased 1.4-fold as compared to the second experimental group (Fig. 4B). The changes in the tested parameters towards the control values after the animals with T2DM received epifamin apparently attest to the fact that the oxidative stress level fell, which resulted in reconstruction of the active site of AH and loss of citrate in the AH-catalyzed reaction.

CONCLUSIONS

The data obtained demonstrate that epifamin has a positive regulating effect on free-radical homeostasis via a reduction in the intensity of oxidative stress in rats with induced T2DM. This fact is supported by the changes in the BCL indicators (I_{\max} and S) that characterize the intensity of free-radical processes; in the $t\alpha_2$ values that show the total antioxidant activity; in the activities of caspase-1 and caspase-3 indicating the rate of apoptotic processes; and in the AH activity and citrate concentration in rat liver under T2DM towards the normal values. ●

REFERENCES

- Balabolkin M.I., Klebanova E.M. // *Problems of Endocrinology*. 2000. № 6. P. 29–34.
- Baynes J.W., Thorpe J.W. // *Diabetes*. 1999. V. 48. P. 1–9.
- Kutsyy M.P., Kuznetsov E.A., Haziyeu A.I. // *Biochemistry*. 1999. V. 64. P. 149–163.
- Woo M., Hakem R., Soengas M.S., Duncan G.S., Shahinian A., Kägi D., Hakem A., McCurrach M., Khoo W., Kaufman S.A., et al. // *Genes Dev*. 1998. V. 12. P. 806–819.
- Gardner P.R., Nguyen D.M., White C.W. // *Proc. Natl. Acad. Sci. USA*. 1994. V. 91. № 25. P. 12248–12252.
- Cadet E., Gadenne M., Capron D., Rochette J. // *Rev. Med. Interne*. 2005. V. 26. P. 315–324.
- Kuhtina E.N., Glushchenko N.N. // *Biochemistry*. 1996. V. 61. № 6. P. 993–997.
- Havinson V.H., Kvetnoy I.M., Yuzhakov V.V., Popuchiev V.V., Kononov S.S. *Peptidergicheskaya regulatsiya gomeostaza (Peptidergic regulation of homeostasis)*. St. Petersburg: Sciencs, 2003. 194 p.
- Anisimov V.N., Khavinson V.Kh. // *Aging interventions and therapies / Ed. Suresh I.S. Rattan*. Singapore: World Scientific. 2005. P. 127–146.
- Reiter R.J., Tan D.X., Osuna C., Gitto E. // *J. Biomed. Sci*. 2000. V. 7. № 6. P. 444–458.
- Reiter R.J., Acuña-Castroviejo D., Tan D.X., Burkhardt S. // *Ann. N. Y. Acad. Sci*. 2001. V. 939. P. 200–215.
- Ulyanov A.M., Tarasov Y.A. // *Vopr Med Khim*. 2000. V. 46. № 2. P. 149–154.
- Bogomolov A.F., Lukyanov I.J., Gorbacheva L.R. *Guidelines on the course of experimental physiology for students of biological department of biology and chemistry faculty*. Ivanovo: Ivanovo State University, 2005. 43 p.
- Kuzmina E.I., Nelyubin A.S., Shchennikova M.K. // *Interuniversity collection: Biochemistry and Biophysics microorganisms*. 1983. P. 179–183.
- Afanasyev V.G., Zaitsev V.S., Wolfson T.I. // *Laboratornoe delo (Lab. Business)*. 1973. № 4. P. 115–116.
- Ha E., Yim S.V., Chung J.H., Yoon K.S., Kang I., Cho Y.H., Baik H.H. // *J. Pineal Res*. 2006. V. 41. № 1. P. 67–72.
- Peschke E. // *J. Pineal Res*. 2008. V. 44. № 1. P. 26–40.
- Lemza S.V., Azhunova T.A., Mondodoev A.G., Nikolaev S.M., Razuvaeva Y.G., Zandanov A.O. // *Bulletin VSNC SO RAMN (Bulletin of East-Siberian Scientific Center of the Siberian Branch of the Russian Academy of Medical Science)*. 2010. V. 72. № 2. P. 181–184.

GENERAL RULES

Acta Naturae publishes experimental articles and reviews, as well as articles on topical issues, short reviews, and reports on the subjects of basic and applied life sciences and biotechnology.

The journal is published by the Park Media publishing house in both Russian and English.

The journal *Acta Naturae* is on the list of the leading periodicals of the Higher Attestation Commission of the Russian Ministry of Education and Science

The editors of *Acta Naturae* ask of the authors that they follow certain guidelines listed below. Articles which fail to conform to these guidelines will be rejected without review. The editors will not consider articles whose results have already been published or are being considered by other publications.

The maximum length of a review, together with tables and references, cannot exceed 60,000 symbols (approximately 40 pages, A4 format, 1.5 spacing, Times New Roman font, size 12) and cannot contain more than 16 figures.

Experimental articles should not exceed 30,000 symbols (20 pages in A4 format, including tables and references). They should contain no more than ten figures. Lengthier articles can only be accepted with the preliminary consent of the editors.

A short report must include the study's rationale, experimental material, and conclusions. A short report should not exceed 12,000 symbols (8 pages in A4 format including no more than 12 references). It should contain no more than four figures.

The manuscript should be sent to the editors in electronic form: the text should be in Windows Microsoft Word 2003 format, and the figures should be in TIFF format with each image in a separate file. In a separate file there should be a translation in English of: the article's title, the names and initials of the authors, the full name of the scientific organization and its departmental affiliation, the abstract, the references, and figure captions.

MANUSCRIPT FORMATTING

The manuscript should be formatted in the following manner:

- Article title. Bold font. The title should not be too long or too short and must be informative. The title should not exceed 100 characters. It should reflect the major result, the essence, and uniqueness of the work, names and initials of the authors.
- The corresponding author, who will also be working with the proofs, should be marked with a footnote *.
- Full name of the scientific organization and its departmental affiliation. If there are two or more scientific organizations involved, they should be linked by digital superscripts with the authors' names. Abstract. The structure of the abstract should be very clear and must reflect the following: it should introduce the reader to the main issue and describe the experimental approach, the possibility of practical use, and the possibility of further research in the field. The average length of an abstract is 20 lines

(1,500 characters).

- Keywords (3 – 6). These should include the field of research, methods, experimental subject, and the specifics of the work. List of abbreviations.

- INTRODUCTION
- EXPERIMENTAL PROCEDURES
- RESULTS AND DISCUSSION
- CONCLUSION

The organizations that funded the work should be listed at the end of this section with grant numbers in parenthesis.

- REFERENCES

The in-text references should be in brackets, such as [1].

RECOMMENDATIONS ON THE TYPING AND FORMATTING OF THE TEXT

- We recommend the use of Microsoft Word 2003 for Windows text editing software.
- The Times New Roman font should be used. Standard font size is 12.
- The space between the lines is 1.5.
- Using more than one whole space between words is not recommended.
- We do not accept articles with automatic referencing; automatic word hyphenation; or automatic prohibition of hyphenation, listing, automatic indentation, etc.
- We recommend that tables be created using Word software options (Table → Insert Table) or MS Excel. Tables that were created manually (using lots of spaces without boxes) cannot be accepted.
- Initials and last names should always be separated by a whole space; for example, A. A. Ivanov.
- Throughout the text, all dates should appear in the “day.month.year” format, for example 02.05.1991, 26.12.1874, etc.
- There should be no periods after the title of the article, the authors' names, headings and subheadings, figure captions, units (s – second, g – gram, min – minute, h – hour, d – day, deg – degree).
- Periods should be used after footnotes (including those in tables), table comments, abstracts, and abbreviations (mon. – months, y. – years, m. temp. – melting temperature); however, they should not be used in subscripted indexes (T_m – melting temperature; $T_{p.t.}$ – temperature of phase transition). One exception is mln – million, which should be used without a period.
- Decimal numbers should always contain a period and not a comma (0.25 and not 0,25).
- The hyphen (“-”) is surrounded by two whole spaces, while the “minus,” “interval,” or “chemical bond” symbols do not require a space.
- The only symbol used for multiplication is “×”; the “×” symbol can only be used if it has a number to its right. The “·” symbol is used for denoting complex compounds in chemical formulas and also noncovalent complexes (such as DNA·RNA, etc.).
- Formulas must use the letter of the Latin and Greek alphabets.

GUIDELINES FOR AUTHORS

- Latin genera and species' names should be in italics, while the taxa of higher orders should be in regular font.
- Gene names (except for yeast genes) should be italicized, while names of proteins should be in regular font.
- Names of nucleotides (A, T, G, C, U), amino acids (Arg, Ile, Val, etc.), and phosphonucleotides (ATP, AMP, etc.) should be written with Latin letters in regular font.
- Numeration of bases in nucleic acids and amino acid residues should not be hyphenated (T34, Ala89).
- When choosing units of measurement, SI units are to be used.
- Molecular mass should be in Daltons (Da, KDa, MDa).
- The number of nucleotide pairs should be abbreviated (bp, kbp).
- The number of amino acids should be abbreviated to aa.
- Biochemical terms, such as the names of enzymes, should conform to IUPAC standards.
- The number of term and name abbreviations in the text should be kept to a minimum.
- Repeating the same data in the text, tables, and graphs is not allowed.

GUIDENESS FOR ILLUSTRATIONS

- Figures should be supplied in separate files. Only TIFF is accepted.
- Figures should have a resolution of no less than 300 dpi for color and half-tone images and no less than 500 dpi.
- Files should not have any additional layers.

REVIEW AND PREPARATION OF THE MANUSCRIPT FOR PRINT AND PUBLICATION

Articles are published on a first-come, first-served basis. The publication order is established by the date of acceptance of the article. The members of the editorial board have the right to recommend the expedited publishing of articles which are deemed to be a priority and have received good reviews.

Articles which have been received by the editorial board are assessed by the board members and then sent for external review, if needed. The choice of reviewers is up to the editorial board. The manuscript is sent on to reviewers who are experts in this field of research, and the editorial board makes its decisions based on the reviews of these experts. The article may be accepted as is, sent back for improvements, or rejected.

The editorial board can decide to reject an article if it does not conform to the guidelines set above.

A manuscript which has been sent back to the authors for improvements requested by the editors and/or reviewers is reviewed again, after which the editorial board makes another decision on whether the article can be accepted for publication. The published article has the submission and publication acceptance dates set at the beginning.

The return of an article to the authors for improvement does not mean that the article has been accepted for publication. After the revised text has been received, a decision is made by the editorial board. The author must return the improved text, together with the original text and responses to all comments. The date of acceptance is the day on which the final version of the article was received by the publisher.

A revised manuscript must be sent back to the publisher a week after the authors have received the comments; if not, the article is considered a resubmission.

E-mail is used at all the stages of communication between the author, editors, publishers, and reviewers, so it is of vital importance that the authors monitor the address that they list in the article and inform the publisher of any changes in due time.

After the layout for the relevant issue of the journal is ready, the publisher sends out PDF files to the authors for a final review.

Changes other than simple corrections in the text, figures, or tables are not allowed at the final review stage. If this is necessary, the issue is resolved by the editorial board.

FORMAT OF REFERENCES

The journal uses a numeric reference system, which means that references are denoted as numbers in the text (in brackets) which refer to the number in the reference list.

For books: the last name and initials of the author, full title of the book, location of publisher, publisher, year in which the work was published, and the volume or issue and the number of pages in the book.

For periodicals: the last name and initials of the author, title of the journal, year in which the work was published, volume, issue, first and last page of the article. Must specify the name of the first 10 authors. Ross M.T., Grafham D.V., Coffey A.J., Scherer S., McLay K., Muzny D., Platzer M., Howell G.R., Burrows C., Bird C.P., et al. // Nature. 2005. V. 434. № 7031. P. 325–337.

References to books which have Russian translations should be accompanied with references to the original material listing the required data.

References to doctoral thesis abstracts must include the last name and initials of the author, the title of the thesis, the location in which the work was performed, and the year of completion.

References to patents must include the last names and initials of the authors, the type of the patent document (the author's rights or patent), the patent number, the name of the country that issued the document, the international invention classification index, and the year of patent issue.

The list of references should be on a separate page. The tables should be on a separate page, and figure captions should also be on a separate page.

The following e-mail addresses can be used to contact the editorial staff: vera.knorre@gmail.com, actanaturae@gmail.com, tel.: (495) 727-38-60, (495) 930-87-07